# A Study of the Change in the Temperature of Maximum Density of Water and Aqueous Solutions as a function of Pressure

*A thesis presented for the degree of*
Doctor of Philosophy

*Presented by*
Gerard Cotter B.Sc.

Department of Experimental Physics
National University of Ireland, Maynooth
Maynooth
County Kildare

23$^{rd}$ September 2010

*Research Supervisor*
Michael F. Cawley M.Sc., Ph.D.

*Head of Department*
J. Anthony Murphy M.Sc., M.S., Ph.D.

NUI MAYNOOTH
Ollscoil na hÉireann Má Nuad

# Contents

# Abstract

The aim of this research is to study the shift in the temperature of maximum density of water and aqueous solutions as a function of pressure. One of the many anomalous properties of water is that it passes through a maximum in density in the liquid state. In order to accurately measure the temperature of maximum density ($T_{md}$), convective flow is monitored in a rectangular container containing the fluid. A temperature gradient is held across the chamber and it is cooled and heated in a quasi-steady state manner. A double cell convection pattern forms in the vicinity of the density maximum. This double cell is tracked by monitoring the temperature at selected points in the fluid. The change in temperature of maximum density due to concentration and applied pressure can be investigated using this technique. At a pressure of one atmosphere, this density maximum occurs in pure water at a temperature of 3.98 °C. It is known that the temperature of maximum density decreases as the pressure increases; for pure water this occurs at a rate of 1 °C per 50 bar. Experimentally the shift in the temperature of maximum density of aqueous solutions is tracked over the pressure range 1 to 100 bar. It is found that the temperature of maximum density drops as the pressure rises for all solutes studied, but that the rate of decrease changes depending on the nature of the solute. For ionic salts, the rate of decrease is steeper than that for pure water, whereas for monohydric alcohols the rate of decrease is less that that for pure water. These divergent trends become more apparent as solute concentrations increase.

The behaviour of the temperature of maximum density is modelled on both macroscopic and microscopic levels. A simple macroscopic model is proposed by combining state functions for water with those of solutes. This approach predicts that the rate of decrease of the temperature of maximum density for ideal (non-interacting) mixtures as a function of pressure is less than for pure water (but not as pronounced as the change observed in the alcohol solutions). Microscopic modelling at the molecular level is done using Monte Carlo methods. Non-ideal mixtures are studied by introducing molecules whose interactions with water are either stronger or

weaker than the water-water interactions. In all cases it is found that the rate of change of the temperature of maximum density as a function of pressure lessens compared to the rate for pure water. The models thus help in understanding some, but not all, of the experimental observations.

# Acknowledgements

There are many people I would like to thank who have helped me over the past three years of research whose help has been without comparison.

I wish to thank my supervisor, Dr. Michael Cawley, for allowing me the opportunity to work with the fluids group at the National University of Ireland Maynooth. His ever present support and inspiration has made this work possible, enjoyable and a significant learning experience.

I thank Professor J. Anthony Murphy for the use of the facilities in the Experimental Physics Department.

Throughout my studies at the National University of Ireland Maynooth Allan Stewart and Andrew Byrne have studied with me in the fluids lab. I would like to thank them for making the lab a pleasant place to work. I would like to thank David Watson for constructing various experimental components and for his patience and time, John Kelly for providing computers and assistance with software issues and all the other technical staff who have helped with ordering, printing and circuit board construction.

I would like to thank the National University of Ireland Maynooth for financial assistance in the form of the John and Pat Hume Scholarship.

As always, I am grateful for the ever present support and patience of my parents, John and Ann Cotter and my sister, Elizabeth Cotter. Finally, I wish like to thank Katie O'Neill for being ever present over my years in college. Thank you for your support and encouragement.

# Chapter 1

# Introduction

## 1.1 Introduction

Water is the most abundant and essential substance on Earth. Sixty five percent of the human body consists of water and nearly eighty percent of the brain consists of water. There are approximately three hundred and twenty six million trillion gallons of water on Earth with the oceans covering seventy percent of the planet. The salt water of the oceans account for approximately ninety eight percent of the water on the planet whereas only two percent is fresh. One point six percent of the Earth's water exists in its solid form comprising of the polar ice caps and glaciers. Water also can be found in its gaseous form as zero to four percent of air consists of water vapour. Despite the vast quantities of water to be found on our planet and the vital role it plays in our lives there are many compelling and unusual peculiarities associated with our most precious substance.

Water is the most anomalous liquid on the planet. At a glance water appears to be a relatively simple molecule consisting of one oxygen and two hydrogen atoms. The molecule is arranged in a v-shape with two hydrogen atoms covalently bonded to one oxygen atom. Two pairs of electrons are involved in these covalent bonds and two lone pairs accumulate at the oxygen atom. A negative charge exists at the oxygen atom and a positive charge at the hydrogen atoms. This polarity causes the two bonded hydrogen atoms to become "bent" giving the molecule its distinctive v-shape with an angle of 104.5° between the bonded hydrogen atoms. This polarity also gives rise to hydrogen bonding between water molecules. The positively charged hydrogen part of one molecule is attracted to the negatively charged oxygen part of another molecule forming a hydrogen bond. This hydrogen bond is about one tenth the strength of the covalent bond formed between the oxygen and hydrogen atoms within a molecule. Hydrogen bonding gives water many unusual or anomalous properties when compared to substances of similar molecular structure [1].
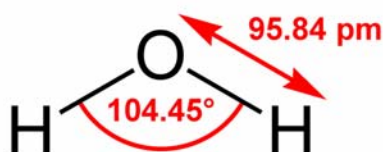


**Figure 1.1-1** *Diagram of a water molecule.*

Some very important and well known anomalous properties of water include its unusually high melting and boiling points. In the solid state water molecules form cage-like structures due to hydrogen bonding. This arrangement is very structured requiring large amounts of energy to break up but there are gaps in the structure giving rise to a lower density. Hence, water has a high melting point of 0 °C. Another very important and well known anomalous property of water is its unusually high boiling point. The boiling point of water is 100 °C. Breaking the residual hydrogen bonds in the liquid requires an abnormally high temperature [2].

A very important anomalous property of water for this work is that water exhibits a maximum density at a temperature of 3.98 °C under one atmosphere of pressure. Hydrogen bonding in liquid water causes it to have a relatively high density. This effect competes with thermal expansion which breaks up structure and lowers density. These competing effects give rise to a temperature of maximum density at 3.98 °C for pure water. Above 3.98 °C hotter water rises and cooler water sinks forming a convective cell. Below 3.98 °C hotter water sinks and cooler water rises forming a convective cell in the opposite direction. For this reason when freshwater lakes freeze over the water at the bottom is hotter than the surface at about 4 °C allowing pond life to survive. The less dense ice floats on top of the lake.

This work is concerned with the effect of pressure on the density maximum of water and many anomalous properties of water are related to pressure. Increased pressure reduces the temperature of the density maximum and ice's melting point. Increasing pressure causes the structure of the water to collapse giving rise to higher density at all temperatures. However, this effect is disproportionate at lower temperatures giving rise to a shift in the temperature of maximum density to lower temperatures. At sufficiently high pressures of about 283.3 bar the density anomaly cannot be seen above the melting point. At a pressure of 133.5 bar ice's melting point is decreased by 1 °C. This is due to collapsing of the ice "cage-like" structure under increased pressures. At increased pressures water can still freeze but it will freeze into different forms of ice such as ice-three, ice-five or ice-seven [3]. It has been suggested that pressure melting of ice accounts for the ability of skaters to glide easily over a smooth ice surface, as a consequence of a layer of water forming between the ice and the narrow blade of the skate [4]. However, as ice skating is

possible at temperatures well below the freezing point of water, the pressure melting effect is unlikely to fully account for the low friction between the ice and the blades of the skate.

Another important anomalous property of water is its unusually high specific heat capacity of 4179 J Kg$^{-1}$ K$^{-1}$ at one atmosphere of pressure at 25 °C [5]. As energy is added to water hydrogen bonds are broken. Much of this energy is absorbed by this process rather than increasing the kinetic energy of the water molecules. For this reason raising the temperature of the water requires a large amount of heat. This is evident if the specific heat capacity of water is compared to a substance with similar mass such as ethanol. Ethanol has a specific heat capacity of 2440 J Kg$^{-1}$ K$^{-1}$ at one atmosphere of pressure at 25 °C [6]. Water's high heat capacity allows bulk water to act as a thermal reservoir. This is most notably seen in the oceans which regulate the Earth's temperature. The specific heat capacity ($C_P$) has a minimum with respect to pressure. At high pressures of approximately 4000 bar at 290 K this minimum is observed [7]. As pressure is increased hydrogen bonds are broken. However, at higher pressures hydrogen bonding networks can penetrate each other creating increased amounts of hydrogen bonding. This process gives rise to a minimum in the specific heat capacity with respect to pressure.

## 1.2 Review of the density maximum of pure water at atmospheric pressure

The earliest known work carried out on the density maximum of water was carried out by a group of court scientists at the Galilean Accademia del Cimento in Florence. The Academy worked on various scientific projects from 1657 to 1667. In 1667 one of the court scientists named Lorenzo Magalotti documented the experiments carried out at the academy [8]. When investigating the freezing point of water the scientists used a bulb connected to a thin graduated tube. This instrument was made of glass and filled with water open at one end like a water thermometer. The degree the water reached was recorded. The bulb of this instrument was immersed in a container with crushed ice. As it cooled the water level started to increase slowly approaching the freezing point indicating that the water must have reached a

minimum volume before the freezing point. This slow rise continued until the freezing point was reached at which point the water level increased very rapidly and unexpectedly. Cooling beyond the freezing point showed that the water level continued to rise until the water transformed to ice and burst the glass bulb. The experiments had revealed two very interesting phenomena, a minimum in the volume (maximum in density) of water before the freezing point and the anomalous expansion of water upon freezing. Both of these phenomena are seen in figure 1.2-1.
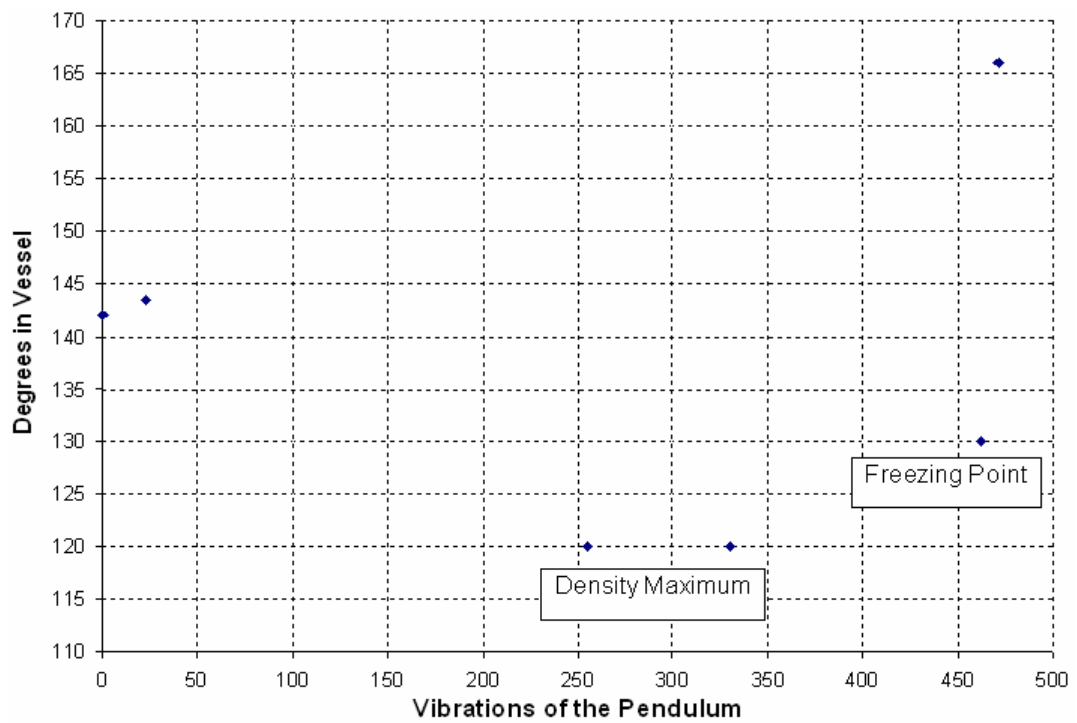


**Figure 1.2-1** *Degrees in vessel versus vibrations in pendulum. Data points are from experiments carried out at the Accademia del Cimento [8].*

This technique relied on the changes in the volume of water due to temperature changes. The volume of the container also changes with temperature giving rise to possible ambiguity in the work of the Academia del Cimento. The slow rise in the water level could have been due to volume changes in the water or the contraction of the vessel.

The first person to record a temperature of maximum density was Thomas Charles Hope by studying the convection patterns in a sample of water. In 1805 he published a paper on his findings [9]. The apparatus Hope used involved a cylindrical

5

container containing water at 0 °C surrounded in the middle by a metal basin containing water at 20 °C. Temperatures of the water above and below the metal basin were recorded using thermometers. The experimental set up is shown in figure 1.2-2. It was expected that if a density maximum did not exist the water would rise as it was heated hence giving hotter temperatures above the basin than below. Hope found that as the water in the cylinder was heated the reading from the higher thermometer above the basin was reading a colder temperature than the one below the basin. As he further heated the water he observed that this trend reversed at some point and water in the bottom of the cylinder was colder than the water in the top. From Hope's experiments as described in his paper [9], he concluded that water had a maximum density in the range of 4.2 °C to 4.4 °C. The temperature of maximum density of pure water is accepted to be 3.98 °C at atmospheric pressure.



**Figure 1.2-2** *Apparatus used by Thomas Hope with bungs where thermometers were situated in holes above and below the basin located halfway up the glass cylinder. This particular apparatus is a replica on display at the National Science Museum of Ireland, St. Patrick's College, Maynooth.*

Detailed investigations into the temperature of maximum density of water at atmospheric pressure were carried out by Thiesen et al. in 1986. Using a method of balancing water columns of different temperatures Thiesen et al. obtained data for the density of water in the range 0 °C to 40 °C [10]. The researchers conducted further explorations in the range 40 °C to 100 °C as described his 1918 paper [11]. In 1907 Chappius obtained detailed data on the density of water in the range 0 °C to 42 °C using a dilatometry technique. Dilatometry is a method used for measuring the compression or expansion of a material over a controlled temperature range. Data from Thiesen et al. and Chappius were compiled and the data quoted in the International Critical Tables of Numerical Data, Physics, Chemistry and Technology published in 1928 [12].

## 1.3 Review of the density maximum of aqueous solutions at atmospheric pressure

In the mid 19th century the first reported investigations into the density maximum of aqueous solutions were conducted. These experiments were carried out in 1839 and 1840 by Despretz and concentrated mainly on salt solutions [13, 14]. From his findings he devised the following rule, now known as the Despretz' law: "the lowering of the temperature of the point of density maximum of water caused by the addition of a solute is directly proportional to the concentration of the latter" [15]. The rate of suppression of the temperature of maximum density does, however, vary from solute to solute (for example, a 0.1 mol/L solution of sodium chloride will have a different value of the temperature of maximum density to a 0.1 mol/L solution of potassium bromide). Thus, the suppression of the temperature of maximum density is not a colligative property (which only depends on number of solute particles present) of water, in contrast to the suppression of the freezing point or the elevation of the boiling point.

Rosetti carried out experiments on the temperature of maximum density and the temperature of the phase change of solutions [16, 17] in 1867 and 1869. Rosetti attempted to connect the lowering of the temperature of maximum density by the addition of a solute to the lowering of the temperature of the phase change. He was

unable to formulate any general law as the depression of the freezing point is a colligative property whereas the density maximum depends on the concentration and the nature of the solute.

Work by later research groups found that various solutes do not obey the Despretz law, perhaps most notably the monohydric alcohols. Ethanol was investigated by Mitchell and Wynne-Jones in 1953 and it was shown that for low concentrations of ethanol the temperature of maximum density in fact increased before decreasing at higher concentrations [18]. Ethanol and various other monohydric alcohols were examined by Wada and Umeda in 1962 [19]. These studies indicated that the monohydric alcohols do not follow the Despretz rule.

Further work was carried out by Franks and Watson on the effects of alcohols and amines on maximum density of water in the 1967 using a dilatometry technique [20]. Once again, they found that some monohydric alcohols produced a rise in the temperature of maximum density at low concentration in agreement with the work of Wada and Umeda.

## 1.4 Recent studies of the temperature of maximum density of aqueous solutions at atmospheric pressure

Recent investigations have been carried out on the behaviour of the temperature of maximum density of aqueous solutions as a function of concentration by Mr. Allan Stewart in the Experimental Physics Department at the National University of Ireland Maynooth. Stewart found that for solutes such as the ionic salts and sugars, the temperature of maximum density decreased in a linear manner as the solute concentration increased ('Despretz law'). However, he observed detailed structure in the concentration profiles of monohydric alcohol solutions at atmospheric pressure. Stewart found that the behaviour of the temperature of maximum density for monohydric alcohol solutions was highly non-linear, moving through several local maxima in the low concentration region for ethanol and 2-propanol. Results of Stewart's work relating to the monohydric alcohols are summarised in figure 1.4-1. It is clear that smooth parabolic models do not give good fits to these profiles. A chi-

squared fit between the ethanol concentration profile and a best fit parabola gives a probability of compatibility of ~$10^{-4}$.  The probability of compatibility for the 2-propanol profile is about 1%.  Stewart's results are given in [21].
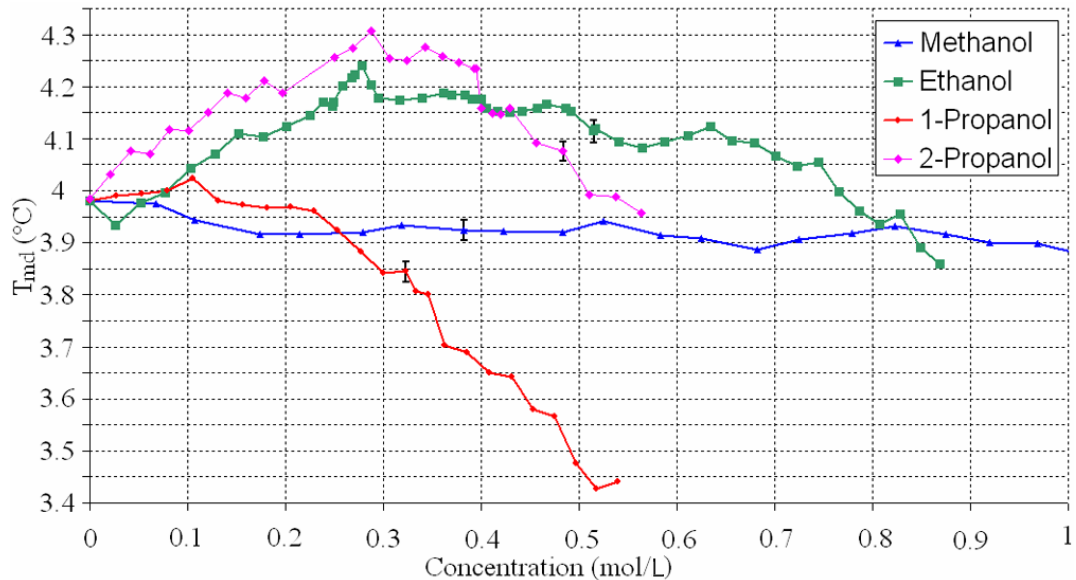


**Figure 1.4-1** *The behaviour of the temperature of maximum density as a function of mass concentration (mol/L) for a range of monohydric alcohols.  The data for all trends have been taken from [21].*

## 1.5 Review of the density maximum under pressure

Physical properties of pure water and saline solutions have been investigated as a function of pressure.  Due to the need for an equation of state for seawater detailed studies have been carried out by various groups.  Specific volume data from all of these groups was used to formulate the most recent equation of state for seawater.  One-atmosphere specific volume data was contributed by Millero et al. in 1976 [22].  High pressure specific volume data was contributed by a number of groups.  In 1970 Bradshaw and Schleicher directly measured the thermal expansion of seawater under pressure using a dilatometry technique [23].  In 1976 Chen and Millero investigated the specific volume of seawater at high pressure using a high pressure magnetic float densimeter [24].  Further studies contributing data to the seawater equation of state were conducted by Chen and Millero in 1978 [25] and Chen et al. in 1977 [26] using sound speed measurements.  Bradshaw and Schleicher produced further data in 1976

(unpublished data).  The new high pressure equation of state for seawater was compiled in 1980 by Millero et al. [27] using data from all of these studies.

In 1978 Caldwell measured the temperature of maximum density for pure water and saline solutions using a technique involving the zero-crossing of the adiabatic gradient [28].  His results were not directly used in the formulation of the seawater equation of state but are useful for comparative purposes.  Henderson and Speedy investigated the temperature of maximum density at negative pressures using a fine helical capillary and the Berthelot tube principle in 1978 [29].

## 1.5.1 The seawater equation

The seawater equation of state is a function that returns a density value for a given salinity, temperature and pressure.  By scanning through a range of temperature values the temperature maximum density can be extracted.  The equation in its most recent form was published in the Unesco algorithms for computation of the fundamental properties of seawater in 1983 [30].  Data from various sources were compiled to create this equation of state as outlined above.  One-atmosphere specific volume data over the entire temperature and salinity range were provided by the relative density measurements of Millero, Gonzalez and Ward in 1976 [22].  The earliest contributor of high pressure data was from Bradshaw and Schleicher in 1970.

Bradshaw and Schleicher measured the thermal expansion of seawater under pressure over a temperature range of -2 °C to 30 °C at 2 °C intervals for salinities of 30.5, 35.0 and 39.5 parts per thousand.  The pressure range they employed was 8 to 1001 bars (absolute).  In order to carry out these investigations Bradshaw and Schleicher used a dilatometer constructed of fused quartz (figure 1.5-1).  The sample under test was held under constant pressure and subjected to a temperature change. The change in volume of the sample under this temperature change was obtained from the change in height of the mercury in the precision bore tubing section of the dilatometer (figure 1.5-1).  In order to change the temperature of the sample under test the dilatometer was placed in a bath of water-ethylene glycol solution.  The

temperature of this bath could be held to an accuracy of 0.001 °C or better once temperature stability had been obtained.
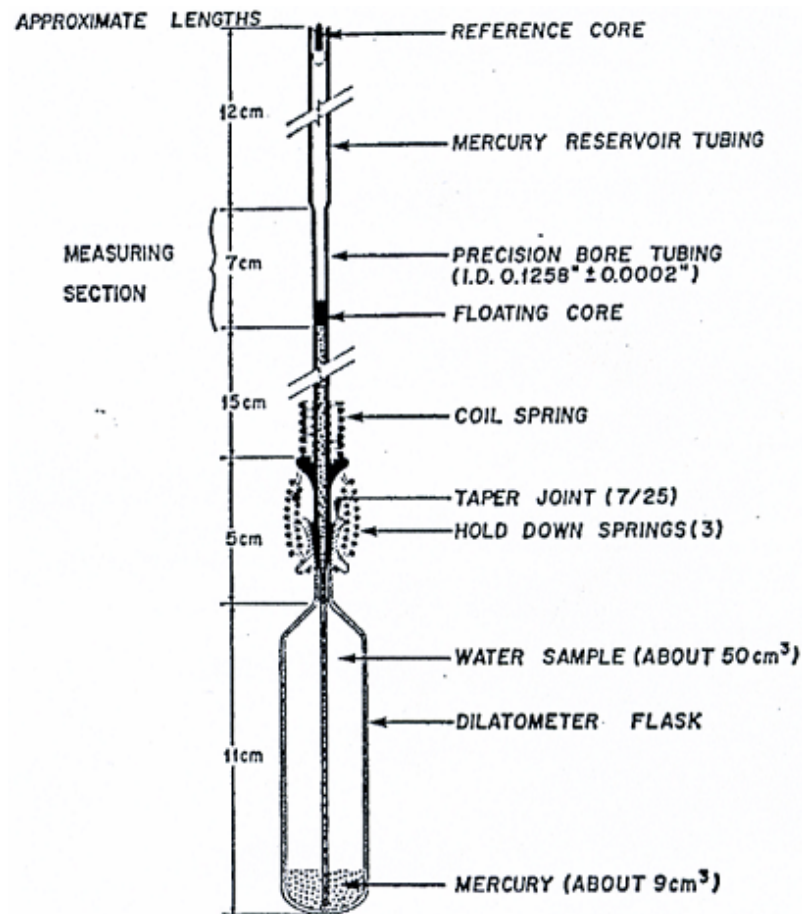


**Figure 1.5-1** *Dilatometer constructed of fused quartz.*

In order to apply pressure to the sample the dilatometer was mounted on a pressure vessel (figure 1.5-2). The pressure fluid used was degassed water which entered the pressure vessel thereby applying pressure. A pressure pump was used to bring the vessel up to the required pressure. A water-oil separator was used to separate oil from the pump and the degassed water from the pressure vessel. When an experimental run was carried out the dilatometer was thoroughly cleaned and filled with a sample of known salinity (30.5, 35.0 and 39.5 parts per thousand were the only salinities tested). Temperature runs were then conducted at pressures from 8 to 1001 bars. All runs were begun at the high end of the temperature range so that the mercury column would retreat over dry glass. Results from observations gave the specific volume changes of the seawater samples from 0 °C to a defined temperature T °C [23]. These values have been used in the compilation of the seawater equation.

11
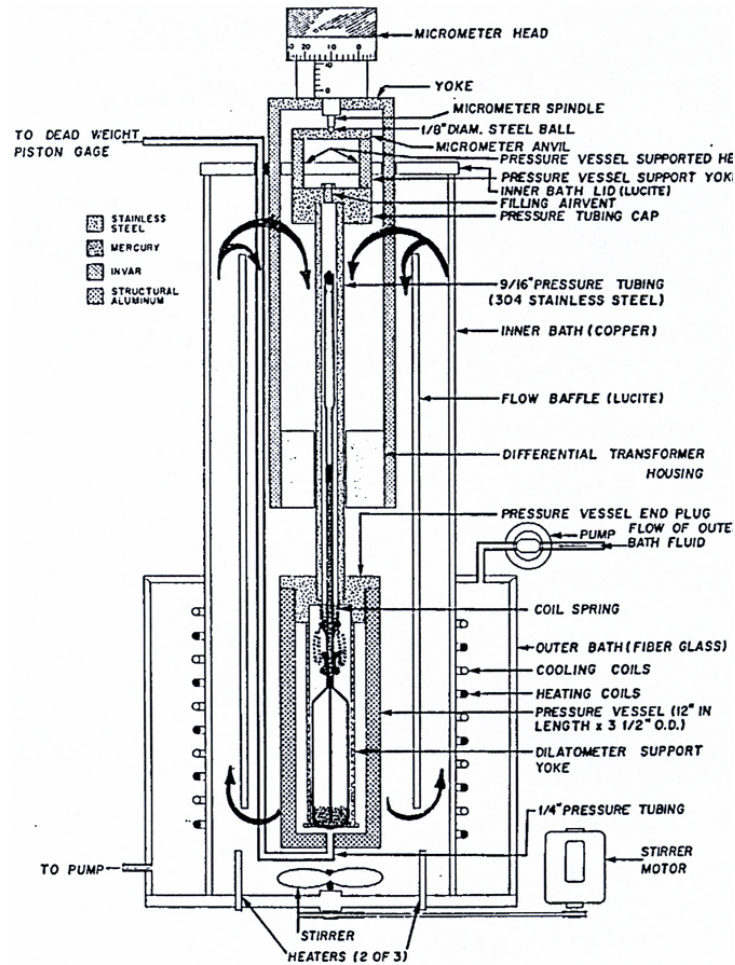
**Figure 1.5-2** *Cross-sectional view of the apparatus used by Bradshaw and Schleicher showing the quartz fused dilatometer mounted on the pressure vessel.*

Chen and Millero contributed to the seawater equation with high pressure data from their 1976 paper [24]. Chen and Millero measured the specific volumes of seawater from 0 to 40 °C, 0 to 1000 bars and over a salinity range of 5 to 40 parts per thousand. They achieved these results using a high pressure magnetic float densimeter. The apparatus consisted of pressure bomb, a magnetic float and auxiliary measuring and control systems. The pressure bomb was cylindrical in shape and made of stainless steel. The top and bottom plugs were sealed with O-rings. The vessel had a volume of 170 cm$^3$. The plug on the bottom of the vessel contained an insert that supported a solenoid. The bomb's windows were made from Plexiglas rod. The floats used were made of thick Pyrex glass and contained a permanent magnet. The floats had a volume of 59.8 cm$^3$ at 0 °C and atmospheric pressure.

The pressure bomb was completely immersed in a 30 litre bath. The temperature of this bath could be controlled to within 0.001 °C. In order to apply pressure to the sample under test an Enerpac hand pump was used. To avoid contamination an oil water separator was used to separate the sample from the pressure generating system. The pressure was accurate to 0.1 bar at a pressure of 1000 bars. The pressure generating system is described in detail by the 1972 paper by Millero et al. [31]. Using this system Chen and Millero measured specific volumes of seawater at various salinities, temperatures and pressures. These values have been used in the formulation of the seawater equation [24].

Both of these methods used by Bradley and Schleicher and Chen and Millero make direct measurements on the specific volume of seawater using a dilatometry technique and a high pressure magnetic float densimeter. In 1977 and 1978 Chen and Millero [25] and Chen et al. [26] used sound speed measurements to derive the P-V-T properties of seawater. Both approaches were used to obtain a reliable equation of state as both approaches are completely independent of each other.

A new high pressure equation of state for seawater was compiled in 1980 using the described data by Millero et al. [27] and is given by Fofonoff and Millard [30] in 1980 as a function of practical salinity ($S$), temperature ($T$, °C) and applied pressure ($P$, decibars):

$$\rho(S,T,P) = \rho(S,T,0)[1 - P/K(S,T,P)] \qquad (1.5\text{-}1)$$

where $K(S,T,P)$ is the secant bulk modulus. Most fluids reduce in volume under applied pressures. The volume of the fluid is a function of applied pressure, compressibility of the fluid and the initial volume of the fluid. Bulk modulus refers to the reciprocal of compressibility and is thus a measure of the resistance to compressibility of a fluid. If applied pressure is plotted against the specific volume of a fluid the bulk modulus defines the slope of the curve. However, this plot is not a straight line so the slope is defined in terms of the secant bulk modulus. The secant bulk modulus is the product of the original fluid volume and the slope of the line drawn from the origin to any specified point on the plot of pressure versus specific

volume [32]. Practical salinity is defined by an electrical conductivity relationship but the difference between practical salinity and absolute salinity is small. Hence, practical salinity is compared to parts per thousand and grams per liter in this work. Using the seawater equation temperature scans can be performed for any salinity and applied pressure. Setting salinity and pressure to zero the density behaviour of pure water is obtained. Figure 1.5-3 shows the density profiles for pure water for different applied pressures. From these profiles the temperature of density maximum can be seen clearly and extracted.
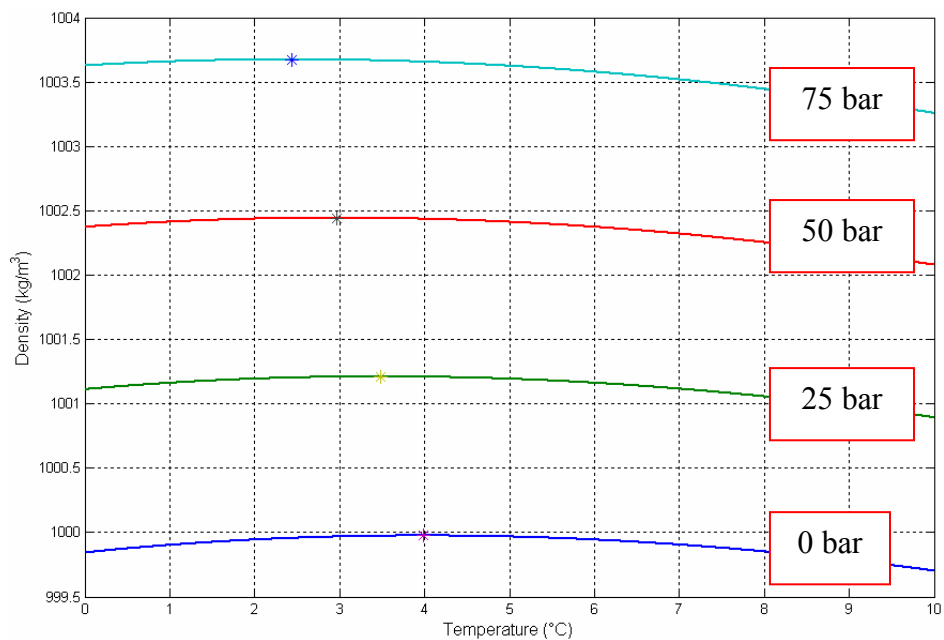


**Figure 1.5-3** *Density versus temperature profiles at various applied pressures for pure water using the seawater state equation [30]. Density maxima are denoted by '\*'.*

The temperature of maximum density for an applied pressure of 0 bar is 3.98 °C as expected. The temperature of maximum density decreases with increasing pressure at a rate of -0.02051 °C/bar for pure water. This is approximately 1 °C per 50 bar which can be seen clearly in figure 1.5-3. For saline solutions the temperature of maximum density is suppressed under pressure by more than the suppression of the temperature of maximum density of pure water. A solution with a salinity of 10 practical salinity units can be investigated under the same applied pressures as pure water (figure 1.5-4). The temperatures of maximum density at each applied pressure

14

value have all been suppressed relative to pure water due to the increased salinity value. The increased salinity also accounts for the increase in density compared to pure water at each applied pressure value. The rate of change of the temperature of maximum density with respect to pressure for this solution is -0.02101 °C/bar. This rate of change of the temperature of maximum density becomes steeper with respect to the pure water rate of change as the salinity is increased.
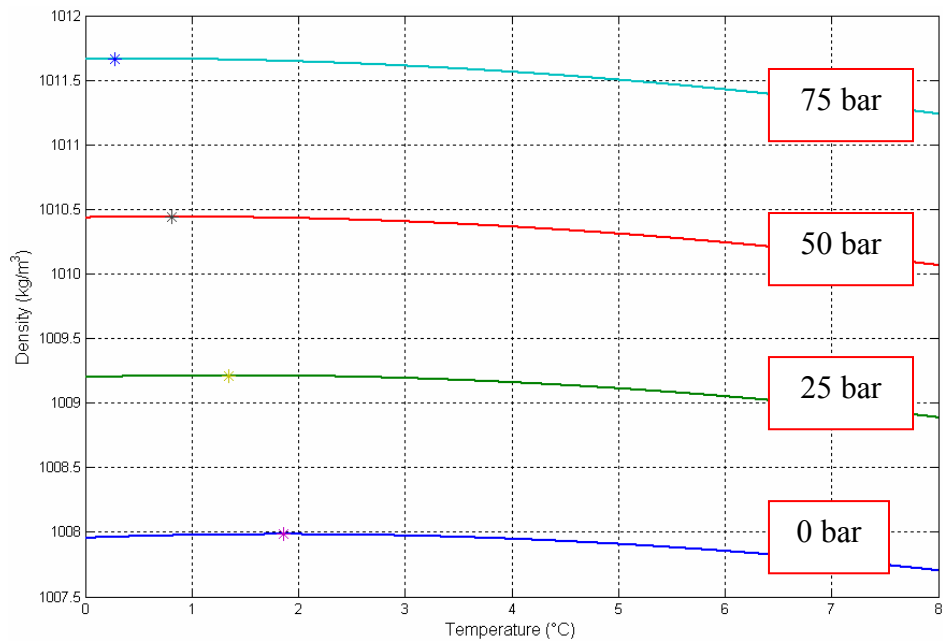


**Figure 1.5-4** *Density versus temperature profiles at various applied pressures for a 10 psu saline solution using the seawater state equation [30]. Density maxima are denoted by '*'.*

There has been a recent update on the equation of state of seawater provided by Feistel and his co-workers as described in the following papers published in 2006, 2008, 2007 and 2010 respectively [33,34,35,36]. It is proposed that this updated equation of state for seawater will be tested in future work in this area.

## 1.5.2 Adiabatic temperature gradient method

Caldwell investigated the density maximum of pure water and saline solution under pressure in 1978 [28]. Unlike contributors to the seawater equation described in section 1.5.1 Caldwell made direct measurements of the temperature of maximum density at various salinities and pressures. The seawater equation was based on

specific volume data at atmospheric and higher than atmospheric pressures. Hence, density profiles were plotted and the temperatures of maximum density extracted. In this study direct measurements of the temperature of maximum density are made so the experiments of Caldwell are of particular interest.

Caldwell used an unusual method to measure the temperature of maximum density of water as a function of salinity and pressure. He measured the adiabatic lapse rate or adiabatic temperature gradient ($\Gamma$) given by:

$$\Delta T = \Gamma \Delta p = \left( \frac{\theta V \beta}{C_p} \right) \Delta p \qquad (1.5\text{-}2)$$

$$\Gamma = \frac{\Delta T}{\Delta p} \qquad (1.5\text{-}3)$$

where $\Delta T$ is the temperature change, $\Delta p$ is the pressure change in bars, $\theta$ is the absolute temperature, $\beta$ is the thermal expansion coefficient, $V$ is the specific volume and $C_p$ is the specific heat at constant pressure. At maximum density the thermal expansion coefficient is zero, but all other quantities in the adiabatic temperature gradient are slowly varying functions of temperature, pressure and salinity. Caldwell held a water sample of known salinity at an ambient temperature and measured the adiabatic temperature gradient for various pressures. By plotting the adiabatic temperature gradient against pressure the point at which the adiabatic temperature gradient passes through zero gave the pressure of maximum density for that salinity and ambient temperature. This process was repeated for various salinities and ambient temperatures.

To measure the adiabatic temperature gradient Caldwell used a pressure vessel containing a very fine thermistor protected from pressure by canulla tubing. The pressure vessel had an inside diameter of 3.75 cm and was 30 cm high. The pressure vessel was placed in a bath which could hold its temperature constant within 0.001 °C. Pressure was applied to the vessel by an oil-filled hand pump. A vertical tube beside the pressure vessel with an oil-water interface provided separation

between the oil and the water. The pressure was accurate to 0.2 bars. In order to measure the adiabatic temperature gradient a rapid change in pressure ($\Delta p$) was made followed by a measurement of the corresponding change in temperature ($\Delta T$). The temperature change was measured by the thermistor in the pressure vessel. The temperature change sensed by this thermistor was from compressive heating of the canulla tubing, followed by compressive heating of the water and finally heat leaking to the bath causing cooling. The value of the temperature change was read 15 s after the pressure change and then the pressure was returned to its original value. Under adiabatic compression, the temperature of the water rises. The value at which the temperature peaked was noted (typically 15 s after the pressure change). The process was very fast and numerous readings of the adiabatic temperature gradient could be made in a short period of time using this method. An example of the adiabatic temperature gradient plotted against pressure from the 1978 paper is shown in figure 1.5-5.
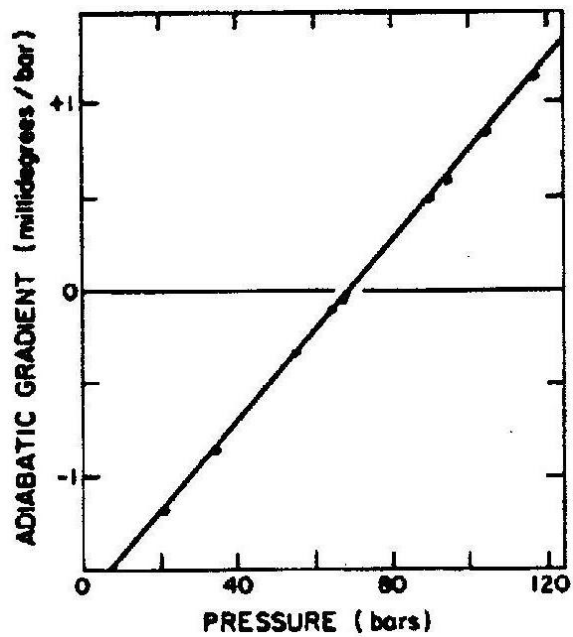


**Figure 1.5-5** *Adiabatic temperature gradient versus pressure for pure water. The ambient temperature was set to 2.52 °C throughout. The graph has been taken from Caldwell's 1978 paper [28].*

In this example, using pure water, the adiabatic gradient passes through zero at a pressure of 72 bar. At an applied pressure of 72 bar the temperature of maximum density is 2.52 °C which corresponds to a suppression of the temperature of

17

maximum density of 1.01 °C per 50 bar in very good agreement to the seawater equation result for pure water. Results from the work of Caldwell are shown in figure 1.5-6. The temperature of maximum density decreases linearly with increasing concentration for an applied pressure value. At a given concentration the temperature of maximum density shifts to lower values under increasing pressure. This is true for all concentrations tested.
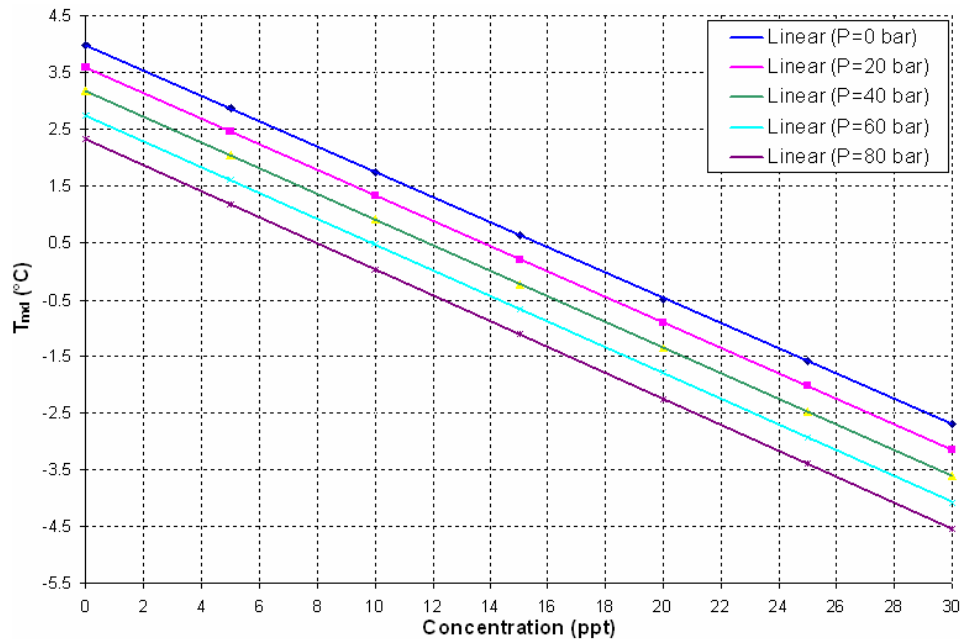


**Figure 1.5-6** *Temperature of maximum density plotted against salinity for various applied pressures. The data for all trends have been taken from [28].*

Plotting this data in a different way shows that the temperature of maximum density is suppressed linearly for all concentrations but that the rate at which it is suppressed varies (figure 1.5-7). The slopes of the trends in figure 1.5-7 become steeper relative to the pure water point as the salinity increases. This is emphasised in figure 1.5-8 as the trends have been normalised with respect to the pure water trend. From this graph it is clear that the slopes become steeper with increasing concentration. These slopes are the rates of change of the temperature of maximum density with respect to applied pressure and follow the same pattern for saline solutions as the seawater equation. For pure water Caldwell gives a rate of change of the temperature of maximum density with respect to pressure of -0.002065 °C/bar. The values of these slopes are plotted against concentration in figure 1.5-9 showing that the rate of

change of the temperature of maximum density with respect to applied pressure clearly becomes steeper with respect to the pure water point.
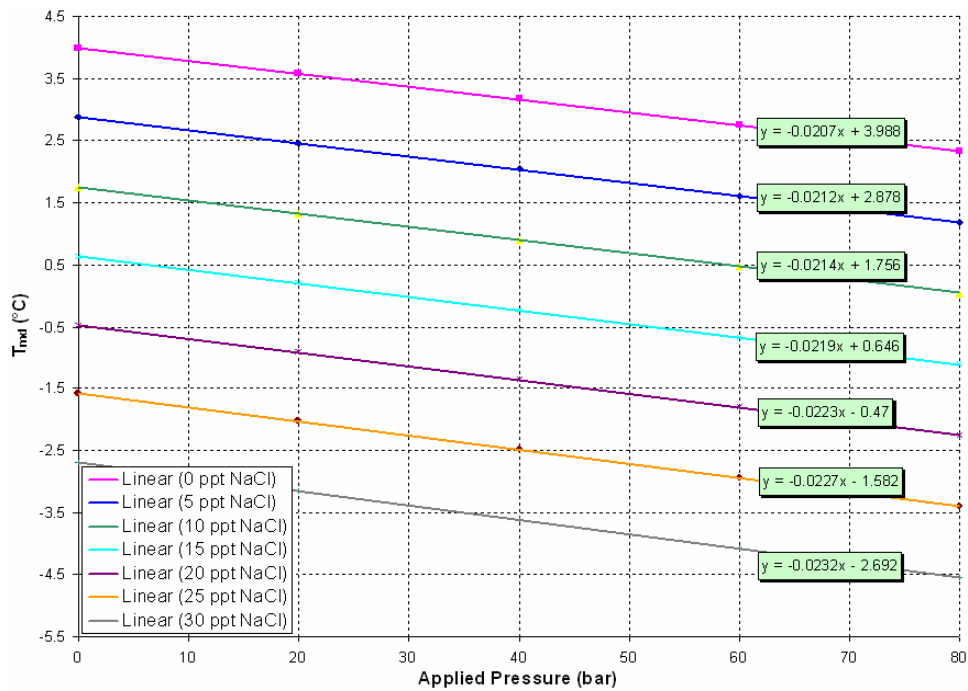


**Figure 1.5-7** *Temperature of maximum density plotted against applied pressure for various salinities. The slopes of the linear trends are shown in the green boxes. The data for all trends have been taken from [28].*
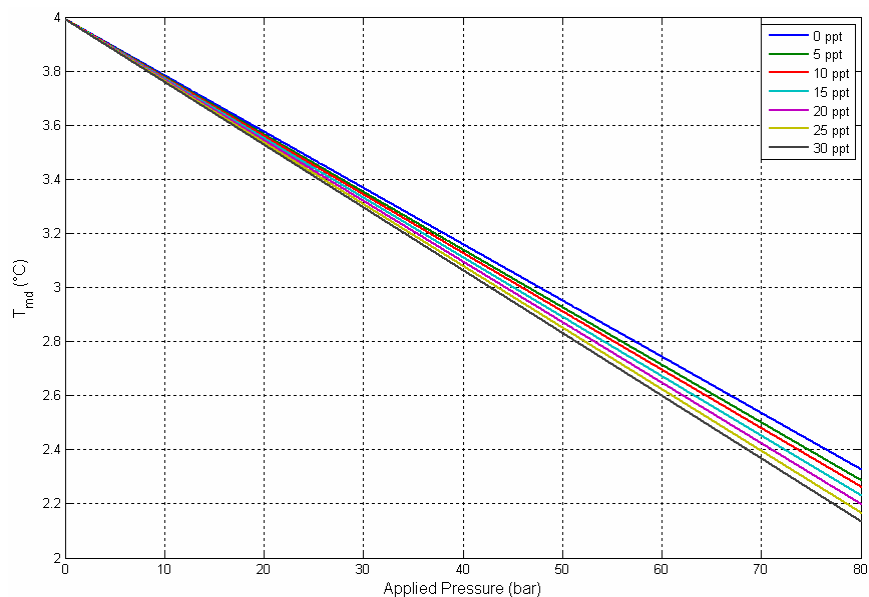


**Figure 1.5-8** *Temperature of maximum density plotted against applied pressure for various salinities. The trends from figure 1.5-7 have been normalised with respect to the pure water trend.*

19
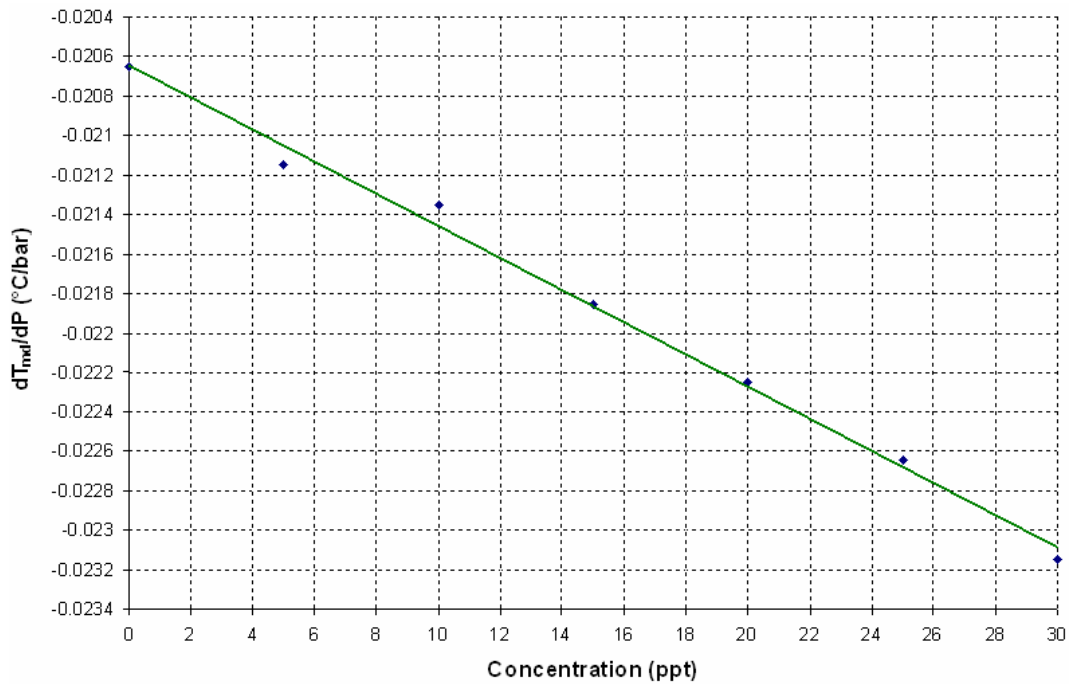
**Figure 1.5-9** *Rate of change of the temperature of maximum density with respect to pressure plotted against concentration. The rates of change have been calculated from Caldwell's results [28].*

## 1.5.3 The temperature of maximum density at negative pressures

Henderson and Speedy investigated the temperature of maximum density in water at negative pressures in 1986 [29]. In order to carry out this study they used the Berthelot method. This method involved using a capillary tube that was sealed at one end and drawn to a fine point at the other. This tube was filled with water and cooled thereby drawing air into the drawn out point. The point was then sealed with flame. Under heating the water expanded and filled the tube. Further heating caused the pressure in the tube to rise. Upon cooling the water occupied the whole volume of the tube at a temperature lower than that at which the water had first filled the tube. Consequently, the water was under negative pressure and further cooling caused the tension to rise. The tension continued to rise until cavitation occurred. Cavitation is the formation of vapour bubbles due to tension or negative pressure. In the work by Henderson and Speedy the straight tube was replaced by a helical capillary supporting a small mirror underneath. This was done as it was much more accurate in measuring pressure. As pressure inside the capillary helix changed, the helix made the mirror rotate slightly. This is an example of a Bourdon tube.

Temperature was measured by a platinum resistance thermometer to an accuracy of 0.1 °C. Using this arrangement, Henderson and Speedy measured temperatures of maximum density over a wide range of negative pressures. For pure water as the pressure becomes more negative the temperature of maximum density increases. At a pressure of -100 bar the temperature of maximum density is 6 °C as opposed to 3.98 °C at atmospheric pressure. Under tension the rate of change of the temperature of maximum density with respect to pressure is -0.017 °C/bar for pure water, i.e. less negative than the slopes for pure water subjected to positive pressure (compression).

## 1.6 Aims of current work

The aim of this work was to extend the investigation of the density maximum of aqueous solutions as a function of pressure and concentration. The only work that has been carried out to date involves pure water and saline solutions. In this study ionic salts (including NaCl), monohydric alcohols, sugars and acetone were investigated. The rate of change of the temperature of maximum density with respect to applied pressure was calculated for differing concentrations of these solutes. This analysis was carried out on all solutes studied over an applied pressure range of 0 to 100 bar and over various concentration ranges.

The technique used directly measures the temperature of maximum density by monitoring the convective flow in the liquid under test using an array of five thermistors within the test chamber. The pressure chamber containing the sample under test was rectangular in shape with inner dimensions of 120×60×60 mm. Pressure was applied to the sample with a hydraulic system and a flexible rubber diaphragm oil-water interface provided separation between the oil and the sample. The technique was readily automated.

## 1.7 Thesis chapter outline

This section is a summary of the content and topics covered in each of the chapters of the thesis.

*Chapter 2* provides a detailed description of the experimental system including the heat exchange and pressure systems. A detailed description of the pressure chamber designed and constructed for these studies is given in this chapter. The thermometry used is also described in detail.

*Chapter 3* describes the procedures involved in determining the temperature of maximum density from experimental results. Experimental results from all investigations are presented in this chapter as well as a description of each solute tested.

*Chapter 4* outlines an approach that attempts to simulate experimental results on a macroscopic level by analysing "ideal" mixtures.

*Chapter 5* describes a microscopic model which was used to attempt to simulate experimental results. Various approaches were taken in microscopic modelling all of which are described in this chapter.

*Chapter 6* outlines overall conclusions about the work carried out as part of this thesis. All significant results pertaining to the behaviour of the temperature of maximum density under pressure are discussed. Possible future work is also discussed in this chapter.

## 1.7.1 Author's direct contribution in this thesis

The work involved in this thesis has been possible thanks to contributions of fellow researchers working in the fluid dynamics group at the National University of Ireland Maynooth over the past decade. This section lists the author's direct contribution to the work described in this thesis for each chapter:

*Chapter 2*
- Converted the dual refrigerator apparatus to a single fridge/freezer system.

- Installed new pumps, relays and plumbing for the heat exchange system.

- Replaced previous control and data acquisition software (Linux-based) with new software written in C.

- Improved the quasi-steady state system.

- Designed and installed a pressure vessel and computer controlled hydraulic system.

*Chapter 3*

- Observed and analysed the behaviour of water and aqueous solutions as a function of pressure. Solutes studied included monohydric alcohols, ionic salts, sugars and ketones.

- Analysed the expected behaviour of the temperature of maximum density of pure water and saline solutions as a function of pressure using the Comsol Multiphysics package.

- Developed and tested a pressure scanning technique.

- Analysed heat transfer in the vicinity of the density maximum using an indirect method.

- Developed and tested an area integration technique to extract the temperature of maximum density values from experimental results.

- Analysed results in terms of the rate of change of the temperature of maximum density with respect to applied pressure as a function of solute concentration.

- Developed error analysis that was applied to all experimental results.

*Chapter 4*

- Developed a model to investigate the behaviour of the temperature of maximum density of "ideal" mixtures of pure water and ethanol and "ideal" mixture of pure water and acetone as a function of pressure and concentration.

- Developed a model to investigate the behaviour of the temperature of the phase change of "ideal" mixtures of pure water and ethanol and

"ideal" mixture of pure water and acetone as a function of pressure and concentration.

*Chapter 5*

- Developed a microscopic model to study the temperature of maximum density of water. The model was a modified two-dimensional gas-lattice approach used by Buzano et al. [67].

- Implemented the model using Monte Carlo simulations realised using Metropolis importance sampling and the Wang-Landau method.

- Tested simulations on Ising and Potts models.

- Modified the model to simulate experimental results using various methods.

# Chapter 2

# Experimental Apparatus and Procedures

## 2.1 Introduction

This chapter describes all elements of the experimental system and the procedures involved in obtaining results. The experimental system is capable of holding temperature gradients, holding applied pressures in a solution under test and monitor temperatures at points in the solution and the system. Temperatures of coolant in chambers either side of a test chamber are held at desired values through the use of computer-controlled pumps allowing a temperature gradient to be set held across the test region. Pressure is applied to the fluid in the test chamber by a hydraulic system consisting of a computer-controlled stepper motor turning gears which in turn controls a ram. The movement of this ram applies pressure to the fluid. Thermistors are strategically placed in the test chamber to monitor temperatures within the fluid and thermistors are also located in the walls of the chamber to monitor side wall temperatures. Readings from the thermistors are converted to temperature values using a data acquisition card and computer software.

## 2.2 Heat exchange system

A horizontal gradient is set up across a rectangular test chamber containing the solutions under test. The system is set up as shown schematically in figure 2.2-1 and pictorially in 2.2-2. The temperature gradient is set up via two isothermal, chambers either side of the test region. The side chambers ($T_L$ and $T_R$) are completely interchangeable. During testing experimental runs were carried out twice, the second time with $T_L$ and $T_R$ interchanged. It was found that interchanging the side chambers did not affect results. The temperatures of the coolant in the side chambers are computer controlled. If a side chamber is hotter than the desired temperature a signal will be sent by the computer to pulse the cold pump for the side chamber in question. If a side chamber is colder than the desired temperature a signal will be sent by the computer to pulse the required hot circuit pump.

The cooling coils are located in the freezer which is maintained at approximately -30 °C. These coils are made of copper and are located in a bath of pure ethylene glycol to avoid freezing. The coils act as heat exchangers containing coolant at very

low temperatures. Pure ethylene glycol is used as the coolant in cooling circuits. When a cold pump is pulsed pure ethylene glycol in the cooling circuit is pumped up to the expansion chamber and cooled ethylene glycol from within the coils in the freezer is pumped down to the relevant side chamber. Expansions chambers have been incorporated into the system to eliminate air bubbles that may enter any of the plumbing circuits. The heating coils are located in an outside reservoir containing water which is kept at room temperature of about 20 °C. A fifty-fifty mixture of ethylene glycol and water is used as the coolant in heating circuits. When a hot pump is pulsed coolant in the heating circuit is pumped to the expansion chamber and room temperature coolant from within the coils in the outside reservoir is pumped to the relevant side chamber. Hence by activating pumps the temperature of the coolant in the side chambers is altered accordingly.
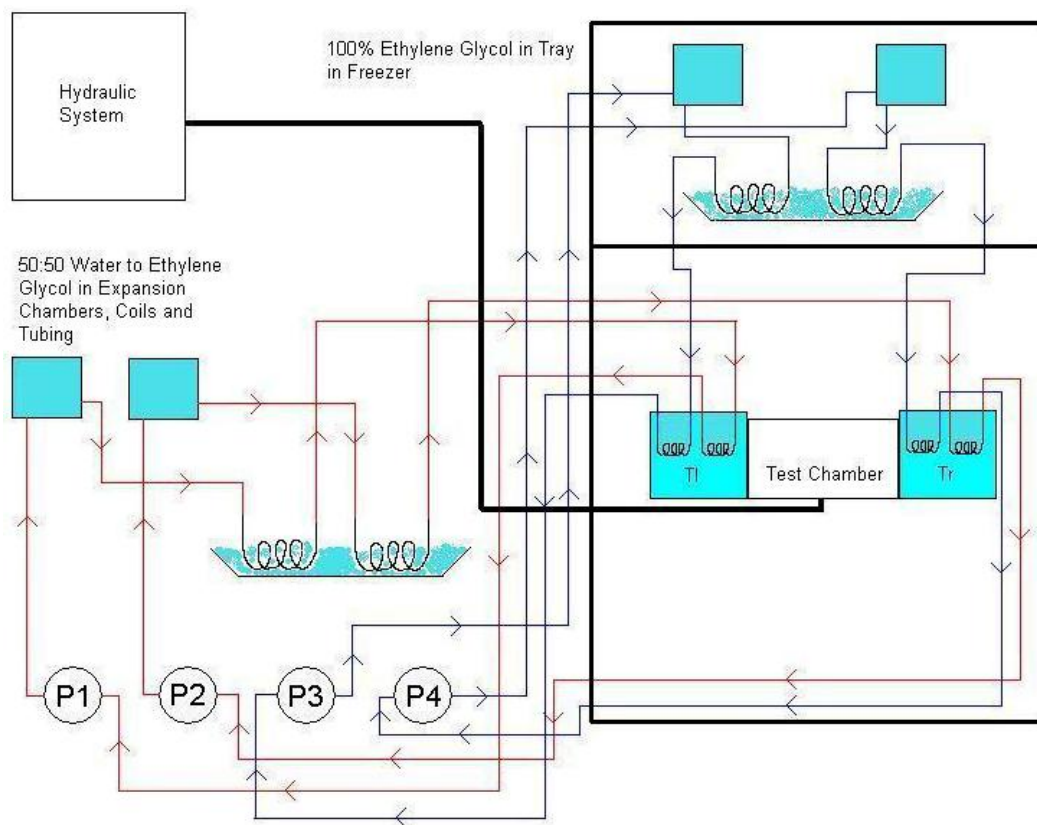


**Figure 2.2-1** *Schematic overview of experimental system.*
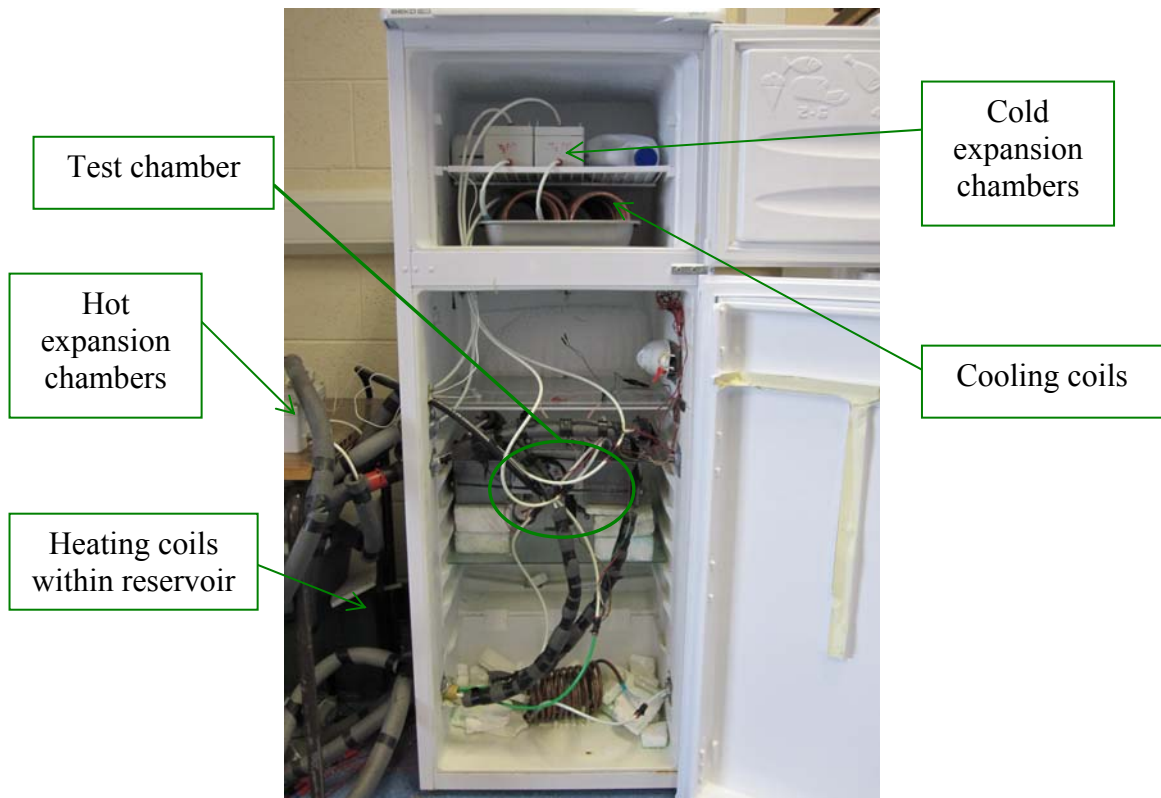
**Figure 2.2-2** *Pictorial overview of experimental system.*

The fridge ambient temperature needs to be controlled as the test and side chambers are within the fridge and hence the fridge ambient affects the temperature of the fluids within these chambers. In order to control the ambient temperature the thermostat was removed and the fridge was placed on a solid-state relay. In software the solid-state relay is switched on and off and hence the fridge compressor depending on the reading from an ambient thermistor. Generally before an experimental run ambient fridge temperature is held at 6 °C as the side chambers usually need to be near to 6 °C at the start of a run. Throughout a run the fridge ambient is set to the average of the desired temperatures of the side chambers. At lower temperatures nearing 0 °C the fridge struggles to maintain the temperature of the average of the side temperatures but this does not affect the side rails maintaining their desired temperatures. In addition to holding the fridge ambient temperature the side chambers are insulated very well with expanded polystyrene. This insulation helps to maintain temperatures within the side chambers since the insulation prevents heat being lost from the chambers to surroundings.

## 2.3 Pressure system

A computer-controlled pressure system was designed to apply pressure to the aqueous solution under test. The hydraulics in use consists of an eight tonne bottle jack and a hydraulic cylinder. Section 2.3.1 illustrates how the hydraulic system is set up. The hydraulic system is controlled through the combination of a computer-controlled stepper motor and a gearing system as described in section 2.3.2.

### 2.3.1 Hydraulic system

The hydraulic system is set up as shown schematically in figure 2.3-1 and pictorially in 2.3-3. An eight tonne bottle jack is anchored to a solid steel bottom plate. On top of this is an inverted hydraulic cylinder, which is bolted to a solid steel top plate. The top and bottom plates to which the ram and bottle jack are bolted are held together with bolts and four thick lengths of threaded bar in such a way that the ram of the bottle jack pushes directly onto the ram of the hydraulic cylinder.
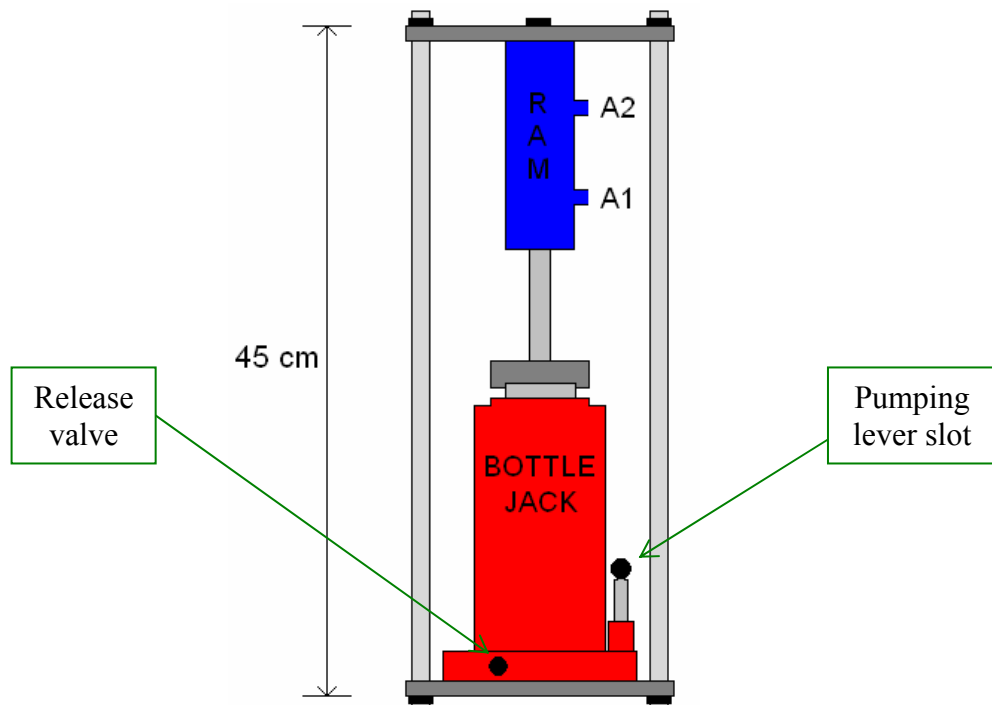


**Figure 2.3-1** *Schematic overview of hydraulic system.*

Before an experimental run the release valve is fully closed, the ram of the cylinder is fully extended and the bottle jack is fully relaxed. When pressure is applied to the test solution the bottle jack is pumped by lifting the lever up and down. This motion of the pumping lever is computer controlled as discussed in section 2.3.2. The ports of the hydraulic cylinder (A1 and A2) are connected to an oil reservoir and the test chamber via two crimped hoses which are pressure rated to 400 bar. The hydraulic cylinder used has a carbon steel body with NBR (Nitrile)/Polyurethane seals. The cylinder is rated to 240 bar static proof pressure and 160 bar working pressure. The hydraulic fluid operating range is from -20 °C to +80 °C.
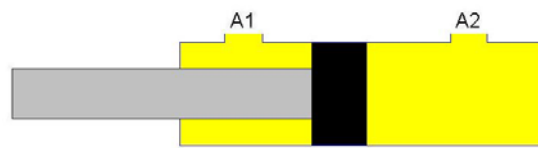


**Figure 2.3-2** *Schematic of hydraulic cylinder.*

As the bottle jack is pumped the ram of the cylinder is forced in and oil is forced out a pressure rated crimped hose connected to port A2 (figure 2.3-2). Oil is simultaneously drawn from a reservoir through a pressure rated crimped hose connected to the A1 port. When the release valve on the bottle jack is activated the ram relaxes and retracts allowing oil to return to the reservoir through A1. The crimped hose leading from A2 is connected to a fitting bolted to the pressure port on the test chamber (section 2.4). The hydraulic system with attached crimped hoses is shown in figure 2.3-3.
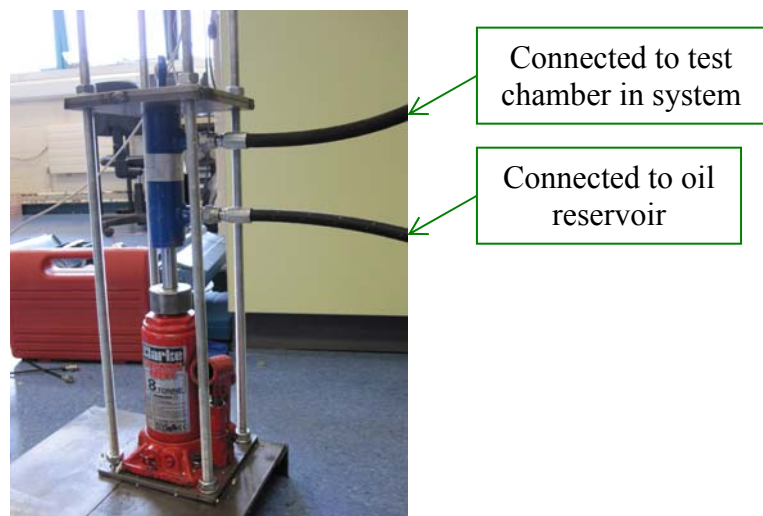


**Figure 2.3-3** *Pictorial overview of hydraulic system.*

## 2.3.2 Motion control of pressure

In order to automate the pumping of the bottle jack a stepper motor in conjunction with a 70:1 worm gear and an 8.3:1 toothed belt gear is used. This combination gives a gear ratio of 581:1 (figure 2.3-4). A high gearing ratio is used for two reasons. Firstly, high torque is needed to pump the bottle jack and apply pressure to the fluid under test. Secondly, the movement of the pumping lever must be kept at a very slow rate as a small movement in the lever and hence the bottle jack will give rise to a large increase in the pressure of the fluid. If a lower gear ratio was employed the required pressure could be easily overshot. As the stepper motor rotates the worm rotates which in turns moves the toothed belt gear. The circular motion of the gear is converted to vertical linear motion to pump the bottle jack. A steel lever with a milled slot was manufactured and placed in the bottle jack pumping lever slot. A bolt was attached to the circular gear perpendicular to motion of the gear. This bolt is placed in the slot of the steel lever so as the gear rotates the lever moves up and down (figure 2.3-5). The stepper motor in use is a Slo-Syn HS50L.
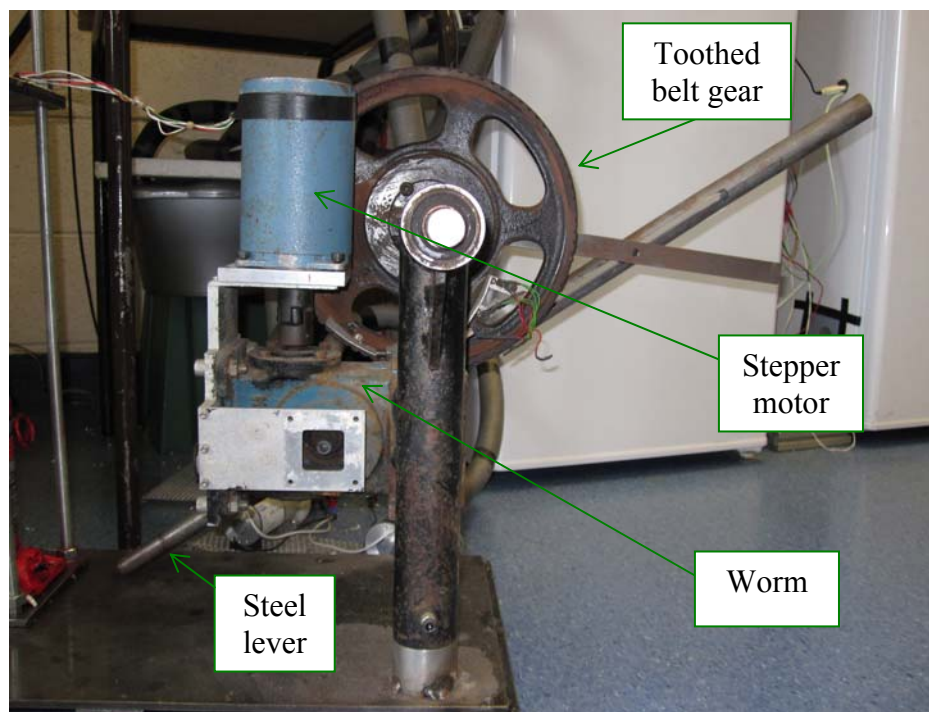


**Figure 2.3-4** *Stepper motor, worm gear (70:1) and toothed belt gear (8.3:1).*
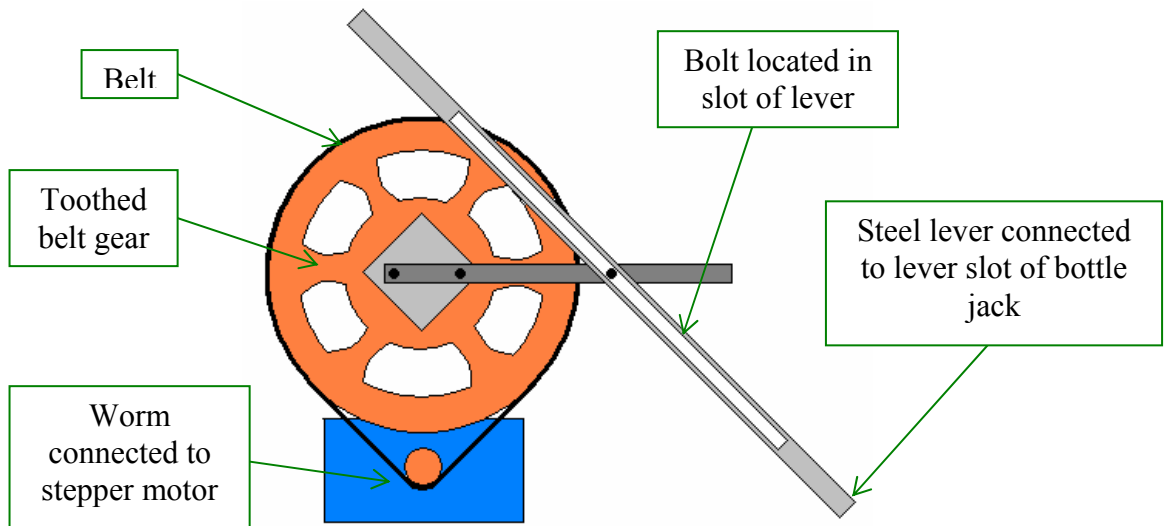
**Figure 2.3-5** *Schematic diagram of gearing system. As the stepper motor rotates the output of the worm rotates turning the larger circular gear which moves the steel lever (connected to bottle jack) up and down.*


### Specifications of Slo-Syn HS50L stepper motor


- Motor type: Permanent magnet stepping motor.
- Windings: 4 bifilar wound electromagnetic coils (two excitation coils wound in opposite directions on the same statorpole).
- Step size: 1.8° fullstep, 0.9° half-step, in half step mode two coils are energised concurrently for 50% of the switching cycle.
- Holding torque: 0.85 Nm, output torque from motor at rest with two windings energised at rated current.
- Power rating/coil: 15.75 W (4.5 V @ 3.5 A max).

To maximise the holding torque the stepper motor is run in full step mode. The holding torque needs to be maximised as a large force on the lever is required to achieve high pressures.

The gearing system with computer-controlled stepper motor is coupled to the hydraulic system as shown in figure 2.3-6.

**Figure 2.3-6** *Pictorial overview of hydraulic system coupled to a computer-controlled gearing system with a steel lever.*

## 2.3.2.1 Control electronics for stepper motor

The stepper motor is controlled in software through the use of a stepper motor controller and four high voltage, high current transistors. The stepper motor has six leads two of which go to ground. By grounding these two leads four coils are effectively created from the two excitation coils. With a control circuit by activating a transistor one of the four coils is energised. The circuit is set up as shown in figure 2.3-7 where Q1 to Q4 are the transistors.

**Specifications of Stmicroelectronics TIP33C transistor**

- Transistor type: Power General Purpose.
- Voltage, $V_{ceo}$: 100 V.
- Current, $I_c$ continuous at max: 10 A.
- Transistor polarity: NPN.
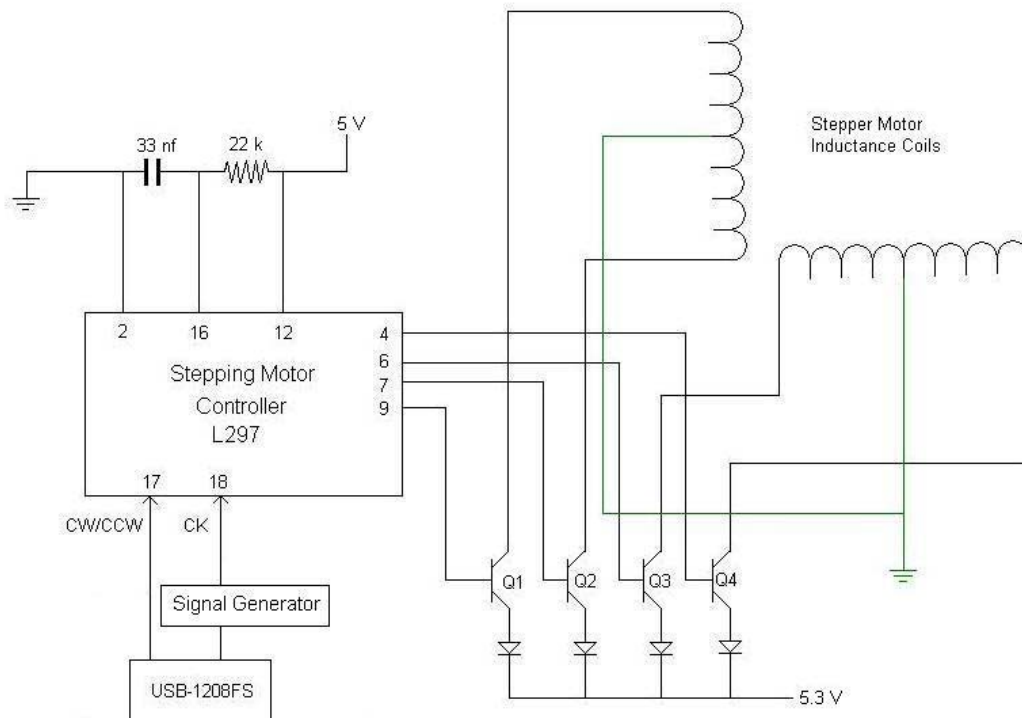
**Figure 2.3-7** *Control circuit for stepper motor.*

Each transistor can supply up to 10 A in each output channel, which can easily drive the stepper motor in use. The controller IC used is the L297 which is capable of generating four phase drive signals and switching sequences for four phase bifilar wound stepping motors. When a pulse is received from the signal generator the controller generates the sequence necessary to rotate the motor through one step in the direction desired (clockwise or anti-clockwise) by setting pin 17 to either high or low. The sequence generated by the controller activates transistors which in turn energise coils in the order required to rotate the stepper motor.

The signal generator is on a solid state relay which is controlled in software via a USB based analogue and digital I/O module. This device also controls the direction of the stepper motor by setting pin 17 to high or low. The signal generator sends a string of digital pulses to the controller. The higher the frequency of the pulses from the signal generator the faster the stepper motor moves. The stepper motor has a maximum speed of 165 motor steps per second with one full revolution taking 200 steps in full step mode. However, holding torque rather than speed is required for holding pressures so the signal generator was set to 80 Hz. Also, at this speed the

pulse rate did not need to be ramped up to 80 Hz. The stepper motor runs smoothly when the controller receives an 80 Hz signal from rest.

## 2.4 Pressure chamber

In order to examine the effect of pressure on the density maximum of water and aqueous solutions a test chamber was required to withstand pressures up to at least 100 bar. In previous work by Cawley et al. [37] perspex chambers of rectangular shape were used but these chambers are not suitable for pressure work. The inner dimensions of the pressure chamber are the same as the inner dimensions of the perspex chambers used by Cawley et al. This was done for comparative purposes. The chamber was designed using the Comsol Multiphysics package [38]. Various designs were tested in this environment with different chamber wall thickness. A chamber was needed that could withstand high pressure but could also maintain a horizontal temperature gradient. The rates of heat flow across possible designs were monitored and experimental runs were simulated on these designs using Comsol Multiphyics. The final design was rectangular aluminium chamber with side walls of thickness 14 mm was constructed. A Comsol representation of the chosen design is shown in figure 2.4-1.

## 2.4.1 The governing equations

In all Comsol Multiphysics studies in this work the same set of governing equations are used to model the behaviour of the fluid under test. These equations are the Navier-Stokes equations and the heat equation. The Navier-Stokes and heat equation are coupled by the temperature dependent density state equation. This coupling is done in the body force term of the momentum equation. Generally the behaviour of fluids computationally is described in terms of conservation of energy, mass and momentum. The Navier-Stokes in this study refers to the conservation of mass and momentum. The conservation of energy is described by the heat equation. The four governing equations are 2.4-1 to 2.4-4.

$$\rho \frac{\partial \vec{v}}{\partial t} + \rho(\vec{v}.\nabla)\vec{v} = -\nabla p + \rho(T)\vec{g} + \mu \nabla^2 \vec{v} \qquad (2.4\text{-}1)$$

$$\nabla.\vec{v} = 0 \qquad (2.4\text{-}2)$$

$$\frac{\partial T}{\partial t} + \vec{v}.\nabla T = \alpha \nabla^2 T \qquad (2.4\text{-}3)$$

where $\rho$ is the density of liquid (kg.m$^{-3}$), $\vec{v}$ is the velocity (m.s$^{-1}$), $T$ is the temperature (K), $t$ is time (s), $p$ is the pressure (Pa), $\mu$ is the viscosity (Pa.s), $\alpha$ is the thermal diffusivity (m$^2$.s$^{-1}$) and $\vec{g}$ is gravity (ms$^{-2}$). Thermal conductivity, specific heat capacity, viscosity and density are obtained from reference [5]. The viscosity and the thermal diffusivity are assumed to be constant and assigned their appropriate values for pure water at 4 °C as given in [6]:

$$\mu = 1.567 \times 10^{-3} \text{ kg m}^{-1} \text{ s}^{-1}$$
$$\alpha = 1.344 \times 10^{-7} \text{ m}^2 \text{s}^{-1}$$
$$g = 9.81 \text{ m s}^{-2}$$

The temperature dependence of the density is only considered in the buoyancy term of the Navier-Stokes equation. This assumption is known as the Boussinesq approximation. This temperature pressure and salinity dependence is described by the equation of state for seawater [30] (section 1.5.1):

$$\rho(T) = \rho(S,T,P) \qquad (2.4\text{-}4)$$

where $P$ is the pressure (decibar) and $S$ is the salinity (psu). These equations are solved in 2D and 3D Comsol simulations. The four governing equations must be solved by discretisation, which involves choosing a finite number of points to represent the fluid flow. These points are known as grid or mesh points. By this discretisation method Comsol Multiphysics is used to find solutions to the governing equations.

## 2.4.2 Final pressure chamber design
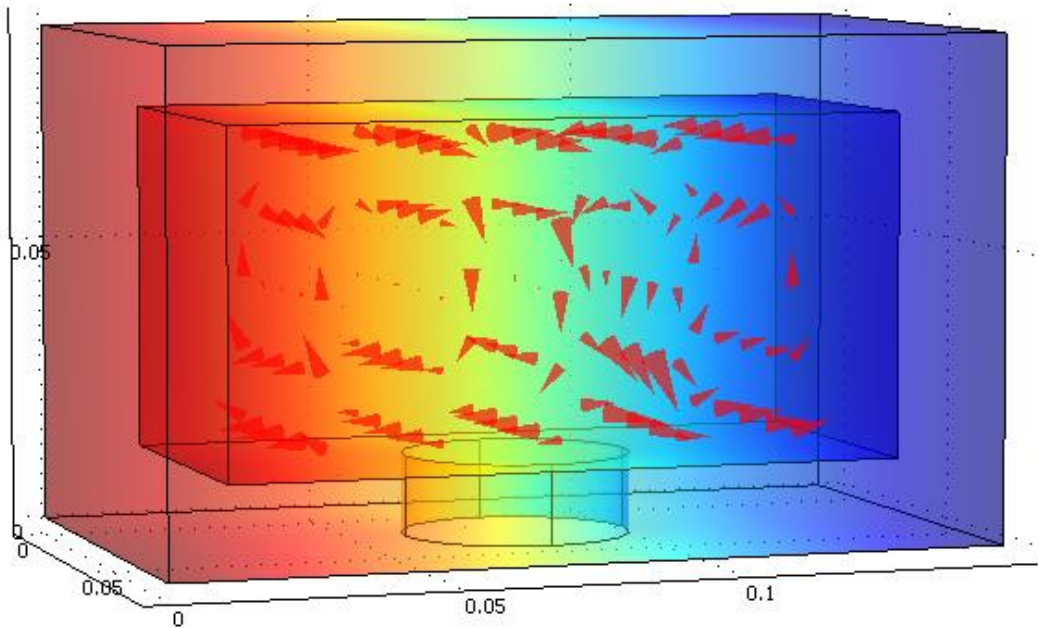


**Figure 2.4-1** *Comsol Multiphysics representation of pressure chamber.*

The main body of the chamber was constructed from a solid piece of aluminium of dimensions 148×88×74 mm into which was milled a hollow of size 120×60×60 mm. Around the top of this was drilled and tapped twenty-two M6 holes for bolts. On the front side was drilled a 40 mm diameter pressure port with eight M6 threaded holes surrounding the port. On the bottom of the chamber two G1/4 holes were bored and tapped, one for the pressure transducers and the other for a ball valve in order to allow easy emptying of the chamber. A lid was constructed of dimensions 148×88×14 mm and twenty-two rebated holes were bored into it to line up with the tapped holes in the main body of the chamber. Two G1/4 sized tapped holes were made in the lid for a filling ball valve and a thermistor feed through system. A circular piece was constructed to bolt onto the pressure port via M6 bolts as with the lid. The pressure chamber without lid or front or circular pressure connection is shown in figure 2.4-2.

Leakage of fluid is a major problem at high pressures; this problem was tackled in a number of ways with the aluminium chamber. Firstly the chamber itself is made of 14mm thick aluminium and hence will not be compromised at pressures within the

desired range. Secondly, all fitting are rated far above pressures of 100 bar and all were sealed to the chamber using a high-pressure thread adhesive. A gasket was constructed from reinforced rubber sheeting and was placed between the chamber and the lid. A groove was milled around the top edge of the main chamber in order to pinch the gasket when the lid was firmly bolted on. This was done to avoid leakage of the fluid under test from the chamber around the lid. A circular diaphragm made from Viton rubber was placed over the pressure port opening and over this was bolted on the specially constructed circular piece of aluminium. Again there was a groove added to the circular piece to create a better seal between the diaphragm and the chamber.
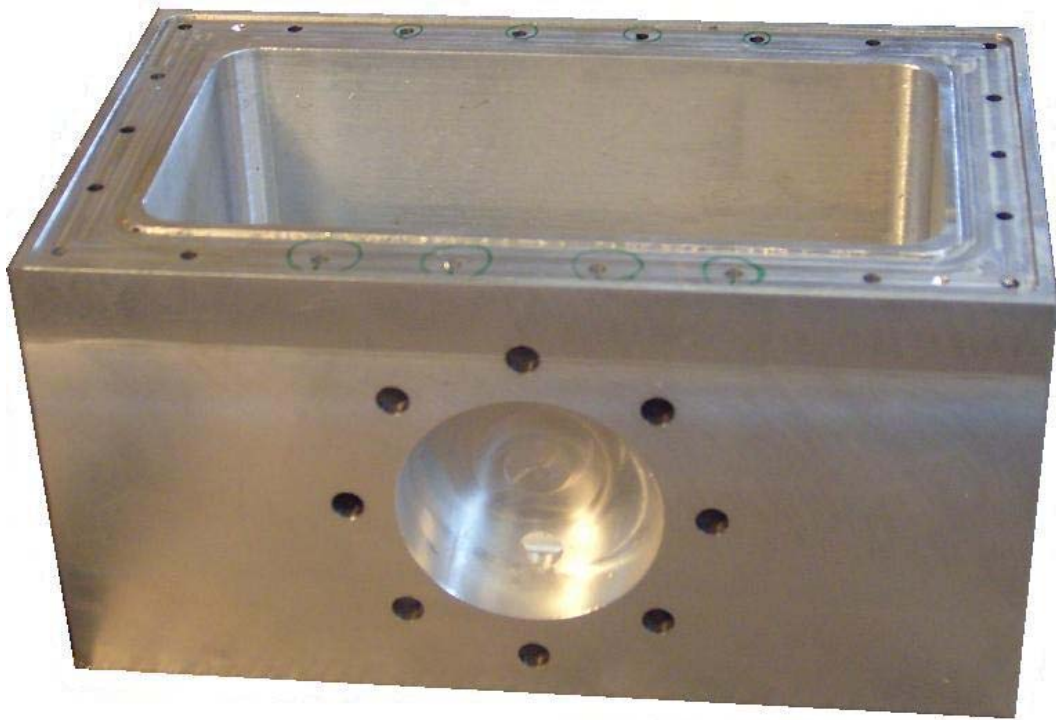


**Figure 2.4-2** *Pressure chamber made from aluminium with front port for pressure connection.*

The circular piece of aluminium bolted to the pressure port pinches a diaphragm between it and the chamber. This connection has a drilled and tapped hole through its centre and a male to male connection for a crimped hose has been screwed into this hole using a high-pressure thread adhesive. To the exposed end of this male to male connection the crimped hose leading from the hydraulic ram is tightly screwed.

When the computer-controlled hydraulic system activates, oil is pumped through this crimped hose through the hole in the circular aluminium connection and against the diaphragm. The diaphragm deforms applying pressure to the fluid in the chamber. Since water is incompressible a very small deformation of the diaphragm increases the pressure by a great amount. Filling of the chamber was done very carefully to avoid air bubbles in the chamber as air bubbles would require the diaphragm to deform by a greater amount to apply pressure to the fluid. If air existed within the chamber the diaphragm could become compromised under high pressure. The chamber can be seen in the system in figure 2.4-3 with the crimped hose from the hydraulic ram attached.
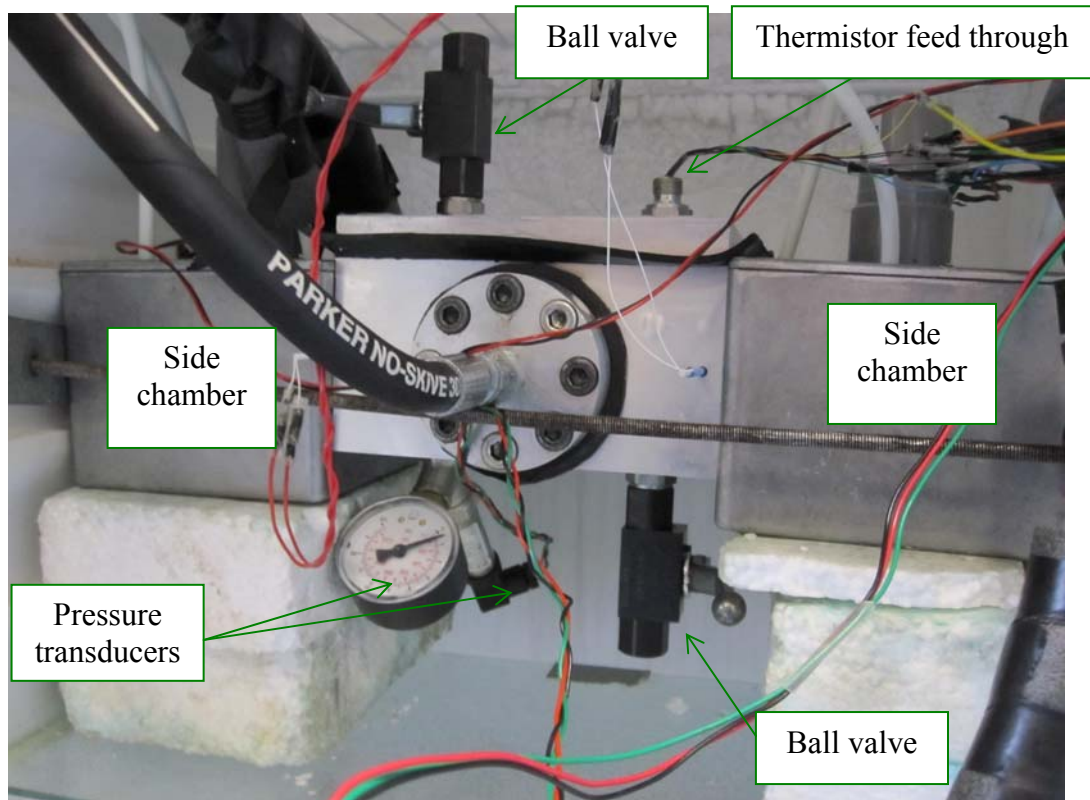


**Figure 2.4-3** *Chamber in system with crimped hose from hydraulic ram attached.*

## 2.5 Thermometry

Thermistors are used to monitor temperatures in the system. The temperature dependant resistors or themistors are chosen as they could be easily incorporated into the software. 5K3A373I Betathem thermistors are used (figure 2.5-1). These are small epoxy coated devices with solid tin plated lead wires. These devices have a

resistance of 5 kΩ at 25 °C and are capable of operating as low as –80 °C and as high as 150 °C. The response time of these temperature-sensing devices is 1 s in typical liquids making them very suitable for temperature sensing in aqueous solutions. The thermistors in use have a negative temperature coefficient (NTC) meaning that the resistance varies inversely with the temperature.



| | Dimensions | | |
|---|---|---|---|
| | A | B | C |
| | 10 ± 2mm | 200 ± 10mm | 2.4mm Maximum |
| Note 1 | 30AWG Solid Silver Plated Copper with White Kynar Insulation | | |
| Note 2 | Black Stycast Epoxy | | |
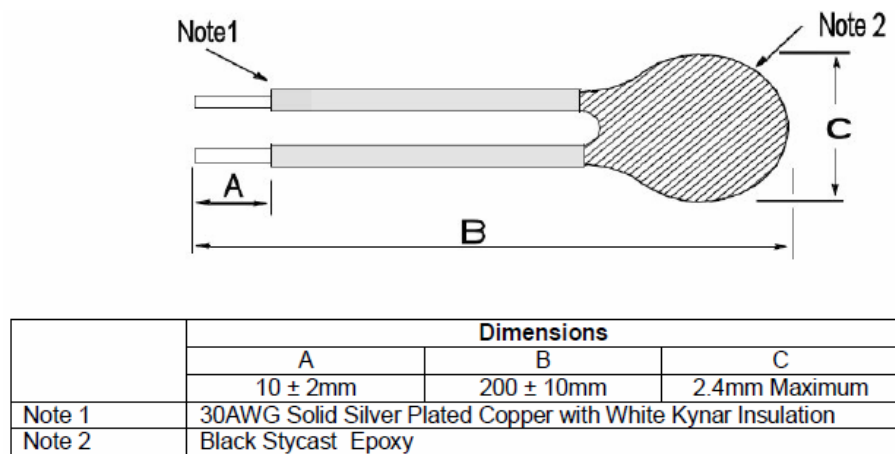
**Figure 2.5-1** *Diagram of a Betatherm thermistor.*

These thermistors are carefully incorporated into the system. Thermistors located in side walls of the chamber are uncoated but all other thermistors require a coating to protect them from fluids they are in contact with. The five sensing thermistors (section 3.1) within the pressure chamber need to be insulated from the fluid under test. The electrical connections at A (figure 2.5-1) are wrapped with insulation tape. The thermistor head and the insulated leads are placed in heatshrink and placed under a heat gun until all air is removed. The open ends of the heatshrink at A and C (figure 2.5-1) are sealed with cyanoacrylate (superglue). Thus, the electrical connections are insulated from each other and the thermistor including the connections is insulated from the fluid. The coated thermistors are affixed to threaded nylon bars attached to exact locations on the interior of the chamber lid to prevent misalignment of thermistors within the chamber.

A temperature-to-voltage circuit consisting of a voltage regulator, a non-inverting amplifier, a voltage follower and a 25 kΩ resistor supplies a constant current of 200 µA to each thermistor (figure 2.5-2). The purpose of the voltage regulator is to maintain a constant output voltage (+5 V) even though the input or load current may

vary.  A 25 kΩ resistor is used to limit the current flow from the regulator to the
thermistor and the non-inverting amplifier provides a positive voltage gain, which
amplifies the voltage from the thermistor by two.  As numerous thermistors are in
use in the experiments that are being carried out many of these circuits were
constructed.  An electronic circuit board was used incorporating eight of these
temperature-to-voltage conversion circuits (figure 2.5-3).  The outputs of each circuit
are sent to a USB data acquisition device and the voltages are recorded and
converted into temperatures via C coding using LabWindows.
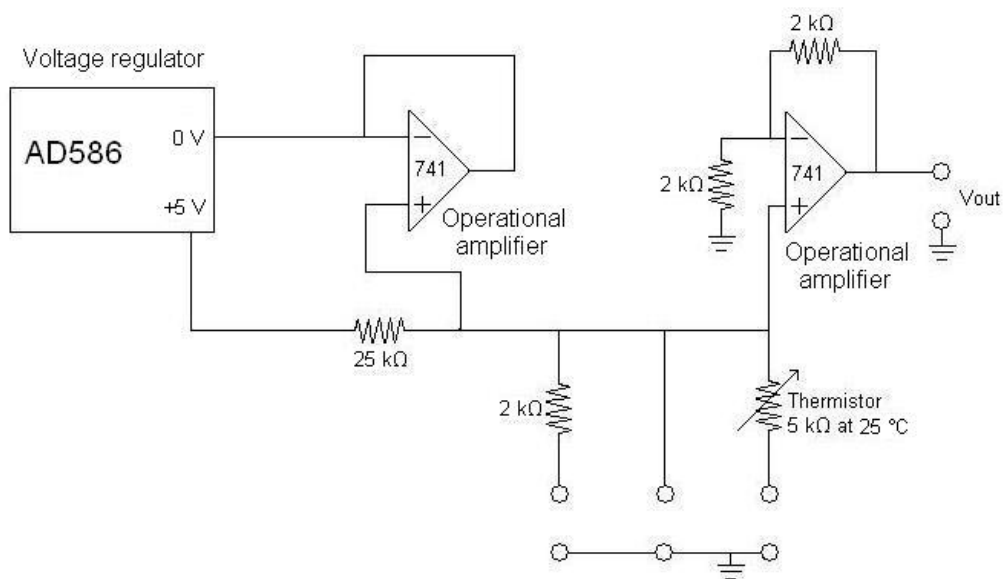


**Figure 2.5-2** *Temperature-to-voltage conversion circuit.*
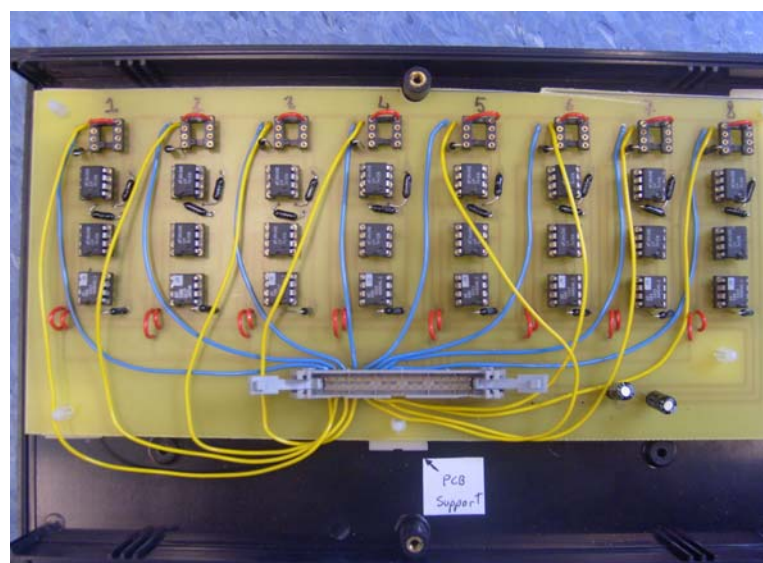


**Figure 2.5-3** *House of eight temperature-to-voltage conversion circuits.*

Once the thermistors are installed in the experimental system they need to be calibrated. The devices are calibrated using a mercury thermometer, which is accurate to 0.1 °C and traceable to the National Institute of Standards and Technology, USA. In order to carry out the calibration all thermistors from the system and the calibrated thermometer are placed in a beaker of ethylene glycol coolant containing a magnetic stirrer to ensure a uniform temperature throughout the liquid. Using a calibration program the ADC number of each thermistor is taken and recorded at various temperatures in the range -2 to 20 °C. This range was chosen for the calibration as most of the experiments were carried out within in this range. The LabWindows graphical user interface for the calibration program is shown in figure 2.5-4.
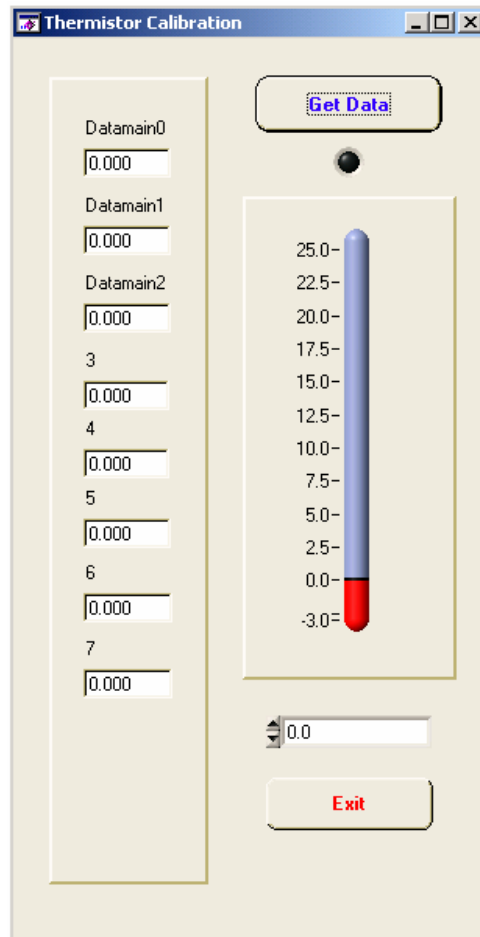


**Figure 2.5-4** *Graphical user interface for calibration program.*

The temperatures corresponding to the ADC values are taken and recorded from the calibrated mercury thermometer. The resistance of a thermistor is directly

proportional to the ADC number or the voltage across it and the resistance of the thermistor is given by the following equation:

$$R = A \exp\left(\frac{E_g}{2k_B T}\right)$$ (2.5-1)

where $R$ is the resistance of the material, $A$ is a constant depending on the physical composition of the semiconductor, $E_g$ is the band gap, $k_B$ is the Boltzmann constant and $T$ is the absolute temperature. Taking the log of both sides of this equation:

$$\ln(R) = \ln(A) + \left(\frac{E_g}{2k_B T}\right)$$ (2.5-2)

By plotting $\ln(R)$ against $1/T$ a straight-line results with a slope of $E_g / 2k_B$ and intercept $\ln(A)$. Since $R$ is directly proportional to the ADC number a straight line also results from a plot of $\ln(ADC\ number)$ against $1/T$. Thus by plotting $1/T$ on the x-axis and $\ln(ADC\ number)$ on the y-axis (figure 2.5-5) and getting the slope and intercept of the best fit trend line the temperature experienced by the thermometer is given by:

$$T = \frac{slope}{\ln(ADC\ number) - intercept}$$ (2.5-3)

This procedure is carried out for each thermistor with all thermistors having unique slope and intercept values. By inputting these values into data acquisition and control software the ADC numbers read from the thermistors are converted to temperatures to an accuracy of 0.1 °C.
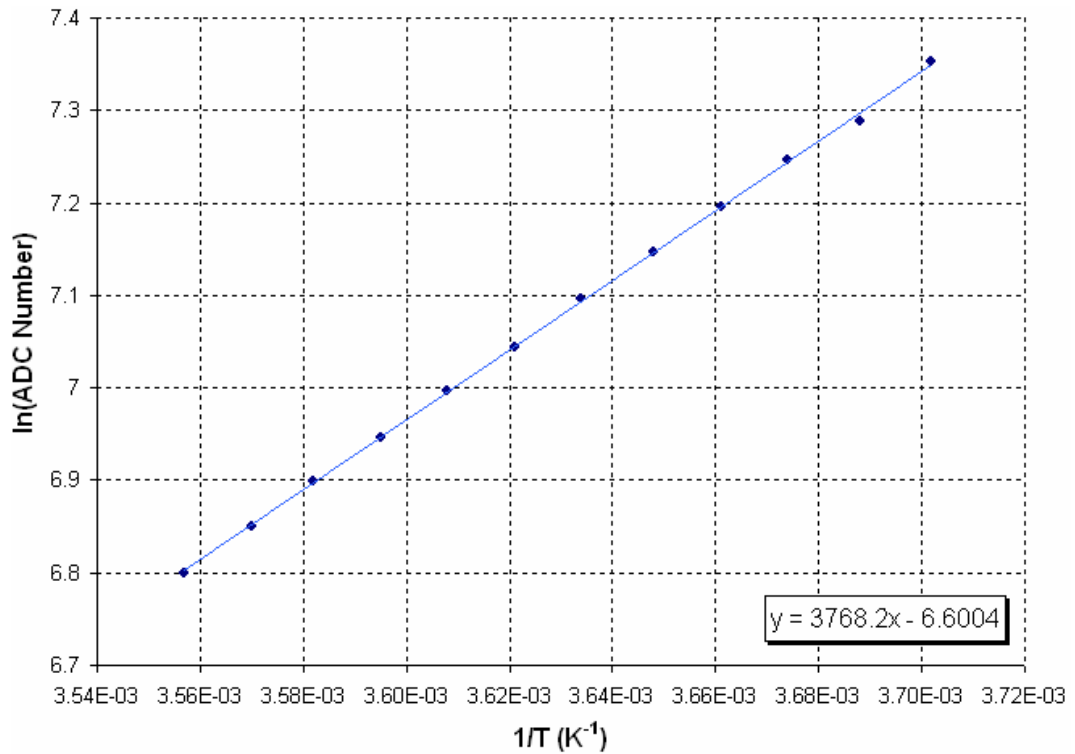
**Figure 2.5-5** *Natural log of ADC number against 1/T*

## 2.6 Data acquisition and control software

A PC is used for control of the system and data acquisition. Software routines are written in C and run using LabWindows (appendix A). Using a USB-based analogue and digital I/O module thermistor and pressure transducer voltages are read in and digital signals sent out to the miniature relays. The USB device employed is a USB-1208LS (figure 2.6-1). This device is interfaced with the PC via a USB port. It has eight 11-bit single ended inputs and 16 digital I/O lines and is powered by a +5 V USB supply from the PC. A specific library was used in LabWindows to interface with the USB module. This library provides loadable kernel drivers and functions for the software routines.

**Figure 2.6-1** *USB based analogue and digital I/O module.*

When the control program is run there are three main options in the graphical user interface (figure 2.6-2):

1. Ramp
2. Hold
3. Fridge

If ramp is chosen the side rail temperatures will ramp down from set values by a certain number of steps then back up to the original values. For example if the ramp starts with side temperatures at 6.7 °C and 5.3 °C and ramps down by 40 steps of 0.1 °C the side walls will be at 2.7 °C and 1.3 °C at the end of the ramp. The system then ramps back up to its original temperatures. At this point the pressure in the fluid is ramped over 10 steps (5400 s) to a pre set value and held at this value for the subsequent down and up ramp. Typically many of these down and up ramps routines take place in a single experimental run with each set at a different applied pressure. Each step takes 540 s, as the test region needs time for the temperature to stabilise after each 0.1°C change. A typical ramp run comprising of four down ramps and four up ramps consists of 350 steps and takes 189000 s or 52.5 hours. If hold is chosen the side chambers will hold set temperature values until the program is

terminated. This is necessary before a ramp run so that the side walls will be at the desired temperature before the run has begun. If fridge is chosen the compressor will come on and off in order for the fridge to hold a set temperature.
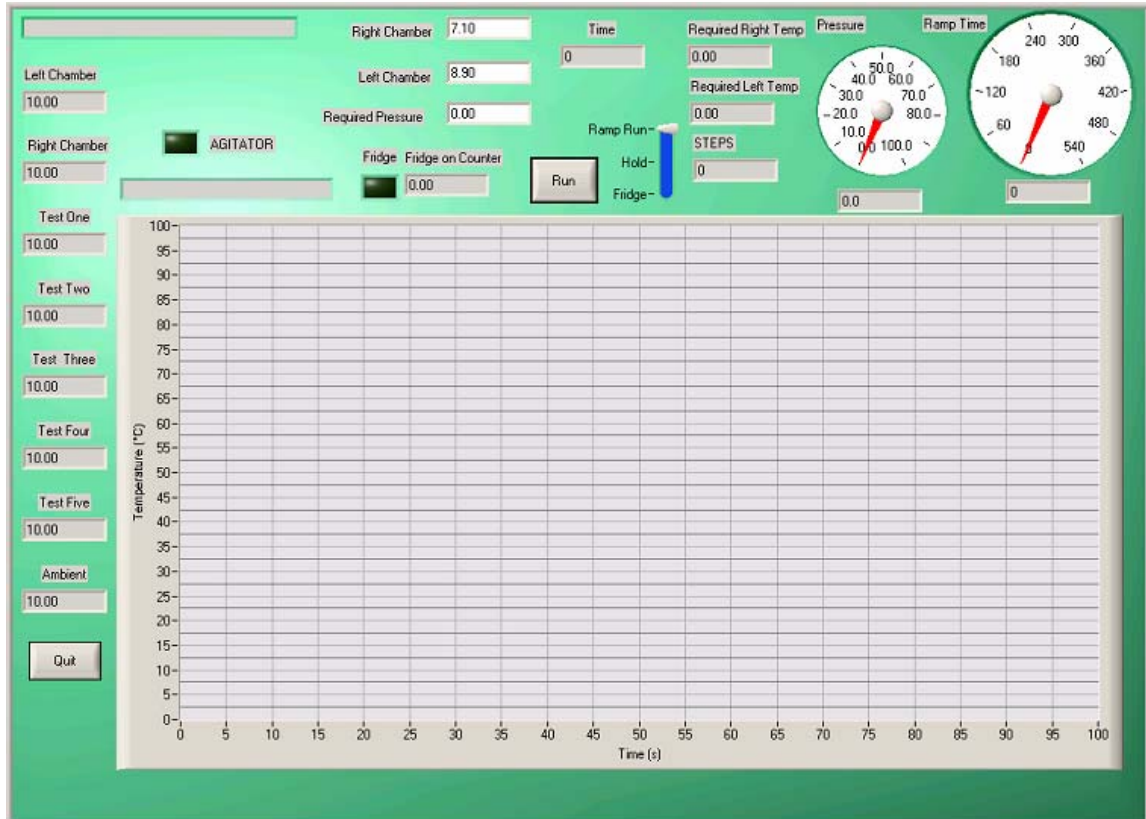


**Figure 2.6-2** *Graphical user interface (GUI) for data acquisition and control software.*

The computer controlling the four magnetic pumps achieves temperature control of the coolant in the $T_L$ and $T_R$ reservoirs. There are thermistors located in the walls of the test chamber. These thermistors send voltages to the USB device, which in turns sends an ADC number to the PC. In the code this ADC number along with calibration data for each thermistors is taken and converted to a temperature in degrees Celsius. These values are printed to the screen. These temperatures are taken and depending on their values and the desired side wall temperatures a heating, cooling or no pump may activate. If the temperature derived from the thermistor is more than 0.1 °C above the desired temperature then the appropriate cooling pump is activated. If the temperature derived from the thermistor is less than 0.1 °C below the desired temperature then the appropriate heating pump is activated. If the

temperature derived from the thermistor is between 0.1 °C above and below the desired temperature no pump is active. No pump is active over this range to prevent the pumps fighting against each other or going into oscillation. In this way a temperature gradient is set up across the test region. Similarly, the ambient fridge temperature is obtained from a thermistor located centrally in the fridge. The fridge compressor turns on if the reading from the ambient fridge thermistor is below the desired fridge temperature. There are five thermistors located in the pressure chamber. These are sensing thermistors and information from them is obtained in the same way as the side wall thermistors. All information from thermistors and time values are recorded.

The pressure transducer also sends a voltage to the USB device corresponding to a pressure in bar. The transducer has been calibrated against an analogue pressure gauge to an accuracy of one bar. The relationship between the voltage output of the transducer and pressure is linear in the range 0 to 100 bar of applied pressure. Using this calibration data voltages from the USB device are converted to pressure readings in bar and printed to the screen. If the reading from the transducer drops below the desired pressure value the stepper motor is activated. Readings from the transducer are recorded in the same file as the thermistor and time data.

Control of the pumps is achieved by controlling the states of miniature relays which are incorporated into the electronic circuit of each pump. A pump activates when a digital signal is sent from the PC to the USB device which sets the relevant output line from the USB device to high. The output lines from the USB device control whether relays are open or closed. If a line is set to high the relay closes and the circuit is complete allowing the pump to be active. After five seconds the line is set back to low and the relay opens breaking the circuit and the pump becomes inactive. Within the miniature relay box (figure 2.6-3) are eight miniature relays with a current driving buffer to increase the current of the digital signal from the USB device. Four of these miniature relays are in use, one for each of the pumps. The relays in use are Omron 12 V DC in type. In previous designs of the miniature relay box 5 V Omron relays were in use but these relays occasionally stayed in the closed state even when the digital signal was removed. Since moving to the 12 V relays this has not been an issue. If the buffer were not in place the relays would draw too much current from

the USB device and may damage it as it is designed to only supply minimal amounts of current.
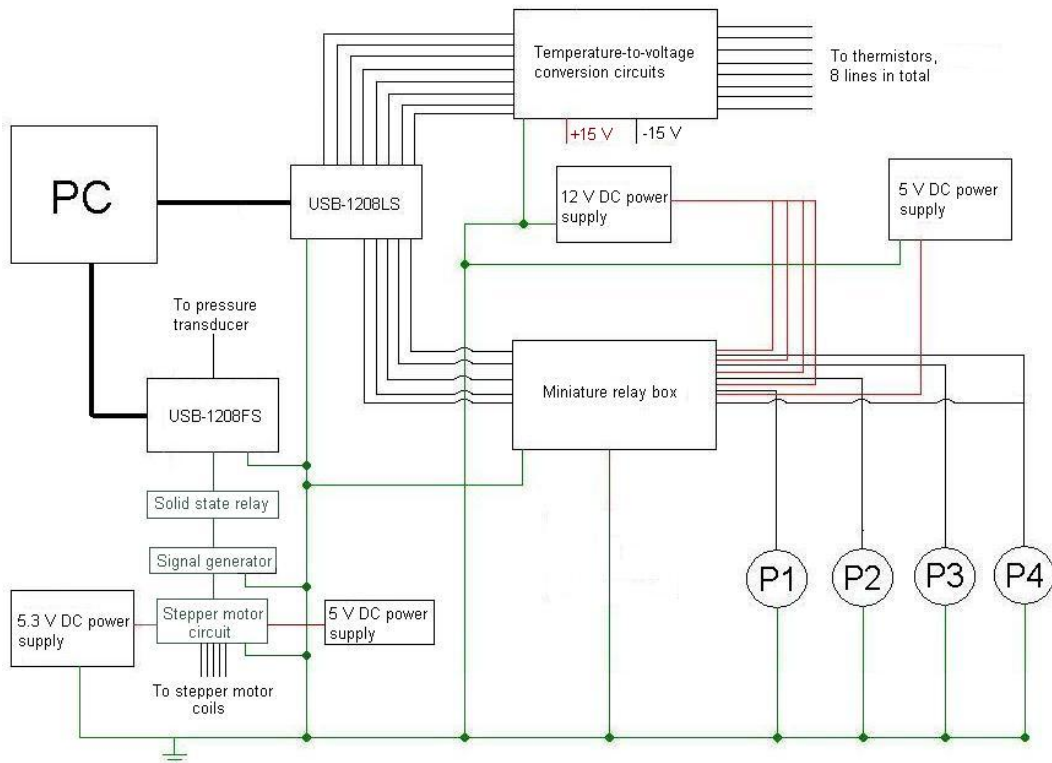


**Figure 2.6-3** *Electronics for data acquisition of thermistors and control of pumps.*

Control of the fridge and the pressure system is achieved through the use of solid-state relays. A buffer is incorporated into the solid-state relays to increase the current from the digital line from the USB device as the solid-state relays would draw too much current from the USB device. The same buffer chip (2891 buffer chip) is used in the miniature relay box as the solid-state relay. One solid-state relay is in use to control the compressor of the fridge. When the fridge turns on a digital signal is sent from the PC to the USB device setting the line connected to the solid-state relay to high. When the line is set to high the solid-state relay allows power to flow to the fridge and the compressor turns on. When the line is set to low the fridge turns off. Similarly, when the pressure system activates the solid-state relay controlling the signal generator allows the signal generator to be on or off depending on whether the relevant line from the USB device is set to high or low.

Within the software are many functions which are described below. These functions allow temperature and pressure control and the recording of data for analysis. A flow chart of the software routine is shown in figure 2.6-4.

**Main functions of data acquisition and control software**

**Initial States:**   Initialises the USB device and opens the file containing calibration data.

**DoRampRun:**   Temperatures are set in the user interface for the side chambers and this function ramps down and up each rail simultaneously by a set number of steps in 0.1°C increments.

**DoHoldRun:**   Reads in all thermistor readings, converts to temperature values and holds side chamber temperatures at desired values.

**DoFridgeRun:**   Holds the fridge ambient temperature at a set value.

**ServoTemperatures**:   Holds required temperatures of side chambers with respect to side wall thermistors.

**PumpActivate:**   Causes a particular pump to activate for a set time or pulse.

**RecordResults:**   Logs time, temperature and pressure values to a file.

**ReadPressure:**   Reads in pressure of solution in the chamber from the pressure transducer.

**Stepper:**   Activates stepper motor as required.
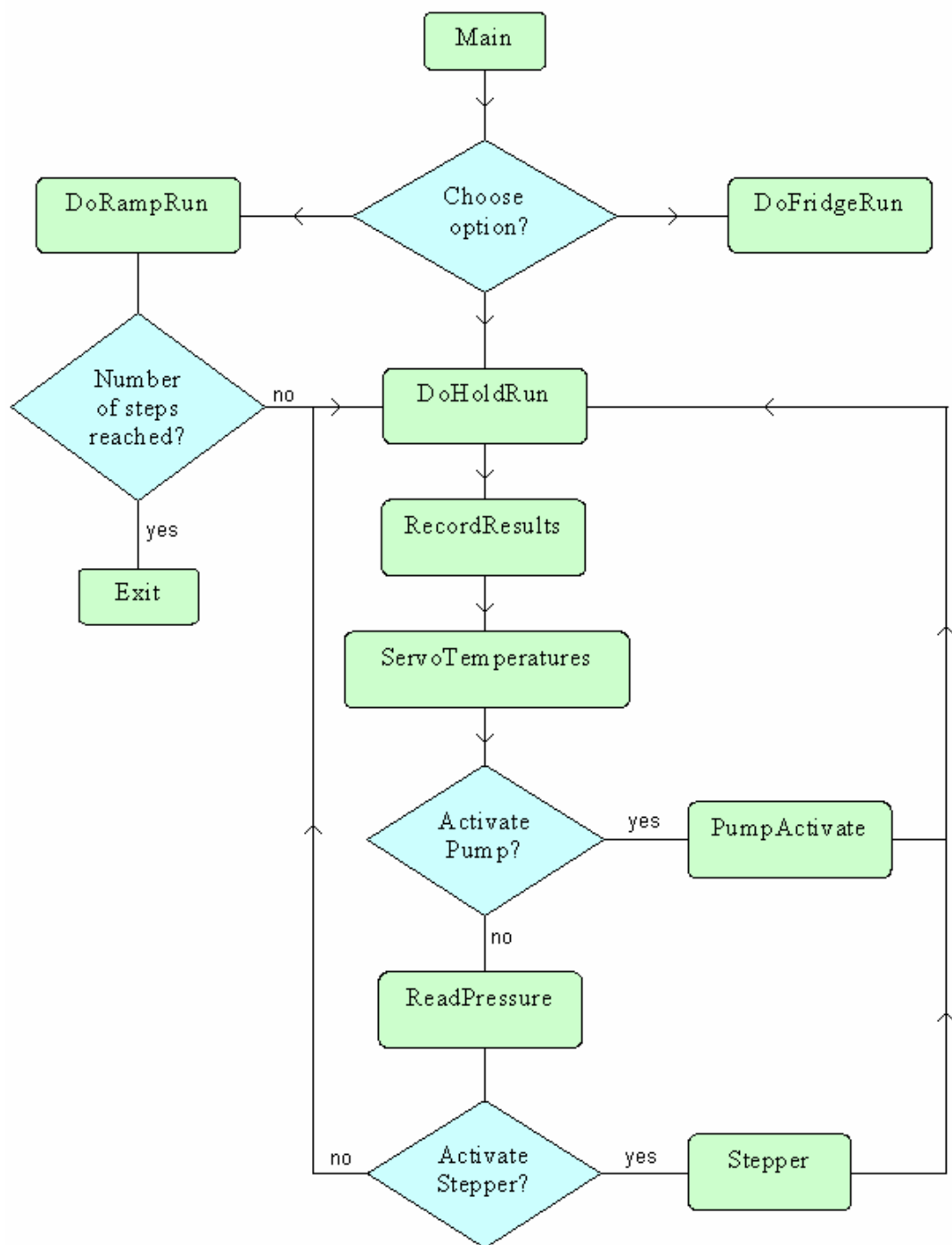
**Figure 2.6-4** *Flow chart showing the* m*ain functions of data acquisition and control software.*

# Chapter 3


# Data Analysis Procedures and Results

## 3.1 Determination of the temperature of maximum density from ramp runs

In order to find the temperature of maximum density a convective flow technique is used. By monitoring temperatures at points in the fluid the convective flows in the fluid are tracked. Temperatures are taken at points in the fluid under test using an array of five thermistors that are located centrally across the rectangular test region. The leftmost thermistor is located 30 mm from the bottom and 30 mm from the front of the inner region containing the liquid under test. This thermistor is also 20 mm from the inner left side wall. The other four sensing thermistor are in line with this thermistor equally spaced across the chamber with 20mm between each thermistor. A schematic of a cross section of the chamber illustrating the location of these thermistors is shown in figure 3.1-1.
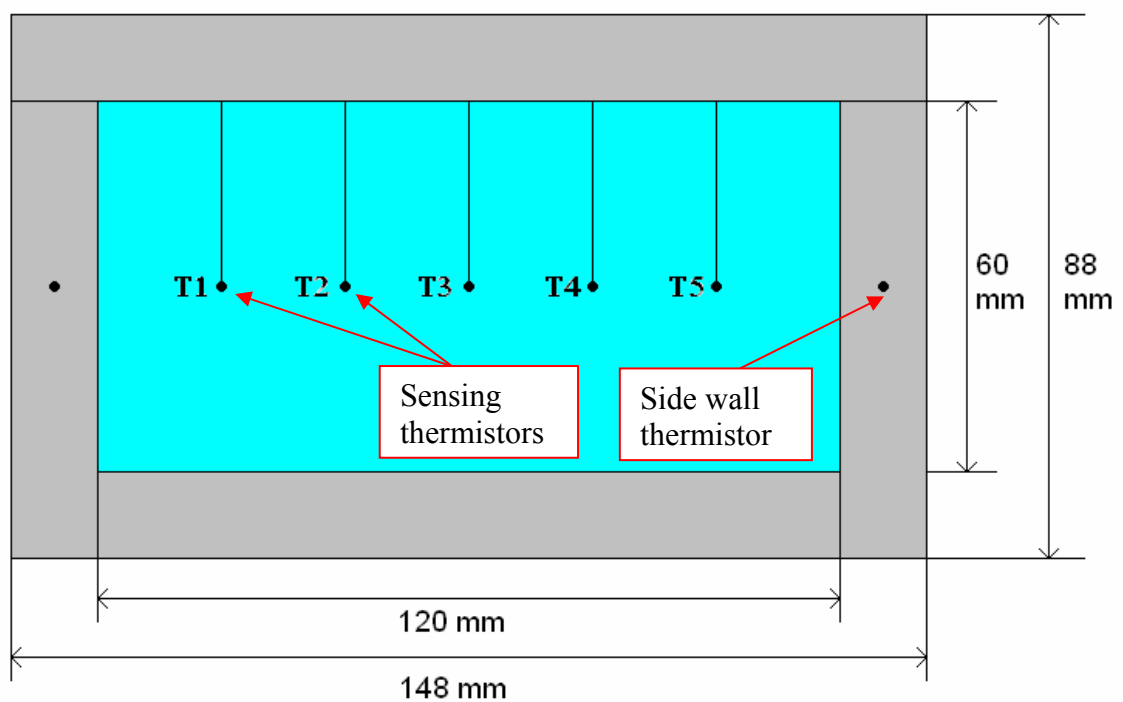


**Figure 3.1-1** *Cross section of chamber showing locations of side wall thermistors and sensing thermistors labelled T1 to T5.*

The side wall thermistors are placed in holes drilled in the front walls of the aluminium chamber. These holes are 44 mm deep so that when thermistors are placed in these holes they will line up with the five sensing thermistors within the

52

chamber.  The chamber wall thickness is 14 mm and the inner test region is 60 mm deep.  Hence, in order for the side wall thermistors to be in line with the sensing thermistors the holes must be half the chamber depth plus the wall thickness.

Side wall temperatures are ramped down and up as described in section 2.6 and temperatures of all thermistors, time values and pressures readings are recorded.  The average temperature of the fluid at the beginning of an experimental run is always above the temperature of maximum density for the solution that is being investigated.  At this temperature a single cell convection pattern exists in the fluid with less dense fluid rising at the hot side wall and more dense colder fluid falling at the cold side wall.  With the hot side wall on the left, this single cell moves in a clockwise direction.  As the average temperature of the fluid drops to within the vicinity of the density maximum a second cell begins to form moving in an anti-clockwise direction.  This secondary cell grows as the side wall temperatures ramp to lower temperatures.  As the fluid cools further this cell takes over the entire region and less dense colder fluid rises and more dense hotter fluid drops.  At this stage a single cell convection pattern exists but now it is moving in an anti-clockwise direction.  This process has been simulated with pure water using the Comsol Multiphysics package (figures 3.1-2 to 3.1-5).  When side walls are ramped up the same process occurs but a second cell moving in a clockwise direction forms in the vicinity of the density maximum and moves across the test fluid until a single cell moving in a clockwise direction exists.  By monitoring the five sensing thermistors the movement of these secondary cells can be tracked and from this information the temperature of maximum density can be extracted.
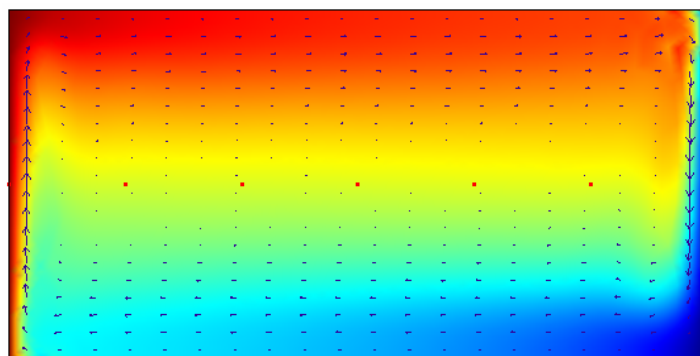


**Figure 3.1-2** *Simulated data for pure water showing single cell convection pattern at beginning of ramp run.*

53
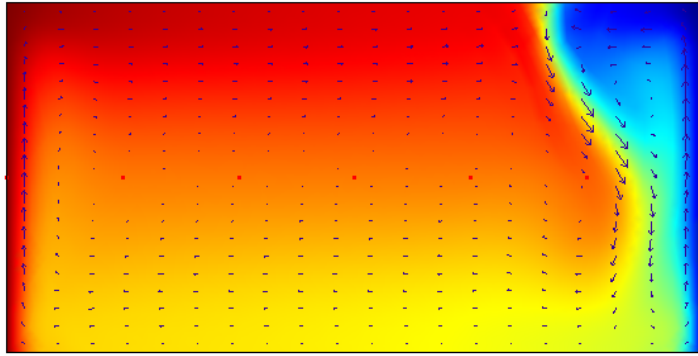
**Figure 3.1-3** *Simulated data for pure water showing the formation of a secondary cell in the vicinity of the density maximum.*
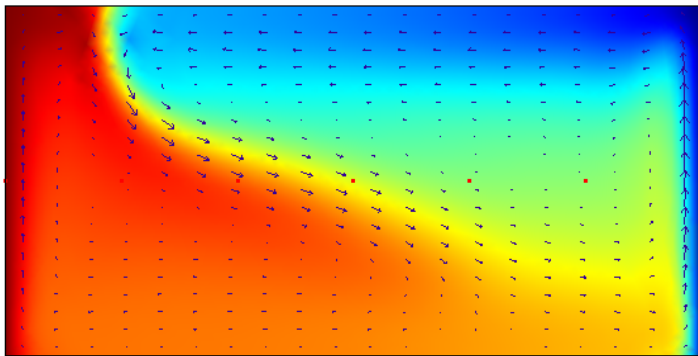


**Figure 3.1-4** *Simulated data for pure water showing the movement of a secondary cell as side wall temperatures are ramped down through the density maximum.*
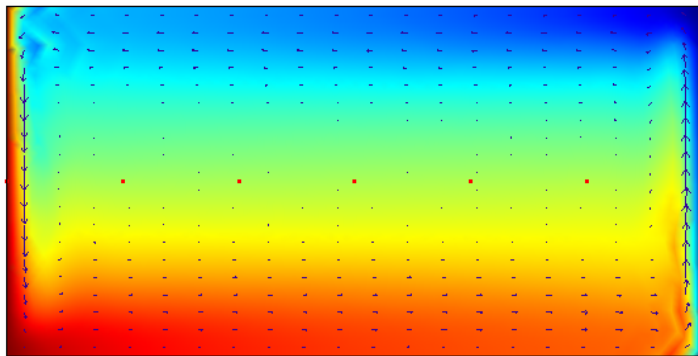


**Figure 3.1-5** *Simulated data for pure water showing single cell convection pattern at end of a down ramp run.*

As side wall temperatures ramp down maintaining a temperature gradient the average temperature approaches the temperature of maximum density and the secondary cell forms and begins to move across the fluid.  As the cell moves past a sensing

thermistor a sudden drop in temperature is recorded by that thermistor.  The termistors record this sudden drop successively as the cell moves thereby spreading out the temperature profiles of the sensing thermistors.  When a single cell exists within the fluid after the density anomaly the thermistor temperature profiles merge together.  This spreading of the thermistor profiles gives rise to a signature of the density anomaly centred on the temperature of maximum density.  As the side wall temperatures are ramped up a sudden increase is recorded by the sensing thermistors giving rise to a signature of the density anomaly centred on the temperature of maximum density in the same way as a down ramp.

A Comsol Multphysics simulation of the experimental procedure is shown in figure 3.1-6, consisting of two sets of down/up ramps.  A temperature gradient of 1.4 °C has been used.  Each ramp in this run was conducted at different pressures.  For the first down ramp the pressure was held at 0 bar applied pressure, the following up ramp at 25 bar applied pressure, the following down ramp at 50 bar applied pressure and the final up ramp at 75 bar applied pressure.  Due to these applied pressures the anomaly features are centred on different temperatures.
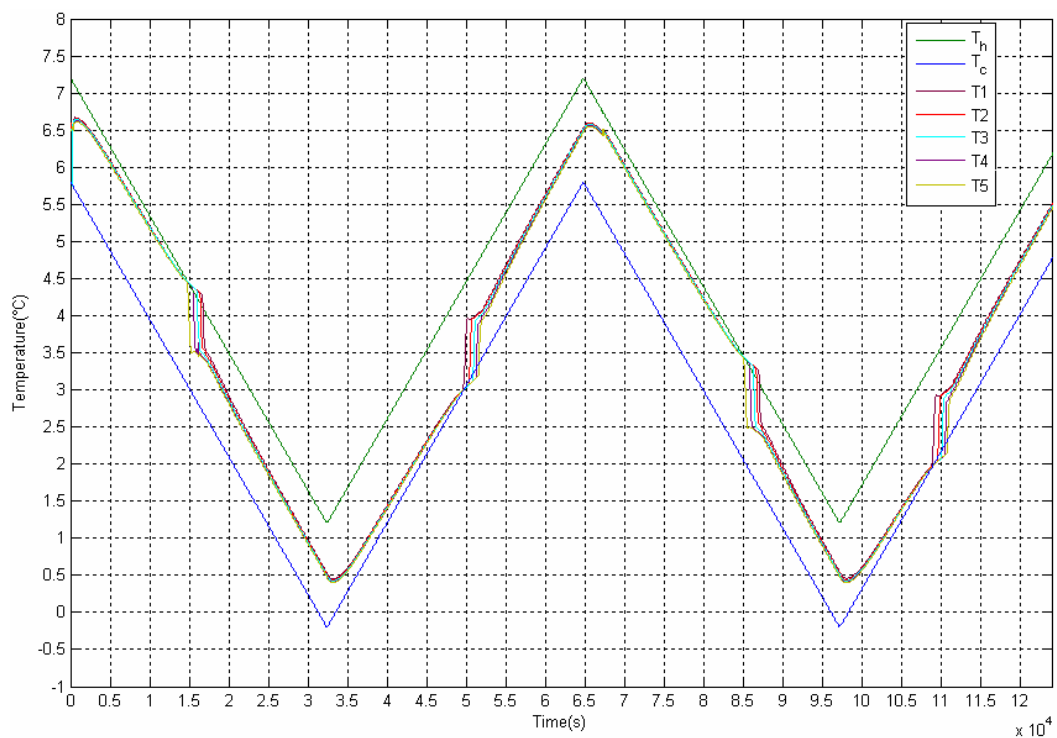


**Figure 3.1-6** *Ramp run using a Comsol Multiphyics model.*

An experimental ramp run is shown in figure 3.1-7 with the corresponding pressure profile (figure 3.1-8). In this case a solution of 60 g/L ethanol is the fluid under test. The run consists of two down and two up ramps. The first down ramp the pressure was held at 3 bar applied pressure, the following up ramp at 25 bar applied pressure, the following down ramp at 50 bar applied pressure and the final up ramp at 75 bar applied pressure. Due to these applied pressures the anomaly features are centred on different temperatures. A temperature gradient of 1.4 °C is typically employed. This temperature gradient is used due to the high rate of heat flow across the thick walled aluminium chamber. Hence larger temperature gradients are not achievable. The gradient is kept as large as possible as smaller gradient produce smaller anomalies and it would be more difficult to extract accurate values of the temperature of maximum density. Insulating the sides, top and bottom may allow for a slightly larger gradient but would not affect the convective flows within the sample under test. The simulation does not have horizontal regions after each ramp as seen in the experimental run. These regions are present due to temperatures being held for a period of time after a ramp to allow pressure to be increased to the desired value using the pressure system before the subsequent ramp. In the simulation pressure is instantly increased to the desired value after a ramp so this flat region is unnecessary.

Typically longer ramps are conducted with a series of down and up ramps. A downward temperature scan is carried out at a fixed applied pressure followed by an upwards scan at the same applied pressure. Most experimental runs are carried out with multiple downward and upward scans with a downward and upward temperature scan at each applied pressure value. This was done to account for possible variations between downward and upward ramps. The beginning of a typical experimental run with 25 g/L 1-propanol as the test fluid is shown in figure 3.1-9. The first downward scan and subsequent upward scan are at atmospheric pressure. The second downward scan and subsequent upward scan are at an applied pressure of 25 bar.
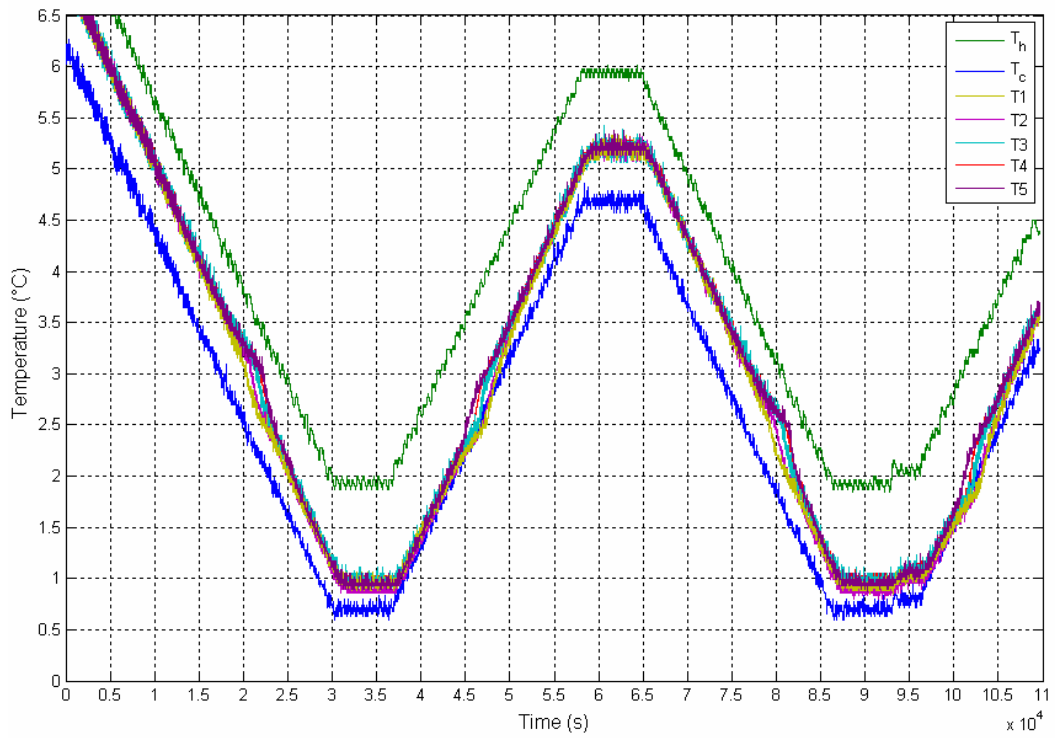
**Figure 3.1-7** *Experimental ramp run with 60 g/L ethanol solution as the test fluid.*
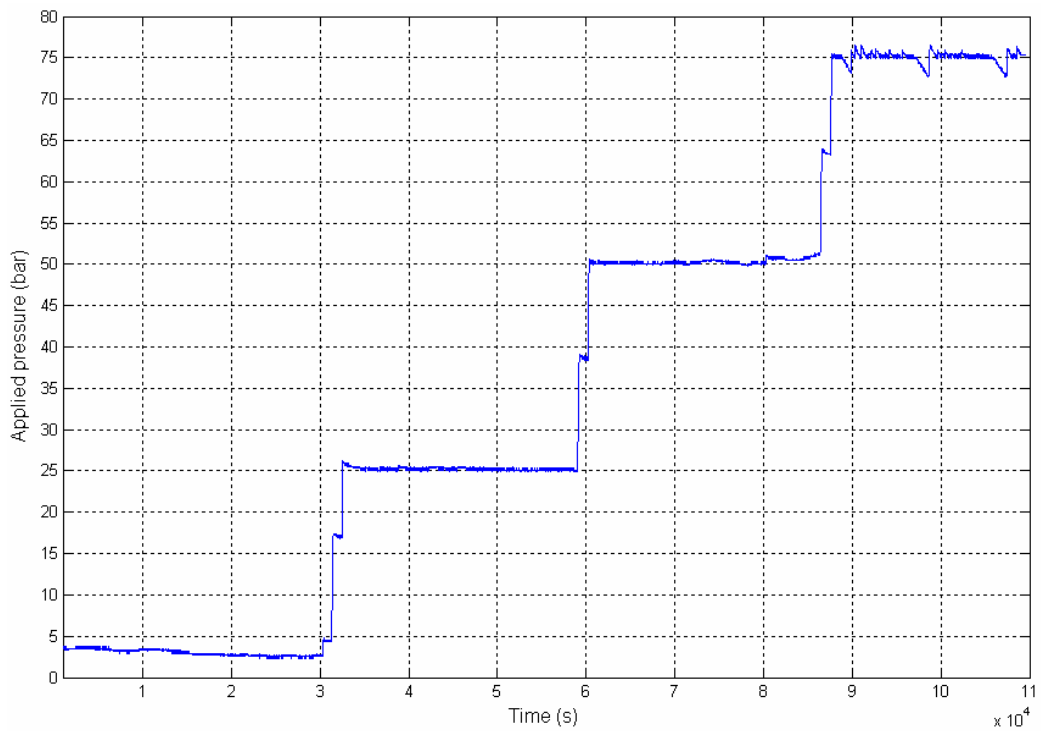


**Figure 3.1-8** *Pressure profile for 60 g/L ethanol solution experimental ramp run.*
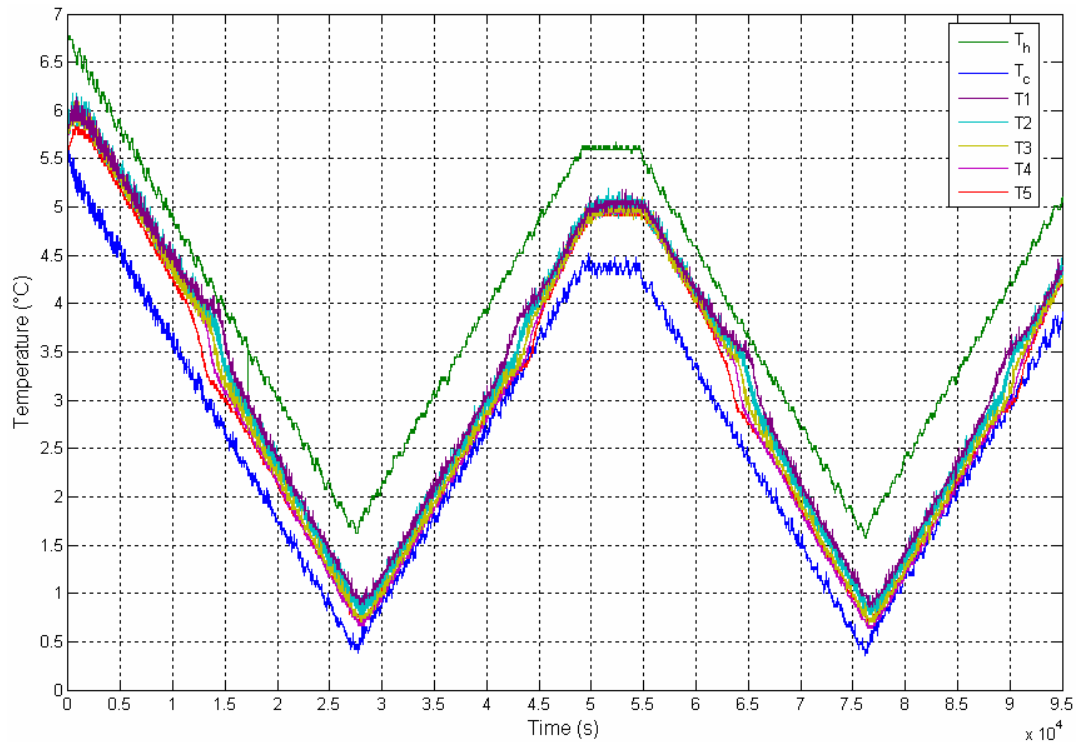
**Figure 3.1-9** *Experimental ramp run with 25 g/L 1-propanol solution as the test fluid.*

In order to extract the temperature of maximum density from the data an area integration technique is employed. The temperature readings from the two sensing thermistors nearest to the side walls of the chamber (the first and fifth thermistors) are taken and the area under each profile is calculated using a trapezoidal integration technique. The difference between these two areas is the area of the anomaly region (figure 3.1-10). The area under the profile of the fifth thermistor is the green plus the tan coloured areas in diagram (A). The area under the profile of the first thermistor is the green area in diagram (A). If we assume that the anomaly feature approximately a parallelogram, then the temperature of maximum density will bisect this anomaly feature. Trapezoidal integration is then used to calculate the point at which the difference in area between the two thermistor profiles is half the calculated area of the anomaly feature. To achieve this, a horizontal threshold line is set above the anomaly and the area difference between the profiles is taken below this line. The threshold line is continually shifted down and the area difference below the line is calculated after each movement of the threshold. When the threshold line reaches halfway down the anomaly it is bisecting the anomaly feature (figure 3.1-10).
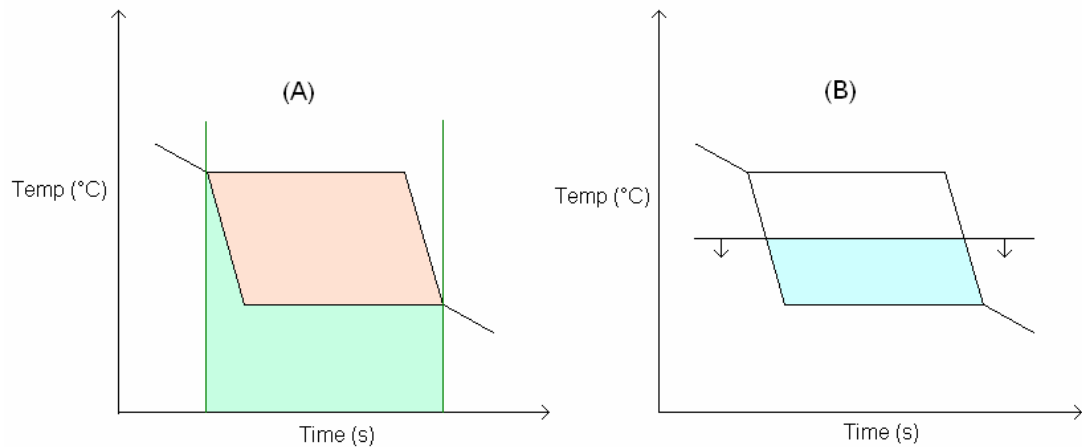
**Figure 3.1-10** *Diagram of anomaly feature showing areas under the first and fifth sensing thermistors (A) and the point at which the threshold bisects the anomaly region (B).*

The area of the cyan region is half the calculated area of the anomaly feature. The corresponding temperature is recorded. This temperature is the temperature of maximum density. This method of locating the temperature of maximum density was tested on data obtained from a run performed using Comsol Multiphysics (figure 3.1-6). This was done as results were known for the simulated data. The area technique returned values of the temperature of maximum density within 0.05 °C of known results for the simulated data for all data tested. The code used to extract the temperature of maximum density using this trapezoidal integration technique was written in Fortran (appendix B).

## 3.2 Pressure scanning

An alternative approach to measuring the temperature of maximum density as a function of pressure is to hold the temperature gradient fixed and scan the pressure over a range which brings the anomaly within the temperature spanned by the gradient. In order to carry out a pressure scan a constant temperature gradient is set up across the test fluid and pressure is ramped up in a controlled manner to a set pressure. Pressure scanning was tested using Comsol Multiphysics. It was found that it was possible to measure the temperature of maximum density by holding side wall temperatures constant and ramping the applied pressure from 0 to 100 bar. The average of the side wall temperatures was chosen to be below the temperature of

59

maximum density and a temperature gradient of 1.8 °C was chosen. At the beginning of the run at atmospheric pressure the sensing thermistors were simply the average of the side wall temperatures as expected. As pressure was ramped the anomaly was seen to emerge (figure 3.2-1). This is due to the fact that as pressure was increased the temperature of maximum density was suppressed and centred on a temperature that was the average of the side wall temperatures.
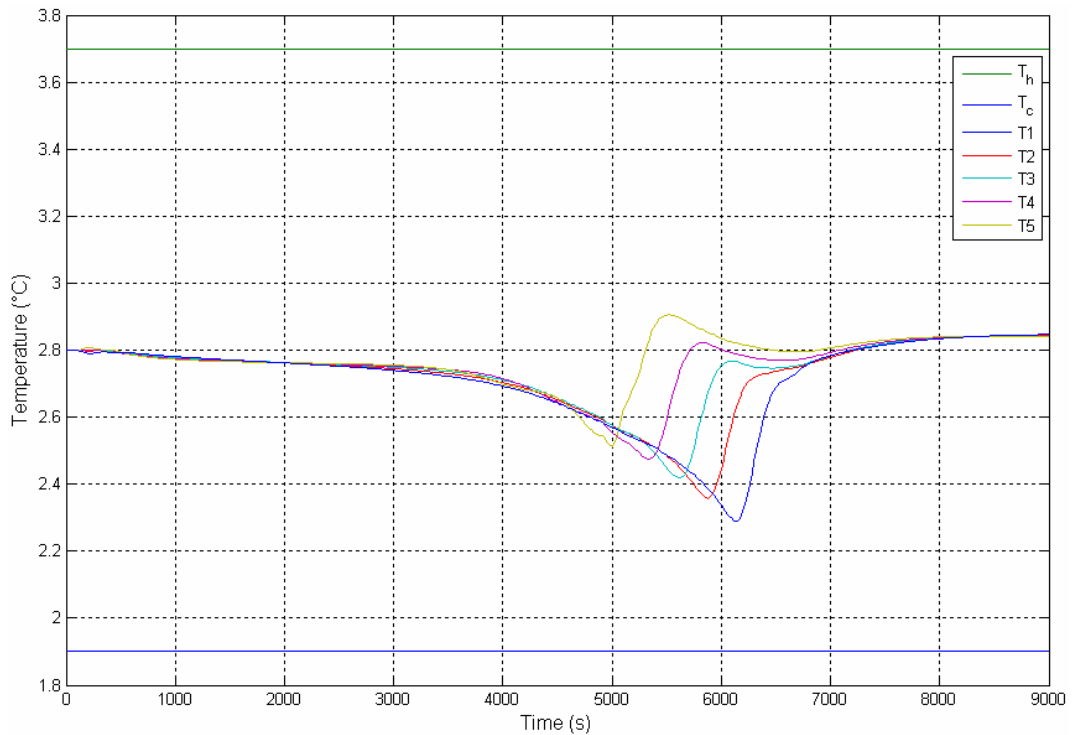


**Figure 3.2-1** *Pressure scan using a Comsol Multiphyics model.*

The only substance tested using this pressure scanning technique was distilled water. Side wall temperatures were held constant and pressure was ramped up to approximately 95 bar. The anomaly shown in figure 3.2-2 is centred on 2.8 °C at 6500 s. The corresponding pressure profile (figure 3.2-3) shows that at this time the sample was under an applied pressure of 60 bar. The temperature of maximum density has been depressed from 3.98 °C to 2.8 °C under 60 bar of pressure. This is equivalent to a depression of 1 °C per 50 bar in agreement with results derived from the seawater equation [30]. Pressure scanning was not used to test aqueous solutions as controlled release of pressure has not been automated. Hence, after each pressure scan the pressure would have to be manually released. For this reason pressure scanning is not efficient and was not pursued further.

60
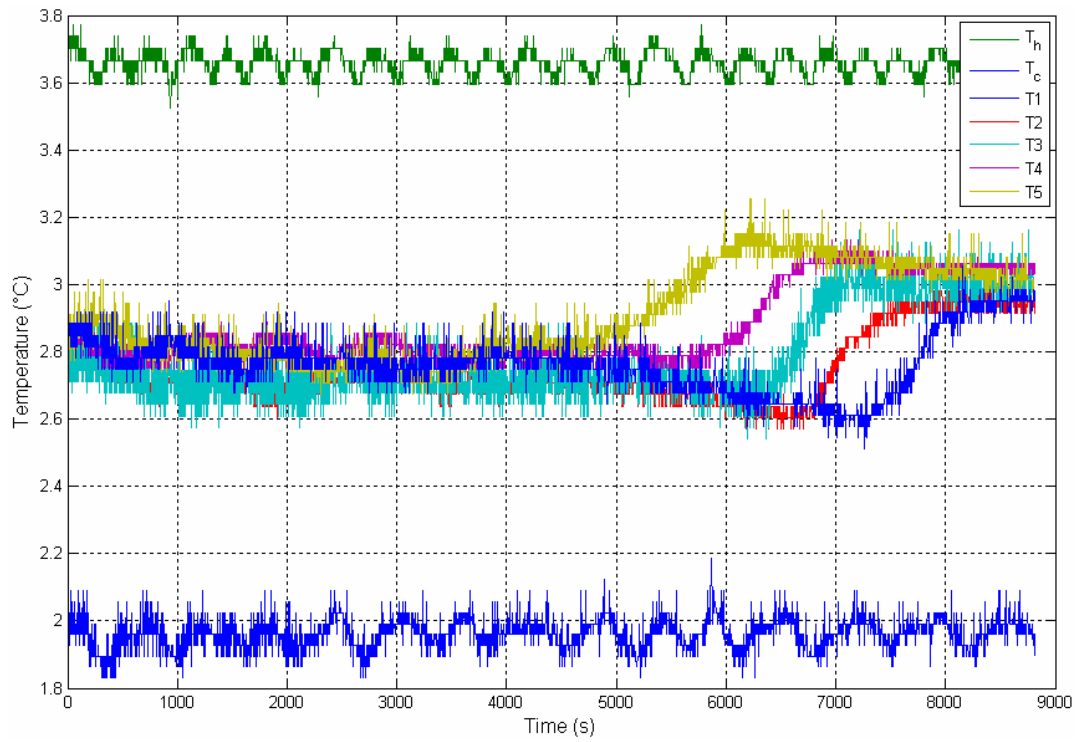
**Figure 3.2-2** *Experimental pressure scan of pure water.*
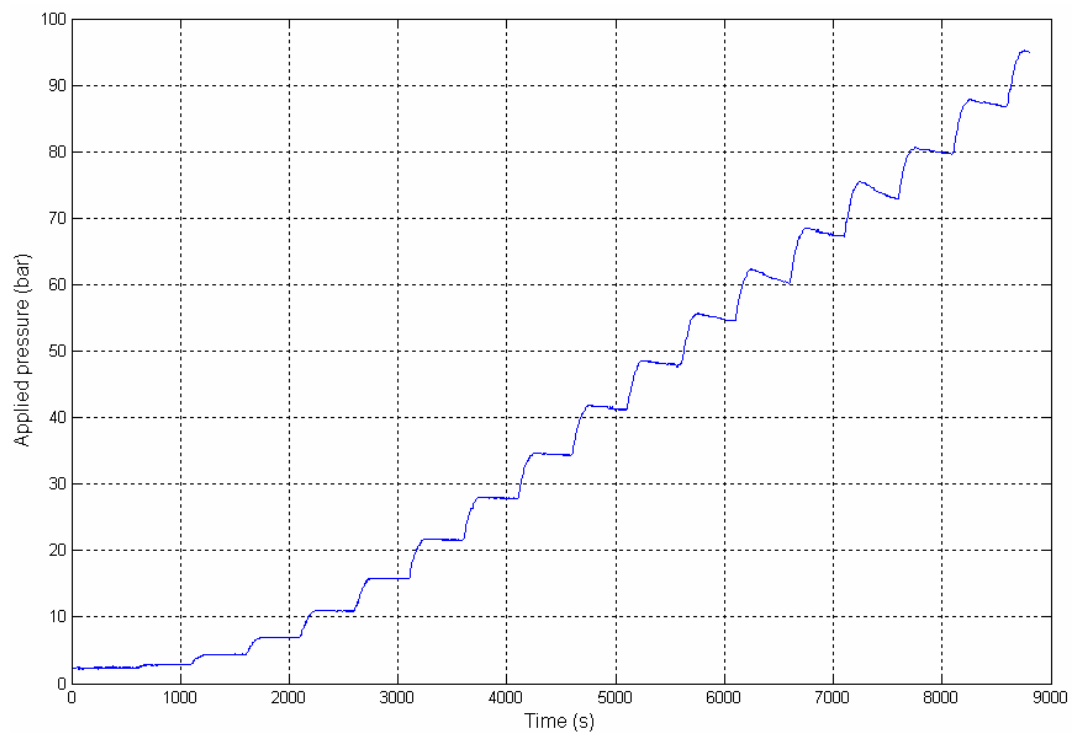


**Figure 3.2-3** *Pressure profile for an experimental pure water pressure scan.*

## 3.3 Heat transfer in the vicinity of the density maximum

It is known that the rate of heat transfer across a region is reduced in the vicinity of the density maximum [39, 40]. This occurs due to the presence of the double convective cell which impedes heat flow across the chamber. The rate of heat flow across a perspex chamber with the same inner dimensions as the pressure chamber used in this work was measured by Cawley et al. [40]. Heat flow across the test region was measured directly by Cawley et al. using a modified version of the longitudinal cut-bar method [40].

The heat flow across the test region was measured indirectly in this work by monitoring the activity of the pumps that control side chamber temperatures. In order to maintain a steady temperature gradient across the sample fluid side wall temperatures must be controlled. This was done in software by activating the required hot or cold pumps from information obtained from side wall thermistors (section 2.6). If the rate of heat flow across the test region was high the pumps needed to be active more often. Conversely, if the rate of heat flow across the test region was low then the pumps were not required to activate as often. Each time a pump activated it was logged to a file and this data has been analysed to investigate the rate of heat flow across the test region in the vicinity of the density maximum.

An experimental pure water temperature scan at atmospheric pressure is shown in figure 3.3-1. Taking this experimental run the number of pump activations versus time displays the length of time taken for each set of 100 pump activations (figure 3.3-2). For example it takes 949 s for the first 100 pump activations and 1252 s for the next 100 pump activations (the first vertical line is at time=949 s, the second is at time=2201 s). Hence, the further apart the vertical lines are on this graph the less active the pumps were over that time period. The lines are spread more in the vicinity of the density maximum implying a reduced rate of heat flow across the test region. The number of pump activations as a function of time has been plotted in a different way (figure 3.3-3). In this case the time has been split into bins of 3000 s and the number of times pumps activated over the time period of that bin was accumulated. The pumps were least active and the rate of heat transfer is at

a minimum in the vicinity of the density maximum as the trend reaches a minimum in the vicinity of the density maximum (figure 3.3-3).
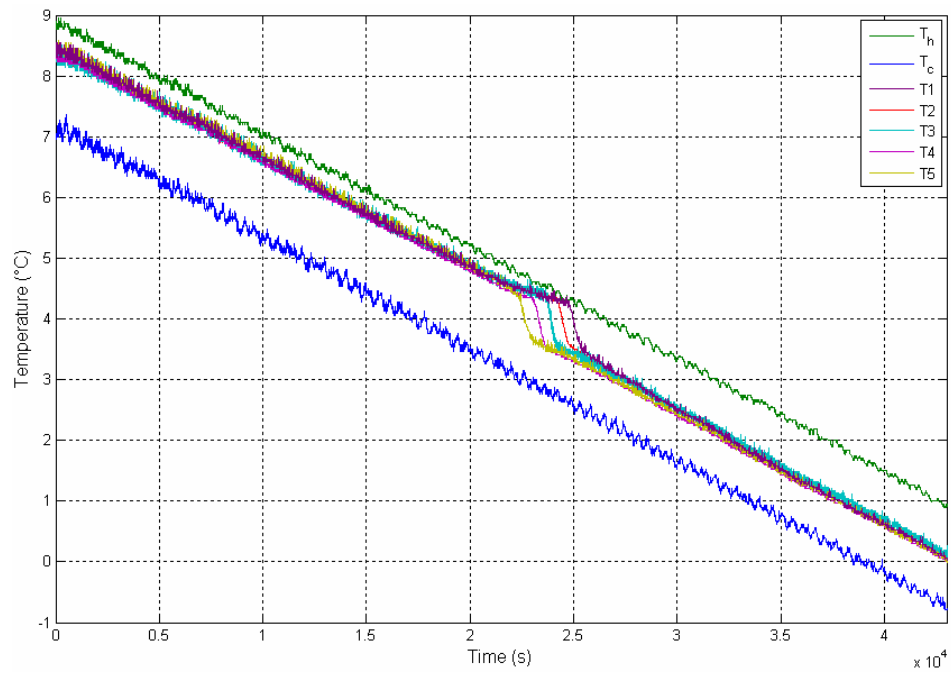


**Figure 3.3-1** *Experimental run with pure water as the test fluid.*
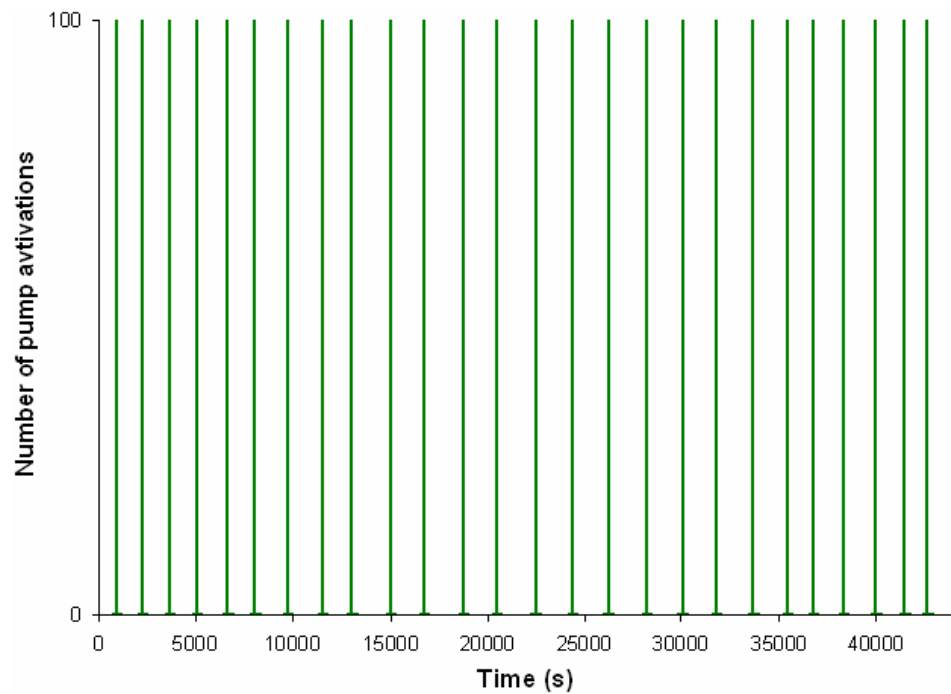


**Figure 3.3-2** *Number of pump activations versus time.*
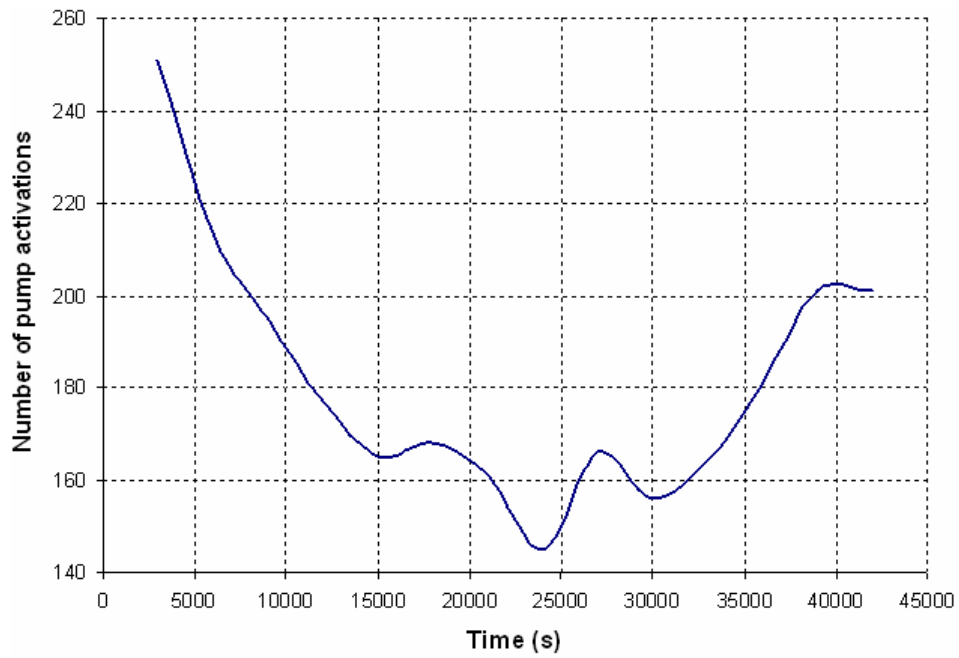
**Figure 3.3-3** *Number of pump activations versus time.*

## 3.4 Pure water results

Pure water was the first fluid to be tested for comparative purposes as results were known.  At atmospheric pressure pure water has a temperature of maximum density of 3.98 °C.  Ramp runs were carried out on a sample of pure water at various applied pressures and the corresponding values of the temperature of maximum density were extracted.  From this data the rate of change of the temperature of maximum density with respect to applied pressure $\left( \dfrac{dT_{md}}{dP} \right)$ could be calculated.  Results for a pure water ramp run comprising of numerous down and up ramps at different applied pressure are shown in table 3.4-1.

| Pure water | |
|---|---|
| $P_{applied}$ (bar) | $T_{md}$ (°C) |
| 0 | 4.137 |
| 0 | 4.002 |
| 0 | 3.966 |
| 0 | 4.067 |
| 10 | 3.807 |
| 10 | 3.857 |

| Pure water (continued) | |
|---|---|
| $P_{applied}$ (bar) | $T_{md}$ (°C) |
| 20 | 3.627 |
| 20 | 3.633 |
| 30 | 3.363 |
| 30 | 3.455 |
| 40 | 3.215 |
| 40 | 3.259 |
| 50 | 3.021 |
| 50 | 3.067 |
| 60 | 2.807 |
| 60 | 2.857 |
| 70 | 2.602 |
| 70 | 2.668 |

**Table 3.4-1** *Temperatures of maximum density for pure water under various applied pressures.*

From this data the rate of change of the temperature of maximum density with respect to pressure can be calculated by plotting applied pressure against the temperature of maximum density and calculating the slope of this trend (figure 3.4-1). The slope of this trend $\left( \dfrac{\mathrm{d}T_{md}}{\mathrm{d}P} \right)$ is -0.0198 ± 0.0005 °C/bar. The graph displays averaged temperature of maximum density values derived from table 3.4-1 with associated errors. The calculation of errors is discussed in section 3.7. This slope value can be compared to similar values derived from Caldwell [28] and the seawater equation of state [30]. By investigating Caldwell's data the value of the rate of change of the temperature of maximum density with respect to pressure is -0.02065 °C/bar for pure water (section 1.5.2). The equation of state for seawater when investigated gives the rate of change of the temperature of maximum density with respect to pressure as -0.02051 °C/bar for pure water (section 1.5.1). The rate of change of the temperature of maximum density with respect to pressure value calculated from experimental work in this study compares very favourably to values derived from Caldwell's results and the seawater equation of state.
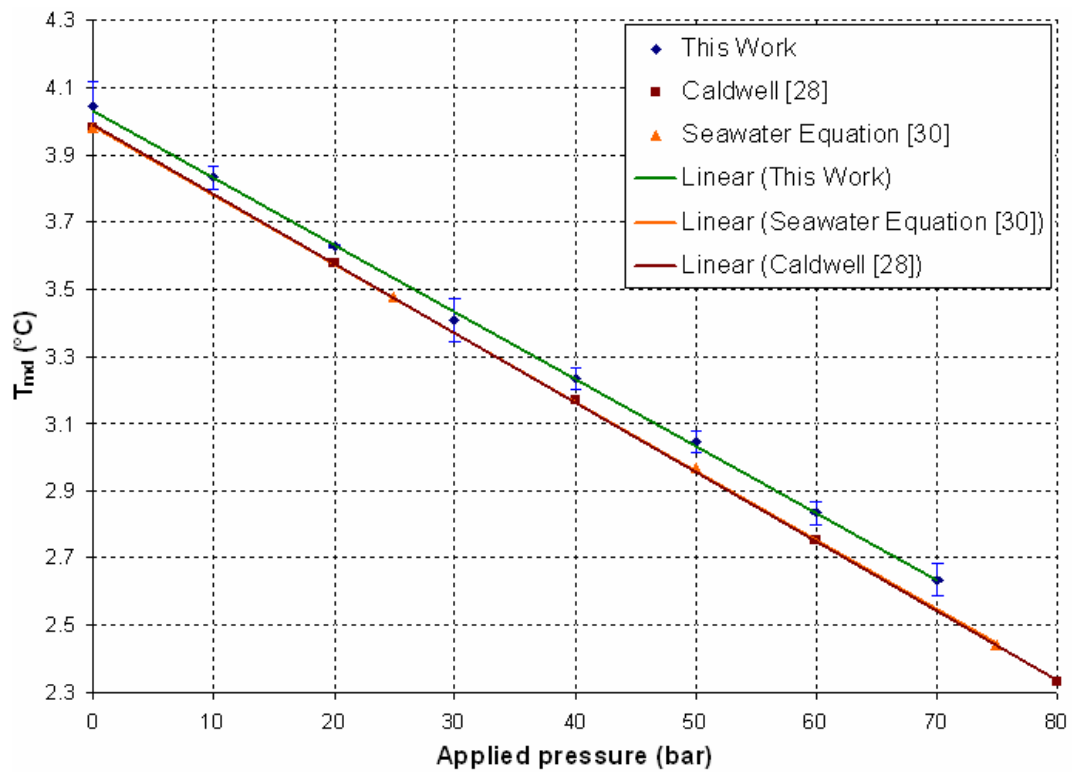
**Figure 3.4-1** *Temperature of maximum density versus applied pressure for pure water.*

## 3.5 Solution results

Three groups of solutes were investigated in this study. These groups are the ionic salts, the monohydric alcohols and the sugars. The salts that were investigated were sodium chloride and potassium bromide (section 3.5.1). Ethanol, 1-propanol and 2-propanol were the monohydric alcohols tested (section 3.5.2). The sugars studied were sucrose and glucose (section 3.5.3). Acetone was the only ketone studied (section 3.5.4). Experiments were conducted for various concentrations of each solute in the same manner as described for pure water in section 3.4. It was found that applying pressure to a solution always reduces the temperature of maximum density but that the rate of decrease changed depending on the nature and concentration of the solute. Results were analysed to find the rate of change of the temperature of maximum density with respect to pressure for each solute at various concentrations. It was found that the three groups of solutes behaved very differently.

### 3.5.1 Ionic salt results

The two ionic salts investigated were sodium chloride and potassium bromide. Sodium chloride and potassium bromide dissolve in water by disassociation. When ionic salts are added to water, partial charges on the water molecules extract ions from of the crystal. For example, $Na^+$ and $Cl^-$ ions are "pulled" out of sodium chloride crystals by water molecules. The water molecules surround the individual ions thereby dissolving the salt. The water molecules orientate themselves differently around the ion depending on its charge. If it is positively charged the negative oxygen ends of the water molecules will surround the positive ion. If it is negatively charged the positive hydrogen ends of the water molecules will surround the negative ion (figure 3.5-1). Water molecules need to surround the ions in order to dissolve the salt. If therefore the supply of water molecules is exhausted no more salt will dissolve. Hence there is a limit to salt concentration in water. Both substances interact in the same way with water molecules but the potassium bromide molecule is about twice as large as the sodium chloride molecule. Sodium chloride has a molecular weight of 58.443 g/mol and potassium bromide has a molecular weight of 119.002 g/mol [6]. Results from the two salts studied were compared to see if there were similarities in their behaviour.
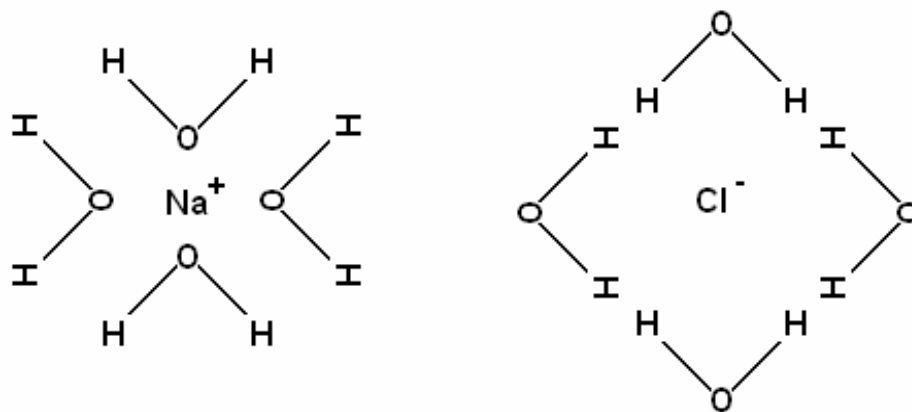


**Figure 3.5-1** *Water molecules arranged about $Na^+$ and $Cl^-$ ions.*

Sodium chloride solutions were studied by Caldwell [28] and also by Fofonoff and Millard [30] in formulating the seawater equation of state. Hence, for comparative purposes sodium chloride was the first solute investigated. Ramp runs were

conducted for differing concentrations of sodium chloride and results pertaining to the temperature of maximum density at applied pressures for each solute concentration were extracted.  For each concentration of sodium chloride the rate of change of the temperature of maximum density with respect to pressure was calculated.  Results from ramps runs are summarised in table 3.5-1.  The rates of change of the temperature of maximum density with respect to applied pressure were calculated from this data and are summarised in table 3.5-2.

| Sodium Chloride NaCl | | | |
|---|---|---|---|
| Concentration (g/L) | Concentration (mol/L) | $P_{applied}$ (bar) | $T_{md}$ (°C) |
| 4.7 | 0.0804 | 5.5 | 2.888 |
| | | 25 | 2.544 |
| | | 51 | 1.979 |
| | | 62 | 1.75 |
| 6.06 | 0.1037 | 0 | 2.652 |
| | | 25 | 2.21 |
| | | 50 | 1.551 |
| | | 70 | 1.273 |
| 10.02 | 0.1714 | 0 | 1.776 |
| | | 25 | 1.364 |
| | | 50 | 0.779 |
| | | 75 | 0.232 |

**Table 3.5-1** *Temperatures of maximum density under applied pressures for various sodium chloride concentrations.  Errors on all $T_{md}$ values are 0.04 °C.*

| Sodium Chloride NaCl | | |
|---|---|---|
| Concentration (g/L) | Concentration (mol/L) | $\frac{dT_{md}}{dP}$ (°C/bar) |
| 4.7 | 0.0804 | -0.0203556 |
| 6.06 | 0.1037 | -0.0204813 |
| 10.02 | 0.1714 | -0.020868 |

**Table 3.5-2** *Rates of change of the temperature of maximum density with respect to pressure for various sodium chloride concentrations.*

By plotting the rate of change of the temperature of maximum density with respect to pressure against concentration it is clear that with increasing concentration of sodium chloride this rate of change becomes steeper with respect to pure water. Caldwell investigated salt solutions in some detail and using his data values of this rate of change were calculated for various salt concentrations. Using the seawater equation of state as compiled by Fofonoff and Millard a similar analysis was conducted to find values of the rate of change of the temperature of maximum density with respect to pressure for salt solutions. These trends are all summarised in figure 3.5-2. Pure water values for the rate of change of the temperature of maximum density with respect to pressure as discussed in section 3.4 have been included in this graph. All trends become steeper with increasing concentration. The slope of the trend derived from this work is $-0.00599 \pm 0.00503$ °C L mol$^{-1}$ bar$^{-1}$. The error in this slope and error bars in figure 3.5-2 are discussed in section 3.7. The slopes of the Caldwell and the seawater equation trends are $-0.00476$ °C L mol$^{-1}$ bar$^{-1}$ and $-0.00359$ °C L mol$^{-1}$ bar$^{-1}$ respectively. Both the Caldwell and seawater equation trends fall within the range of values calculated in this study.
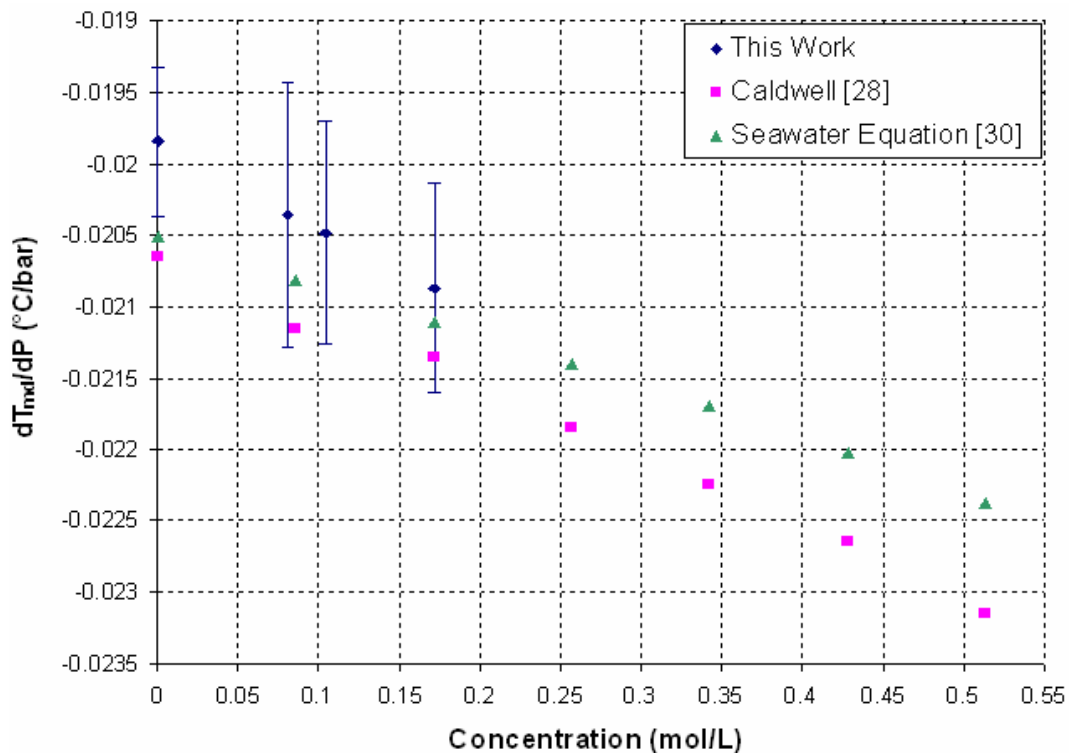


**Figure 3.5-2** *Rate of change of the temperature of maximum density with respect to pressure plotted against NaCl concentration for various data sets.*

Potassium bromide was another ionic salt investigated in this work. Potassium bromide interacts with the water molecules in the same manner as sodium chloride. Ramp runs were carried out for various concentrations of potassium bromide and results were extracted. Downward and upward temperature scans were conduceted at each applied pressure value. This was done to account for possible variations between downward and upward ramps (section 3.1). The rates of change of the temperature of maximum density with respect to pressure were calculated. Results from ramps runs are summarised in table 3.5-3. The rates of change of the temperature of maximum density with respect to applied pressure are summarised in table 3.5-4.

| Potassium Bromide KBr | | | |
|---|---|---|---|
| Concentration (g/L) | Concentration (mol/L) | $P_{applied}$ (bar) | $T_{md}$ (°C) |
| 5 | 0.042 | 0 | 3.521 |
| | | 0 | 3.526 |
| | | 20 | 3.072 |
| | | 20 | 3.067 |
| | | 40 | 2.644 |
| | | 40 | 2.629 |
| | | 60 | 2.304 |
| 10 | 0.084 | 0 | 2.956 |
| | | 0 | 2.954 |
| | | 20 | 2.511 |
| | | 20 | 2.519 |
| | | 40 | 2.116 |
| | | 40 | 2.085 |
| | | 60 | 1.732 |
| | | 60 | 1.701 |
| 20 | 0.1681 | 0 | 1.918 |
| | | 0 | 1.844 |
| | | 20 | 1.516 |
| | | 20 | 1.411 |
| | | 40 | 1.067 |
| | | 40 | 1.0 |
| | | 60 | 0.574 |

**Table 3.5-3** *Temperatures of maximum density under applied pressures for various potassium bromide concentrations. Errors on all $T_{md}$ values are 0.04 °C.*

| Potassium Bromide KBr | | |
| :---: | :---: | :---: |
| Concentration (g/L) | Concentration (mol/L) | $\frac{\mathrm{d}T_{md}}{\mathrm{d}P}$ (°C/bar) |
| 5 | 0.042 | -0.0204575 |
| 10 | 0.084 | -0.02065 |
| 20 | 0.1681 | -0.021755 |

**Table 3.5-4** *Rates of change of the temperature of maximum density with respect to pressure for various potassium bromide concentrations.*

By plotting the rate of change of the temperature of maximum density with respect to pressure against concentration it is observed that potassium bromide behaves in a similar way to sodium chloride. Both trends become steeper with increasing concentration (figure 3.5-3). The sodium chloride trend has a slope of -0.00599 °C L mol$^{-1}$ bar$^{-1}$ and the potassium bromide trend is steeper with a slope of -0.01108 °C L mol$^{-1}$ bar$^{-1}$. These trends are analysed further in section 3.6.
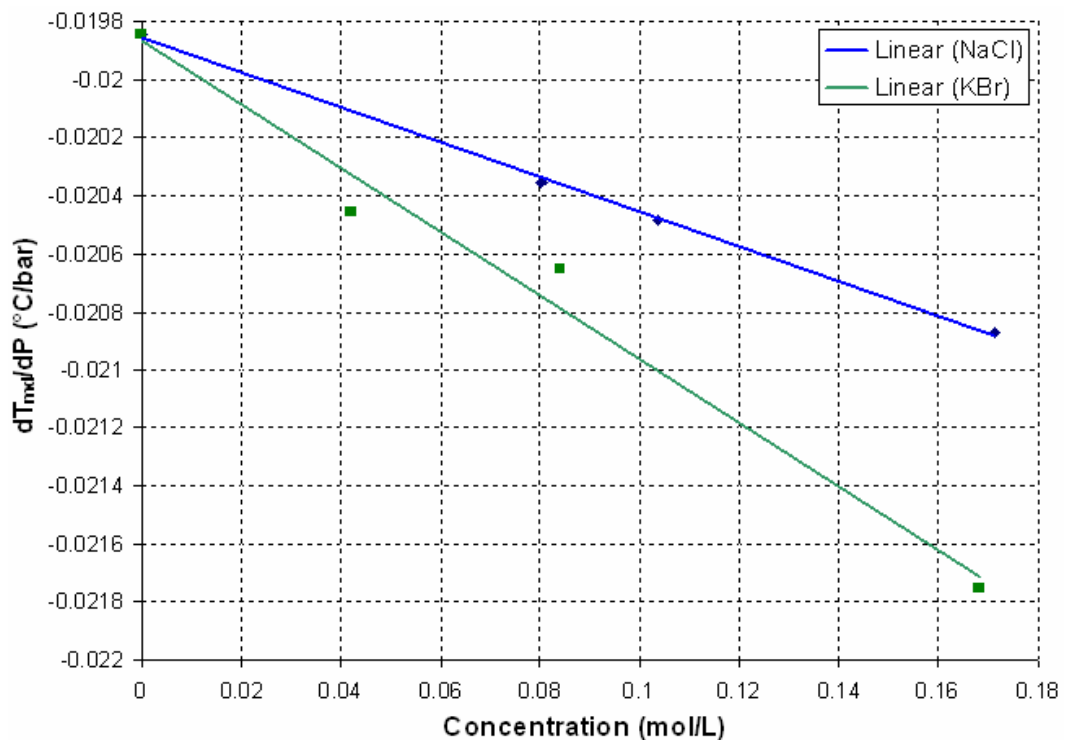


**Figure 3.5-3** *Rate of change of the temperature of maximum density with respect to pressure plotted against NaCl and KBr concentrations.*

## 3.5.2 Monohydric alcohol results

The monohydric alcohols investigated were methanol, ethanol, 1-propanol and 2-propanol. Methanol, ethanol and propanol are completely miscible in water. This is because methanol, ethanol, propanol and water are all polar molecules. The water molecules are interchangeable with the alcohol molecules in solution. Hydrogen bonds will readily form with the alcohol molecules as if they were other water molecules due to the hydroxyl groups of the alcohol molecules. For this reason there is no limit to the concentration of these alcohols in water or water in alcohol. All three alcohols tested interact with water in a similar manner but the molecules differ in size. Larger alcohol molecules are not completely miscible in water. These molecules have longer hydrocarbon chains that will not form hydrogen bonds with water molecules. Alcohols that have four carbons or more have reduced solubility. The solubility of the simplest five alcohols and their isomers are shown in table 3.5-5.

| Substance | Isomer | Solubility (g/L) |
|---|---|---|
| methanol | - | Miscible |
| ethanol | - | Miscible |
| propanol | 1-propanol | Miscible |
| | 2-propanol | Miscible |
| butanol | 1-butanol | 74 |
| | 2-butanol | 181 |
| | 2-methyl-1-propanol | 81 |
| | 2-methylpropan-2-ol | Miscible |
| pentanol | 1-pentanol | 22 |
| | 2-pentanol | 43 |
| | 3-pentanol | 56 |
| | 2-methyl-1-butanol | 30 |
| | 3-methyl-1-butanol | 27 |
| | 2-methyl-2-butanol | 110 |
| | 3-methyl-2-butanol | 56 |
| | 2,2-dimethyl-1-propanol | 35 |

**Table 3.5-5** *Solubility of some monohydric alcohols at 25 °C and atmospheric pressure using data from [41], [42] and [43].*

Methanol has a molecular weight of 32.04 g/mol, ethanol has a molecular weight of 46.07 g/mol and both propanol isomers have a molecular weight of 60.1 g/mol [6]. Both 1-propanol and 2-propanol have the molecular formula $C_3H_8O$ and thus have the same molecular mass. They are structural isomers of propanol meaning that the molecules are arranged differently. 1-Propanol is often shown as $CH_3CH_2CH_2OH$ and 2-propanol as $(CH_3)_2CHOH$ to illustrate the structural difference in the molecules. The structural isomers are shown in figure 3.5-4. There are no structural isomers of methanol and ethanol.
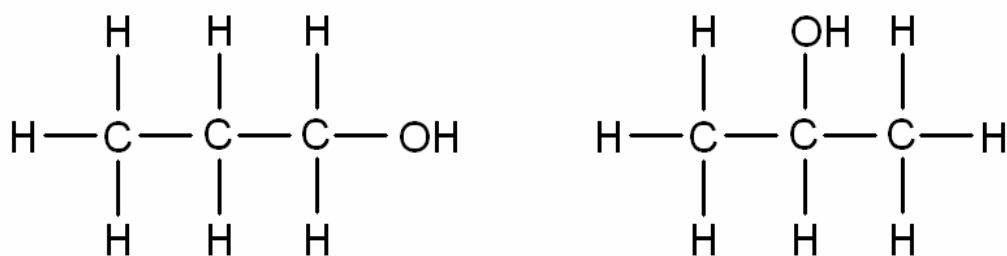


**Figure 3.5-4** *Structural isomers of propanol. (left: 1-propanol, right: 2-propanol).*

Experimental runs were conducted for differing concentrations of methanol, ethanol, 1-propanol and 2-propanol. The rates of change of the temperature of maximum density with respect to pressure were calculated for each solute concentration. Results for methanol ramp runs are summarised in tables 3.5-6. The rates of change of the temperature of maximum density with respect to applied pressure were calculated from this data and are summarised in table 3.5-7. Experimental results for ethanol solutions are shown in tables 3.5-8 with corresponding values for the rates of change of the temperature of maximum density shown in table 3.5-9. 1-Propanol results from ramp runs can be seen in tables 3.5-10. The rates of change of the temperature of maximum density with respect to applied pressure were calculated for 1-propanol and are summarised in table 3.5-11. Results for 2-propanol are summarised in table 3.5-12 and corresponding rates of change of the temperature of maximum density with respect to applied pressure in table 3.5-13.

| Methanol CH₃OH | | | |
|---|---|---|---|
| Concentration (g/L) | Concentration (mol/L) | $P_{applied}$ (bar) | $T_{md}$ (°C) |
| 20 | 0.6242 | 0 | 3.842 |
| | | 0 | 3.819 |
| | | 20 | 3.51 |
| | | 20 | 3.475 |
| | | 40 | 3.168 |
| | | 40 | 3.122 |
| | | 60 | 2.813 |
| | | 60 | 2.791 |
| 40 | 1.2484 | 0 | 3.336 |
| | | 0 | 3.297 |
| | | 25 | 3.031 |
| | | 25 | 2.956 |
| | | 40 | 2.734 |
| | | 40 | 2.654 |
| | | 60 | 2.368 |
| | | 60 | 2.318 |

**Table 3.5-6** *Temperatures of maximum density under applied pressures for various methanol concentrations. Errors on all $T_{md}$ values are 0.04 °C.*

| Methanol CH₃OH | | |
|---|---|---|
| Concentration (g/L) | Concentration (mol/L) | $\frac{dT_{md}}{dP}$ (°C/bar) |
| 20 | 0.6242 | -0.017165 |
| 40 | 1.2484 | -0.0161 |

**Table 3.5-7** *Rates of change of the temperature of maximum density with respect to pressure for various methanol concentrations.*

| Ethanol C₂H₅OH | | | |
|---|---|---|---|
| Concentration (g/L) | Concentration (mol/L) | $P_{applied}$ (bar) | $T_{md}$ (°C) |
| 10 | 0.2171 | 0 | 4.219 |
| | | 0 | 4.23 |

| Ethanol (continued) | | | |
| C$_2$H$_5$OH | | | |
| Concentration (g/L) | Concentration (mol/L) | P$_{applied}$ (bar) | T$_{md}$ (°C) |
|---|---|---|---|
| 10 | 0.2171 | 50 | 3.358 |
| | | 74 | 2.935 |
| 12 | 0.2605 | 0 | 4.271 |
| | | 0 | 4.283 |
| | | 0 | 4.225 |
| | | 0 | 4.264 |
| | | 4 | 4.208 |
| | | 4.5 | 4.215 |
| | | 19 | 3.919 |
| | | 25 | 3.807 |
| | | 25 | 3.805 |
| | | 25 | 3.832 |
| | | 31 | 3.711 |
| | | 31.8 | 3.725 |
| | | 37.6 | 3.609 |
| | | 50 | 3.364 |
| | | 50 | 3.42 |
| | | 75 | 2.881 |
| 20 | 0.4341 | 0 | 4.233 |
| | | 0 | 4.267 |
| | | 25 | 3.863 |
| | | 50 | 3.484 |
| | | 75 | 3.046 |
| 25 | 0.5427 | 6 | 4.119 |
| | | 25 | 3.829 |
| | | 70 | 3.119 |
| 30 | 0.6512 | 0 | 4.249 |
| | | 25 | 3.82 |
| | | 50 | 3.453 |
| | | 75 | 3.047 |
| 60 | 1.3024 | 3 | 2.909 |
| | | 25 | 2.703 |
| | | 50 | 2.346 |
| | | 75 | 2.059 |
| 70 | 1.5194 | 0 | 2.314 |
| | | 0 | 2.348 |
| | | 25 | 2.136 |
| | | 50 | 1.714 |

| Ethanol (continued) | | | |
| :---: | :---: | :---: | :---: |
| C$_2$H$_5$OH | | | |
| Concentration (g/L) | Concentration (mol/L) | P$_{applied}$ (bar) | T$_{md}$ (°C) |
| 70 | 1.5194 | 50 | 1.796 |
| | | 75 | 1.507 |
| 80 | 1.7365 | 0 | 1.45 |
| | | 3 | 1.476 |
| | | 25 | 1.285 |
| | | 25 | 1.291 |
| | | 50 | 1.027 |
| | | 50 | 1.036 |
| | | 75 | 0.679 |
| | | 75 | 0.741 |

**Table 3.5-8** *Temperatures of maximum density under applied pressures for various ethanol concentrations Errors on all T$_{md}$ values are 0.04 °C.*

| Ethanol | | |
| :---: | :---: | :---: |
| C$_2$H$_5$OH | | |
| Concentration (g/L) | Concentration (mol/L) | $\frac{\mathrm{d}T_{md}}{\mathrm{d}P}$ (°C/bar) |
| 10 | 0.2171 | -0.0174111 |
| 12 | 0.2605 | -0.01823 |
| 20 | 0.4341 | -0.015964 |
| 25 | 0.5427 | -0.0156526 |
| 30 | 0.6512 | -0.015892 |
| 60 | 1.3024 | -0.0120833 |
| 70 | 1.5194 | -0.011412 |
| 80 | 1.7365 | -0.0100033 |

**Table 3.5-9** *Rates of change of the temperature of maximum density with respect to pressure for various ethanol concentrations.*

| 1-Propanol | | | |
| :---: | :---: | :---: | :---: |
| CH$_3$CH$_2$CH$_2$OH | | | |
| Concentration (g/L) | Concentration (mol/L) | P$_{applied}$ (bar) | T$_{md}$ (°C) |
| 10 | 0.1664 | 0 | 3.927 |

| 1-Propanol (continued) $CH_3CH_2CH_2OH$ | | | |
|---|---|---|---|
| Concentration (g/L) | Concentration (mol/L) | $P_{applied}$ (bar) | $T_{md}$ (°C) |
| 10 | 0.1664 | 0 | 4.006 |
| | | 20 | 3.556 |
| | | 20 | 3.657 |
| | | 40 | 3.176 |
| | | 40 | 3.257 |
| | | 60 | 2.816 |
| | | 60 | 2.941 |
| 25 | 0.416 | 0 | 3.535 |
| | | 0 | 3.627 |
| | | 25 | 3.196 |
| | | 25 | 3.228 |
| | | 40 | 2.934 |
| | | 40 | 2.921 |
| | | 60 | 2.642 |
| 50.4 | 0.8386 | 0 | 2.442 |
| | | 25 | 2.174 |
| | | 50 | 1.8 |
| | | 75 | 1.487 |
| 70 | 1.1647 | 0 | 0.728 |
| | | 0 | 0.742 |
| | | 20 | 0.463 |
| | | 20 | 0.514 |
| | | 40 | 0.255 |
| | | 40 | 0.316 |
| | | 60 | 0.094 |

**Table 3.5-10** *Temperatures of maximum density under applied pressures for various 1-propanol concentrations.  Errors on all $T_{md}$ values are 0.04 °C.*

| 1-Propanol $CH_3CH_2CH_2OH$ | | |
|---|---|---|
| Concentration (g/L) | Concentration (mol/L) | $\frac{dT_{md}}{dP}$ (°C/bar) |
| 10 | 0.1664 | -0.01827 |
| 25 | 0.416 | -0.0158479 |
| 50.4 | 0.8386 | -0.012956 |

| 1-Propanol (continued) | | |
|---|---|---|
| $CH_3CH_2CH_2OH$ | | |
| Concentration (g/L) | Concentration (mol/L) | $\frac{dT_{md}}{dP}$ (°C/bar) |
| 70 | 1.1647 | -0.011 |

**Table 3.5-11** *Rates of change of the temperature of maximum density with respect to pressure for various 1-propanol concentrations.*

| 2-Propanol | | | |
|---|---|---|---|
| $(CH_3)_2CHOH$ | | | |
| Concentration (g/L) | Concentration (mol/L) | $P_{applied}$ (bar) | $T_{md}$ (°C) |
| 10 | 1.664 | 2 | 4.185 |
| | | 25 | 3.748 |
| | | 50 | 3.275 |
| | | 75 | 2.856 |
| 10 | 1.664 | 0 | 4.382 |
| | | 0 | 4.287 |
| | | 25 | 3.877 |
| | | 25 | 3.873 |
| | | 50 | 3.411 |
| | | 50 | 3.4 |
| 20 | 0.3328 | 0 | 4.42 |
| | | 0 | 4.322 |
| | | 25 | 3.928 |
| | | 28 | 3.912 |
| | | 50 | 3.569 |
| | | 50 | 3.554 |
| | | 75 | 3.142 |
| | | 75 | 3.115 |
| 40 | 0.6656 | 0 | 4.014 |
| | | 0 | 3.884 |
| | | 25 | 3.641 |
| | | 25 | 3.613 |
| | | 50 | 3.292 |
| | | 50 | 3.246 |
| | | 75 | 2.955 |

| 2-Propanol $(CH_3)_2CHOH$ | | | |
|---|---|---|---|
| Concentration (g/L) | Concentration (mol/L) | $P_{applied}$ (bar) | $T_{md}$ (°C) |
| 40 | 0.6656 | 75 | 2.896 |

**Table 3.5-12** *Temperatures of maximum density under applied pressures for various 2-propanol concentrations.  Errors on all $T_{md}$ values are 0.04 °C.*

| 2-Propanol $(CH_3)_2CHOH$ | | |
|---|---|---|
| Concentration (g/L) | Concentration (mol/L) | $\frac{dT_{md}}{dP}$ (°C/bar) |
| 10 | 0.1664 | -0.0182713 |
| 10 | 0.1664 | -0.01858 |
| 20 | 0.3328 | -0.0163978 |
| 40 | 0.6656 | -0.013714 |

**Table 3.5-13** *Rates of change of the temperature of maximum density with respect to pressure for various 2-propanol concentrations.*

The behaviour of the monohydric alcohols is very different to the behaviour of the salts.  The rate of change of the temperature of maximum density with respect to pressure becomes less steep with increasing concentration with respect to the pure water point for all alcohols tested.  This behaviour is in contrast to the behaviour of the salts which display a clear increase in the rate of change of the temperature of maximum density with respect to pressure for increasing solute concentration.  Further analysis of results is discussed in section 3.6.

### 3.5.3 Sugar results

The sugars investigated in this study were glucose and sucrose.  Glucose has the molecular formula $C_6H_{12}O_6$.  Sucrose has the molecular formula $C_{12}H_{22}O_{11}$.  Both sugars dissolve in water but are not completely miscible in water.  Glucose and sucrose are large molecules made of carbon, hydrogen and oxygen.  Both molecules

contain ring structures with many attached hydroxyl groups (O-H) with the O having a slightly negative charge and the H having a slightly positive charge (figure 3.5-5). Since water is polar, water molecules attach to these hydroxyl groups of the sugar molecule via dipole-dipole forces. Attractive forces between the water molecules can overcome attractive forces between sugar molecules in the crystal. When this occurs the sugar molecule is extracted from the crystal. The sugar molecule is surrounded by water molecules and thus dissolved. This process repeats until the sugar is completely dissolved or the supply of unattached water molecules runs out. Since there are a definite number of water molecules needed to dissolve a sugar molecule there is a limit to the concentration of sugar in water. Glucose and sucrose interact with water in a similar manner but the molecules differ in size. Glucose has a molecular weight of 180.16g/mol and sucrose has a molecular weight of 342.3 g/mol [6].
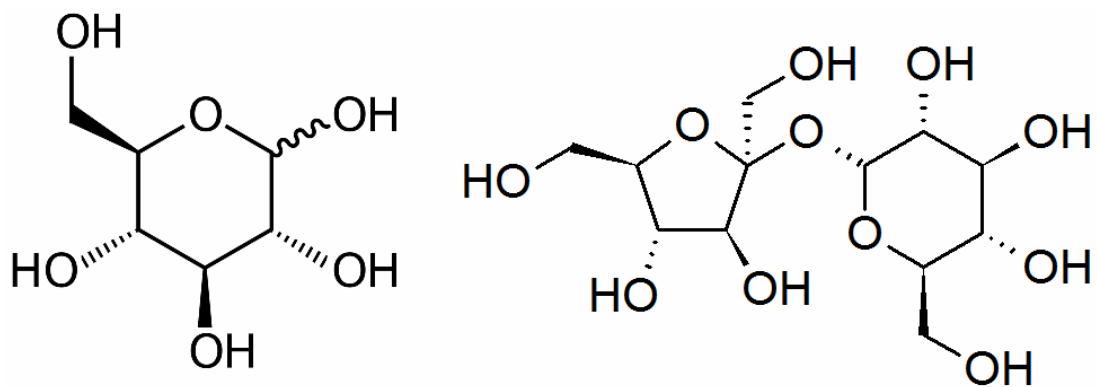


**Figure 3.5-5** *Structural diagrams of glucose and sucrose.*

Experimental results for glucose solutions showing the temperatures of maximum density at applied pressure are displayed in tables 3.5-14. Table 3.5-15 gives the rates of change of the temperature of maximum density with respect to pressure for the glucose solutions tested. Sucrose results are quoted in tables 3.5-16 with corresponding rates of change of the temperature of maximum density with respect to pressure for the various sucrose solutions shown in table 3.5-17.

| Glucose $C_5H_{12}O_6$ | | | |
|---|---|---|---|
| Concentration (g/L) | Concentration (mol/L) | $P_{applied}$ (bar) | $T_{md}$ (°C) |
| 5 | 0.0278 | 0 | 3.774 |
| | | 0 | 3.752 |
| | | 40 | 2.927 |
| | | 40 | 2.902 |
| | | 60 | 2.568 |
| | | 60 | 2.5 |
| 15 | 0.0833 | 0 | 3.218 |
| | | 0 | 3.235 |
| | | 20 | 2.773 |
| | | 20 | 2.756 |
| | | 40 | 2.429 |
| | | 40 | 2.375 |
| 30 | 0.1665 | 0 | 2.389 |
| | | 0 | 2.383 |
| | | 20 | 1.981 |
| | | 20 | 2.001 |
| | | 40 | 1.563 |
| | | 40 | 1.579 |

**Table 3.5-14** *Temperatures of maximum density under applied pressures for various glucose concentrations.  Errors on all $T_{md}$ values are 0.04 °C.*

| Glucose $C_5H_{12}O_6$ | | |
|---|---|---|
| Concentration (g/L) | Concentration (mol/L) | $\frac{dT_{md}}{dP}$ (°C/bar) |
| 5 | 0.0278 | -0.0205875 |
| 15 | 0.0833 | -0.0206125 |
| 30 | 0.1665 | -0.020375 |

**Table 3.5-15** *Rates of change of the temperature of maximum density with respect to pressure for various glucose concentrations.*

| Sucrose C$_{12}$H$_{22}$O$_{11}$ | | | |
|---|---|---|---|
| Concentration (g/L) | Concentration (mol/L) | P$_{applied}$ (bar) | T$_{md}$ (°C) |
| 20 | 0.0584 | 0 | 3.135 |
| | | 25 | 2.634 |
| | | 50 | 2.11 |
| | | 75 | 1.608 |
| 20 | 0.0584 | 0 | 3.133 |
| | | 10 | 2.94 |
| | | 25 | 2.667 |
| | | 35 | 2.424 |
| 30 | 0.0876 | 0 | 2.489 |
| | | 25 | 2.029 |
| | | 50 | 1.484 |
| | | 75 | 0.992 |

**Table 3.5-16** *Temperatures of maximum density under applied pressures for various sucrose concentrations.  Errors on all T$_{md}$ values are 0.04 °C.*

| Sucrose C$_{12}$H$_{22}$O$_{11}$ | | |
|---|---|---|
| Concentration (g/L) | Concentration (mol/L) | $\frac{\mathrm{d}T_{md}}{\mathrm{d}P}$ (°C/bar) |
| 20 | 0.0584 | -0.02042 |
| 20 | 0.0584 | -0.0199379 |
| 30 | 0.0876 | -0.020144 |

**Table 3.5-17** *Rates of change of the temperature of maximum density with respect to pressure for various sucrose concentrations.*

The behaviour of the sugars tested appears to differ to that of the salts and monohydric alcohols.  The rate of change of the temperature of maximum density with respect to pressure does not appear to change significantly with increasing concentration with respect to the pure water point for both sugars tested.  This is in contrast to the behaviour of the salts and alcohols which both display a clear increase or decrease in the rate of change of the temperature of maximum density with respect

to pressure for increasing solute concentration. Further analysis of results is discussed in section 3.6.

### 3.5.4 Acetone results

Acetone is an organic compound which is the simplest substance in the ketone family. Acetone is completely miscible in water. Hydrogen bonds will readily form with the acetone molecules as if they were other water molecules. For this reason there is no limit to the concentration of acetone in water or water in acetone. This is similar to the behaviour of methanol, ethanol and the propanols in water. Acetone has a molecular weight of 58.08 g/mol [6]. The molecular formula for acetone is $(CH_3)_2CO$. The structure of the molecule is shown in figure 3.5-6.
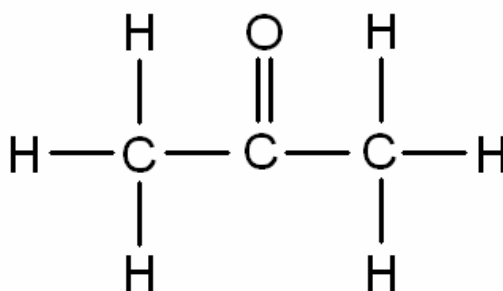


**Figure 3.5-6** *Structure of acetone.*

Experimental results from ramp runs for acetone solutions are shown in tables 3.5-18 with corresponding values for the rates of change of the temperature of maximum density shown in table 3.5-19. The rate of change of the temperature of maximum density with respect to pressure becomes less steep with increasing concentration with respect to the pure water point for acetone. This is similar to the behaviour of the monohydric alcohols.

| Acetone $(CH_3)_2CO$ | | | |
|---|---|---|---|
| Concentration (g/L) | Concentration (mol/L) | $P_{applied}$ (bar) | $T_{md}$ (°C) |
| 10 | 0.172 | 0 | 2.266 |
| | | 0 | 2.186 |

| Acetone (continued) $(CH_3)_2CO$ | | | |
|---|---|---|---|
| Concentration (g/L) | Concentration (mol/L) | $P_{applied}$ (bar) | $T_{md}$ (°C) |
| 10 | 0.172 | 20 | 1.896 |
| | | 20 | 1.789 |
| | | 40 | 1.578 |
| | | 40 | 1.462 |
| | | 60 | 1.197 |
| | | 60 | 1.139 |
| 20 | 0.344 | 0 | 3.102 |
| | | 0 | 3.087 |
| | | 20 | 2.733 |
| | | 20 | 2.727 |
| | | 40 | 2.335 |
| | | 40 | 2.324 |
| | | 60 | 2.024 |
| | | 60 | 2.026 |

**Table 3.5-18** *Temperatures of maximum density under applied pressures for various acetone concentrations. Errors on all $T_{md}$ values are 0.04 °C.*

| Acetone $(CH_3)_2CO$ | | |
|---|---|---|
| Concentration (g/L) | Concentration (mol/L) | $\frac{dT_{md}}{dP}$ (°C/bar) |
| 10 | 0.172 | -0.0175689 |
| 20 | 0.344 | -0.0175213 |

**Table 3.5-19** *Rates of change of the temperature of maximum density with respect to pressure for various acetone concentrations.*

## 3.6 Overview of results

The rate of change of the temperature of maximum density with respect to pressure has been calculated for many concentrations of various solutes. These rates of change have been plotted against concentration for the solutes tested in figures 3.6-1 to 3.6-4. From the figures the differences in the behaviour of the solutes is clear.

The pure water point is taken as a base point for the behaviour of the rate of change of the temperature of maximum density with respect to applied pressure. The ionic salt solutions display an increase in the rate of suppression of the temperature of maximum density with respect to applied pressure for increasing concentration. In contrast to this behaviour the monohydric alcohols display a decrease in the rate of suppression of the temperature of maximum density with respect to pressure for increasing concentration. The sugars are perhaps a third family as the rate of change of the temperature of maximum density with respect to pressure does not appear to change significantly with increasing concentration.

The salts display very linear trends on all figures. The monohydric alcohols show a very different trend as discussed but in addition there is also evidence of possible structure in the ethanol trend. Each point on all of these figures has an associated error. Error analysis is discussed in section 3.7. The rate of change of the phase change for salt solutions has been included on the graph to illustrate the difference between the rate of change of the density maximum with respect to applied pressure and the rate of change of the temperature of the phase change with respect to applied pressure for salt solutions. This data for this trend was taken from the 1974 Doherty and Kester paper [44].
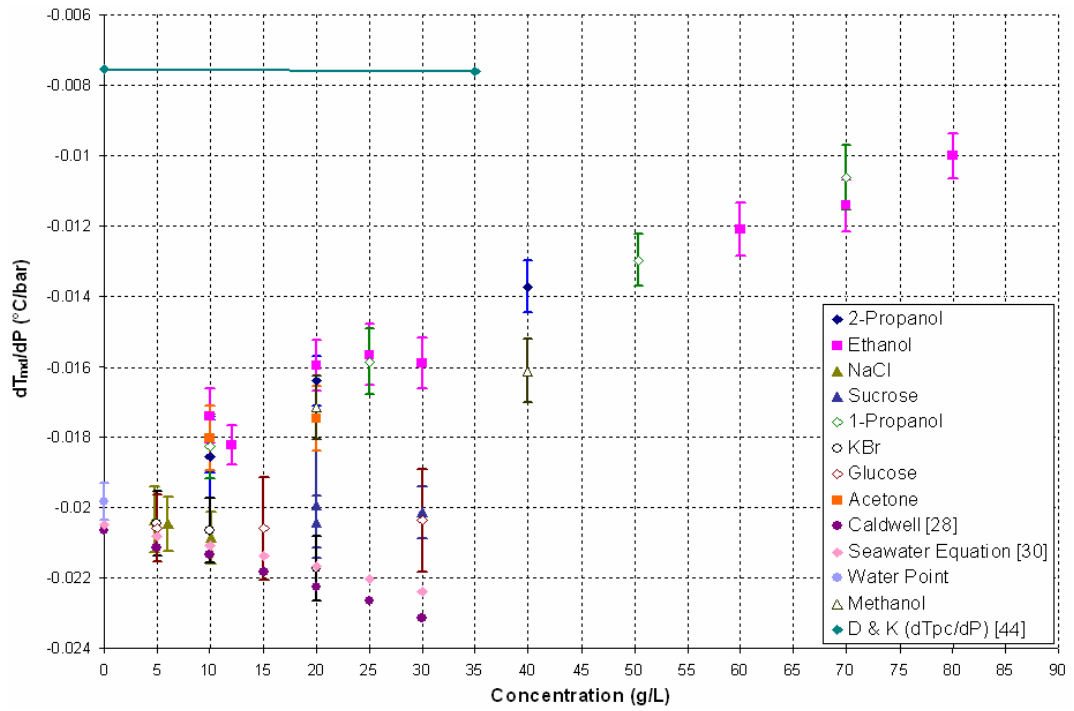
**Figure 3.6-1** *Rate of change of the temperature of maximum density with respect to applied pressure for differing concentrations (g/L) of various solutes.*
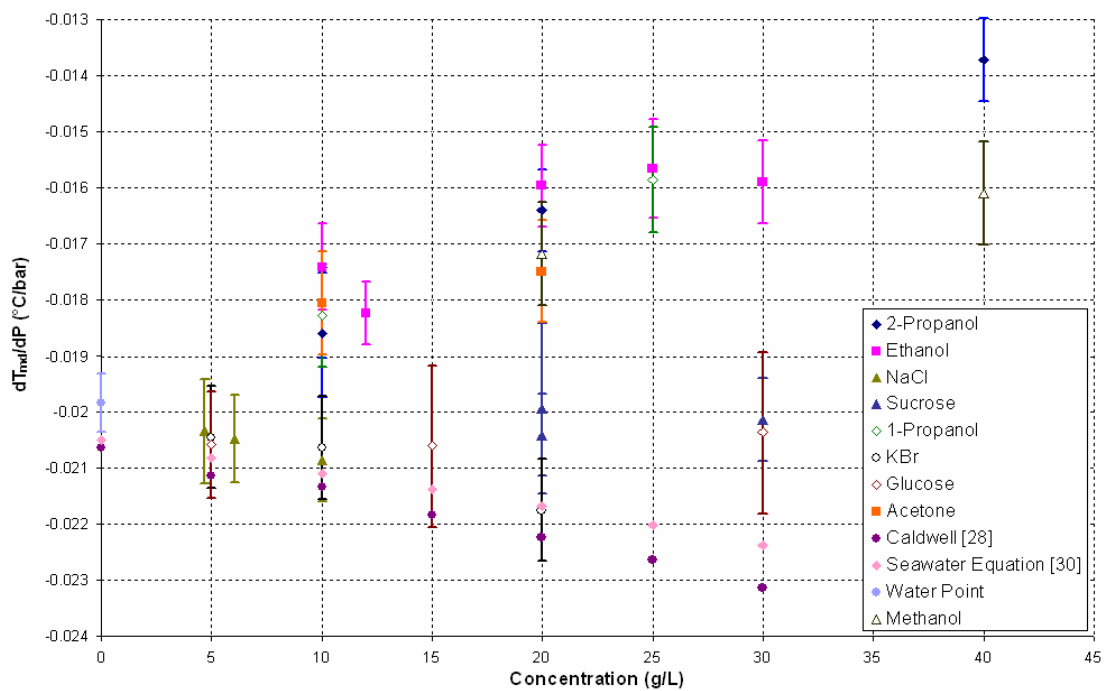


**Figure 3.6-2** *Rate of change of the temperature of maximum density with respect to applied pressure for differing concentrations (g/L) of various solutes-low concentration region.*
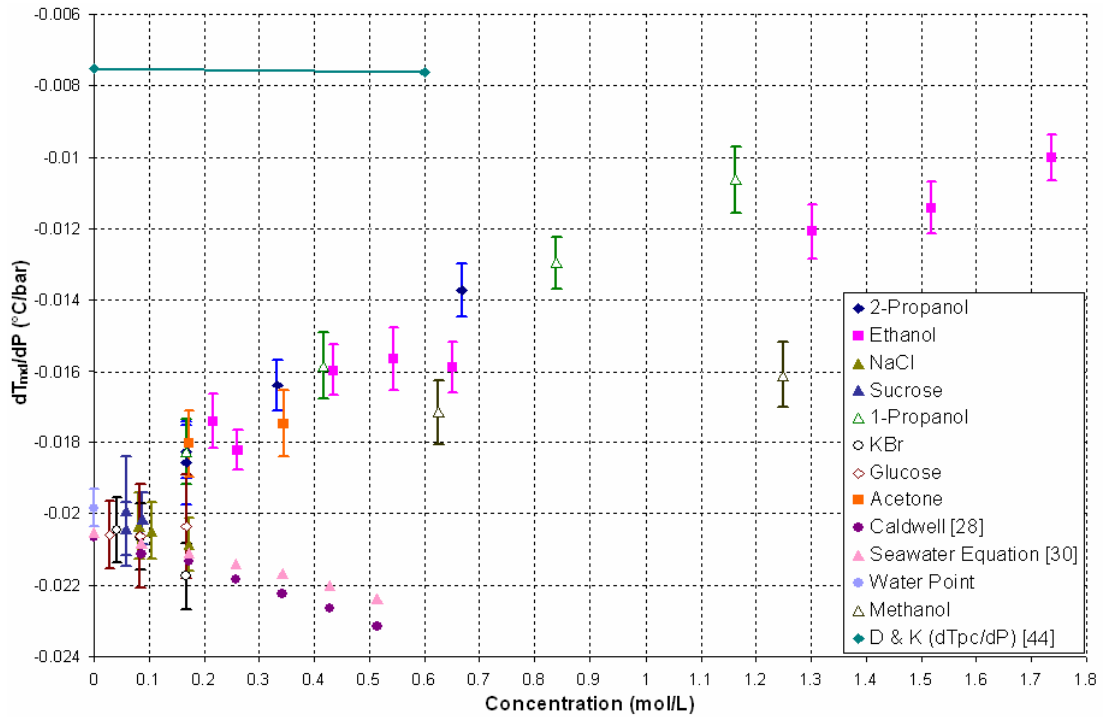
**Figure 3.6-3** *Rate of change of the temperature of maximum density with respect to applied pressure for differing concentrations (mol/L) of various solutes.*
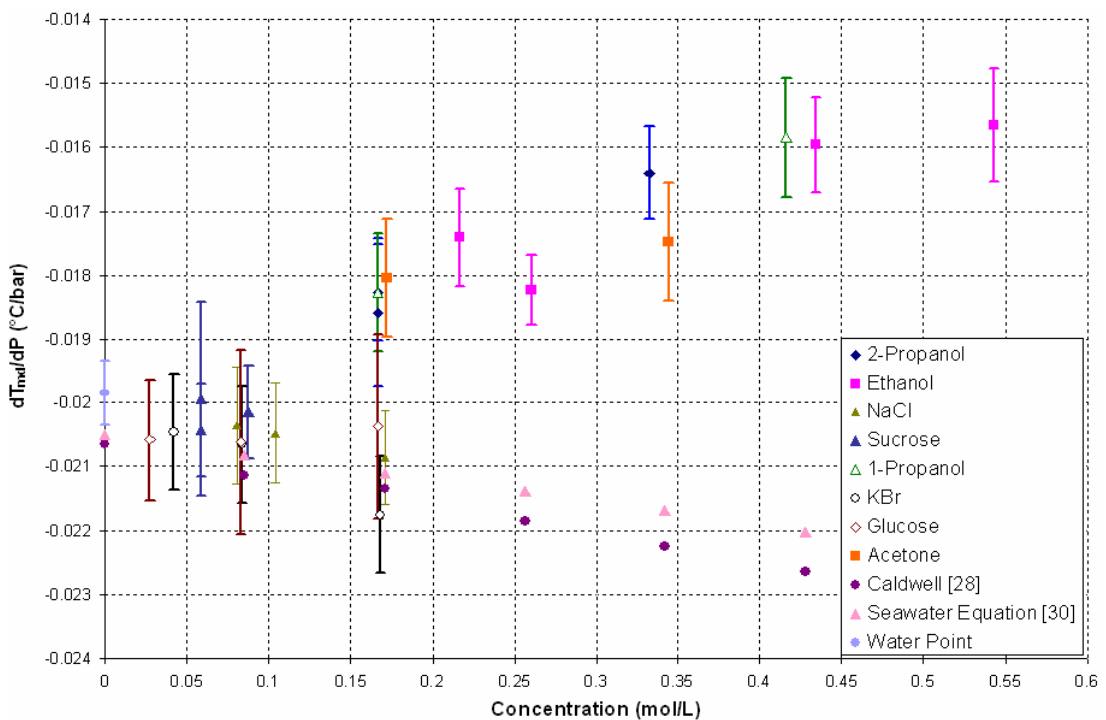


**Figure 3.6-4** *Rate of change of the temperature of maximum density with respect to applied pressure for differing concentrations (mol/L) of various solutes-low concentration region.*

Ethanol and sodium chloride solutions have been examined in a more detail outlining clearly the differences in the behaviour of the two solutes. Graphs of the temperature of maximum density versus concentration at various applied pressures were constructed from the ethanol results (figure 3.6-5). A similar graph was constructed from the salt solution results (figure 3.6-6). Ten curves and trends are shown in figures 3.6-5 and 3.6-6. Values of the temperature of maximum density were not explicitly taken for each trend but were extrapolated from the experimental data. Using least squares fitting (section 3.7) the slope and intercept of temperature of maximum density versus pressure graphs such as figure 3.4-1 were found. The slope is the rate of change of the temperature of maximum density with respect to pressure. For any concentration of solute tested a unique slope and intercept were obtained whereby:

$$\textbf{T}_{\textbf{md}}=\textbf{slope(pressure in bar)+intercept} \qquad (3.6\text{-}1)$$

For any concentration of solute tested a temperature of maximum density could be calculated at any pressure.

Figure 3.6-5 illustrates that at atmospheric pressure, i.e. the top curve at P=0 bar, the temperature of maximum density of ethanol solutions rise and then fall with increasing concentration in agreement with work done by Wada and Umeda [19]. Pressure increases from the top curve to the bottom curve. If a vertical cross-section is taken anywhere on the graph it is clear that as applied pressure increases the temperature of maximum density decreases which is also as expected. However, interestingly as concentration increases the curves come closer together. This is in agreement with figure 3.6-3. As concentration is increased the temperature of maximum density is suppressed by a lesser amount under increasing pressure as the curves are converging. Hence the rate of change of the temperature of maximum density with respect to pressure is decreasing with increasing concentration.
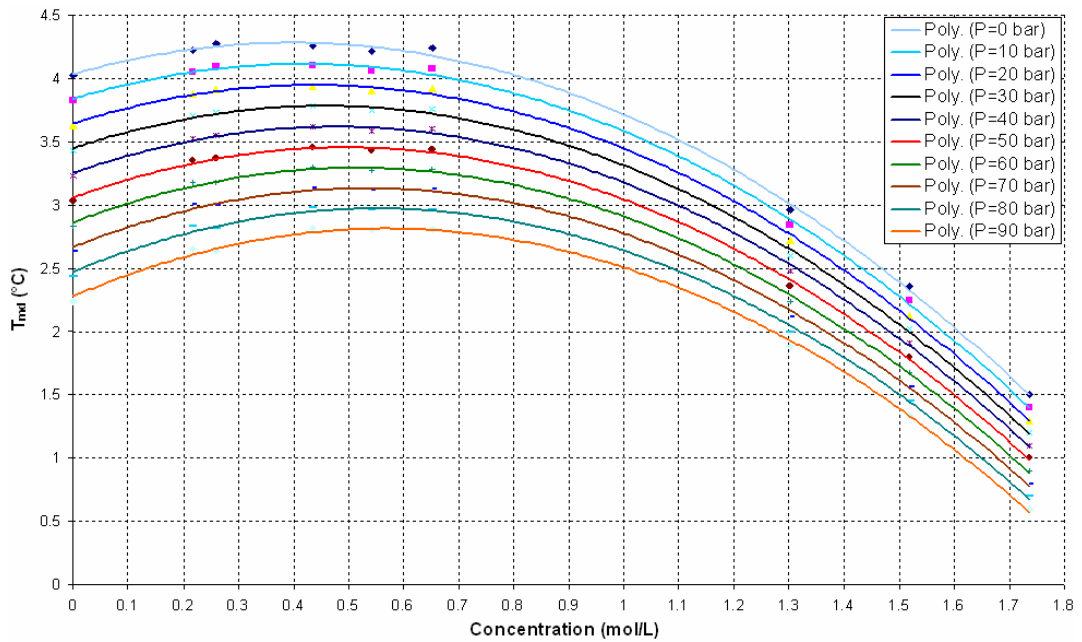
**Figure 3.6-5** *Temperature of maximum density versus concentration for ethanol solutions under various applied pressures.*

Figure 3.6-6 shows that at atmospheric pressure, i.e. the top curve at P=0 bar, the temperature of maximum density of salt solutions decreases linearly with increasing concentration in agreement with Caldwell [28]. As pressure increases from the top trend to the bottom trend if a vertical cross-section is taken anywhere on the graph it is clear that as applied pressure increases the temperature of maximum density decreases similar to ethanol solutions. However, in contrast to the behaviour of ethanol as concentration increases the trends diverge. As concentration is increased the temperature of maximum density is suppressed by a greater amount under increasing pressure as the trends are diverging. The rate of change of the temperature of maximum density with respect to pressure is increasing with increasing concentration. The linear trends in figure 3.6-6 have been extrapolated for clarity as only low salt solution concentrations were examined (figure 3.6-7).
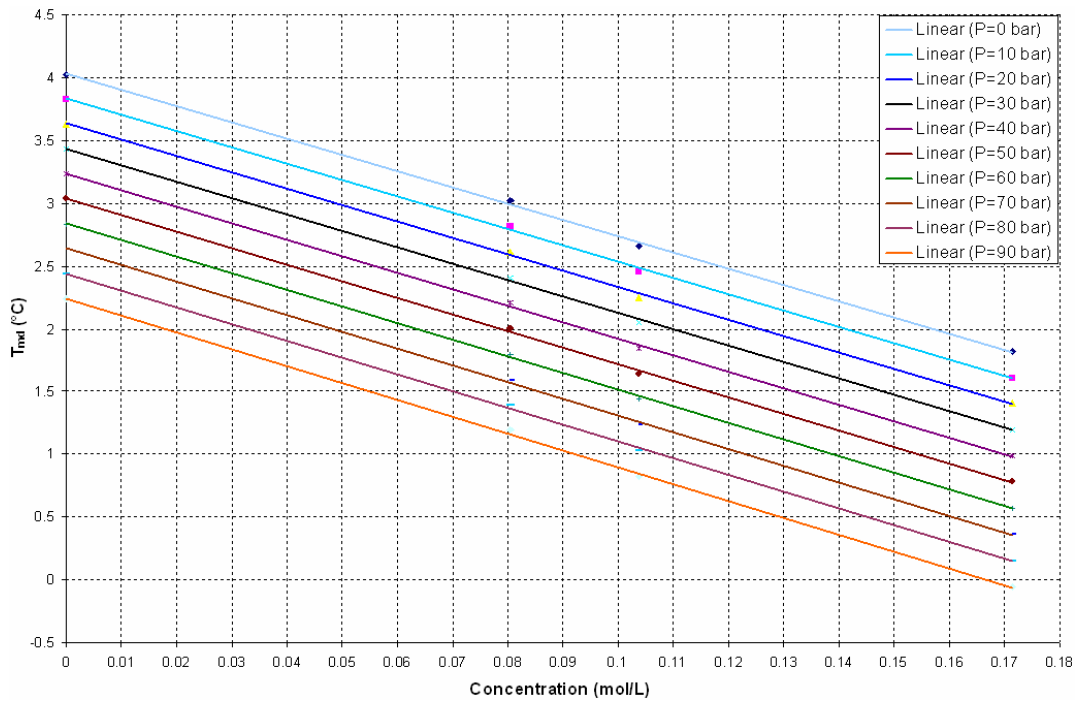
**Figure 3.6-6** *Temperature of maximum density versus concentration for sodium chloride solutions under various applied pressures.*
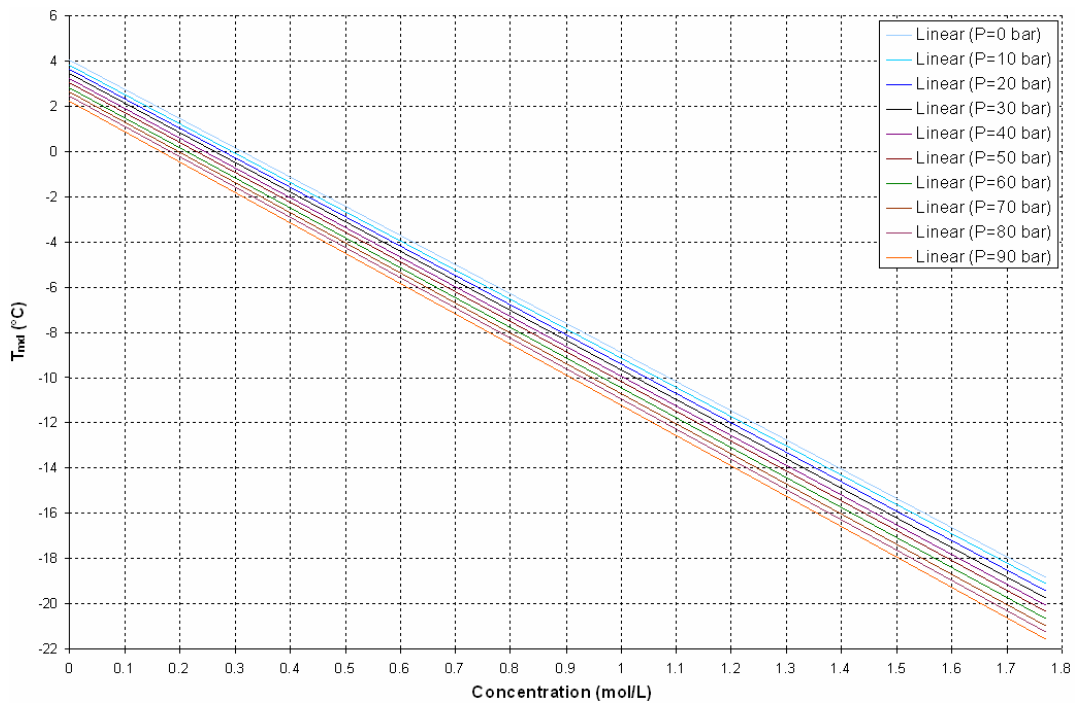


**Figure 3.6-7** *Temperature of maximum density versus concentration for sodium chloride solutions under various applied pressures (extrapolated from figure 3.5-6).*

## 3.7 Error analysis

Errors are associated with each point on the figures 3.6-1 to 3.6-4. In order to calculate these errors firstly the temperature of maximum density versus applied pressure data for pure water needed to be analysed (table 3.4-1). For each applied pressure the average value for the temperature of maximum density was calculated with a corresponding standard deviation given by:

$$s = \sqrt{\frac{1}{N-1} \sum_{i=1}^{N} (x_i - \bar{x})^2} \qquad (3.7\text{-}1)$$

Where $N$ is the number of temperature of maximum density values at a specific applied pressure, $\{x_1, x_2, ..., x_N\}$ are temperature of maximum density values and $\bar{x}$ is the average value of the temperature of maximum density at an applied pressure. Using this method the errors were calculated on the average temperature of maximum density value for each applied pressure (table 3.7-1).

| Pure water | | |
|---|---|---|
| $P_{applied}$ (bar) | $T_{md}$ (average) (°C) | Error (°C) |
| 0 | 4.043 | 0.075 |
| 10 | 3.832 | 0.035 |
| 20 | 3.63 | 0.004 |
| 30 | 3.409 | 0.065 |
| 40 | 3.237 | 0.031 |
| 50 | 3.044 | 0.0325 |
| 60 | 2.832 | 0.035 |
| 70 | 2.635 | 0.047 |

**Table 3.7-1** *Applied pressure, average temperature of maximum density values and associated errors.*

This information is graphed in figure 3.4-1. The average error from this table is 0.04 °C. This average error is typical for all experimental runs as when extracting the temperature of maximum density all runs were carried out in the same way. For all solutes tested the average temperature of maximum density for a particular

applied pressure was taken and this average value was given an error of 0.04 °C.  In
order to work out the rate of change of the temperature of maximum density with
respect to applied pressure a least squares fitting program was used.  The errors
associated with the rates of change have been calculated using the function FIT.M
that has been adapted from Press et al. [45].  The routine LEASTSQ.M calls FIT.M
and reads in applied pressures, the average values of the temperature of maximum
density and standard deviations and returns slope and intercept values with
associated errors given by the formulae:

$$Slope = \frac{\sum\left(\frac{1}{\sigma_i^2}\right)\sum\left(\frac{x_iy_i}{\sigma_i^2}\right) - \sum\left(\frac{x_i}{\sigma_i^2}\right)\sum\left(\frac{y_i}{\sigma_i^2}\right)}{\sum\left(\frac{1}{\sigma_i^2}\right)\sum\left(\frac{x_i}{\sigma_i^2}\right) - \left(\sum\left(\frac{x_i}{\sigma_i^2}\right)\right)^2} \qquad (3.7\text{-}2)$$

$$\sum\left(\frac{y_i}{\sigma_i^2}\right) = Intercept\sum\left(\frac{1}{\sigma_i^2}\right) + Slope\sum\left(\frac{x_i}{\sigma_i^2}\right) \qquad (3.7\text{-}3)$$

All summations are from $i$ to $N$.  The applied pressure values, $x_i$, are assumed to have
no associated error, $y_i$ are the average of the temperature of maximum density
values with associated standard deviations $\sigma_i$.  The program also returns errors in the
slope, intercept, a chi-squared value and a goodness of fit value.  Standard deviations
associated with the $y_i$ values for pure water are given in table 3.7-1.  This gives rise
to a rate of change of the temperature of maximum density of
$-0.0198 \pm 0.0005$ °C/bar.  Standard deviations associated with the $y_i$ values for all
solutes were set to 0.04 °C as discussed above.  All calculated slopes and associated
errors are shown on graphs 3.6-1 to 3.6-4.

The sizes of the error bars vary due to the linearity of the temperature of maximum
density versus applied pressure graphs such as figure 3.4-1.  If these points were
scattered a large error would be obtained in the slope reading using the least squares
fitting routine.  The points could be scattered due to slightly inaccurate temperature
of maximum density values.  These values were extracted from ramp runs using an

area integration technique discussed in section 3.1.  If anomalies were unusual in shape or not approximately a parallelogram then the temperature of maximum density would not have bisected the anomaly feature.  Misshapen anomalies therefore gave rise to large errors in the rate of change of the temperature of maximum density with respect to applied pressure.  The 30 g/L glucose point on figures 3.6-1 and 3.6-2 is an example of a point with a large error due to this effect.

Note that all errors on graphs 3.6-1 to 3.6-4 have been calculated individually from information extracted from separate ramp runs at differing solute concentrations.  For this reason, it is possible that trends in graphs 3.6-1 to 3.6-4 may appear linear but still have relatively large uncertainties associated with the individual points (the sodium chloride trend is an example of such a case).  Equations 3.7-2 and 3.7-3 can be used to calculate the slope and intercept with associated errors for all trends in figures 3.6-1 to 3.6-4 where the concentration values, $x_i$, are assumed to have no associated error, $y_i$ are the rates of change of the temperature of maximum density with respect to applied pressure with associated standard deviations $\sigma_i$.  This analysis has been carried out on the sodium chloride trend as discussed in section 3.5-1.

# Chapter 4

# Macroscopic Modelling

## 4.1 Introduction

In macroscopic models solutions are assumed to be "ideal" meaning that there are no interactions between the water and solute molecules. In order to conduct this study density information for pure water and the solute under test was needed. The seawater equation of state has been used to model the density behaviour of pure water [30]. This function returns the density of water for a given salinity, temperature and pressure. For the macroscopic approach the salinity variable has been set to zero throughout. State functions for pure ethanol were obtained from work conducted by Dillon and Penoncello [46]. The density of pure acetone was modelled from work carried out by Lago and Albo [47]. The phase change behaviour of pure water, ethanol and acetone has also been studied. The phase change behaviour of pure water has been studied by Fofonoff and Millard [30]. The phase change behaviour of pure ethanol and acetone has been carried out by Sun et al. [48] and Richter and Pistorius respectively [49]. Investigating the phase change is important as models need to be able to replicate the behaviour of the temperature of maximum density and the phase change. Some solutes such as sodium chloride display a decrease in the temperature of maximum density and the phase change with increasing solute concentration. However, solutes such as ethanol display an increase in the temperature of maximum at low concentration whereas the phase change temperature decrease with increasing concentration for all solutes. Models need to replicate this unusual and contrasting behaviour.

## 4.2 Density of pure water and solutes under applied pressure

Using the seawater equation of state, density has been plotted against temperature at various applied pressures for pure water (figure 4.2-1). The values of the temperature of maximum density at the applied pressures were extracted. By graphing applied pressures against temperatures of maximum density the rate of change of the temperature of maximum density with respect to pressure was calculated to be -0.0205 °C/bar. This point is the pure water point for the seawater equation. (figures 3.6-1 to 3.6-4). Using information from Dillon and Penoncello similar plots can be made to model the behaviour of the density of pure ethanol at

various applied pressures (figure 4.2-2).  Similarly, figure 4.2-3 shows density profiles for pure acetone at applied pressures as derived from information in the 2009 Lago and Albo paper.  For both ethanol and acetone at applied pressure the density decreases linearly with increasing temperature.  At fixed temperature the density of both solutes increases with increasing pressure.  No density maximum is visible for these trends unlike the density profiles for pure water.
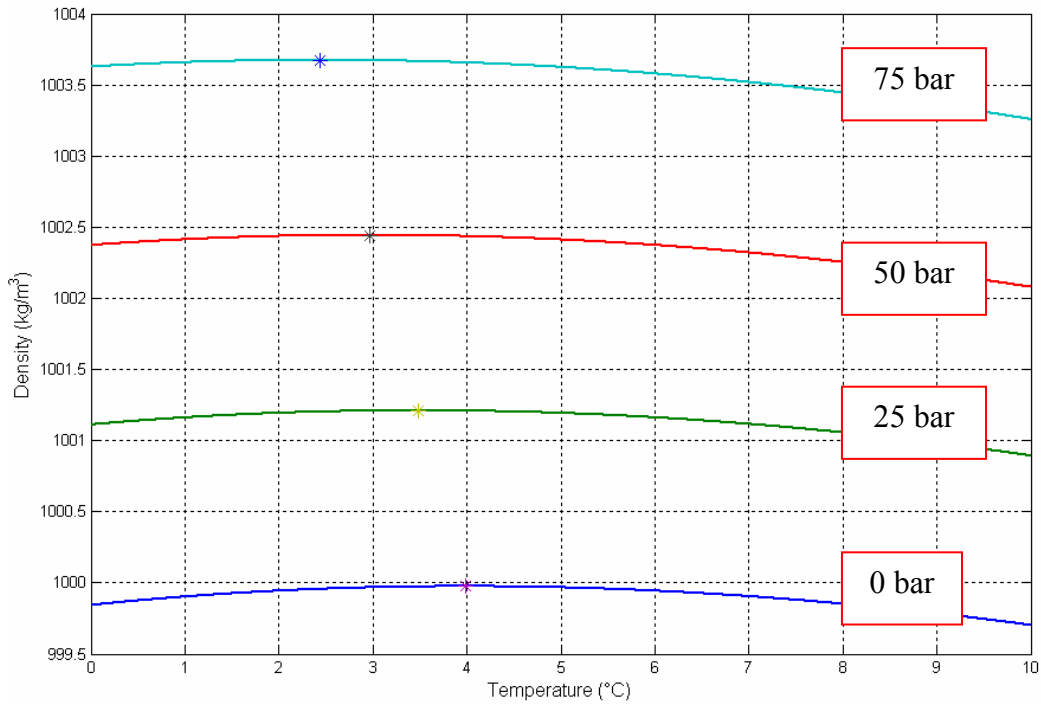


**Figure 4.2-1** *Density versus temperature profiles at various applied pressures for pure water using the seawater state equation [30]. Density maxima are denoted by '\*'.*
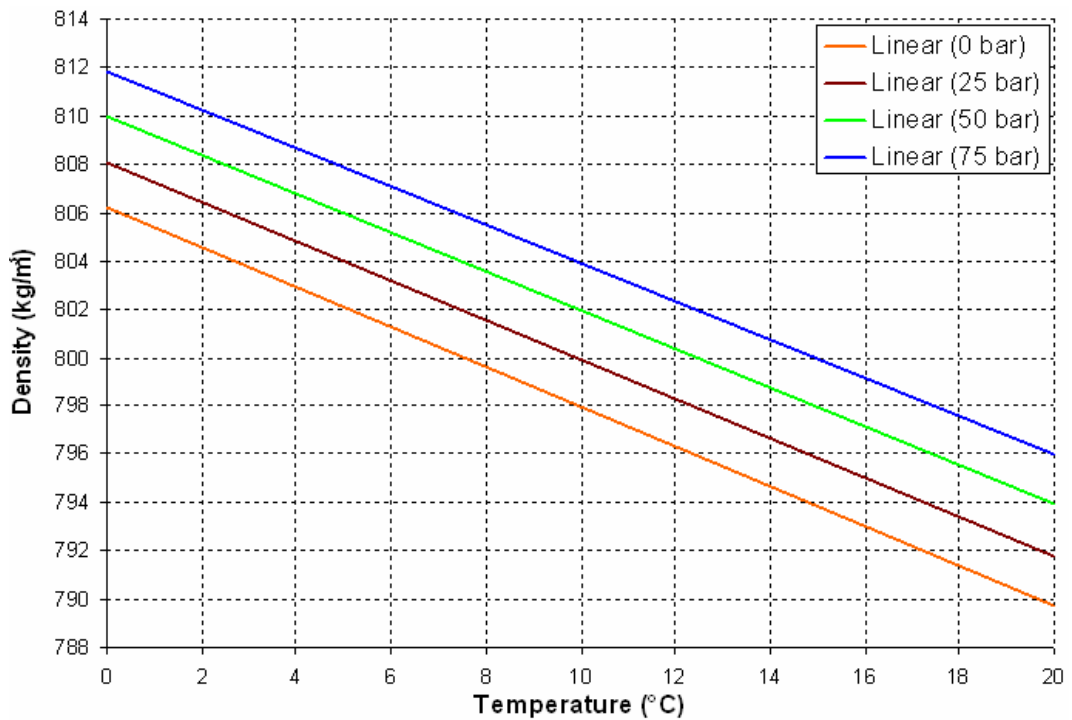
**Figure 4.2-2** *Density versus temperature profiles at various applied pressures for pure ethanol. The data for all trends has been derived from Dillon and Penoncello [46].*
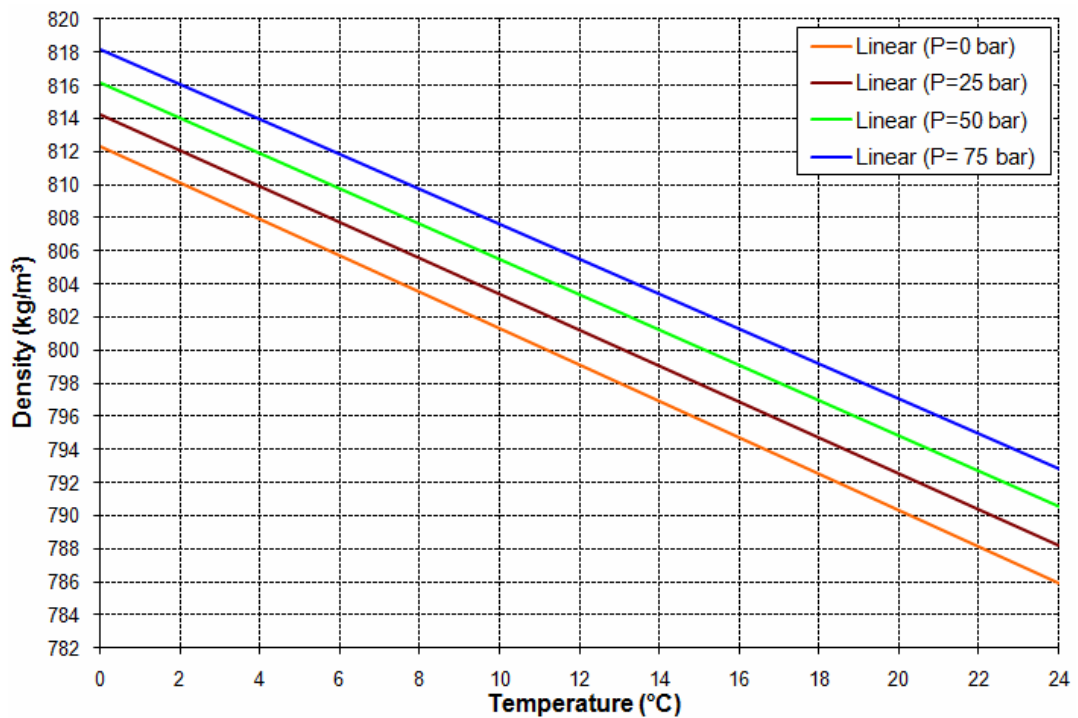


**Figure 4.2-3** *Density versus temperature profiles at various applied pressures for pure acetone. The data for all trends has been derived from Lago and Albo [47].*

## 4.3 Macroscopic modelling of the behaviour of the density maximum of mixtures

By combining the state functions for pure water with those for pure ethanol and acetone at specific applied pressures (0 bar, 25 bar, 50 bar and 75 bar), density versus temperature profiles were obtained for "ideal" mixtures of pure water and the solute under test. It was assumed that the density of an aqueous solution was equal to the density of the water plus the density of the solute added. This assumption was only used for low concentrations. The total density at a fixed applied pressure and T °C is given by:

$$\rho = x\rho_s(T) + (1-x)\rho_w(T) \tag{4.3-1}$$

where $\rho_s$ is the density of the solute at T °C in $kgm^{-3}$, $\rho_w$ is the density of water at T °C in $kgm^{-3}$ and $x$ is the percentage of solute concentration. The solute density $(\rho_s)$ was found to decrease linearly under increasing temperature (figures 4.2-2 and 4.2-3) and the the density of water $(\rho_w)$ was given by the seawater equation [30]:

$$\rho_s = aT + b \tag{4.3-2}$$

$$\rho_w = \rho(0, T, P) \tag{4.3-3}$$

where $a$ and $b$ are constants and $P$ is pressure in decibars. There were a different set of constants ($a$ and $b$) for each solute at each fixed pressure. From the density versus temperature profiles the rates of change of the temperature of maximum density with respect to pressure were calculated for various percentages of ethanol or acetone and water. An example of results from an 8% ethanol and 92% water is shown in figure 4.3-1. The rate of change of the temperature of maximum density with respect to pressure for this combination is -0.0195 °C/bar. Results from all "ideal" mixtures of ethanol and pure water are summarised in figure 4.3-2. Results from all "ideal" mixtures of acetone and pure water are shown in figure 4.3-3.
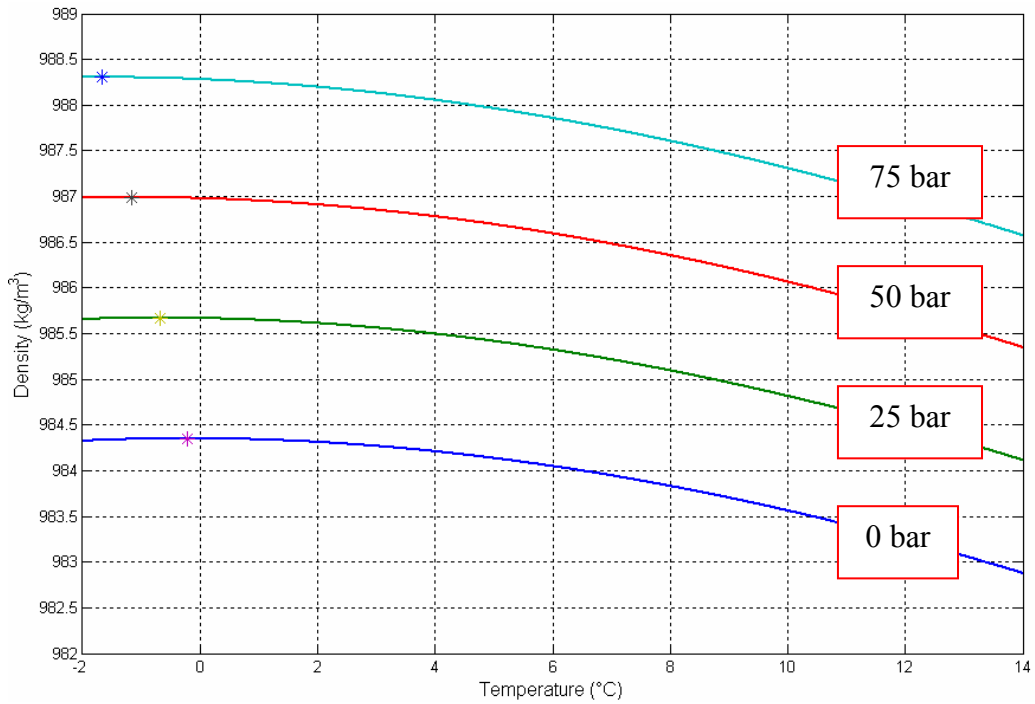
**Figure 4.3-1** *Density versus temperature profiles at various applied pressures for 8% ethanol and 92% water using combined state functions. Density maxima are denoted by '∗'.*
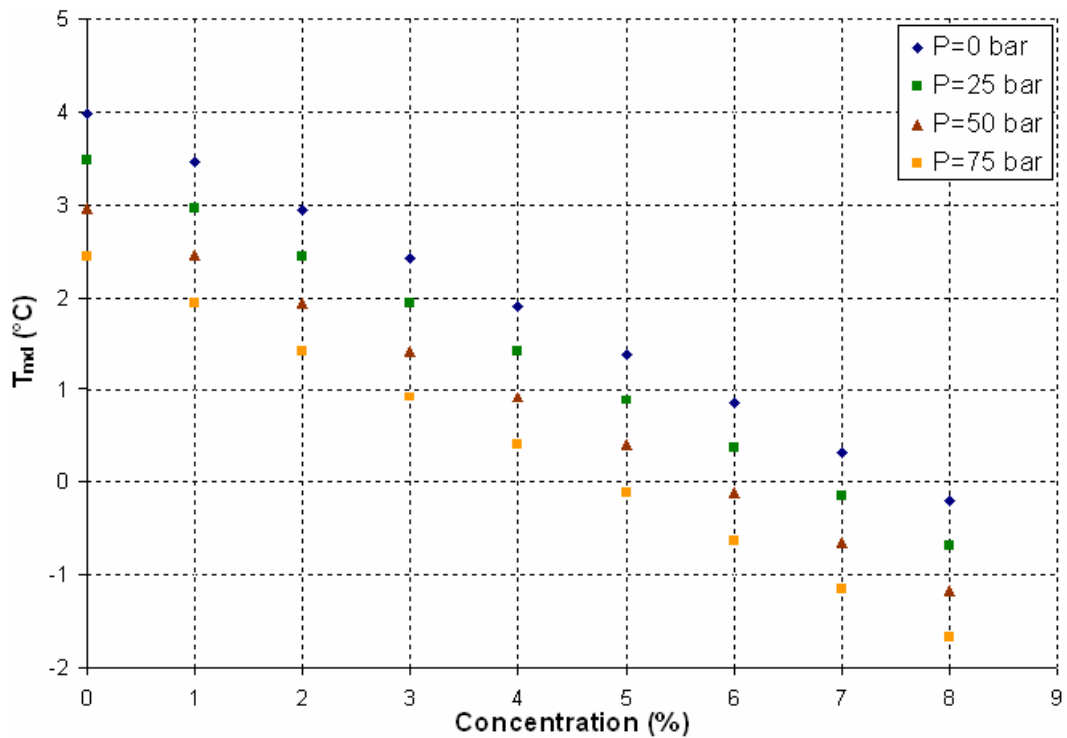


**Figure 4.3-2** *Temperature of maximum density versus concentration for "ideal" mixtures of pure water and ethanol under applied pressures.*
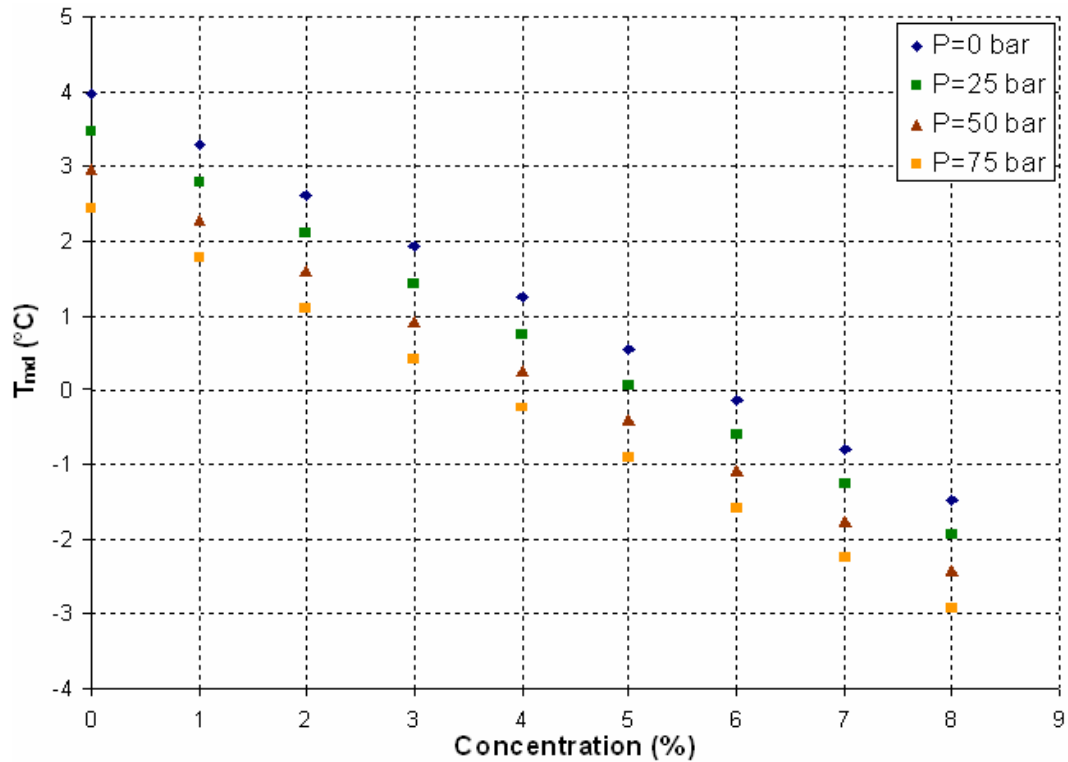
**Figure 4.3-3** *Temperature of maximum density versus concentration for "ideal" mixtures of pure water and acetone under applied pressures.*

Figures 4.3-2 and 4.3-3 show that at fixed concentration the temperature of maximum density is shifted to lower values with increasing pressure as expected. At fixed pressure the temperature of maximum density decreases linearly as concentration increases. This is not the case experimentally for ethanol solutions. In reality at low concentrations and at fixed pressure ethanol solutions display an increase in the temperature of maximum density followed by a decrease in the temperature of maximum density at higher concentrations. The macroscopic model does not predict this initial rise in the temperature of maximum density for low concentrations as interactions between molecules have been ignored in the macroscopic model. Figure 4.3-4 compares linear trends for ethanol from the macroscopic approach to experimental results. The non-linear curves have been derived from experimental data. Acetone solutions display a linear decrease in the temperature of maximum density at fixed pressures as a function of concentration experimentally and macroscopically. However, experimental trends are steeper than corresponding macroscopic trends (figure 4.3-5).
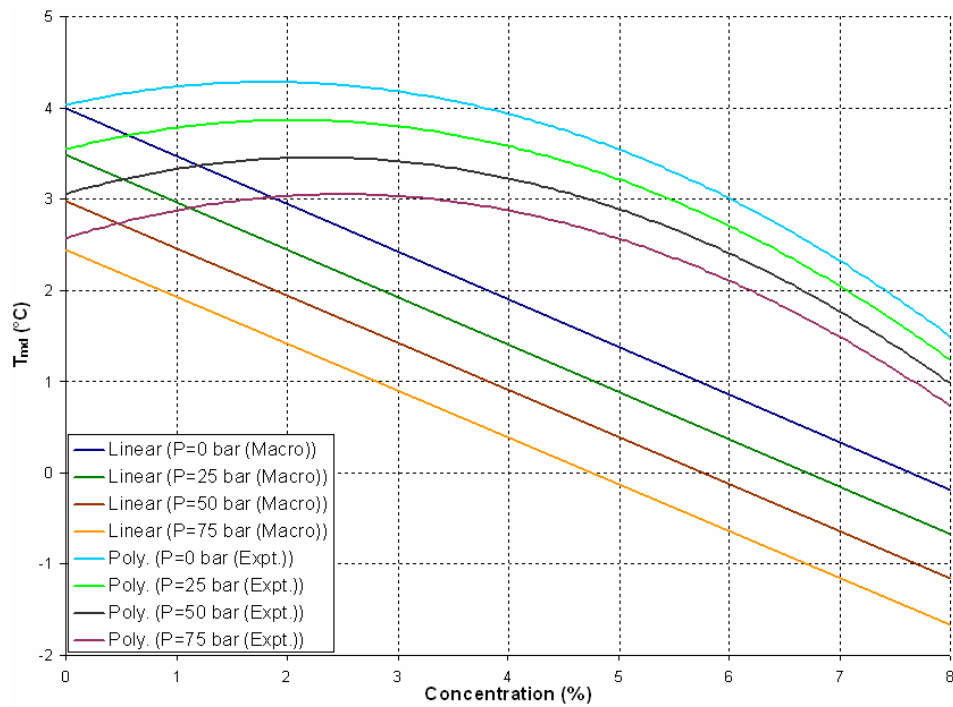
**Figure 4.3-4** *Temperature of maximum density versus concentration behaviour for ethanol solutions under fixed pressures derived from experimental results and the macroscopic model.*
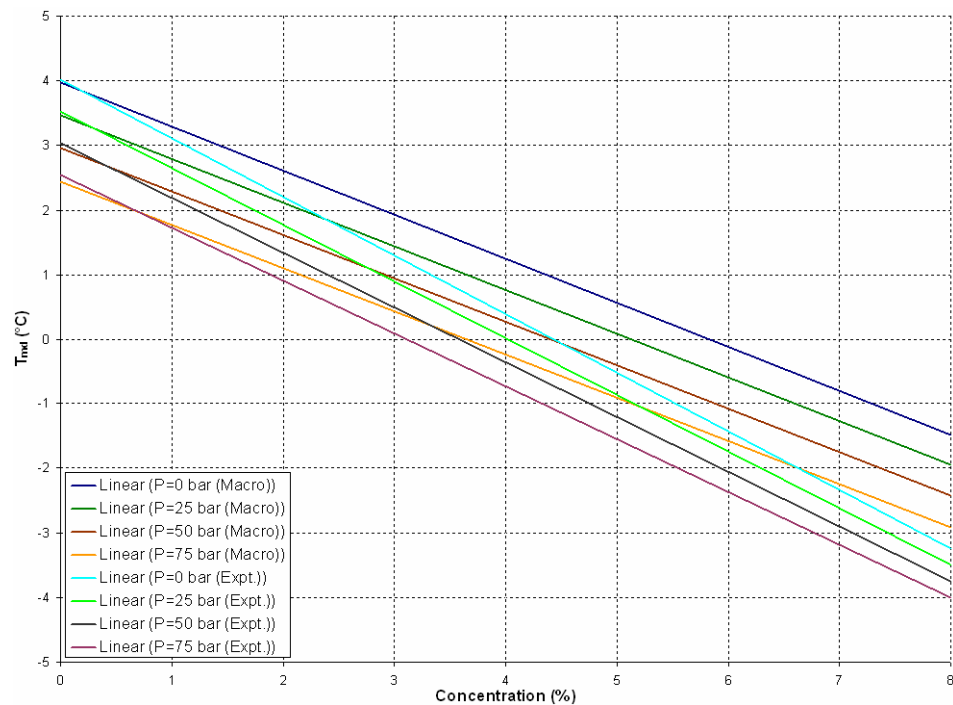


**Figure 4.3-5** *Temperature of maximum density versus concentration behaviour for acetone solutions under fixed pressures derived from experimental results and the macroscopic model.*

Various "ideal" mixtures have been investigated in the range from pure water to an 8% solute and 92% pure water mixture. This range was chosen as experimental runs have been conducted over approximately the same range of solute concentration. The rate of change of the temperature of maximum density with respect to applied pressure has been plotted against concentration of solute (figure 4.3-6). The rates of change derived from macroscopic investigations become less steep with respect to pure water as concentration increases. The trend for "ideal" acetone mixtures is slightly steeper than the trend for "ideal" ethanol mixtures but both "ideal" trends are significantly less negative than experimental results (figure 4.3-7). The reason for this could be that "ideal" mixing is assumed in the macroscopic approach and hence interactions between molecules are completely neglected. The concentration values for the experimental results were converted to a percentage by dividing the concentrations in grams by 10. This is an approximation.
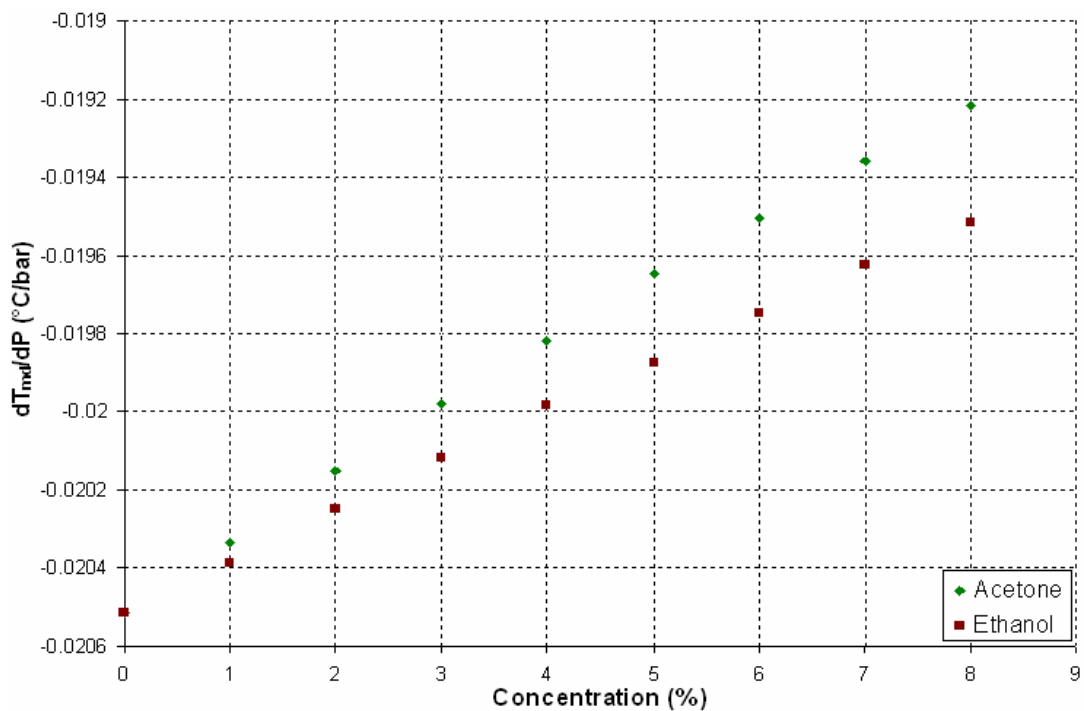


**Figure 4.3-6** *Rate of change of the temperature of maximum density with respect to applied pressure for differing "ideal" mixtures of ethanol and water and acetone and water. The zero concentration point in this graph is derived from the seawater equation [30].*
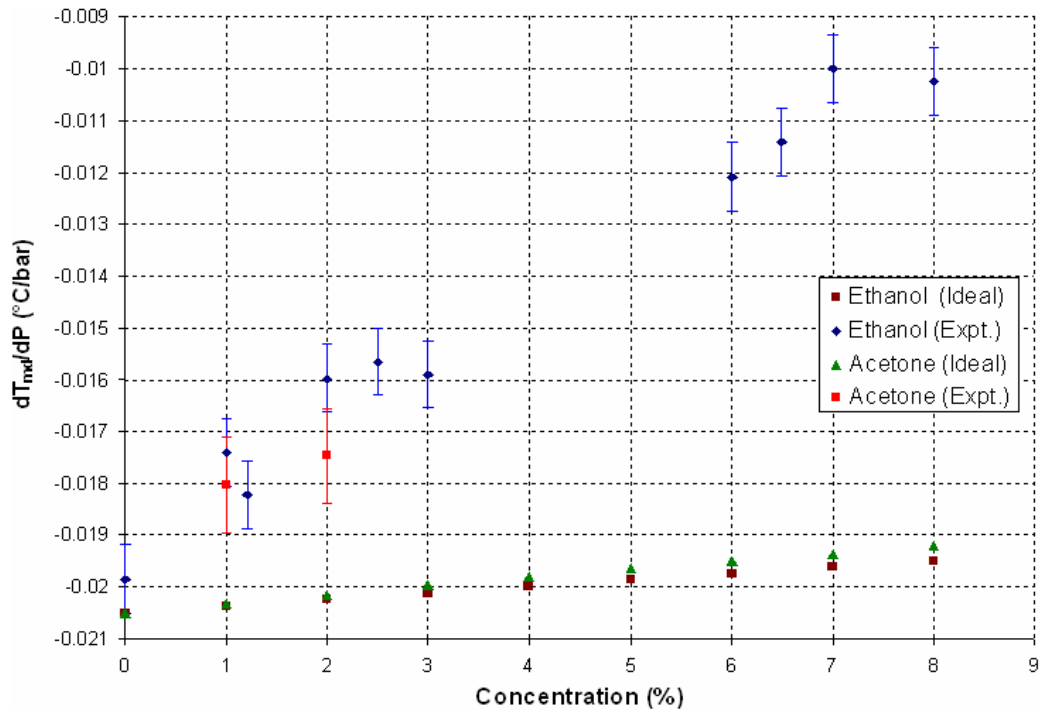
**Figure 4.3-7** *Rate of change of the temperature of maximum density with respect to applied pressure for differing concentrations of ethanol (ideal and experimental) and acetone (ideal and experimental). There is a slight difference between the measured zero concentration point and the point derived from the seawater equation (see figure 3.5-2).*

## 4.4 The phase change of pure water and solutes as a function of pressure

A seawater equation that returns a freezing point temperature for a given salinity and pressure as compiled by Fofonoff and Millard was employed [30]. For the macroscopic approach the salinity variable has been set to zero throughout. The temperature of the phase change for pure water has been plotted against pressure using this freezing point equation (figure 4.4-1). On this graph the behaviour of the temperature of maximum density for pure water with increasing pressure has been added showing that the temperature of the phase change and the temperature of maximum density intersect at an applied pressure of about 270 bar.
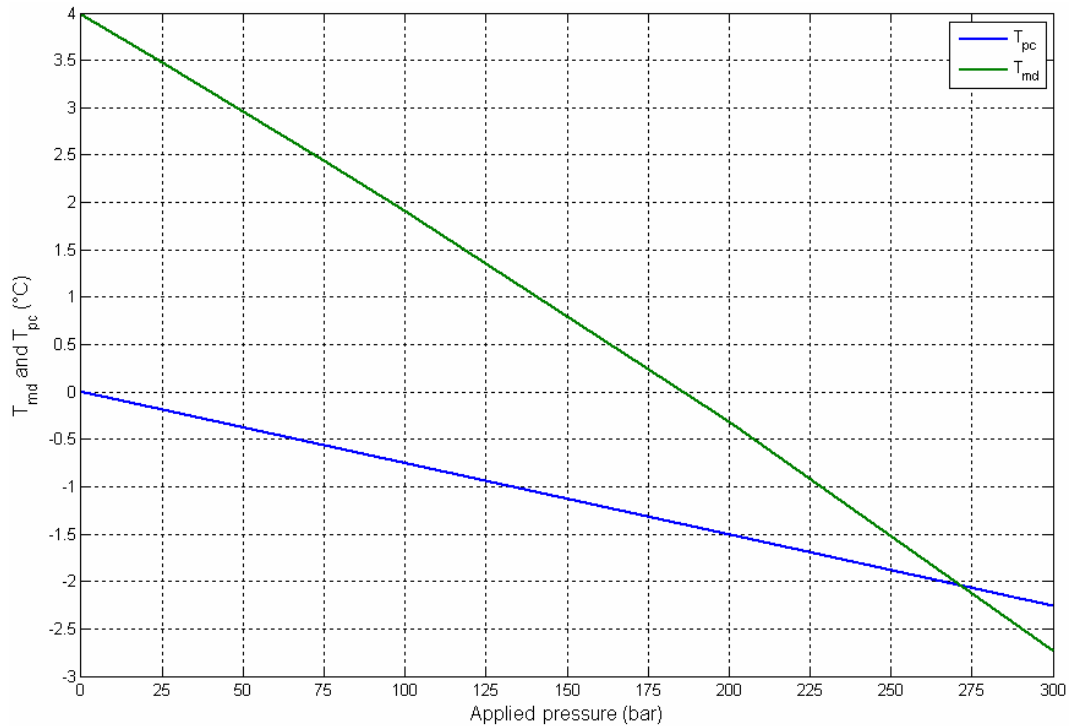
**Figure 4.4-1** *The temperature of maximum density and the temperature of the phase change plotted against pressure for pure water. Both trends have been derived using seawater equations as given in [30].*

A function was used to model the behaviour of the freezing point of pure ethanol under pressure. This function was derived from work conducted by Sun et al. [48]. The temperature of the phase change for pure ethanol has been plotted against pressure using this function (figure 4.4-2). Another function was used to model the behaviour of the freezing point of pure acetone under pressure. This function was derived from work conducted by Richter and Pistorius [49]. The behaviour of the freezing point of pure acetone with respect to pressure is shown in figure 4.4-3. Unlike pure water the freezing point of pure ethanol and pure acetone increase as pressure increases. The lowering of the freezing point of water under pressure (pressure melting) is one of the many water anomalies.
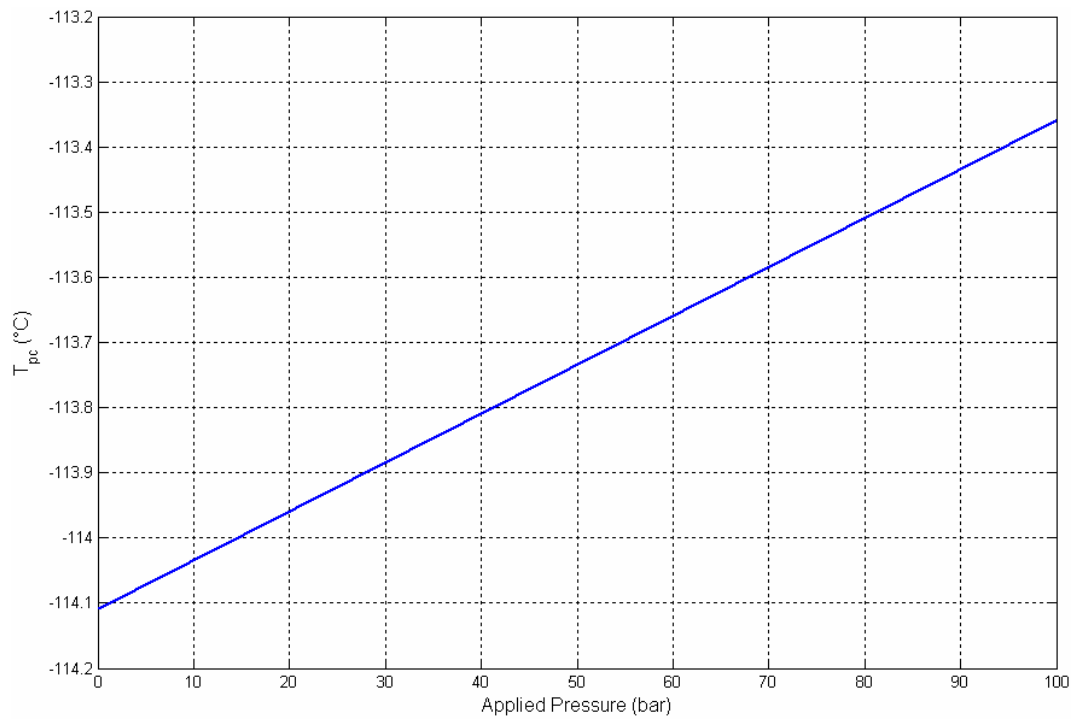
**Figure 4.4-2** *Temperature of the phase change plotted against pressure for pure ethanol.  The data for this trends has been derived from Sun et al. [48].*
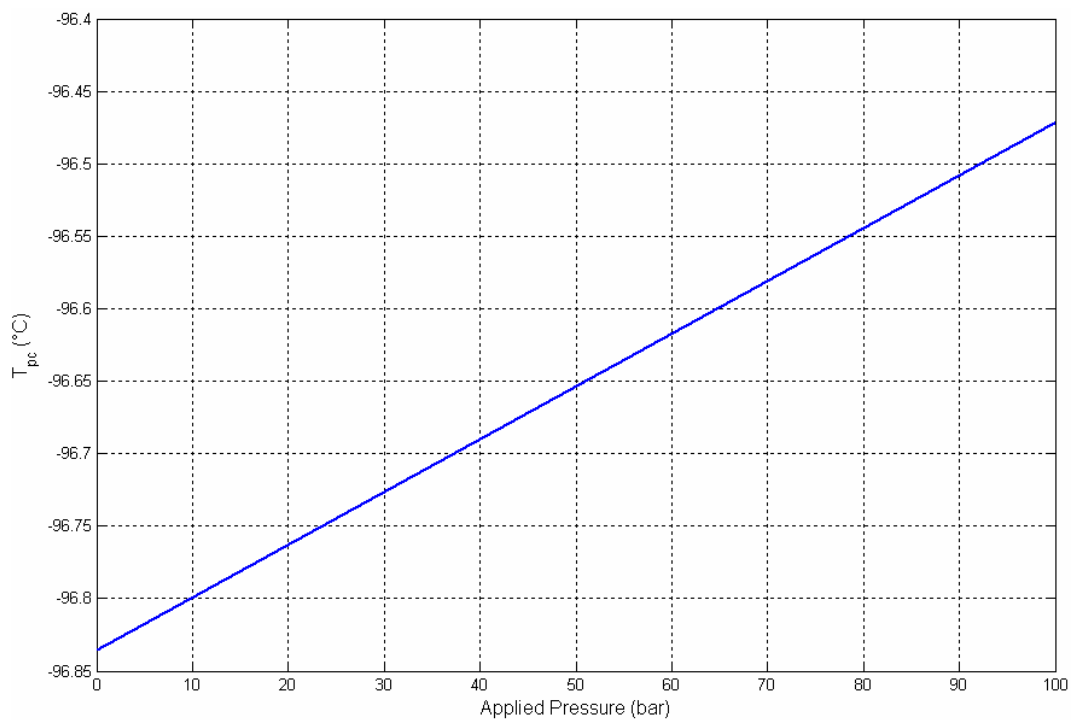


**Figure 4.4-3** *Temperature of the phase change plotted against pressure for pure acetone. The data for this trend has been derived from Richter and Pistorius [49].*

## 4.5 Macroscopic modelling of the phase change of mixtures

The functions governing the temperature of the phase change of pure water and pure ethanol and acetone under applied pressure were combined. The temperature of the phase change of a mixture at $P$ bar is given by:

$$T_{pc} = xT_{pc(s)}(P) + (1-x)T_{pc(w)}(P) \qquad (4.5\text{-}1)$$

where $T_{pc(s)}$ is the phase change temperature of the solute, $T_{pc(w)}$ is the phase change temperature of water and $x$ is the percentage of solute concentration. The behaviour of the phase change temperature of the solute is given by the equation of a line and the temperature of the phase change of water was given by a freezing point equation obtained from [30]:

$$T_{pc(s)} = aP + b \qquad (4.5\text{-}2)$$

$$T_{pc(w)} = sw\_fp(0, P*10) \qquad (4.5\text{-}3)$$

where $a$ and $b$ are constants and $P$ is pressure in bar. The function $sw\_fp$ refers to the seawater freezing point. This function returns the freezing point temperature in degrees Celsius for given pressure and salinity values. In this study salinity has been set to zero as only pure water mixtures were investigated. There were a different set of constants ($a$ and $b$) for each solute. Results from all "ideal" mixtures of ethanol and pure water solutions are summarised in figure 4.5-1. Results from all "ideal" mixtures of acetone and pure water solutions are shown in figure 4.5-2.
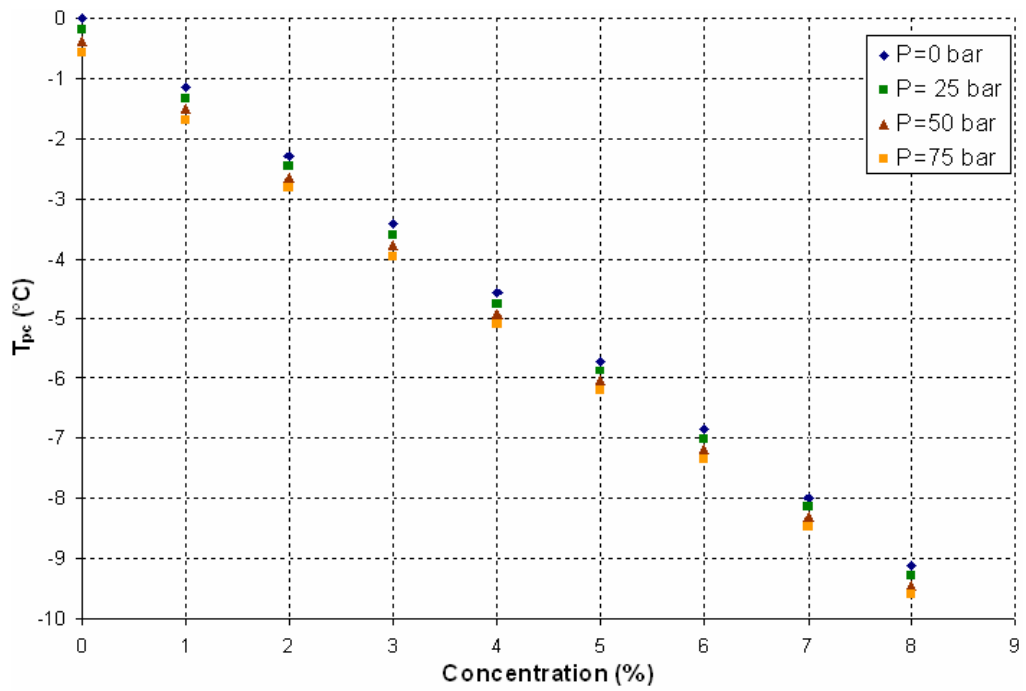
**Figure 4.5-1** *Temperature of the phase change versus concentration for " ideal" mixtures of pure water and ethanol under applied pressures.*
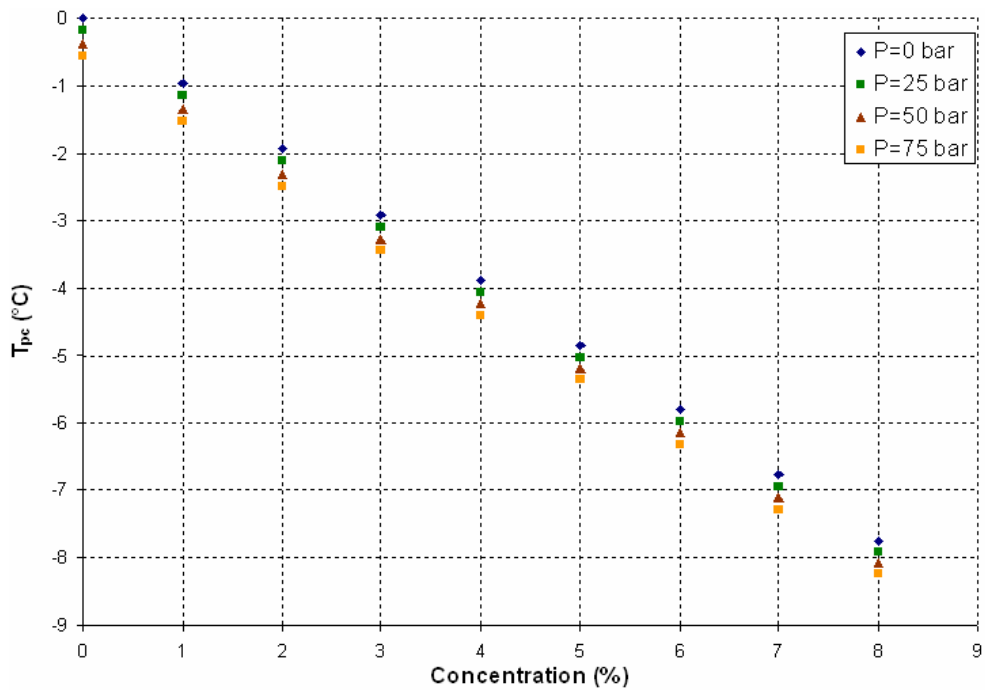


**Figure 4.5-2** *Temperature of the phase change versus concentration for " ideal" mixtures of pure water and acetone under applied pressures.*

Figures 4.5-1 and 4.5-2 show that at fixed concentration the temperature of the phase change is shifted to lower values with increasing pressure as expected. At fixed

pressure the temperature of the phase change decreases linearly as concentration increases using the macroscopic model. Experimentally at atmospheric pressure the temperature of the phase changes of ethanol and acetone solutions decrease linearly with increasing concentration. This linearity is predicted by the macroscopic model for both solutes tested but the rate of suppression of the phase change experimentally is not as steep as predicted by the macroscopic models. Experimental data from the CRC Handbook [6] relating to the temperature of the phase change of ethanol as a function of concentration at atmospheric pressure has been compared to the atmospheric pressure (P=0 bar) trend from macroscopic studies (figure 4.5-3). A similar graph compares the experimental and macroscopic behaviour of the phase change of acetone at atmospheric pressure (figure 4.5-4). Data pertaining to the phase change of ethanol and acetone soltutions at pressures other than atmospheric pressure could not be found. For this reason only concentration trends at atmospheric pressure have been included in figures 4.5-3 and 4.5-4.
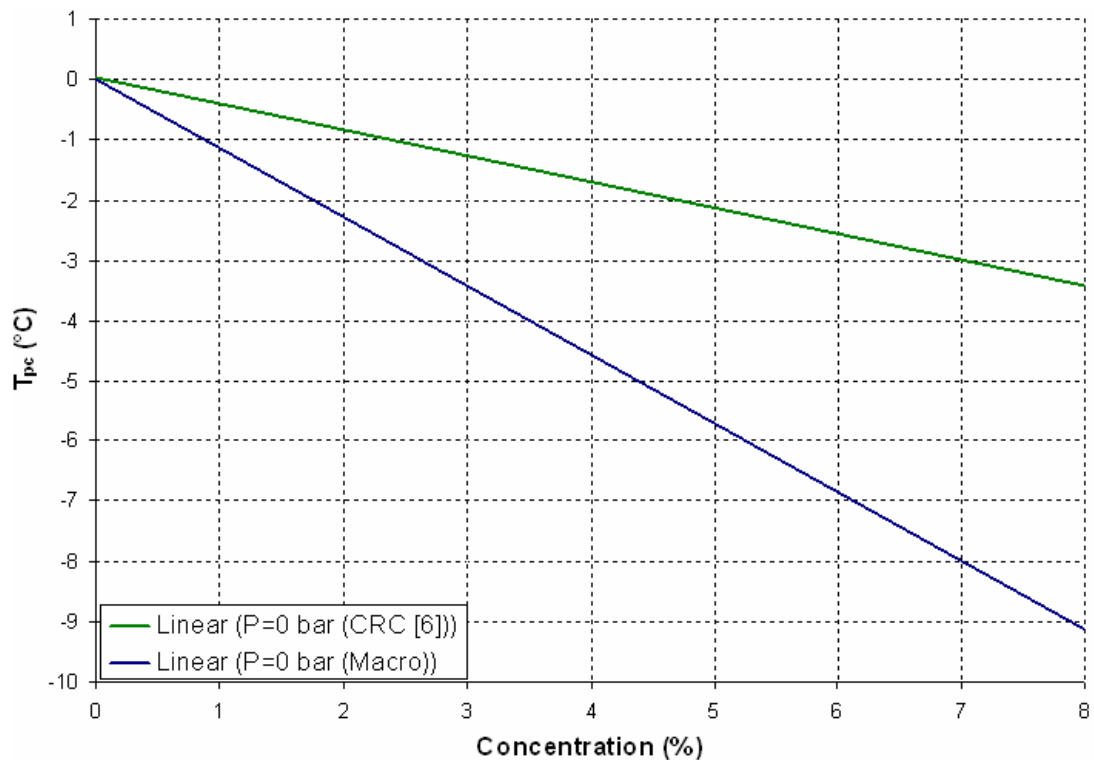


**Figure 4.5-3** *Temperature of the phase change versus concentration behaviour for ethanol solutions using experimental data and the macroscopic model at atmospheric pressure.*
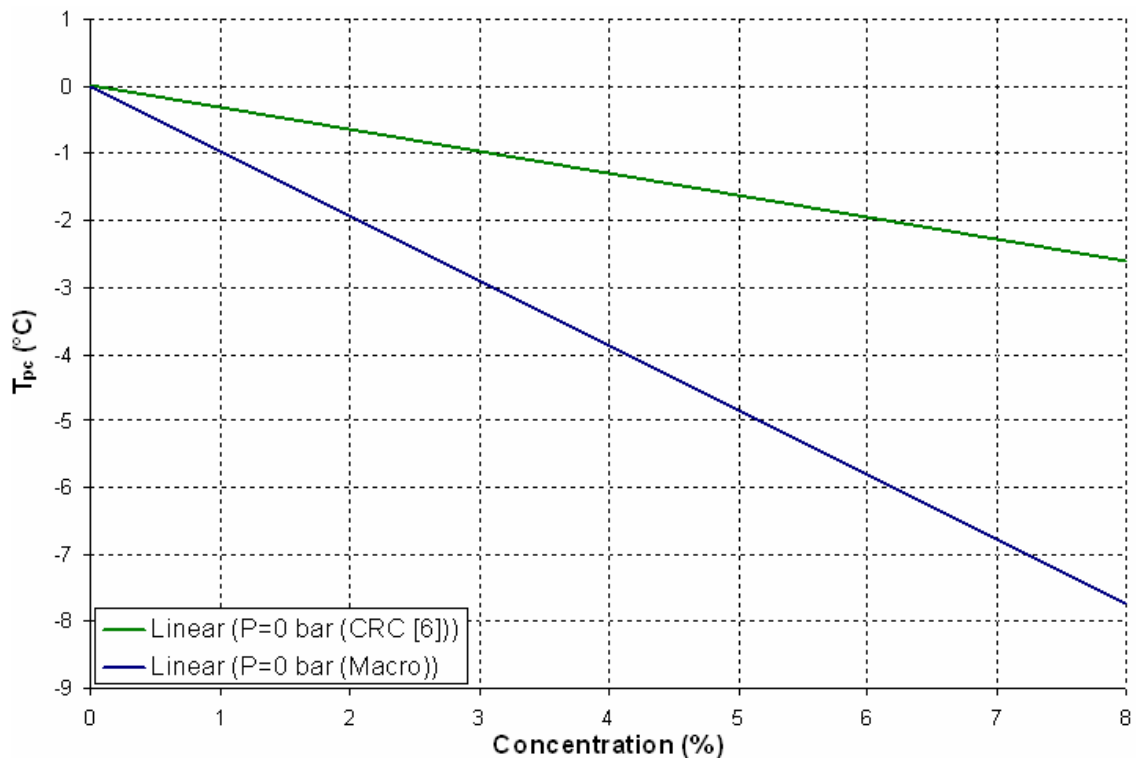
**Figure 4.5-4** *Temperature of the phase change versus concentration behaviour for acetone solutions using experimental data and the macroscopic model at atmospheric pressure.*

The rate of change of the temperature of the phase change with respect to pressure has been plotted against concentration of solute in figure 4.5-5. The trends derived from macroscopic investigations become less steep with respect to pure water as concentration increases. The trend for "ideal" ethanol mixtures is slightly steeper than the trend for "ideal" acetone mixtures. This is in contrast to the behaviour of the rate of change of the temperature of maximum density with respect to pressure for the "ideal" mixtures. The trend for "ideal" acetone mixtures is slightly steeper than the trend for "ideal" ethanol mixtures in relation to the rate of change of the temperature of maximum density (figure 4.3-6). To the author's knowledge there has been no experimental work carried out to date on the phase change of ethanol and acetone solutions under applied pressures. Only the phase change behaviour of saline solutions has been studied as a function of pressure [44]. For this reason the trends in figure 4.5-5 cannot be compared to experimental data.
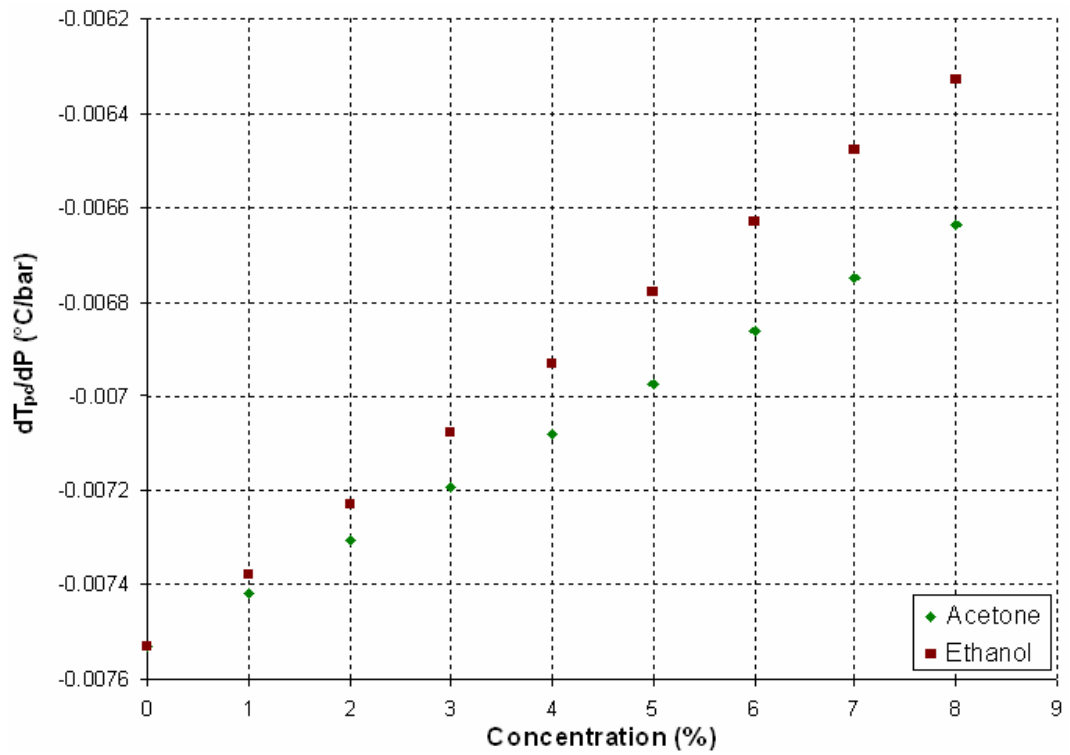
**Figure 4.5-5** *Rate of change of the temperature of the phase change with respect to pressure for differing "ideal" mixtures of ethanol and water and acetone and water. The graph only includes results from the macroscopic model.*

# Chapter 5

# Microscopic Modelling

## 5.1 Introduction

Molecular simulations can be broken down into two main approaches. These approaches are molecular dynamics and the Monte Carlo method. The molecular dynamics deterministic approach simulates the time evolution of the molecular system and tracks the actual trajectories of the molecules in the system. In a molecular dynamics simulation an initial set of molecule positions and molecule velocities are set up. Based on the potential energy function components of the force acting on the molecule are calculated and using Newton's second law the acceleration of the molecule is found. From this acceleration value the velocity of the molecule at the next time step can be calculated. Thus, a molecule's position and velocity can be calculated at any moment in time from the molecule's position, velocity and acceleration at the previous time step. By integrating these infinitesimal steps the trajectory of the system for any desired time range can be calculated. In molecular dynamics the systems are computationally very complex and often require long times and enormous amounts of processor power to achieve meaningful results [50]. For these reasons the Monte Carlo method was mainly used in this study.

In the Monte Carlo approach a large number of geometries of the system are constructed and the potential energy function is calculated in turn for each of them. Geometries are accepted or rejected before a new geometry is tested. In this way a system evolves giving data that is used to calculate thermodynamic properties of the system. In contrast to molecular dynamics the Monte Carlo approach is stochastic rather than deterministic and does not allow for time evolution of the system. However, this does not necessarily mean that the molecular dynamics approach is better at deriving the thermodynamic properties of systems. Many problems are approached more efficiently using the Monte Carlo method. The Monte Carlo approach was mainly used in this work as it was far more efficient, less computationally demanding and yielded meaningful results. The Monte Carlo approach can be realised in many ways. The most popular way of realising the Monte Carlo method is the Metropolis method which was explored. The Wang-Landau approach was also investigated. The Wang-Landau approach is a very powerful and useful approach which will be discussed in detail in section 5.4. A

chart summarising the approaches investigated in microscopic studies is shown in figure 5.1-1.
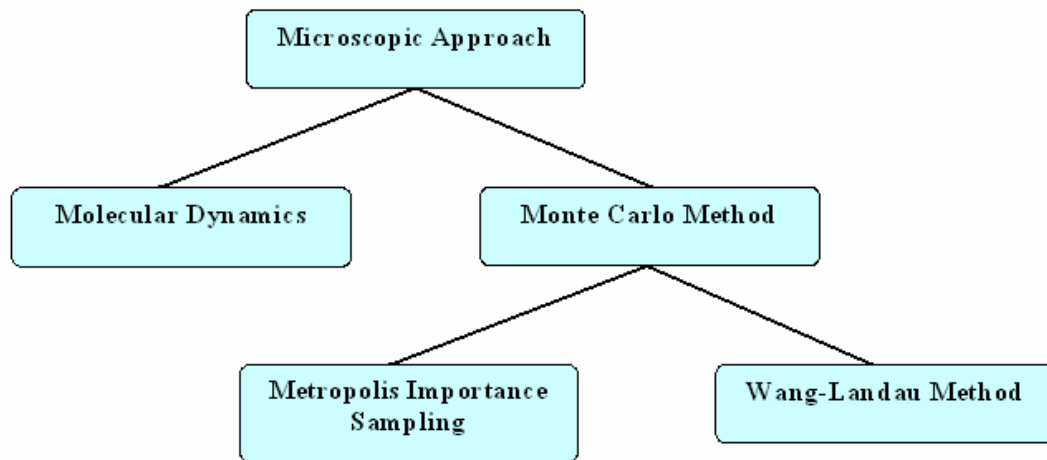


**Figure 5.1-1** *Summary of the main aspects of microscopic modelling investigated in this work.*

## 5.2 Review of molecular models

Studies have been carried out by various groups on the temperature of maximum density at the molecular level. These studies attempted to provide an explanation of presence of a density maximum in water. In 1891 W.C. Röntgen developed a molecular model proposing that liquid water is a mixture of two forms of ice at different densities. The ratio of these two ice forms is temperature dependent. Röntgen proposed that the density maximum arises due to a trade-off between thermal expansion and transformations from one form of ice to another. Using this model Röntgen also devised explanations for the increase in the thermal expansion coefficient with pressure and the decrease of viscosity with pressure. Röntgen published his findings in his 1892 paper [51] (translated in [52]).

In 1997 Cho et al. investigated the number and density of nearest neighbours in hydrogen bonded networks in water to account for the presence of a density maximum. This group proposed that changes in the disposition of the second nearest neighbours cause a change in the structure and thus increase the density. The analytical model devised by produces a density maximum which matches

experimental data well [53]. Cho et al. published another paper accounting for other anomalous water properties most notably the depression of the melting point and density maximum under pressure [54].

A theory proposed in 1998 by Tanaka [55] attributes the density maximum in water to the competition between normal thermal expansion and bond ordering. Bond ordering refers to hydrogen bonding. Tanaka introduced a bond order parameter into his molecular model that has a negative dependence on temperature. This parameter decreases the density on cooling. Normal thermal expansion is governed by van der Waals forces and has a smaller temperature dependence than the bond order parameter. These opposing effects give rise to a maximum in density.

The density maximum in water is caused by the presence of interstitial water molecules in the cavities of the tetrahedral network as proposed in 2000 by Jedlovszky at al. [56]. Jedlovszky et al. used x-ray diffraction studies of water at temperatures above and below the density maximum showing that at lower temperatures the number of neighbours at a distance of 3-4 angstroms decreases. The number of neighbours at a distance of 4-5 angstroms was found to increase. Consequently there is a decrease in the number of interstitial molecules and a decrease in density at lower temperatures accounting for the existence of a density maximum in water.

Chatterjee et al. used a statistical mechanics model to investigate the effect of adding nonpolar solutes at atmospheric pressure on the temperature of maximum density of water [57]. This approach was also used by Ashbaugh and Truskett [58] and Truskett and Debenedetti [59]. Chaterjee et al. published his work in 2005, Ashbaugh and Truskett in 2002 and Truskett and Debenedetti in 1999. These models predicted that the maximum elevation of the temperature of maximum density would increase as the hydrocarbon chain length increased. This is a consequence of increased hydrophobicity. The increased hydrophobicity caused a shift in the temperature of maximum density towards lower concentrations.

## 5.3 Metropolis importance sampling

Monte Carlo simulations are most commonly realised using Metropolis importance sampling. In this process five steps are followed as discussed in [60]:

1. Specify the initial atom coordinates.
2. Select some atom *i* randomly and move it by random displacement: $\Delta X_i$, $\Delta Y_i$, and $\Delta Zi$.
3. Calculate the change of potential energy $\Delta V$ corresponding to this displacement.
4. If $\Delta V < 0$ accept the new coordinates and go to step 2.
5. Otherwise, if $\Delta V \geq 0$, select a random number R in the range [0,1] and:

   A. if $e^{-\Delta V / kT} > $R accept the new coordinates and go to step 2.

   B. if $e^{-\Delta V / kT} \leq $R keep the original coordinates and go to step 2.

All iterations are independent of one another. This is a stochastic process which is conditional on the present state of the system, its future and past are independent. This is known as a Markov process. The Boltzmann factor ($e^{-\Delta V / kT}$) is a weighting factor that determines the relative probability of a particle to be in an energy state $E_i$ in a multi-state system. It is this weighting factor that allows the energy of a system to reach a minimum for a given temperature in a relatively short period of time.

## 5.3.1 Lattice models and Metropolis importance sampling

A lattice model consists of a set number of sites. The lattice size is chosen, for example a 9x6 lattice, giving rise to a fixed number of sites. Early models devised were based on the 2-D Ising model. In this model a discrete set of spins is chosen which can take on two values 1 or –1. Spin down is denoted by –1 and spin up is denoted +1. A lattice is constructed of chosen size whereby each element is in orientation up or down. Each spin only interacts with spins above below to the left and right. The energy of one spin is given by:

$$H = -J\sum s_i s_j \qquad (5.3\text{-}1)$$

Where J is the coupling constant, $s_i$ is the value of the spin under investigation and $s_j$ are the values of the four neighbouring spins. The total energy of the system is obtained by summing all values of H for the entire system and dividing the total by two, as all interactions are included twice in calculations. The evolution of the system is governed by Monte Carlo Metropolis importance sampling. A random site is chosen and the spin is "flipped" to the opposite value and the energy of the new configuration is calculated. The energy of the previous configuration is subtracted from the new configuration's energy to give $\Delta V$ or the change in energy of the system. If the change in energy is greater than zero the Boltzmann test is carried out as discussed in section 5.3, step 5. This process is repeated until the system reduces to its lowest energy configuration.

Figure 5.3-1(a) shows an initial random scattering of spins in a 10x10 square lattice Ising model. After Metropolis importance sampling is carried out the system settles to a minimum energy configuration with all spins aligned at low temperatures (figure 5.3-1(b)). At low temperatures the energy is at a minimum.

| -1 | 1 | 1 | 1 | -1 | 1 | -1 | 1 | 1 | -1 | | 1 | 1 | 1 | 1 | 1 | 1 | 1 | 1 | 1 | 1 |
| 1 | 1 | 1 | 1 | -1 | -1 | 1 | 1 | 1 | -1 | | 1 | 1 | 1 | 1 | 1 | 1 | 1 | 1 | 1 | 1 |
| -1 | 1 | -1 | 1 | -1 | -1 | -1 | 1 | 1 | -1 | | 1 | 1 | 1 | 1 | 1 | 1 | 1 | 1 | 1 | 1 |
| 1 | 1 | 1 | -1 | -1 | -1 | 1 | 1 | 1 | -1 | | 1 | 1 | 1 | 1 | 1 | 1 | 1 | 1 | 1 | 1 |
| 1 | -1 | -1 | -1 | 1 | -1 | 1 | -1 | 1 | -1 | | 1 | 1 | 1 | 1 | 1 | 1 | 1 | 1 | 1 | 1 |
| 1 | 1 | -1 | -1 | 1 | -1 | -1 | -1 | 1 | -1 | | 1 | 1 | 1 | 1 | 1 | 1 | 1 | 1 | 1 | 1 |
| -1 | 1 | 1 | 1 | 1 | 1 | 1 | 1 | -1 | 1 | | 1 | 1 | 1 | 1 | 1 | 1 | 1 | 1 | 1 | 1 |
| 1 | 1 | 1 | -1 | -1 | 1 | 1 | 1 | 1 | -1 | | 1 | 1 | 1 | 1 | 1 | 1 | 1 | 1 | 1 | 1 |
| -1 | 1 | 1 | 1 | -1 | -1 | 1 | -1 | -1 | 1 | | 1 | 1 | 1 | 1 | 1 | 1 | 1 | 1 | 1 | 1 |
| 1 | -1 | -1 | -1 | 1 | 1 | -1 | -1 | -1 | -1 | | 1 | 1 | 1 | 1 | 1 | 1 | 1 | 1 | 1 | 1 |

<div align="center">(a)       (b)</div>
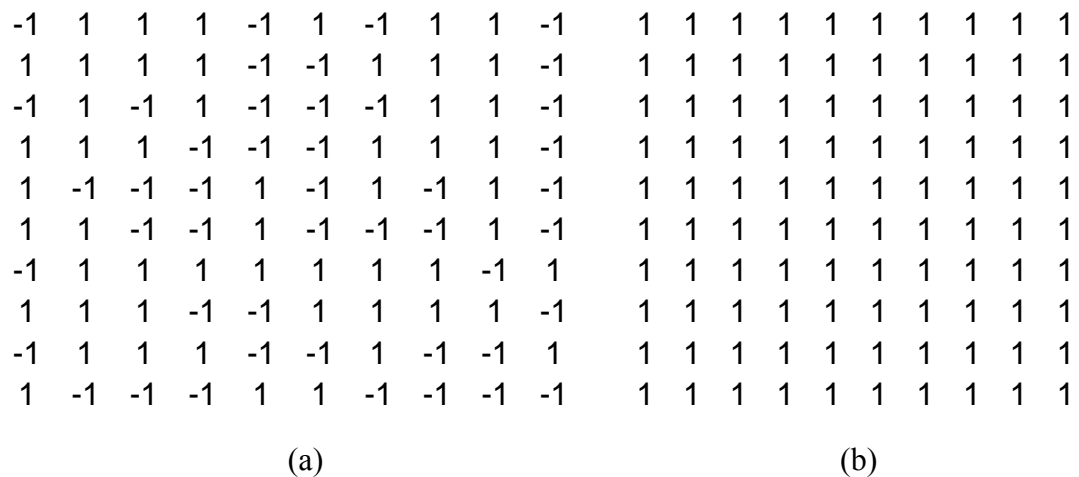
**Figures 5.3-1** *Spin configurations initially and after Metropolis importance sampling has been performed. In this simulation 100,000 random "flips" were performed.*

A two-dimensional Potts model was then expanded as an extension to the Ising model. The Potts model is very similar to the Ising model except that each site can

have 'q' different values of spin rather than just –1 or +1 with the Ising model.  The energy of one spin is given by:

$$H = -J\sum\sum\delta(s_i s_j)$$  (5.3-2)

Where J is the coupling constant, $s_i$ is the value of the spin under investigation and $s_j$ are the values of the four neighbouring spins.  If $s_i = s_j$ 1 is returned and 0 otherwise.  If q=2 the Ising and Potts models are very similar.  As with the Ising model the total energy of the system is obtained by summing all values of H for the entire system and dividing the total by two, as all interactions are included twice in calculations.  The evolution of the system is governed by Metropolis importance sampling.  When a random "flipping" of a site is performed the site can take on any integer spin value from 1 to q.  At sufficiently low temperatures total energy of the system is at a minimum.  This occurs when all spins align.  Figure 5.3-2(a) shows a random scattering of spins in a 10x10 lattice with q=6.  After Metropolis importance sampling is performed the system settles to a minimum energy configuration with all spins aligned with q=6 at low temperatures (figure 5.3-2(b)).

```
1  5  4  6  3  4  1  5  5  3        6  6  6  6  6  6  6  6  6  6
4  6  4  4  2  2  5  5  6  1        6  6  6  6  6  6  6  6  6  6
2  6  2  4  3  2  3  6  5  1        6  6  6  6  6  6  6  6  6  6
6  5  5  1  3  3  6  6  6  2        6  6  6  6  6  6  6  6  6  6
5  1  3  2  6  2  4  1  5  3        6  6  6  6  6  6  6  6  6  6
6  5  2  1  4  3  1  3  4  3        6  6  6  6  6  6  6  6  6  6
2  6  5  4  4  4  5  6  2  6        6  6  6  6  6  6  6  6  6  6
5  4  4  1  2  5  4  6  5  2        6  6  6  6  6  6  6  6  6  6
1  6  4  5  1  1  5  1  2  4        6  6  6  6  6  6  6  6  6  6
4  3  3  3  5  4  1  2  1  2        6  6  6  6  6  6  6  6  6  6
```

           (a)                                    (b)
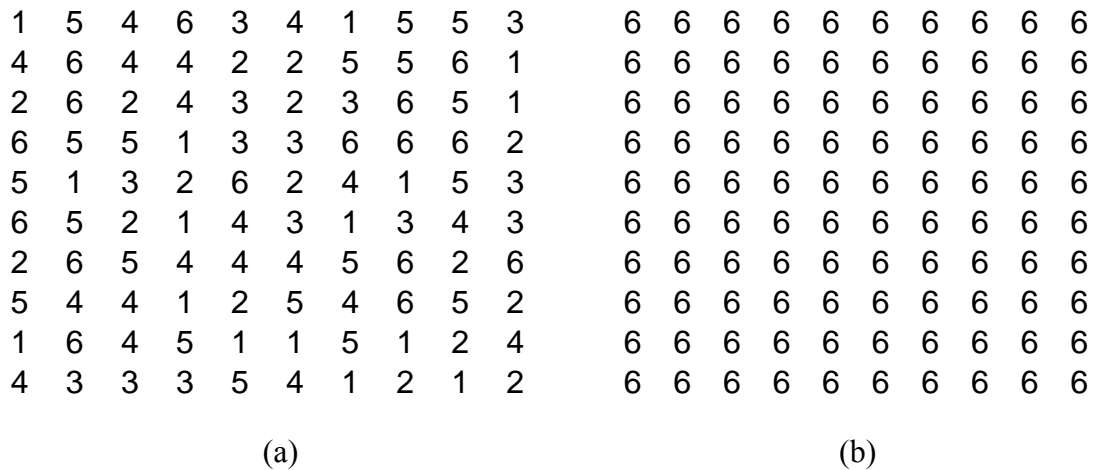
**Figures 5.3-2** *Spin configurations initially and after Metropolis importance sampling has been performed.  In this simulation 100,000 random "flips" were performed.*

Figures 5.3-1(b) and 5.3-2(b) show how the system finds the lowest possible energy configuration for low temperatures using Metropolis importance sampling. The configuration shown in figure 5.3-1(b) corresponds to a total energy of -200 since all spins are aligned at low temperature. When all spins are aligned each spin that is investigated contributes -4 to the total energy of the system according to equation 5.3-1. There are 100 spin sites thus the total energy of the system is -400 but this must be divided by 2 as all interactions are included twice in calculations. This gives rise to total system energy of -200. Similarly, figure 5.3-2(b) corresponds to a total energy of -200 since all spins are aligned at low temperature. When all spins are aligned each spin that is investigated contributes -4 to the total energy of the system according to equation 5.3-2. This gives rise to total system energy of -200.

With the Potts model temperature scans were also carried out with q=6 giving rise to a first order phase change (figure 5.3-3). At low temperatures as discussed the system settles into a configuration whereby all spins align corresponding to a total energy value of -200. As the temperature is increased a first order phase change occurs and the energy increases rapidly and then levels out as a plateau. In this simulation 60,000 random Monte Carlo "flips" were performed at each of the 200 points.
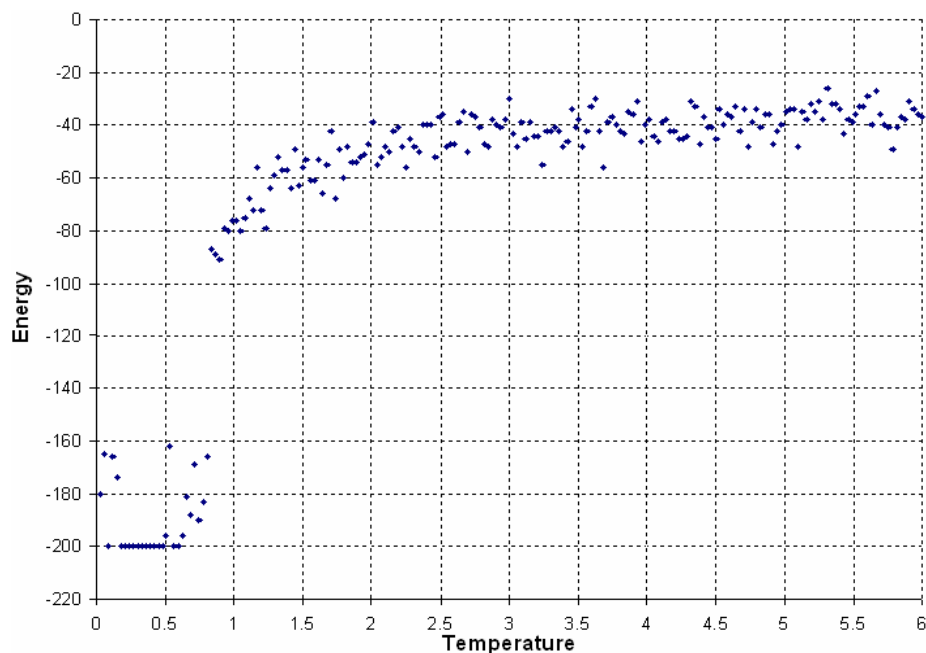


**Figure 5.3-3** *Energy versus temperature profile using the Potts model (q=6). The energy is given in units of k.*

## 5.4 Wang-Landau approach

In this approach a random walk is performed in energy space to extract an estimate for the density of states rather than sampling the probability distribution at a fixed temperature [61]. The probability can be computed at any temperature by weighing the density of states by the appropriate Boltzmann factor. With derivatives of the partition function thermodynamic properties can be computed directly. The Wang-Landau algorithm is a very powerful method which can yield vast amounts of information from a single simulation.

The Wang-Landau method is a Monte Carlo algorithm which is highly successful in estimating the density of states (DOS) $g(E)$ of a variety of statistical systems. In Wang-Landau sampling, Metropolis acceptance criterion for the transition probability from a conformation energy $E_1$ to a conformation with energy $E_2$ is replaced by an expression involving the instantaneous density of states given by:

$$p(E_1 \rightarrow E_2) = \min\left(\frac{g(E_1)}{g(E_2)}, 1\right) \qquad (5.4\text{-}1)$$

The simulation will hence have a tendency to sample conformations with small $g(E)$ with a higher probability. If the density of states is known the Wang-Landau algorithm will generate a random walk in energy space with a flat histogram [62].

Using this method the density of states is iteratively determined by undertaking a random walk in energy space and attempting to sample a flat energy distribution. Initially, $g(E)=1$ for all $E$ and a histogram is set up that will track the number of visits to each energy level, $E$. A Monte Carlo step is performed and the density of states of the new conformation with energy $E_2$ (if accepted) is multiplied by a modification factor, $f$, which is set at the beginning of the simulation and the corresponding histogram is incremented. The $E_2$ energy state will always be accepted if $g(E_2) < g(E_1)$. Otherwise, it is accepted with a probability of $g(E_2)/g(E_1)$. If the new conformation is rejected the previous density of states with energy $E_1$ is multiplied by $f$ and its histogram incremented. Once the energy distribution is sufficiently flat $f$

is reduced to $\sqrt{f}$ the histogram is set to zero and a new iteration begins.  At the beginning of the simulation a threshold is set for $f$ and the simulation continues until that threshold is reached.  A suitable value for this threshold is chosen, normally such that $\ln(f) \leq 10^{-6}$ such that the density of states has converged to the correct state.  For more details on the Wang-Landau method see [61, 63].

In this study the density of states is used to explore multidimensional parameter space using a code written in C (appendix C).  A random walk is performed in energy and density rather than just energy.  Hence, a two-dimensional density of states function is evaluated, g($E, N$) where $E$ is energy and $N$ is the number of occupied sites (see section 5.6).  The partition function, $Z$, is derived using a post-processing code also written in C and is given by:

$$Z = \sum_{E,N} g(E,N) e^{-E/kT} e^{\mu N/kT}$$
(5.4-2)

where $\mu$ is the chemical potential.  In post-processing thermodynamic properties such as energy and density are computed directly (appendix D).  These thermodynamic properties are functions of temperature and chemical potential.

## 5.4.1 A simple example of the Wang-Landau approach

In order to describe how the Wang-Landau algorithm calculates the density of states function a simple 1-D program is examined.  This program deals with the example from statistical mechanics whereby two dice are thrown and the density of states function for the "energy" of the result calculated.  The "energy" of the result is simply the sum of the upturned faces.  There are 36 possible configurations ranging from 2 to 12.  Only one configuration gives rise to an energy of 2 (one and one) whereas 6 configurations give rise to an energy of 7 which is the most probable value of energy.  The Wang-Landau algorithm aims to reproduce the possible energies and the corresponding number of possibilities for that energy or the density of states. Initially only a very approximate density of states function is produced (figure 5.4-1). The system evolves until the density of states function is refined.  The program does

indeed give back the expected density of states, g($E$), which has been graphed below (figure 5.4-2).

The most probable result is an energy value of 7 with 6 possible configurations giving rise to this energy. The total number of configurations is 36, from summing all g($E$) values, as expected. This is a simple 1-D algorithm, which illustrates how the method works, but when applying Wang-Landau sampling to water a 2-D algorithm is needed.
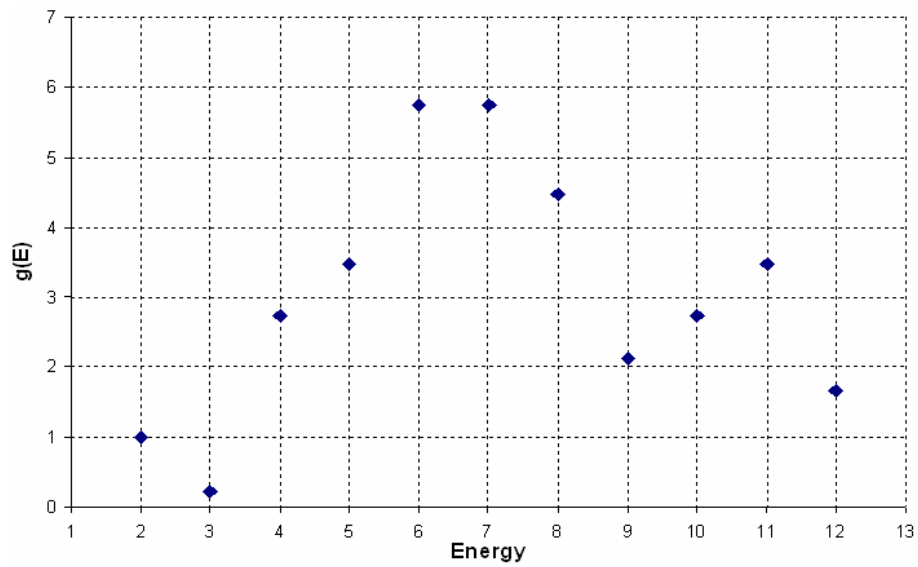


**Figure 5.4-1** *Density of states versus energy initially.*
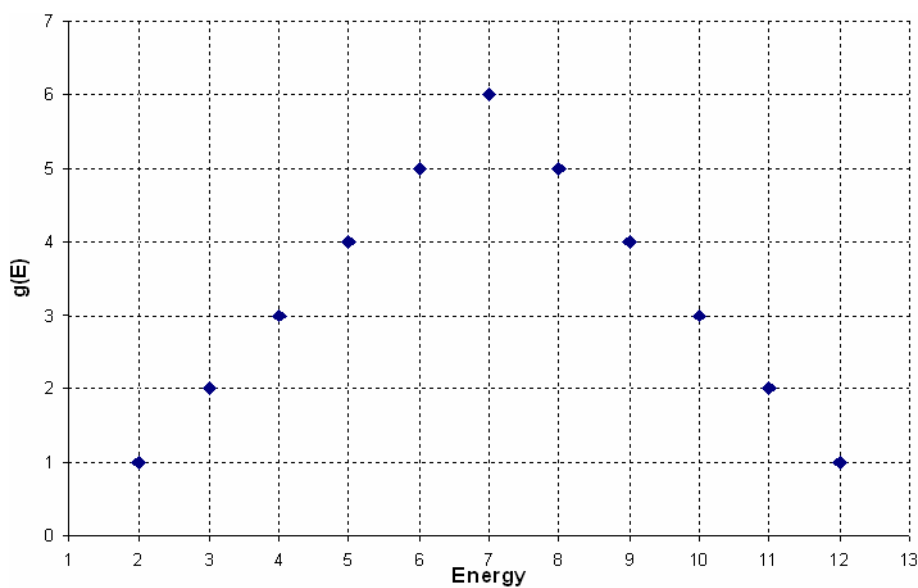


**Figure 5.4-2** *Density of states versus energy after refining the density of states.*

## 5.4.2 Metropolis importance sampling versus the Wang-Landau approach

There are advantages to both Monte Carlo methods investigated in this work. The Metropolis importance sampling method enables a "snap-shot" of the system configuration to be obtained for a particular temperature. This is because the Metropolis method allows the user to extract the information for all molecules for a particular temperature. However, in the Wang-Landau method a density of states function is formed and thus at one particular temperature value it is not possible to extract information on the molecules in the system. When temperature scans are performed energy and density profiles are obtained and it can be seen that the Wang-Landau method gives rise to far smoother curves when compared to a similar curves derived using the Metropolis sampling method. The reason for this is that the Wang-Landau approach estimates the density of states and in doing so gleans information from all steps in the process. Even if a move is rejected, a histogram is incremented which is subsequently used to bias the simulation towards less visited regions of the density of states. In Metropolis importance sampling a rejected move is discarded and the same move is as likely to happen again and the system reverts to a previous state. This can lead to slowing down of the simulation if the system becomes trapped in a local minimum. These local minima give rise to noisy energy and density profiles when dealing with Metropolis importance sampling. These profiles are discussed further in section 5.7.

The Wang-Landau method produces the density of states function which in conjunction with the partition function gives all thermodynamic properties at all temperatures and chemical potentials. The Metropolis sampling method only gives rise to a sample of the probability function. Hence, many simulations would have to be conducted using the Metropolis method to obtain the same wealth of information that one Wang-Landau simulation produces.

## 5.5 Mercedes-Benz 2-D model

Water molecules are modelled as Mercedes Benz symbols, to realistically model the energy of the interaction between molecules in the lattice. The model is based on the Mercedes Benz logo which consists of a two-dimensional disk with three symmetrically arranged arms, separated by an angle of 120° [64]. In water molecules the angle between the bonded hydrogen atoms is 104.5° and there are two lone pairs that accumulate at the oxygen atom giving rise to a molecule that is 3-D in geometry. In this model angles between atoms are 120° and the two lone pairs of electrons are simplified to one bonding arm representing the oxygen atom. These simplifications allow for highly structured arrangements to form and hence are very useful in modelling the behaviour of water. This would not be possible if the separation between two of the arms was 104.5°. A 3-D model would be needed in order to incorporate both lone pairs and the actual angle between the bonded hydrogen atoms but this would not necessarily give more accurate results. Mercedes-Benz molecules are free to move within a rectangular region which is allowed to vary in size in an off-lattice model. In off-lattice models the interaction of the molecules is governed by a Lennard-Jones (LJ) term and an explicit hydrogen-bonding (HB) term whereby:

$$U(X_i, X_j) = U_{LJ}(r_{ij}) + U_{HB}(X_i, X_j)$$  (5.5-1)

The model is represented using Ben-Naim's notation:
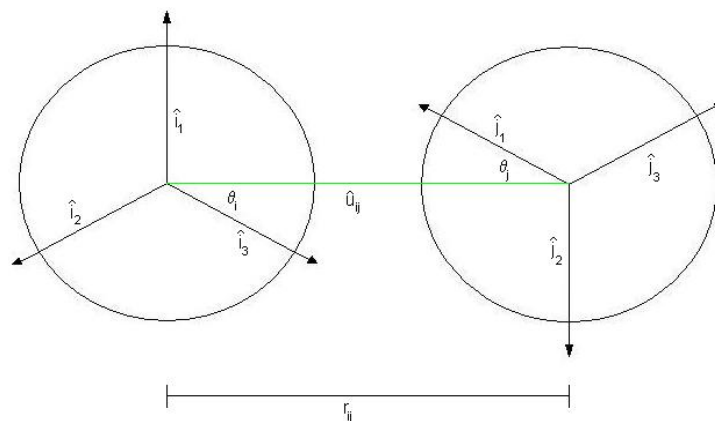


**Figure 5.5-1** *Two MB water molecules using Ben-Naim notation.*

$X_i$ denotes the vector representing the coordinates and the orientation of the ith particle. The distance between the centres of molecules $i$ and $j$ is denoted by $r_{ij}$. Each molecule has three hydrogen bonding arm vectors and the intermolecular axis vector, $\hat{u}_{ij}$ makes angles $\phi_i$ and $\phi_j$ with the closest arm of each molecule [65]. The Lennard-Jones potential is defined by:

$$U_{LJ}(r_{ij}) = 4\varepsilon_{LJ}\left[\left(\frac{\sigma_{LJ}}{r_{ij}}\right)^{12} - \left(\frac{\sigma_{LJ}}{r_{ij}}\right)^{6}\right]$$

(5.5-2)

where $r_{ij} = r_i - r_j$ and $r_{ij} \equiv |r_{ij}|$, $\varepsilon_{LJ}$ is a well-depth parameter and $\sigma_{LJ}$ is a contact parameter. The Lennard-Jones potential is shown graphically in figure 5.5-2.
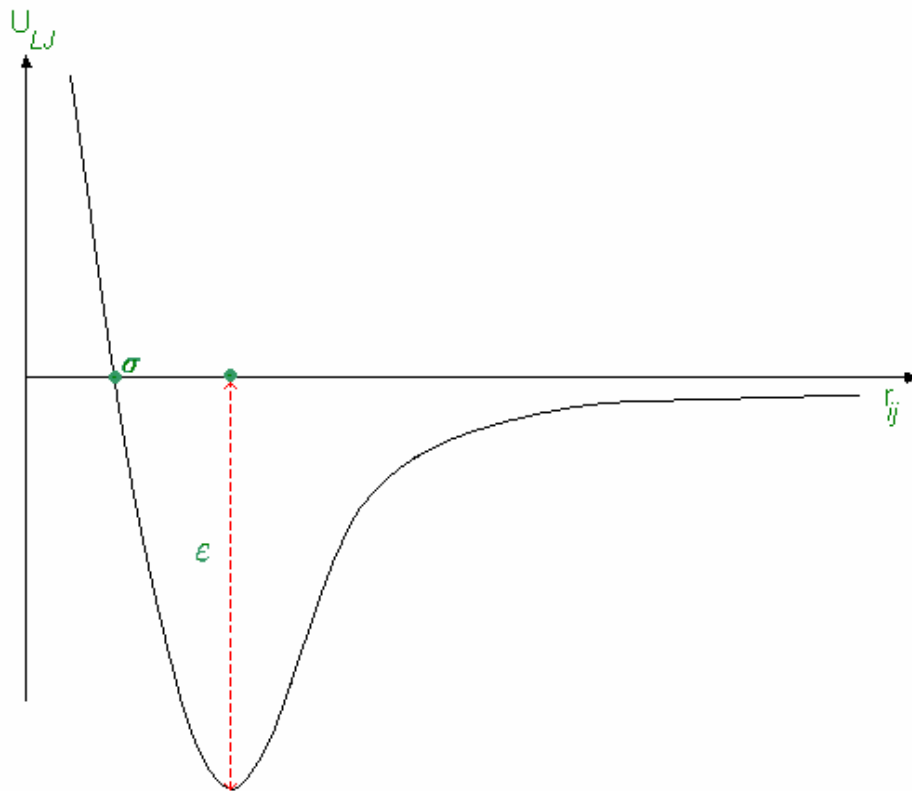


**Figure 5.5-2** *Graphical representation of the Lennard-Jones potential.*

When the arm of one molecule aligns with the arm of another molecule a hydrogen bond is formed with an energy defined by a Gaussian function of separation and angle:

124

$$U_{HB}\left(X_i, X_j\right) = \varepsilon_{HB} G(r_{ij} - r_{HB}) \sum_{k,l=1}^{3} G(\hat{i}_k \cdot \hat{u}_{ij} - 1) G(\hat{j}_k \cdot \hat{u}_{ij} + 1) \qquad (5.5\text{-}3)$$

where $G(x)$ is an unnormalised Gaussian function:

$$G(x) = \exp[-x^2 / 2\sigma^2] \qquad (5.5\text{-}4)$$

The unit vector $\hat{i}_k$ represents the $k$th arm of the $i$th particle ($k$=1,2,3) and the unit vector joining the centre of molecule $i$ to the centre of molecule $j$ is $\hat{u}_{ij}$. The optimal hydrogen bond energy is defined by $\varepsilon_{HB}$ =-1 and the optimal bond length by $r_{HB}$=1. Therefore the strongest hydrogen bond occurs when an arm of one molecule is perfectly aligned with an arm of another molecule. Any arm of a molecule can align with any arm of another molecule. The energy contribution is only defined by the degree to which the arms line up. This method only applies to off-lattice models.

## 5.5.1 Off-Lattice Monte Carlo Simulations

In this model the Mercedes-Benz molecules are free to move within a rectangular region which is allowed to vary in size. Interactions between the molecules are governed by a Lennard-Jones term and an explicit hydrogen bonding term (equation 5.5-1). The Lennard-Jones potential is given by equation 5.5-2. Molecules will not interact with each other if they are further apart than a set limiting separation called the cut off distance ($r_c$) [66]. If the distance between molecules is less than the cut-off distance the potential is defined by equation 5.5-2 and if the distance between molecules is greater than or equal to the cut-off distance then the potential is set to zero. The strength of the interaction is governed by $\varepsilon_{LJ}$ and $\sigma_{LJ}$ defines the length scale. The Monte Carlo off-lattice model is based on an NPT (constant number of molecules, constant pressure and constant temperature) ensemble with $\varepsilon_{LJ}$ and $\sigma_{LJ}$ set to unity. The Monte Carlo method has been realised using Metropolis importance sampling. As the simulation evolves the position of a random molecule is changed or the area of the region is altered by a small amount. The change in energy is calculated and the steps outlines in section 5.3 are followed.

The model is written in C++ using a structured style. The main functions are defined below. A flow chart of the software routine is shown in figure 5.5-3.

**<u>Main functions of the off-lattice model</u>**

**SetParams:** Defines many initial parameters such as temperature, pressure, number of molecules, the cut-off distance ($r_c$) and various other parameters.

**InitCoords:** Sets up random vector co-ordinates for the initial positions of all the molecules.

**Total_e:** This function calculates the Lennard-Jones and hydrogen bond energies between pairs of molecules if the distance between molecules is less than the cut-off distance. The energy due to the pair of molecules is added to the total energy of the system.

**Mc_move:** This function moves the molecules from one position to another within the region. If a move is rejected by Metropolis importance sampling the original positions of the molecules are saved so that the previous state of the system can be restored.

**Mc_vol:** Changes the volume of the region containing the molecules by a small amount. If a move is rejected by Metropolis importance sampling the original positions of the molecules are saved so that the previous system configuration can be restored.

**CalcCorrections:** Computes tail-corrections associated with using a cut-off, $r_c$, in the Lennard-Jones potential.

**WritePositions:** Writes the start and end positions or vectors of each molecule to files.
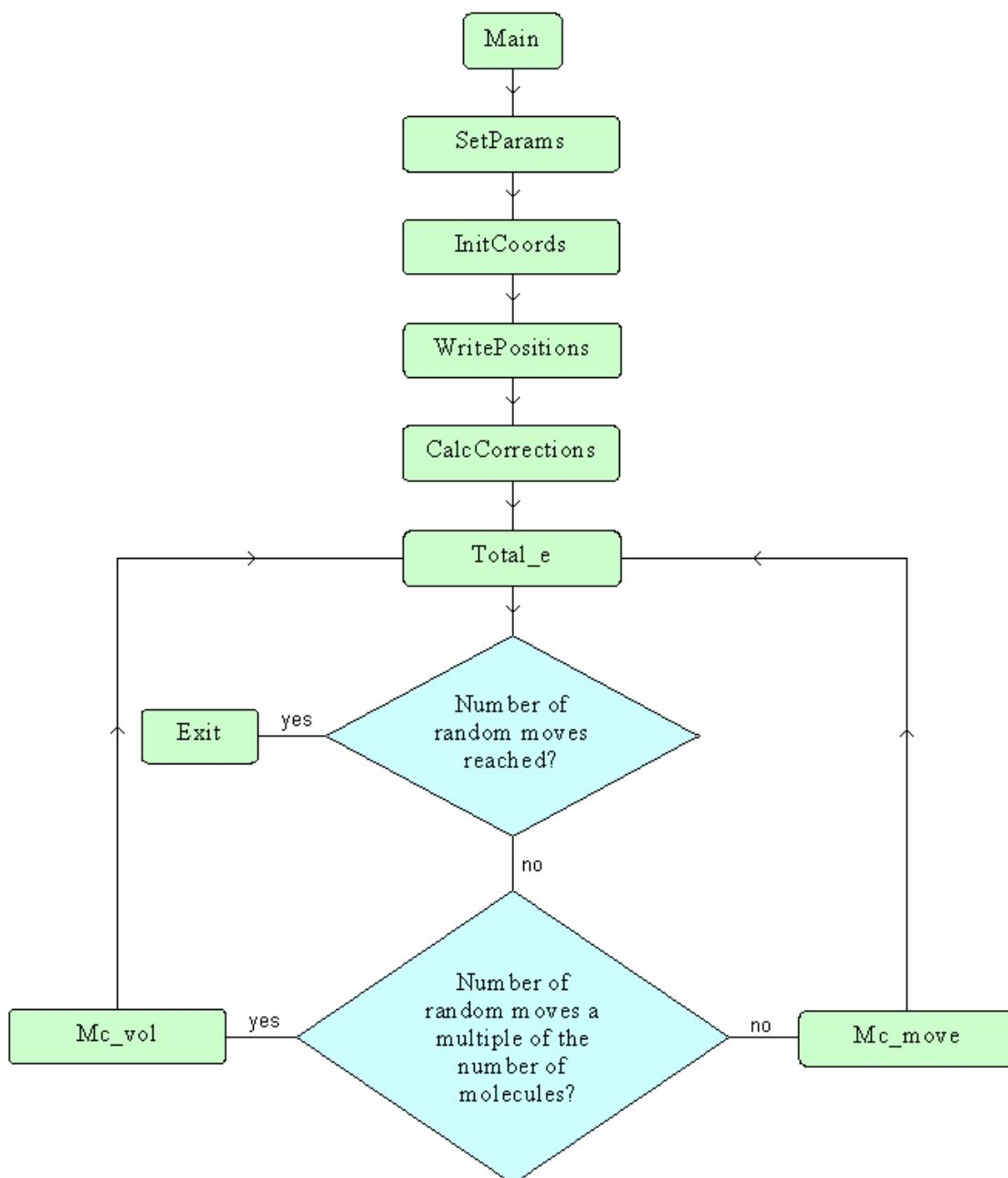
**Figure 5.5-3** *Flow chart showing main functions of the off- lattice model using the Metropolis importance sampling method.*

## 5.5.2 Off-lattice results

Off-lattice Monte Carlo simulations were carried out on systems of 8 and 16 molecules. The region containing the molecules was repeated nine times to illustrate wrap-around effects. This wrapping effect allows molecules on one side of the lattice to interact with corresponding molecules on the opposite side of the lattice allowing the system to behave more realistically (discussed further in section 5.6).

Initially molecules are randomly located (figure 5.5-4 and 5.5-6). At low temperatures the system 8 molecule system forms Mercedes-Benz ice (figure 5.5-5). Simulations are very time consuming and require enormous amounts of processor power. Temperature scans were not conducted for this reason. The 16 molecule system does not form Mercedes-Benz ice but still produces a very structured low density configuration (figure 5.5-7). These types of formations are not possible with a lattice based model.

In order to achieve Mercedes-Benz ice (figure 5.5-5) 20,000,000 Monte Carlo steps needed to be carried out. In gas-lattice models significantly less Monte Carlo steps are required to form Mercedes-Benz ice. The ice structure shown in figure 5.7-2 using a Buzano gas-lattice model (section 5.6) required 200,000 steps. A factor of a hundred times more steps is needed to produce similar results as gas-lattice models.
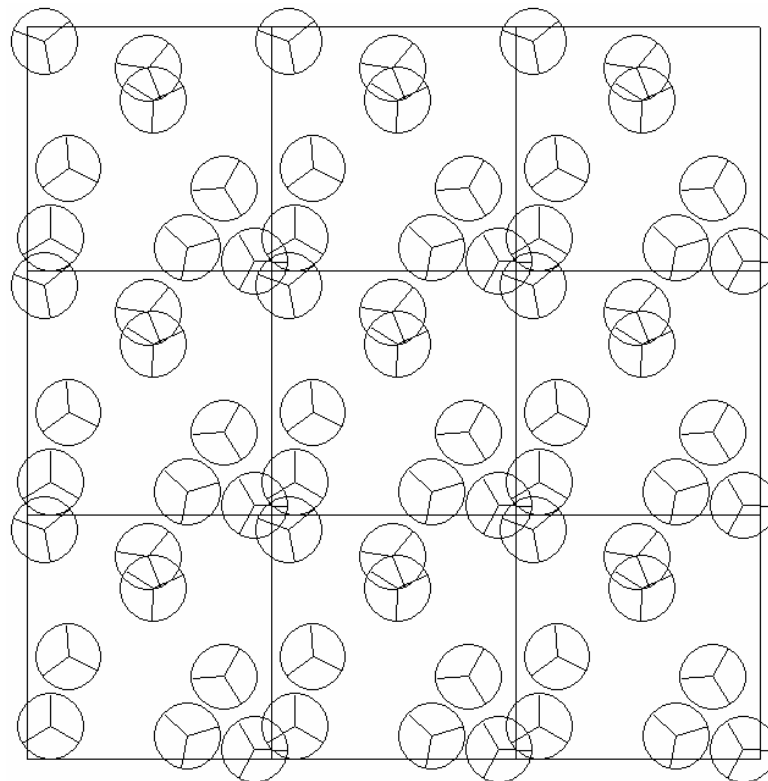


**Figure 5.5-4** *Randomly configured sites at beginning of simulation. System of 8 molecules.*
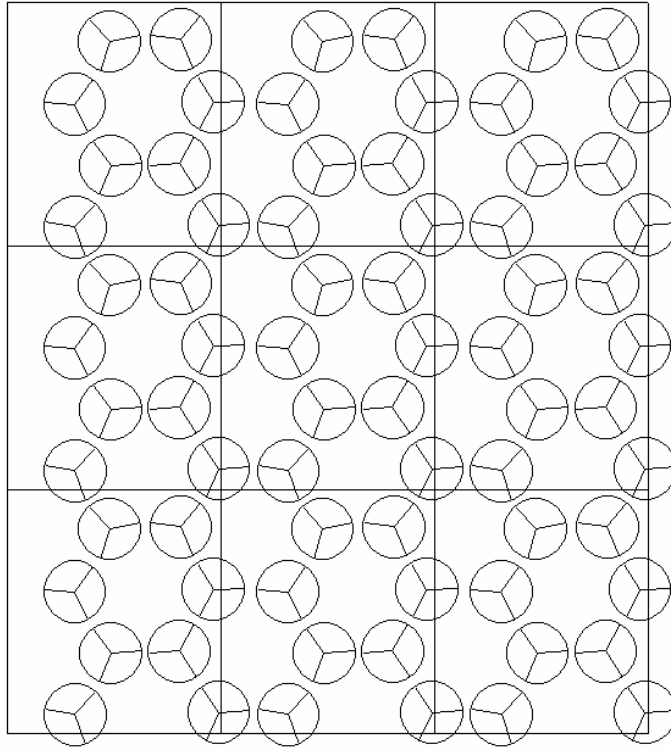
**Figure 5.5-5** *Mercedes-Benz ice for off-lattice model. System of 8 molecules.*
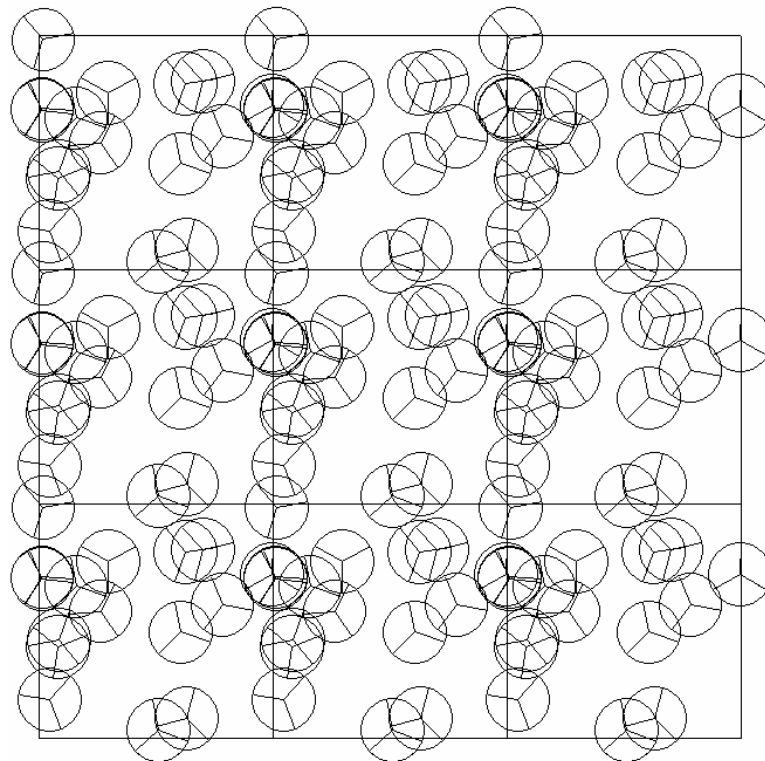


**Figure 5.5-6** *Randomly configured sites at beginning of simulation. System of 16 molecules.*
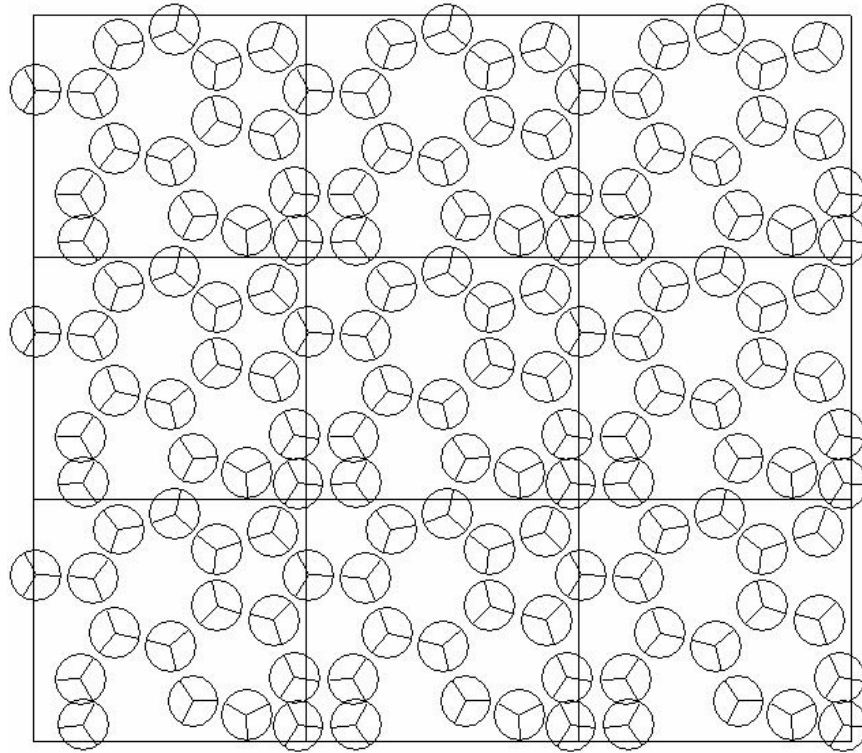
**Figure 5.5-7** *Structured arrangement of molecules at end of simulation. System of 16 molecules.*

## 5.6 Buzano gas lattice model

This model is defined on a two-dimensional hexagonal gas lattice. Molecules are arranged on a hexagonal lattice (figure 5.6-1). Molecules are located along a row equally spaced then the molecules in the rows above and below will be offset by half the distance between the molecules (figure 5.6-1). The water molecules are modelled as Mercedes-Benz symbols. A lattice site can be occupied by a Mercedes-Benz molecule or it can be vacant. The energy contributions due to active molecules and hydrogen bonds are defined by Buzano et al. [67, 68, 69]. In the lattice each molecule has six nearest neighbours (figures 5.6-1 and 5.6-2). Active nearest neighbours cause the total energy of the system to be reduced by $\varepsilon$. The value of $\varepsilon$ is set to unity. If arms of nearest neighbour molecules line up a hydrogen bond is formed and an energy term of $-\eta < 0$ is added to the total energy of the system where eta ($\eta$) is equal to $3\varepsilon$.
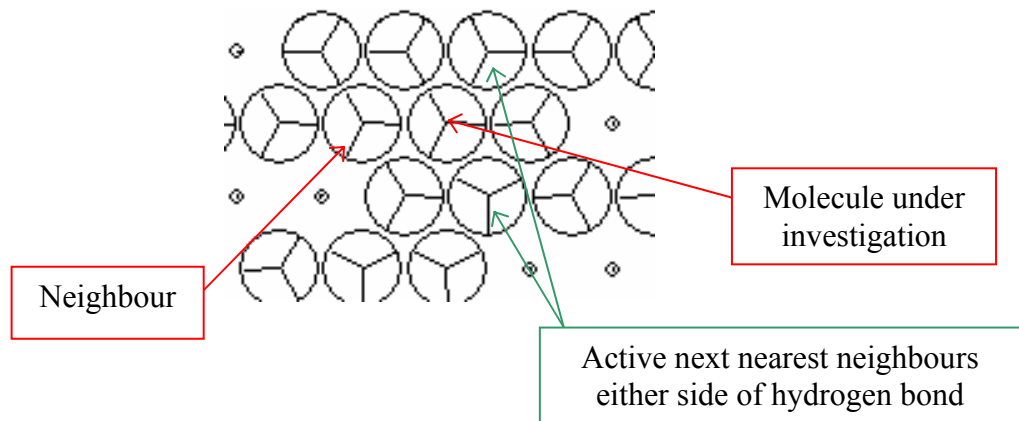
**Figure 5.6-1** *Sample of lattice showing the molecule under test, neighbours and active next nearest neighbours.*

In this model next nearest neighbours are taken into account (figure 5.6-1). If a next nearest neighbour is active a formed hydrogen bond is weakened by an energy term $c\eta/2$ $(c \in [0,1])$. In the hexagonal lattice there are two next nearest neighbours per hydrogen bond such that when both are occupied as in figure 5.6-1 the hydrogen bond contributes a reduced energy of $-(1-c)\eta$. The weakening term is an effective three body interaction. Thus the bond formation is dependent on both orientation and local density which mimics the fact that hydrogen bonds may be perturbed when water molecules are too close to one another [67].
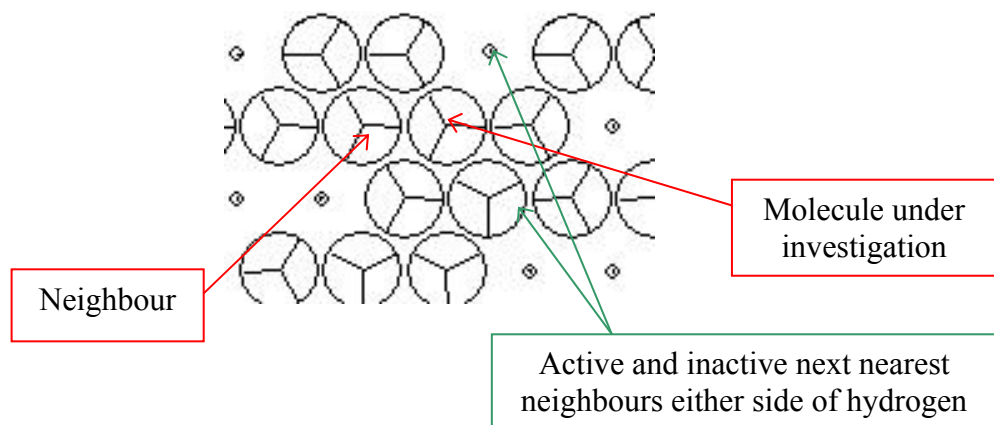


**Figure 5.6-2** *Sample of lattice showing the molecule under test, neighbours and active and inactive next nearest neighbours.*

The smallest meaningful lattice size possible using the Buzano model is 3x2. A lattice this size is capable of reproducing low-density Mercedes-Benz ice (two sites vacant and four sites active). This 3x2 lattice is known as the primitive cell. Larger lattice sizes should be multiples of this primitive cell in order to achieve an 'ice' configuration at low temperatures. Figure 5.6-3 shows the low density 'ice' configuration and the primitive cell.
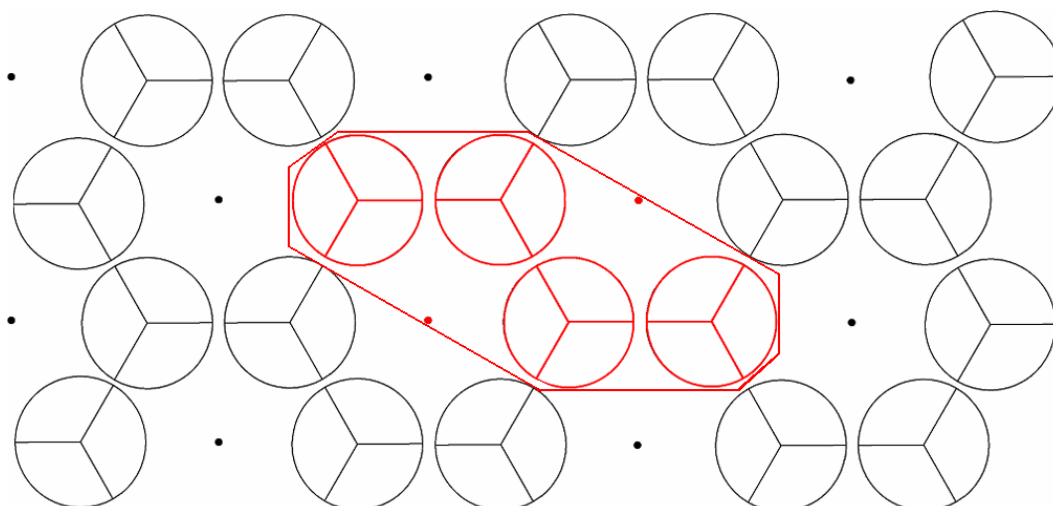
**Figure 5.6-3** *Mercedes-Benz ice configuration showing the primitive cell in red.*

A Mercedes-Benz water molecule can only form a maximum of three hydrogen bonds due to the lattice structure. A water molecule only has two possible bonding orientations. The bonding orientations arise when the arms neighbouring molecules are aligned. The two bonding orientations are shown in figure 5.6-4.
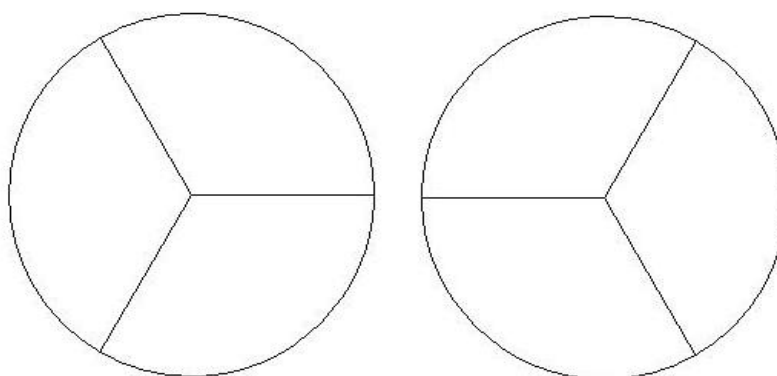
**Figure 5.6-4** *Bonding orientations for Mercedes-Benz molecules.*

## 5.6.1 Modifications to the Buzano gas lattice model

The Mercedes-Benz molecules can be either in bonding or non-bonding orientations. In the original version of the model [67] there are two bonding orientations and twenty non-bonding orientations giving a total of twenty-two possible orientations. With twenty-two orientations simulations that were carried out whereby density was graphed against temperature a very sharp first order phase change was seen but the density maximum was nearly undetectable. Since a well defined density maximum is required for this study the number of orientations was changed to 3, namely the two bonding orientations and one non-bonding orientation (figure 5.6-5). This gave rise to results displaying a very clear signature of the density maximum. These results are discussed in section 5.7.
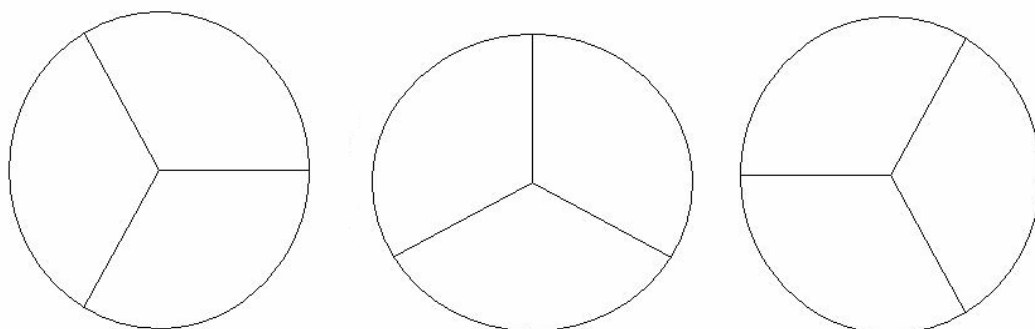


**Figure 5.6-5** *Three possible orientations for the modified Buzano model.*

The code implementing the Buzano gas lattice model was written in C and compiled using Dev-C++. The main subroutines are described below. A flow chart of the software routine is shown in Figure 5.6-7.

### Main subroutines of the modified Buzano gas lattice model

**calc_coords:** sets up the initial hexagonal lattice with sites randomly active or inactive and active sites in random rotational orientations.

**total_e:** this subroutine sums the energy contribution from each site as and also sums the total density.

**RandomFlip:** this subroutine takes a random site and either rotates it to a random orientation or alters the activity of a site. Half the time a molecule will be rotated randomly and half the time this subroutine is called the sites activity will be "flipped".

**wrap:** this subroutine "wraps" molecules in the lattice so that molecules on one side of the lattice interact with corresponding molecules on the opposite side of the lattice. This gives the ability of a smaller lattice to behave more realistically due to the periodic boundaries. In reality even a small volume of water will have a vast number of molecules ($6.022x10^{23}$ molecules per 18 grams of water) and a very small number of these will be in contact with the boundaries of the container. In these simulations comparatively very few molecules are involved and thus boundary effects would affect a large percentage of molecules in the lattice. To avoid these effects periodic boundaries are employed.

**energy_hb2:** cycles through each of the neighbours of the molecule under test and calls the wrap and buzano subroutines.

**buzano:** calculates the energy contribution due to the molecule under test and the neighbour in question.

**arm_arm:** this subroutine checks if the molecule under test aligns with the neighbour in question. In other words this subroutine checks if a hydrogen bond exists.
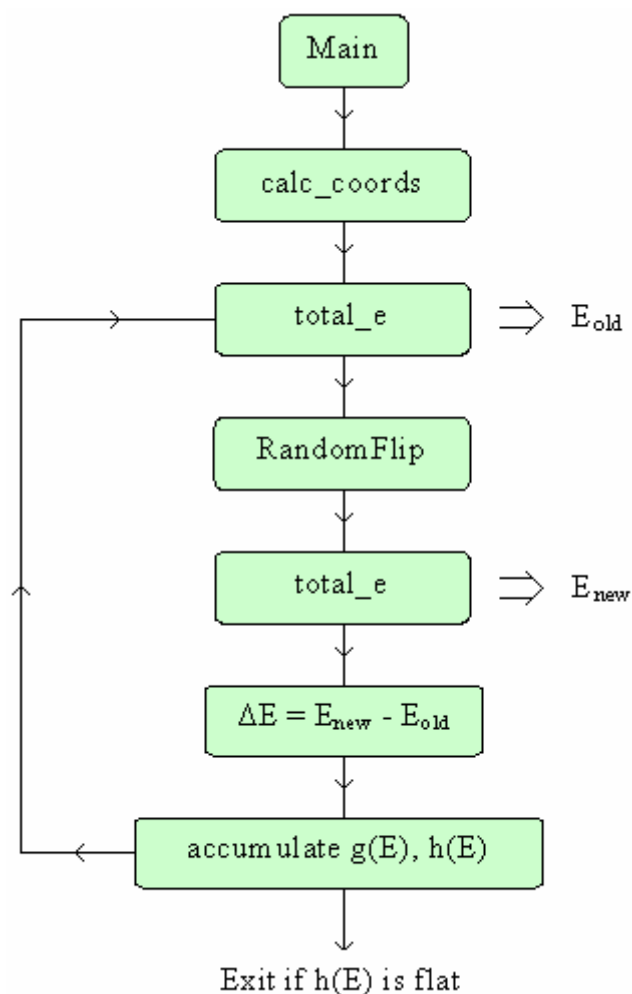
**Figure 5.6-7** *Flow chart showing main subroutines of the Buzano gas lattice model using the Wang-Landau method.*

## 5.7 Monte Carlo simulation results

Monte Carlo simulations have been explored in this study using Metropolis importance sampling and the Wang-Landau approach.  Simulations were carried out mainly on gas lattice models but some work was also conducted on off lattice models (section 5.5).  For both off lattice and gas lattice simulations water molecules were modelled as Mercedes-Benz symbols.  All gas lattice water models were based on the modified Buzano approach as discussed in section 5.6.  Attempts were made to replicate experimental results using the Buzano gas lattice model.

## 5.7.1 Metropolis importance sampling results

Before the system was allowed to evolve a lattice size was chosen and each site was randomly set to be active or inactive and in a random orientation. This can be seen clearly in figure 5.7-1. Some sites are active in bonding or non-bonding orientations and some are inactive denoted by the smaller circles. The system was allowed to evolve over 200,000 cycles in order to find the lowest possible energy for the given temperature. 200,000 random "flips" were made altering the activity or rotational orientation of a randomly chosen molecule and Metropolis importance sampling was carried out. In this case the temperature was set to a low value so an ice structure was expected (figure 5.7-2). This hexagonal structure is typical of Mercedes Benz ice. The molecules have locked into positions whereby they form hydrogen bonds with neighbouring molecules forming a cage like structure. The molecule within the cage has become inactive as is energetically most favourable in this case. The molecules have locked into a highly structured low-density formation, which requires thermal energy to break up analogous to physical ice. In figures 5.7-1 and 5.7-2 the lattice size was 9x6, i.e. 54 molecules and was repeated nine times to include wrap around effects.
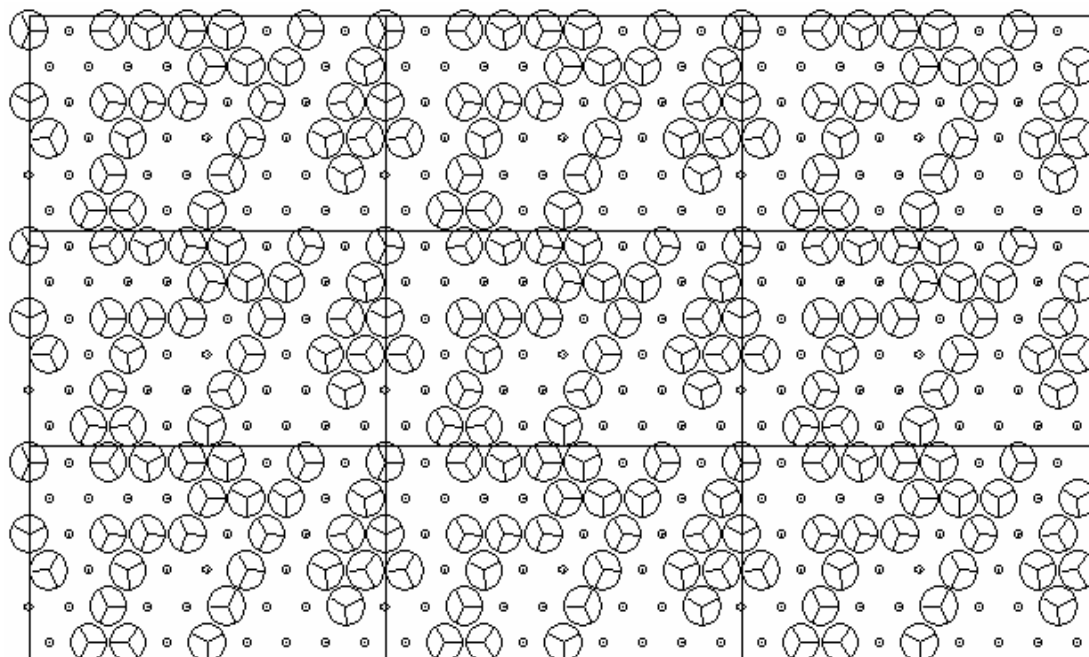


**Figure 5.7-1** *Randomly configured sites at beginning of simulation.*
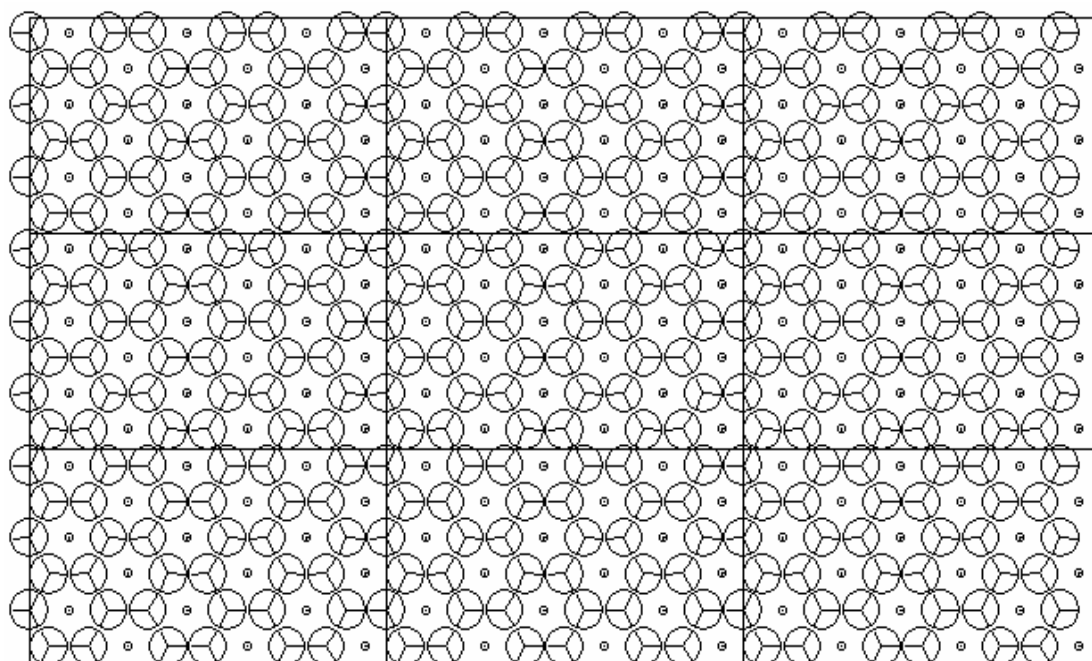
**Figure 5.7-2** *Ice structure Metropolis importance sampling has been performed. In this simulation 200,000 random "flips" were performed.*

Figures 5.7-1 and 5.7-2 are "snap-shots" of the system configuration at a particular temperature. This is possible because the Metropolis importance sampling method allows the information to be extracted for all molecules for a particular temperature. The Wang-Landau method creates a density of states function and thus at one a particular temperature value it is not possible to extract information on the molecules in the system. These "snap-shots" are only possible using the Metropolis importance sampling method.

In order to attempt to reproduce the density versus temperature and energy versus temperature profiles for water a temperature scan was conducted. In the density curve it was hoped to see a first order phase change from the ice to liquid state and to see the density maximum. Since this research is concerned mainly with the density maximum it was more important to have a well-defined density maximum. The temperature was incremented and Metropolis importance sampling was performed after each increment. The temperature values and corresponding reduced energy and reduced density values were printed to file and are graphed below (figures 5.7-3 and 5.7-4).
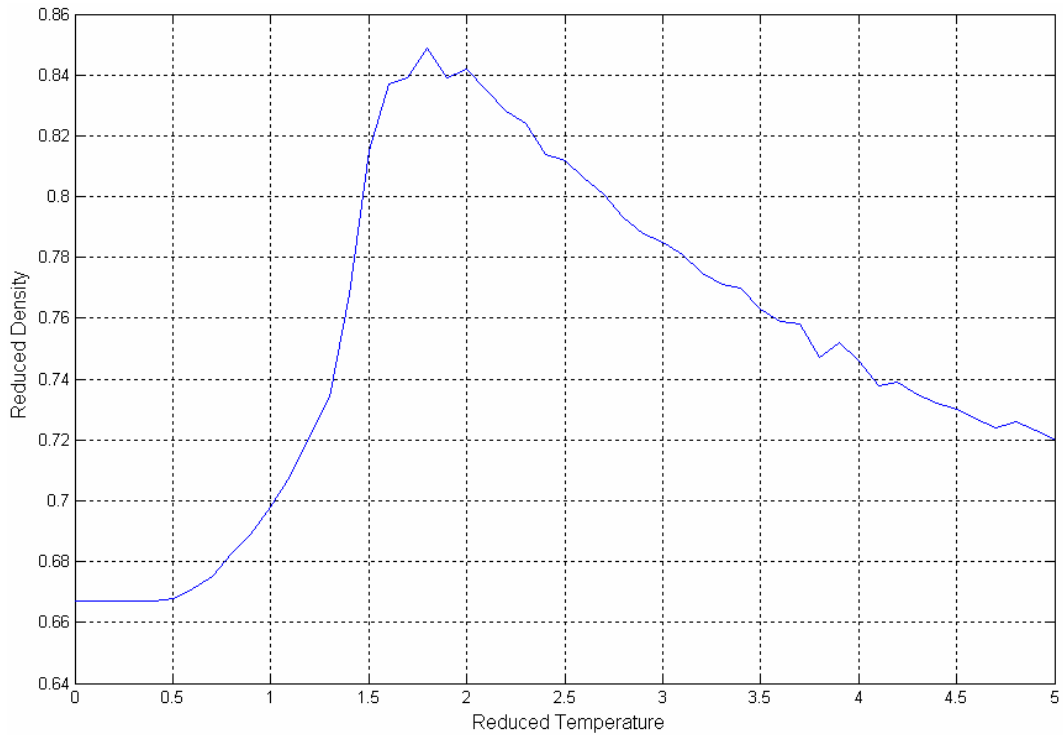
**Figure 5.7-3** *Reduced density versus reduced temperature profile for the Buzano gas lattice water model. 200,000 random flips were performed at each point.*
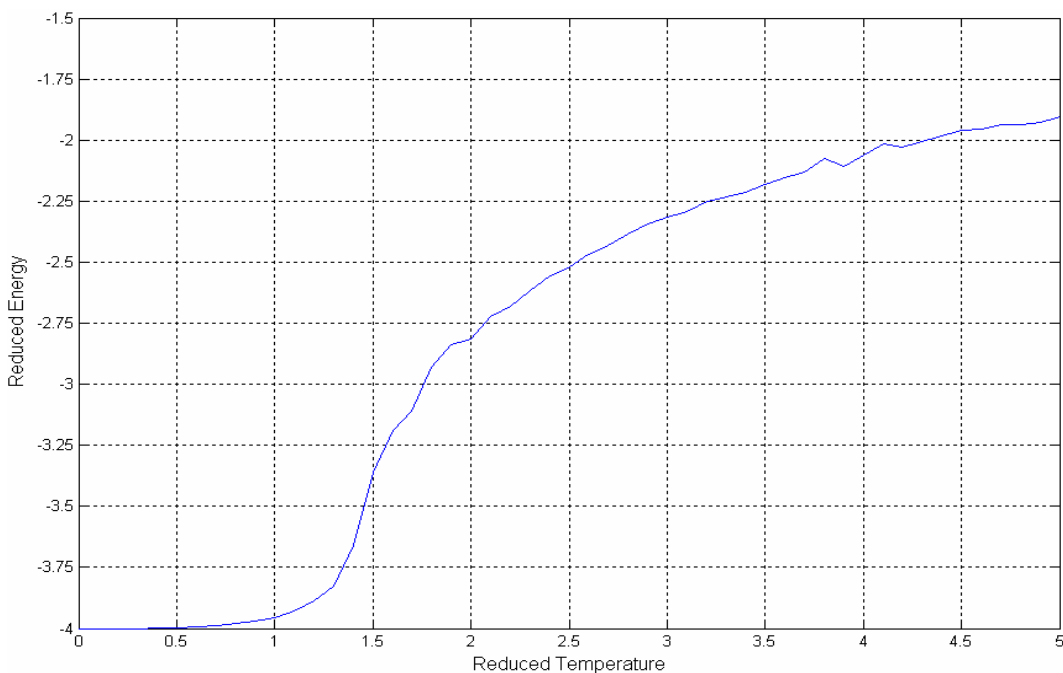


**Figure 5.7-4** *Reduced energy versus reduced temperature profile for the Buzano gas lattice water model. 200,000 random flips were performed at each point.*

The ice phase is clearly visible (figure 5.7-3) at a normalised density of 0.667. This value makes logical sense as when Mercedes-Benz ice forms it forms in cages such

as figure 5.7-2. In this formation two thirds of the sites are active giving rise to a normalised density of 0.667. For example if figure 5.7-2 is analysed taking one of the nine boxes 18 sites are inactive and 36 are active, i.e. 36/54 or 2/3 are active. As thermal energy is added to the system these cages break up, inactive sites become active and the density rises rapidly. The density reaches a maximum at a temperature of 1.8 and as thermal energy is further increased the density drops off, as the higher density state is not sustainable with increasing temperature. Figure 5.7-4 shows the corresponding energy curve.

## 5.7.2 Wang-Landau method results

As with the Metropolis importance sampling approach simulations were carried out to reproduce the density versus temperature and energy versus temperature profiles for water. Temperature scans of Helmholtz free energy and entropy were conducted. All these scans, figures 5.7-5 to 5.7-8 were performed on a 9x6 lattice. Figures 5.7-5 and 5.7-6 are comparable to the results of the Metropolis sampling method. The density profiles compare very favourably. The density maximum is located at a temperature of 1.78 in figure 5.7-5 whereas it is located approximately at a temperature of 1.8 in figure 5.7-3. The ice phase is seen at a normalised density of 0.667 as expected. Reduced energy and reduced density refer to the fact that the Boltzmann constant and the energy associated with the Van der Waals type forces ($\varepsilon$) have been set to unity.

The Wang-Landau density of states approach gives very smooth profiles when compared to Metropolis importance sampling results. Possible reasons for this are discussed in section 5.4.2. All these Wang-Landau simulations were conducted using a two dimensional density of states function, g($E,N$), where $N$ is the number of occupied sites and the partition function is given by equation 5.4-2.
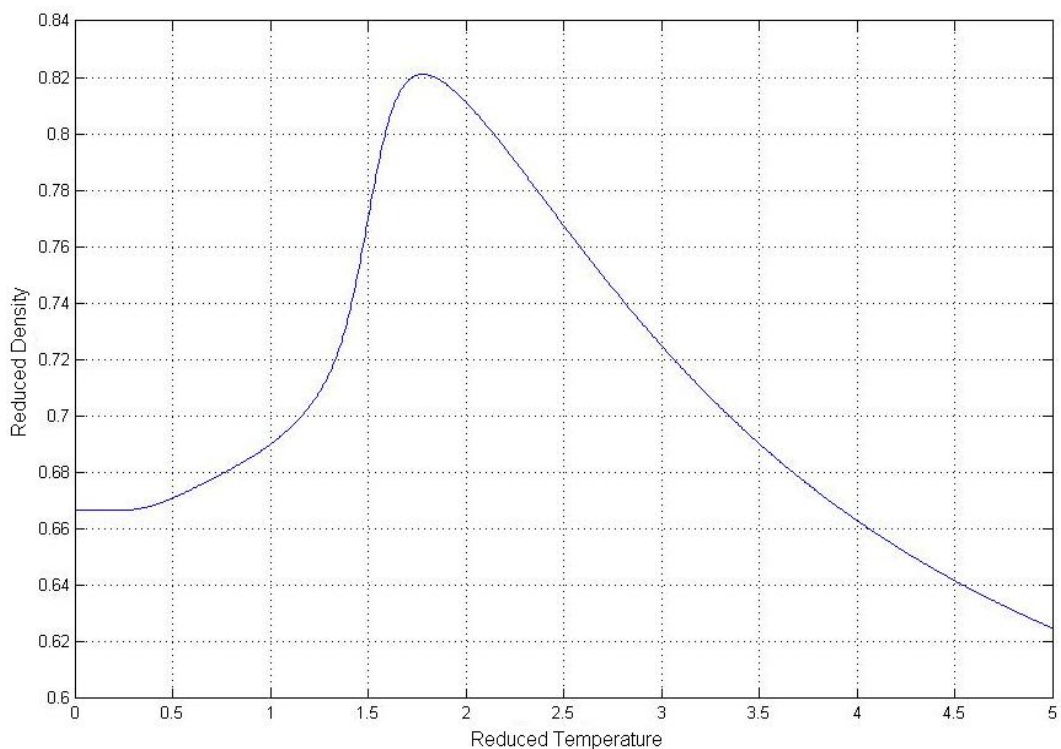
**Figure 5.7-5** *Reduced density versus reduced temperature profile for the Buzano gas lattice water model using the Wang-Landau approach.*
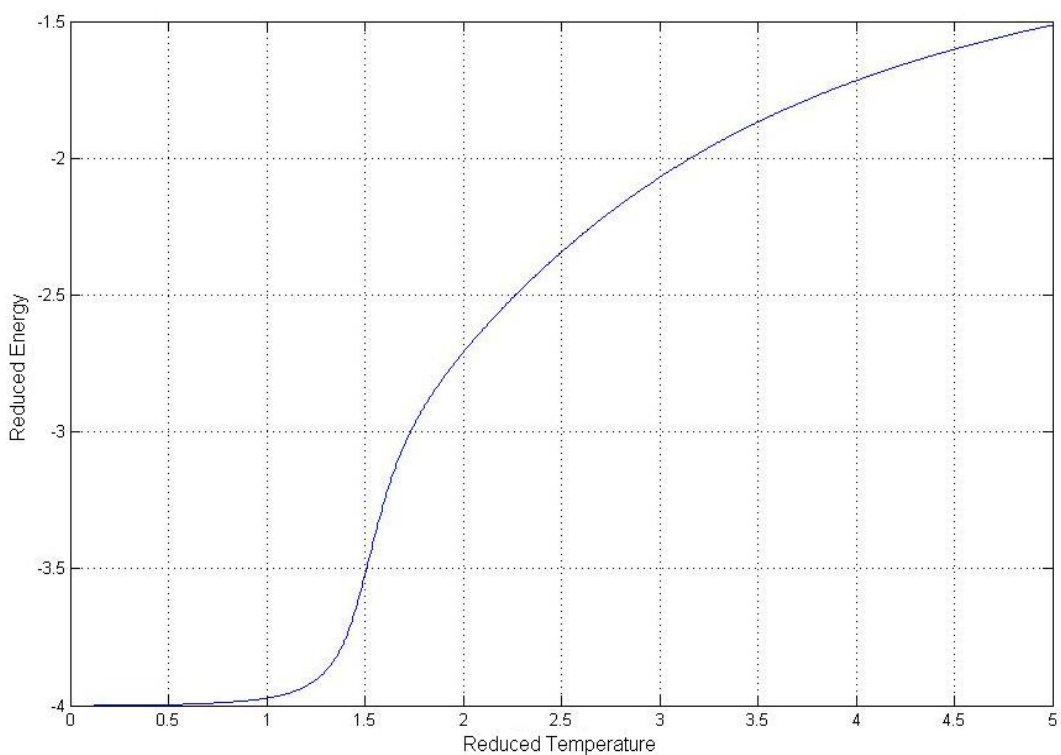


**Figure 5.7-6** *Reduced energy versus reduced temperature profile for the Buzano gas lattice water model using the Wang-Landau approach.*
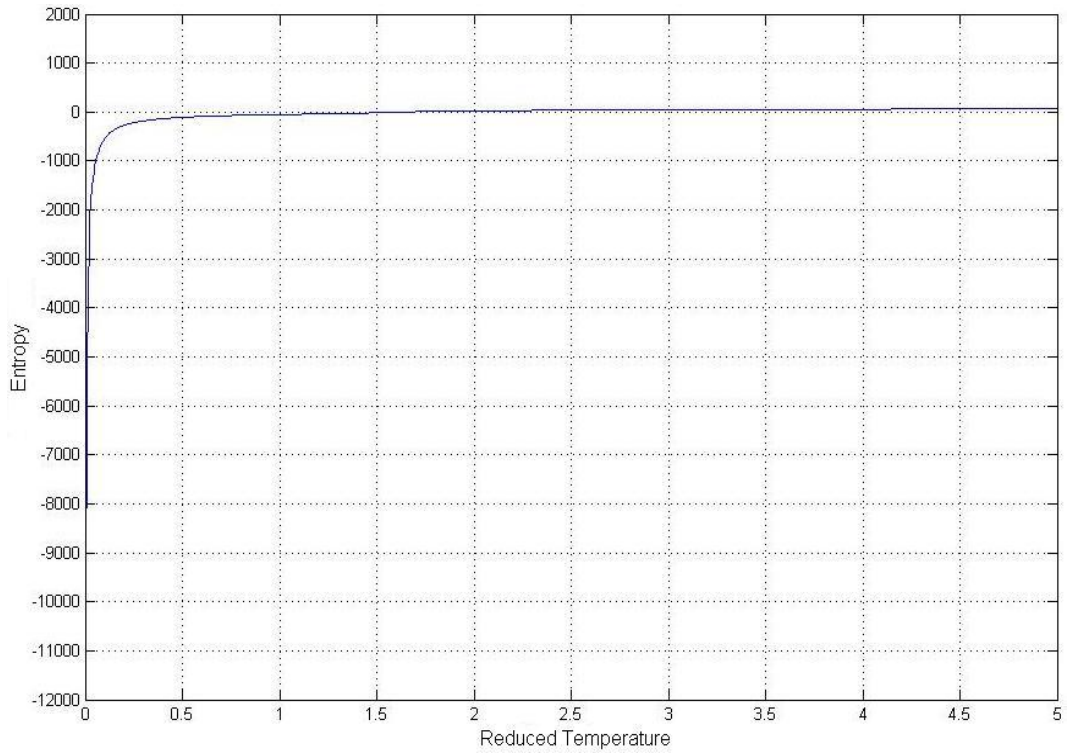
**Figure 5.7-7** E*ntropy versus reduced temperature profile for the Buzano gas lattice water model using the Wang-Landau approach.*
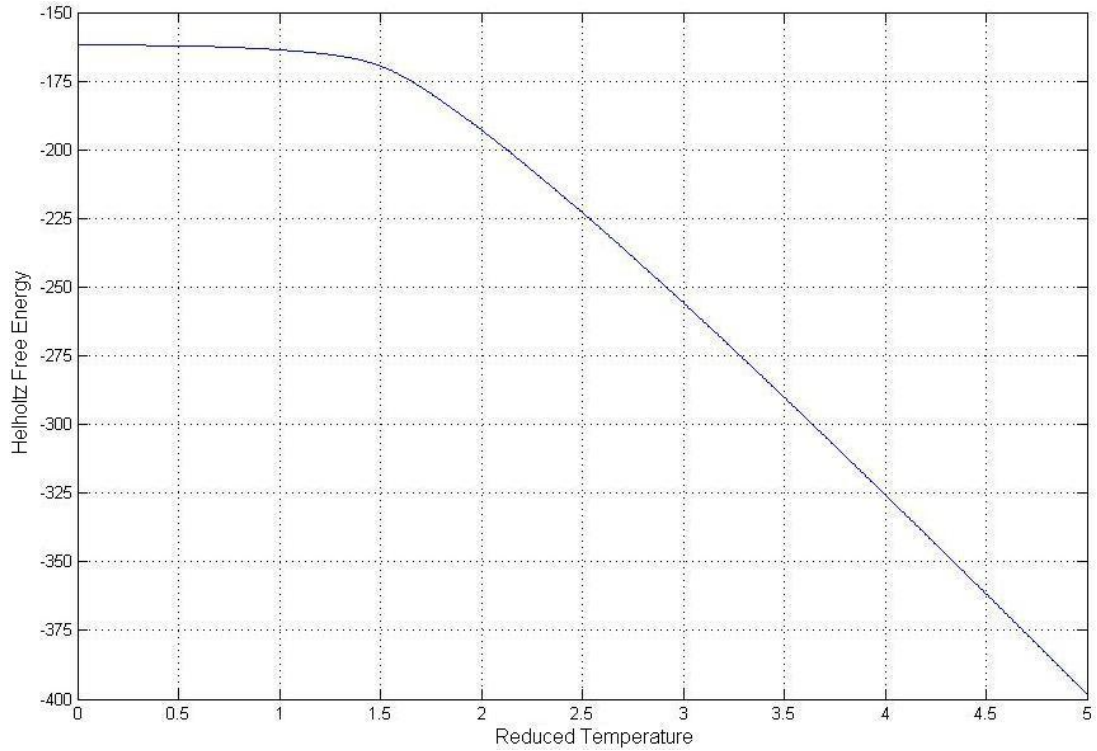


**Figure 5.7-8** *Helmholtz free energy versus reduced temperature profile for the Buzano gas lattice water model using the Wang-Landau approach.*

### 5.7.3 Simulating experimental results

To simulate experimental results a pressure variable is needed. In gas lattice simulations there is no pressure variable but each molecule carries a chemical potential contribution, mu ($\mu$), to the energy function used to evaluate the acceptance probability as described by Buzano et al. [67]. The acceptance rate is high at high chemical potential values and low at low chemical potential values. The chemical potential variable in gas lattice simulations is analogous to the pressure variable in off-lattice simulations. In off-lattice models the chemical potential is associated with solute concentration. However, that is not the case with gas lattice models. Concentration is altered in this work in numerous ways as desribed in sections 5.7.3.1 to 5.7.3.3 and 5.8. In a high chemical potential (pressure) regime, bulk water freezing is prevented by lack of vacancies. Conversely, in a low chemical potential (pressure) regime, the number of vacancies is large enough to allow the formation of a long-ranged ordered hydrogen bond network [67]. All results up to this section have been performed with the chemical potential set to -1.5. Figure 5.6-9 displays a density versus temperature profile with the chemical potential set to 5. As temperature increases density decreases as expected.
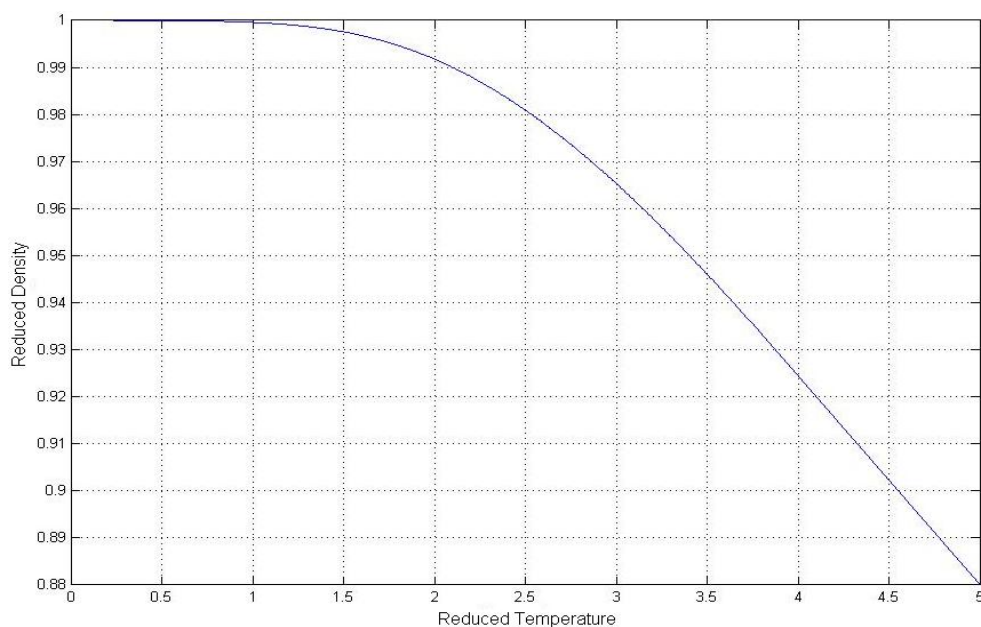


**Figure 5.7-9** *Reduced density versus reduced temperature profile for the Buzano gas lattice water model using the Wang-Landau approach with the chemical potential set to 5.*

If the chemical potential is set to a sufficiently high value Mercedes-Benz ice
(figure 5.7-2) will not form.  All sites become occupied (figure 5.7-10) and the
density becomes unity.
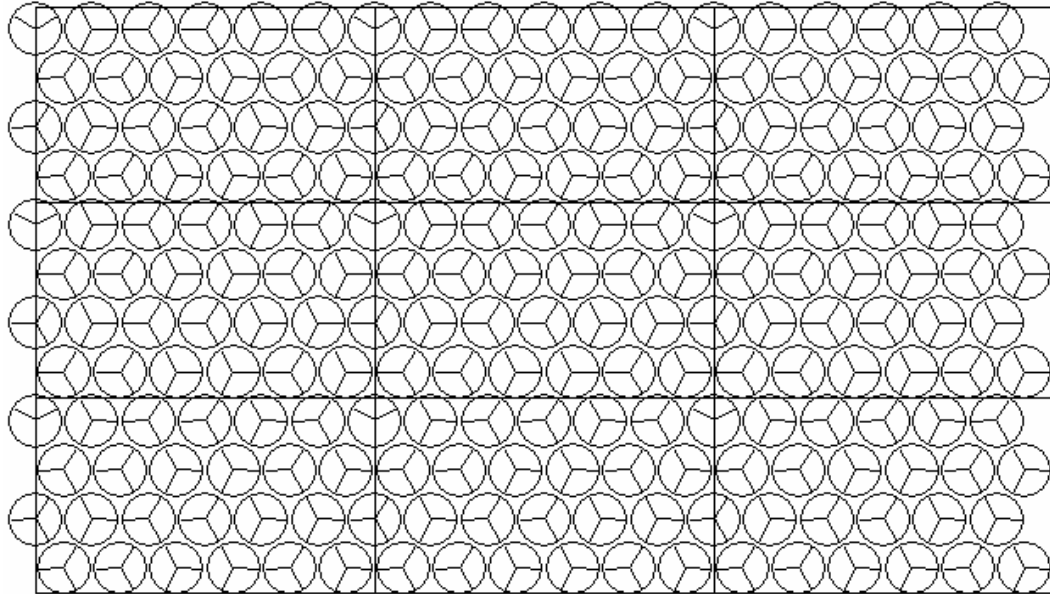


**Figure 5.7-10** *Low temperature "snap-shot" of the system at high pressure.  All sites
are occupied despite hydrogen bonding throughout the lattice giving rise to a density
of unity.  This "snap-shot" was obtained from the Metropolis importance sampling
method.*

Thus, at high chemical potential the maximum density feature is not visible at all.
However, experiments can be conducted using intermediate chemical potentials and
the movement of the density maximum can be tracked.  Figure 5.7-11 shows density
versus temperature profiles for various different chemical potential.  As chemical
potential increases the temperature of maximum density shifts to lower temperatures.
Plotting the temperatures of maximum density against the corresponding chemical
potential and calculating the slope of this trend gives the rate of change of the
temperature of maximum density with respect to chemical potential $\left( \frac{\mathrm{d}T_{md}}{\mathrm{d}\mu} \right)$

(figure 5.7-12).  The rate of change of the temperature of maximum density with
respect to chemical potential is analogous to the rate of change of the temperature of
maximum density with respect to applied pressure in experimental results.  The slope

given in figure 5.7-12 is the rate of change of the temperature of maximum density with respect to chemical potential for pure water.
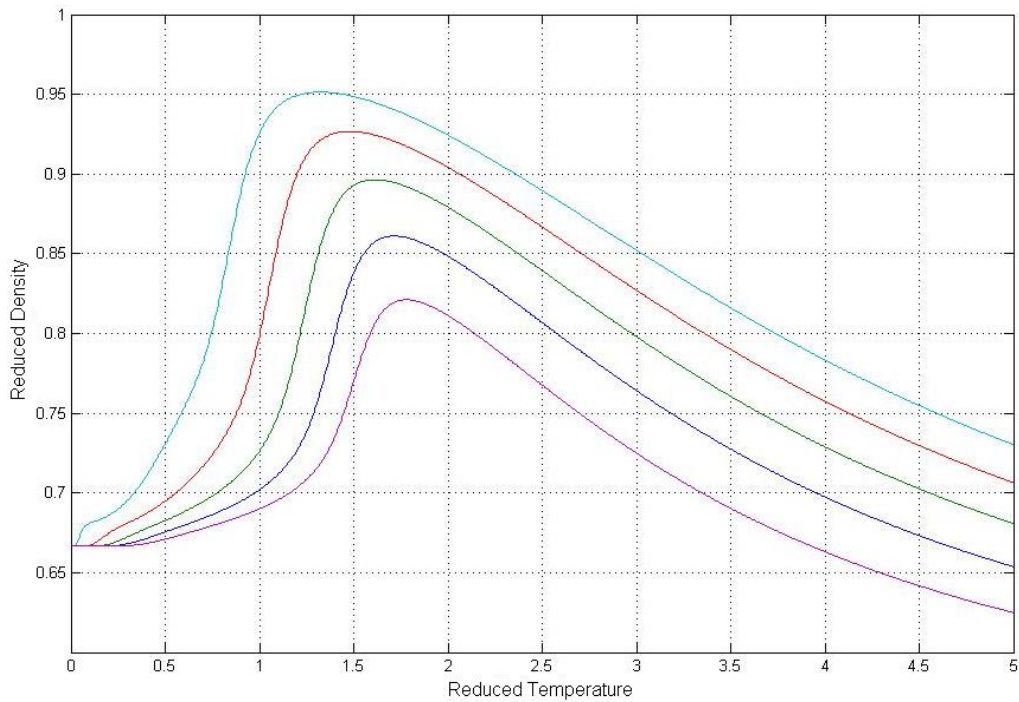


**Figure 5.7-11** *Reduced temperature versus reduced density for pure water at various values of chemical potential. $\mu = -1.5$ (magenta), $\mu = -1.0$ (blue), $\mu = -0.5$ (green), $\mu = 0.0$ (red) and $\mu = 0.5$ (turquoise).*
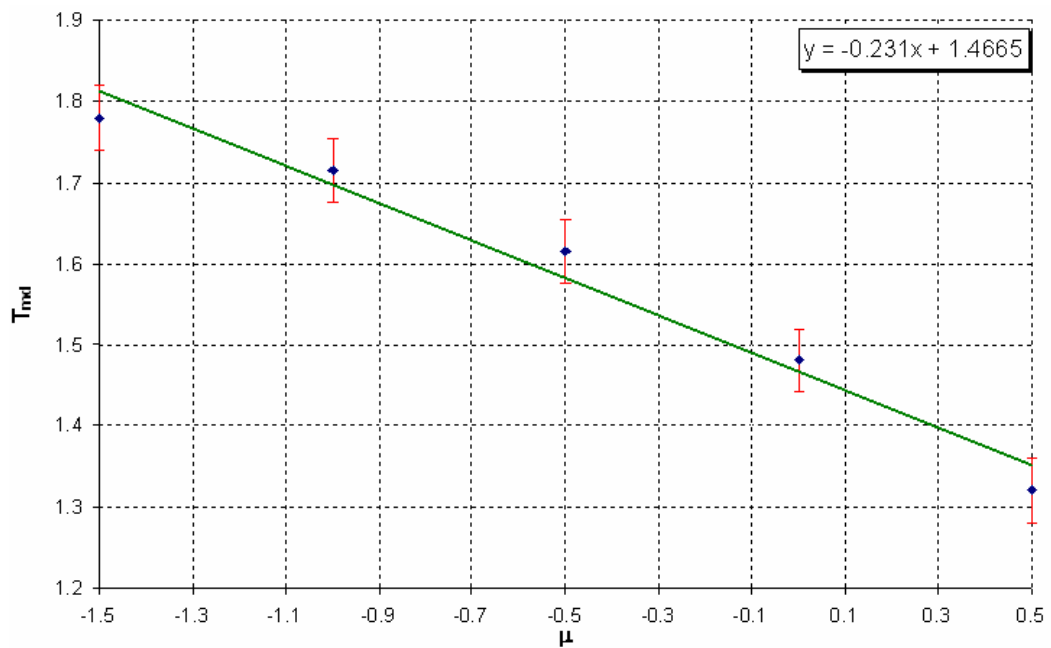


**Figure 5.7-12** *Temperature of maximum density versus chemical potential for pure water.*

## 5.7.3.1 Addition of hydrophilic molecules to the lattice

In order to explore this rate of change of the temperature of density maximum with respect to chemical potential at different concentrations something had to be added to the lattice that did not behave like a water molecule. In one approach this was done by adding molecules to the lattice that have greater affinity to form hydrogen bonds. For the pure water Buzano model if arms of nearest neighbour molecules lined up a hydrogen bond was formed and an energy term of $-\eta < 0$ was added to the total energy of the system where $\eta$ was equal to 3. Molecules were added to the lattice with an $\eta$ value of 4. These molecules were more likely to form hydrogen bonds with nearest neighbours. The rate of change of the temperature of maximum density with respect to temperature was calculated for various numbers or concentration of added molecules. Figure 5.7-13 summarises results from Wang-Landau simulations at each concentration. All simulations were performed on a 9x6 lattice.

Results shown in figure 5.7-13 are from Wang-Landau simulations carried out using the same random number seed. Added molecules were in random locations but these locations remained the same as the number of added molecules increased. For example if the first added molecule was in location (1, 1) the second molecule added would have been in a different location, for example location (2, 2). However, when the simulation was carried out for two added molecules the first molecule was still in location (1, 1). When three molecules were added to the lattice two of the added molecules would be in locations (1, 1) and (2, 2) and so on. Simulations have been carried out with different random number seeds to see if results are comparable. Plotting the rate of change of the temperature of maximum density with respect to pressure against molecules added it can be seen that the rate of change of the temperature of maximum density with respect to chemical potential becomes less steep with increasing concentration with respect to the pure water point (figure 5.6-14). This is similar to the behaviour of the monohydric alcohols studied experimentally.
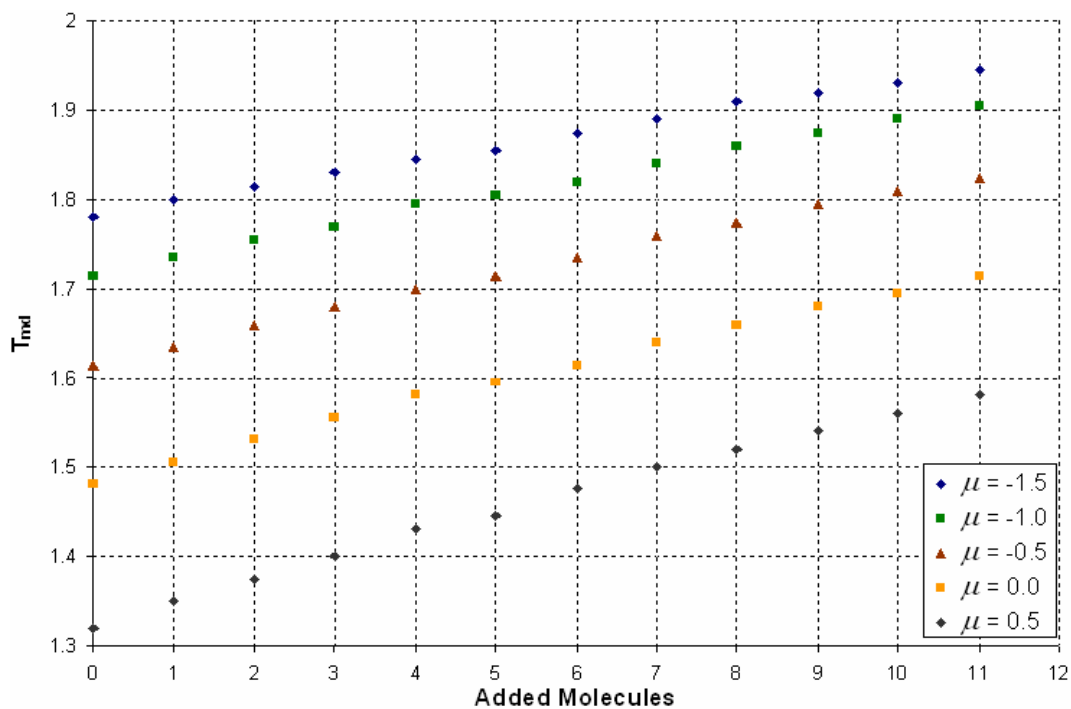
**Figure 5.7-13** *Temperature of maximum density versus added molecules (hydrophilic) for various chemical potentials.*
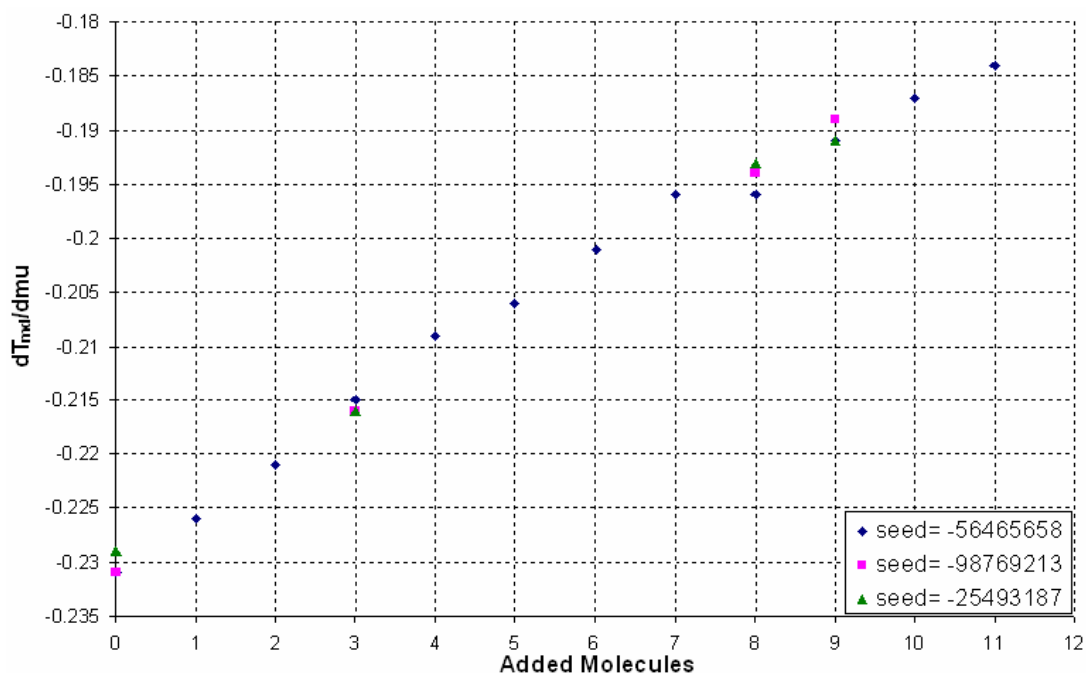


**Figure 5.7-14** *Rate of change of the temperature of maximum density with respect to chemical potential for differing numbers of added molecules with $\eta =4$. Different random seeds used to compare results as different seeds give rise to a different set of locations for added molecules.*

## 5.7.3.2 Addition of non-bonding molecules to the lattice

Non-bonding molecules were added to the lattice to model the addition of hydrophobic molecules to water. Mercedes-Benz molecules can be present or absent from the lattice and if a molecule is present it can be in one of three rotational orientations (figure 5.6-5). Two of these orientations allow for bonding with neighbouring molecules but one orientation forbids bonding with adjacent molecules. Non-bonding molecules were added to the lattice in random locations and were set to be always present and in the non-bonding rotational orientation (figure 5.7-15). Consequently, at low temperatures the lattice could not condense to Mercedes-Benz ice. The non-bonding molecule could not form a hexagonal cage which is necessary to form the low-density 'ice' configuration (figure 5.7-2). The rate of change of the temperature of maximum density with respect to temperature was calculated for various numbers or concentration of added molecules. Figure 5.7-16 summarises results from Wang-Landau simulations at each concentration. All simulations were performed on a 9x6 lattice.
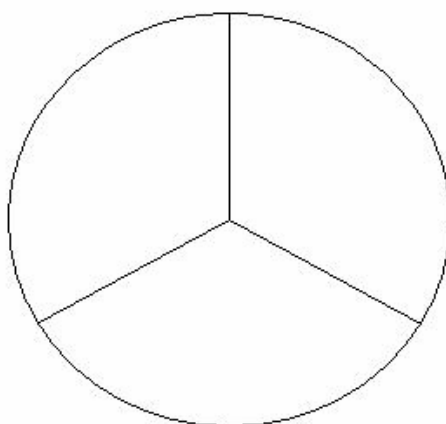


**Figure 5.7-15** *Mercedes Benz molecule in non-bonding orientation.*

The rate of change of the temperature of maximum density with respect to pressure was plotted against non-bonding molecules added. It can be seen that the rate of change of the temperature of maximum density with respect to chemical potential becomes less steep with increasing concentration with respect to the pure water point (figure 5.6-17). This is similar to the behaviour of the monohydric alcohols studied experimentally.
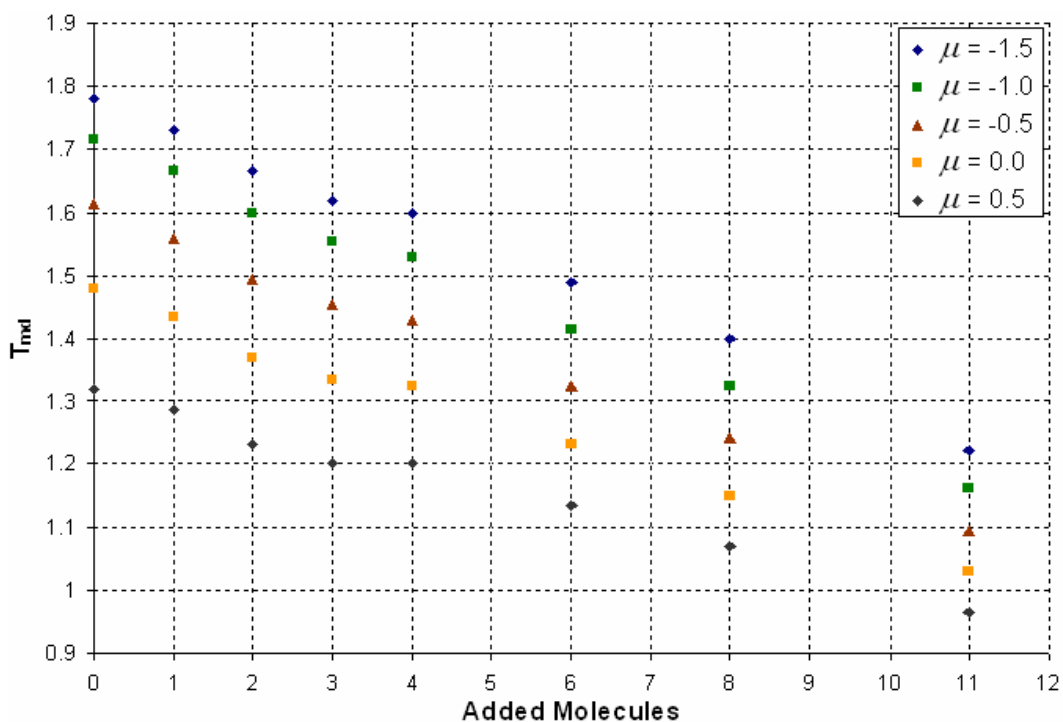
**Figure 5.7-16** *Temperature of maximum density versus added molecules (hydrophobic) for various chemical potentials.*
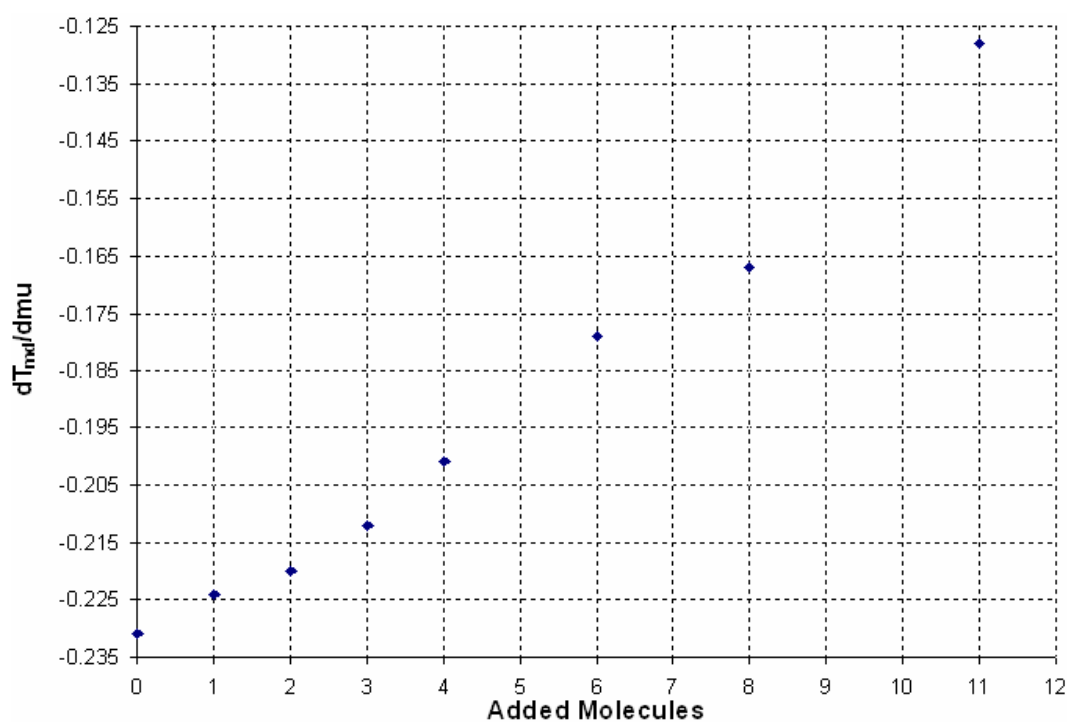


**Figure 5.7-17** *Rate of change of the temperature of maximum density with respect to chemical potential for differing numbers of hydrophobic molecules added.*

148

The behaviour of the temperature of maximum density with respect to chemical potential (pressure) under increasing concentrations of hydrophilic and hydrophobic molecules has been compared (figure 5.7-18). The rate of change of the temperature of maximum density becomes less negative as the number of added molecules increases for both trends but at a faster rate for the hydrophobic trend.
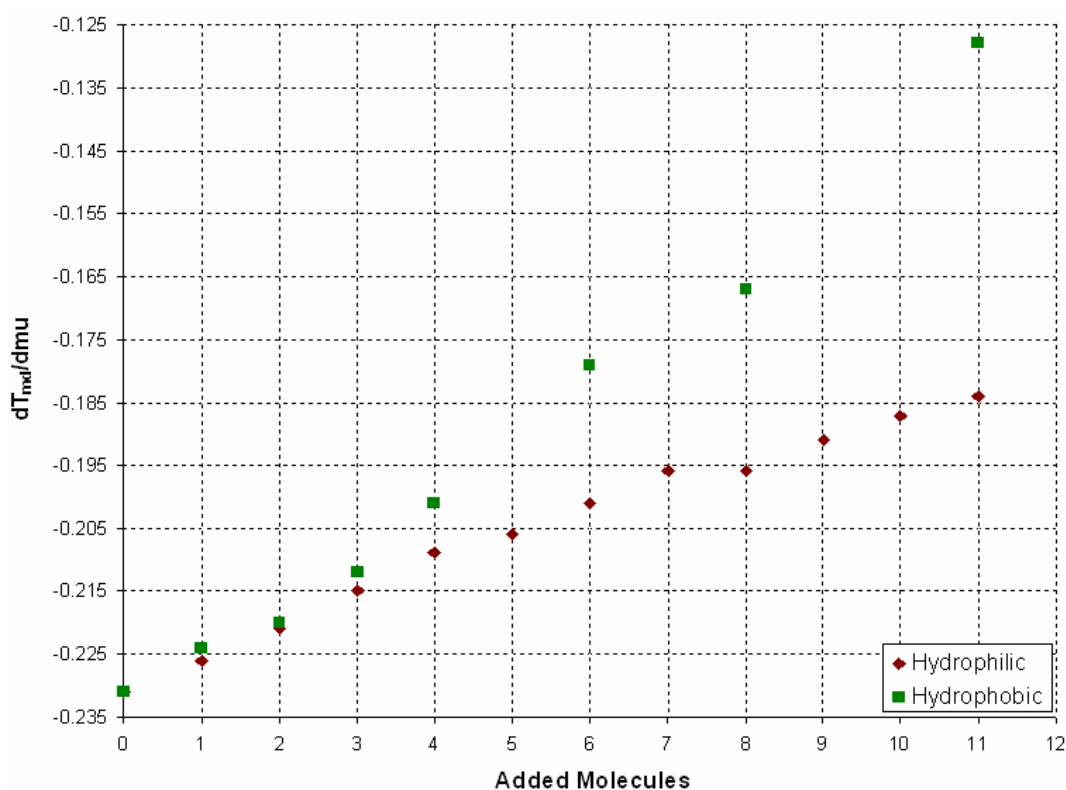


**Figure 5.7-18** *Rate of change of the temperature of maximum density with respect to chemical potential for differing numbers of hydrophobic and hydrophilic molecules added.*

### 5.7.3.3 Increased hydrogen bond strength

Another approach taken to investigate the rate of change of the temperature of density maximum with respect to chemical potential was to increase the hydrogen bond strength of every molecule in the lattice. For the pure water model if arms of nearest neighbour molecules lined up a hydrogen bond was formed and an energy term of $-\eta < 0$ was added to the total energy of the system where $\eta$ was equal to 3. In this model the hydrogen bond strength was increased to a maximum of 5 in 0.2 increments. As the hydrogen bond strength was increased all molecules were more

likely to form hydrogen bonds with nearest neighbours. At each new global $\eta$ value analysis of the temperature of maximum density with respect to chemical potential was carried out. All simulations were performed on a 9x6 lattice.

Figure 5.7-19 summarises results from Wang-Landau simulations at each global $\eta$ value. The rate of change of the temperature of maximum density with respect to chemical potential becomes less steep with increasing values of $\eta$ (hydrogen bond strength) with respect to the pure water point (figure 5.6-20). This is similar to the behaviour of the monohydric alcohols studied experimentally. The values of the rate of change of the temperature of maximum density are positive above an $\eta$ value of approximately 4.7. This is unusual as no other attempt to reproduce experimental behaviour has shown this result.
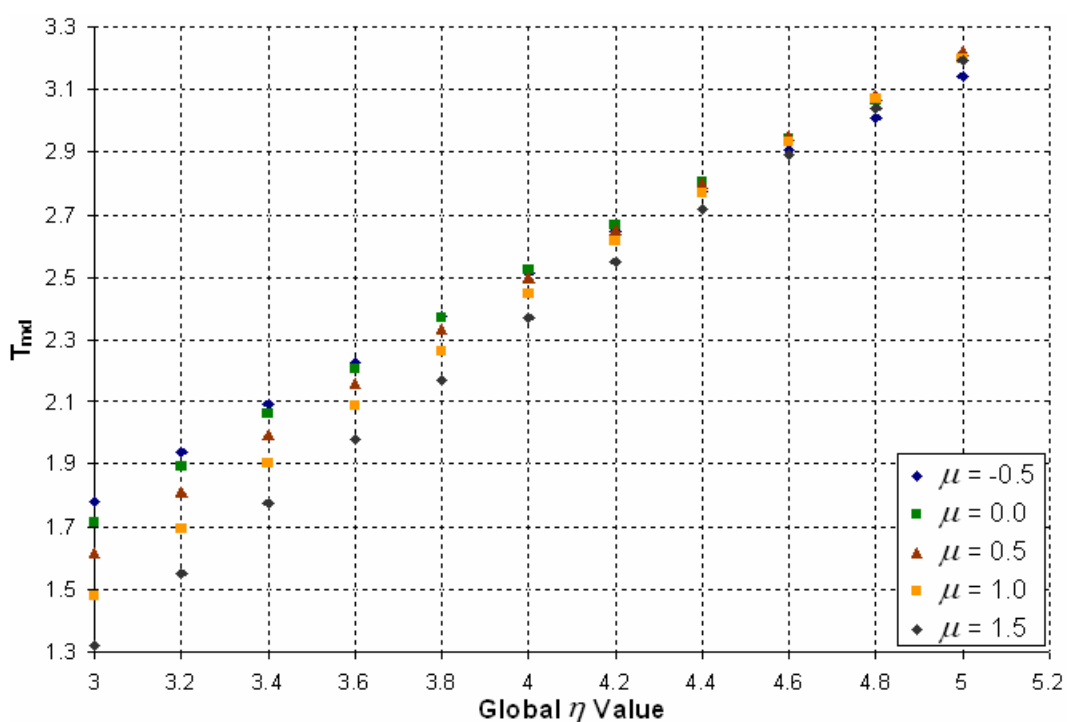


**Figure 5.7-19** *Temperature of maximum density versus global $\eta$ value (hydrogen bond strength).*
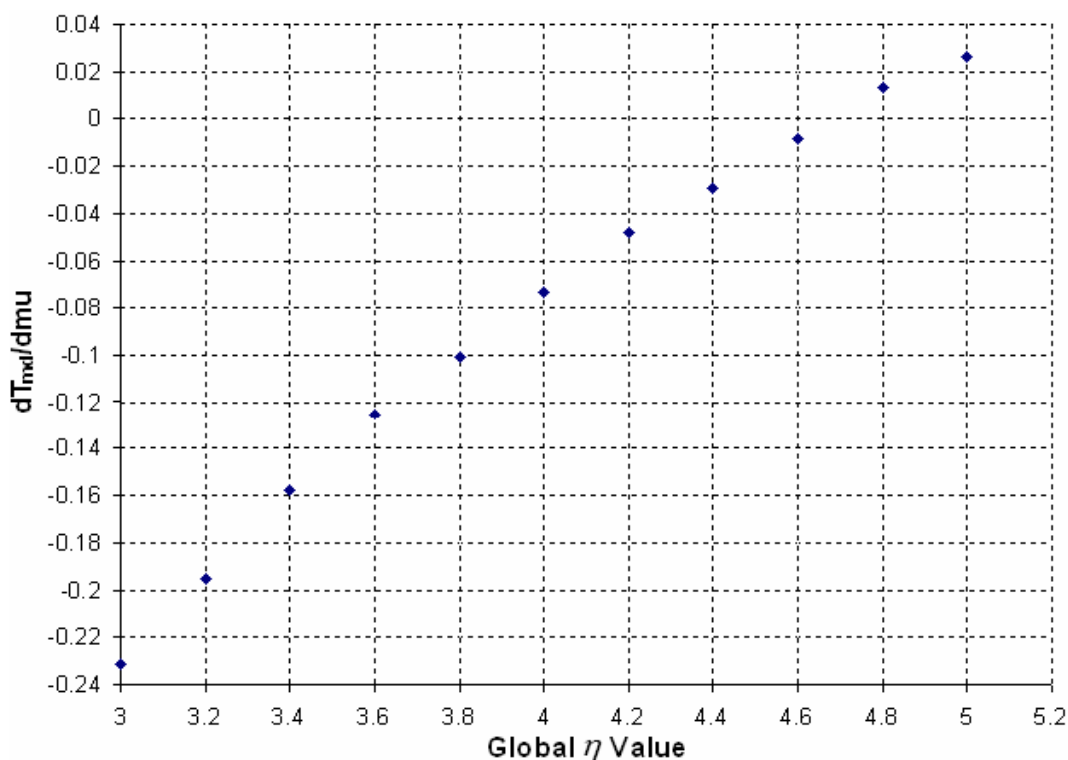
**Figure 5.7-20** *Rate of change of the temperature of maximum density with respect to chemical potential for increasing global $\eta$ value (hydrogen bond strength).*

## 5.8 Strong and weak water

Simulations were performed involving pure water ('o'), strong water ('s') and weak water ('w'). Mixtures of pure water with strong water and pure water with weak water were investigated. By investigating mixtures the expected influence of simple solutes on the behaviour of the temperature of maximum density can be studied at various concentrations. Ordinary water is modelled using the Buzano et al. model [67] as described in section 5.6. Strong water effectively increases the energy associated with each molecule, ($\varepsilon$), which in turn increases the hydrogen bond strength $\eta$ (section 5.6). Weak water effectively reduces the magnitude of $\varepsilon$ (and hence $\eta$). The increase or reduction in the energy parameters is achieved by altering the radii of the strong and weak water molecules with respect to the ordinary water molecules. Strong water molecules have a larger radius than ordinary water molecules. Weak water molecules have a smaller radius than ordinary water molecules. Although the radii vary the centres of all molecules are fixed at lattice points. The energy parameters are then scaled by the square of the radius. For all

Wang-Landau simulations the radius of pure water Mercedes-Benz water molecules is 0.25. Strong water molecules have a radius of 0.3 and weak water molecules have a radius of 0.125 (figure 5.8-1).



'w' water molecule          'o' water molecule          's' water molecule
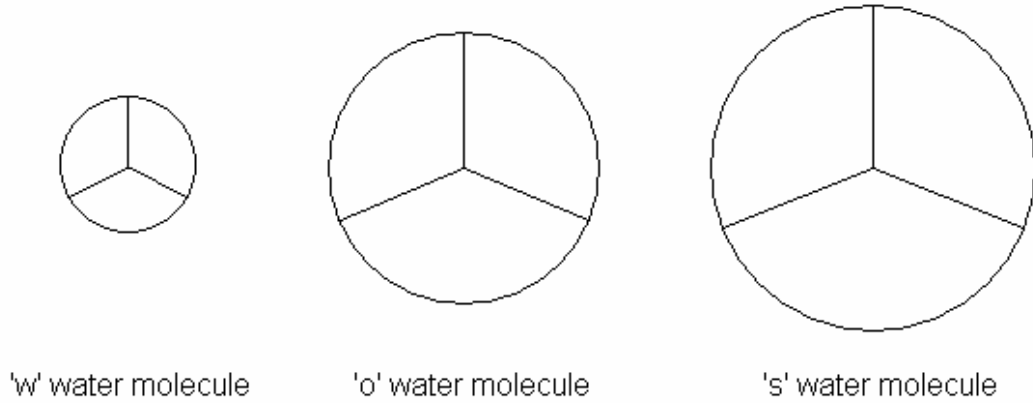
**Figure 5.8-1** *Graphical representation of weak, ordinary and strong water molecules (molecules are to scale).*

In Wang-Landau simulations up to this point a two-dimensional density of states function, g($E$, $N$), was evaluated. For this approach a three-dimensional density of states function, g($E$, $d$, $c$), is evaluated, where $d$ is the density given by:

$$d = \frac{(N_0 + N_s)}{N_{site}} \qquad (5.8\text{-}1)$$

and the concentration by:

$$c = \frac{N_s}{N_0 + N_s} \qquad (5.8\text{-}2)$$

where $N_{site}$ is the number of lattice sites used in the simulation, $N_0$ is the number of sites occupied by 'o' water and $N_s$ is the number of sites occupied by 's' water. If a pure water and weak water mixture is under investigation $N_s$ is replaced by $N_w$. The partition function for this three-dimensional model is given by:

152

$$Z = \sum_{E,d,c} g(E,d,c)e^{-E/kT}e^{\mu_d d/kT}e^{\mu_c c/kT} \qquad (5.8\text{-}3)$$

where $\mu_d$ is the chemical potential which is analogous to pressure as discussed in section 5.7.3, $c$ is the concentration and $\mu_c$ is the concentration parameter which controls the number of added strong or weak water molecules.  The advantage of using this three-dimensional parameter space is that from a single Wang-Landau simulation information can be obtained at any chemical potential or pressure and at any concentration of strong or weak molecules.  The two-dimensional density of states function requires that a different Wang-Landau simulation must be performed for every concentration value.

## 5.8.1 Strong and weak water results

Since strong water molecules have higher hydrogen bond strengths than ordinary water molecules it is expected that mixtures of ordinary water and strong water will cause an elevation in temperature of maximum density.  Conversely, it is expected that mixtures of weak water and ordinary water will cause the temperature of maximum density to fall.  Plots of density against temperature for pure ordinary water over a range of pressure values are shown in figure 5.8-2(a).  At low pressures and low temperatures the density is 0.667 corresponding to Mercedes-Benz ice where two thirds of the lattice sites are occupied by 'o' molecules and one third of the sites are vacant.  This highly structured arrangement accounts for the relatively low density.  With increasing temperature the ice structure breaks up and vacant sites become occupied thereby increasing the density.  As the temperature increases further the density reaches a limiting value of 0.5.  This process gives rise to a clear signature of the density maximum in the density profile.  The density profiles are similar to that of figure 5.7-5 as expected.

Density profiles at various values of $\mu_d$ were investigated to study the effect of pressure on the temperature of maximum density.  As expected the temperature of maximum density shifts to lower values as pressure increases (figure 5.8-2(b)).  At sufficiently high values of $\mu_d$ even at low temperatures the density is at unity.  This

occurs because at high pressure the Mercedes-Benz ice structure is forced to collapse and all sites become occupied giving rise to a density of unity. Consequently, at high pressure values the temperature of maximum density vanishes.
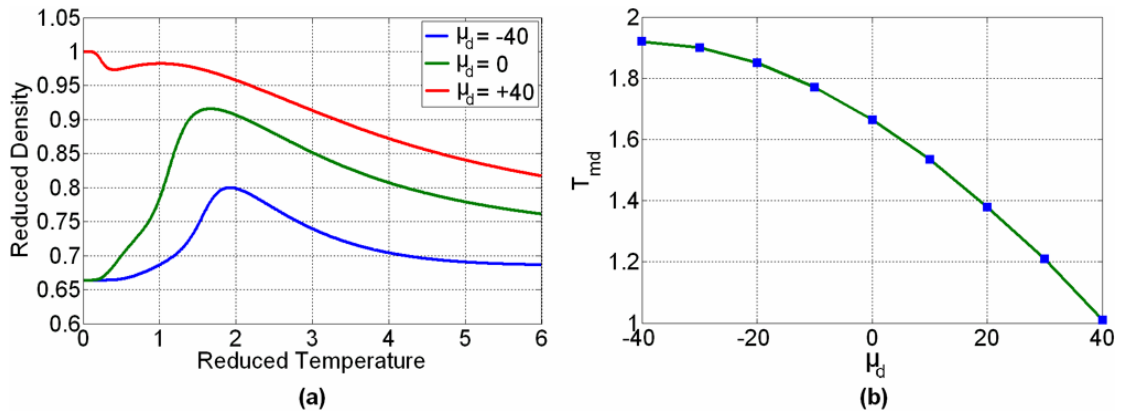


**Figure 5.8-2(a)** *Reduced density versus reduced temperature for pure 'o' water at various pressures.*

**Figure 5.8-2(b)** *Temperature of maximum density ($T_{md}$) versus pressure for pure 'o' water.*

In order to study the effect of ordinary and strong water and ordinary and weak water mixtures the concentration parameter ($\mu_c$) was varied over a wide range (-200 to +200). By using a wide range it was possible to simulate mixtures which ranged from pure water when $\mu_c$ was large and negative to pure strong (or pure weak) water when $\mu_c$ was large and positive. At low concentrations both mixtures behave like pure ordinary water (figures 5.8-3(a) and 5.8-4(a)) and the values of the temperatures of maximum density in both cases were comparable with ordinary water. At higher concentrations of strong water the temperatures of maximum density are all shifted to higher values for a fixed pressure (figure 5.8-3(b)). At higher concentrations of weak water the temperatures of maximum density are all shifted to lower values for a fixed pressure (figure 5.8-4(b)).
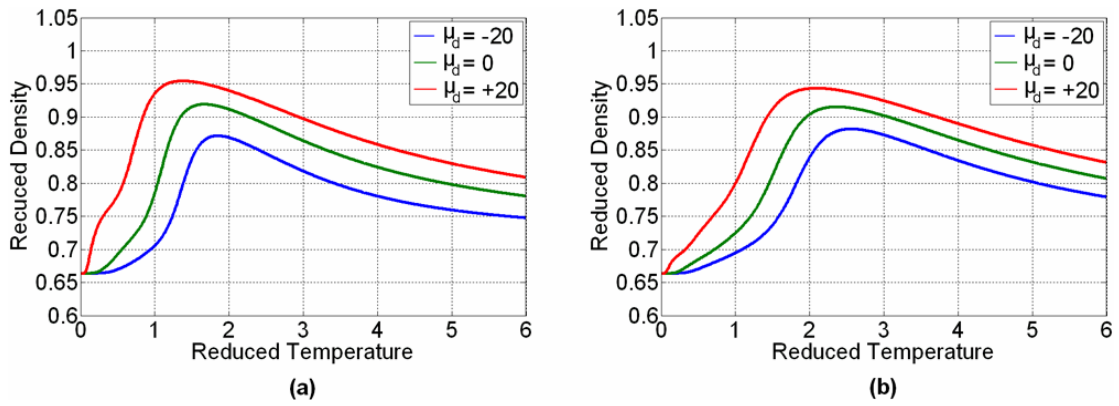
**Figure 5.8-3(a)** *Reduced density versus reduced temperature for a mixture of 'o' and 's' waters at a concentration parameter of -200 for various pressure values.*

**Figure 5.8-3(b)** *Reduced density versus reduced temperature for a mixture of 'o' and 's' waters at a concentration parameter of +200 for various pressure values.*
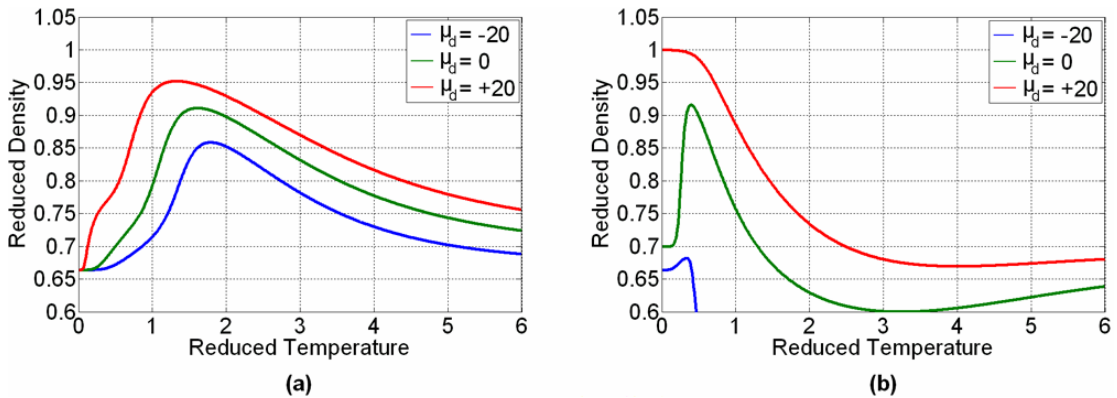


**Figure 5.8-4(a)** *Reduced density versus reduced temperature for a mixture of 'o' and 'w' waters at a concentration parameter of -200 for various pressure values.*

**Figure 5.8-4(b)** *Reduced density versus reduced temperature for a mixture of 'o' and 'w' waters at a concentration parameter of +200 for various pressure values.*

The effect of concentration on the temperature of maximum density is summarised in figures 5.8-5 and 5.8-6. For mixtures of ordinary and strong waters the temperature of maximum density rises with increasing concentration to a maximum value of 2.4 at the set pressure (figure 5.8-5). For mixtures of ordinary and weak waters the temperature of maximum density decreases with increasing concentration to a value of 0.4 at the set pressure (figure 5.8-6). At low concentrations of -200 both mixtures behave like ordinary water and the temperature of maximum density is approximately 1.6 for both mixtures as expected.
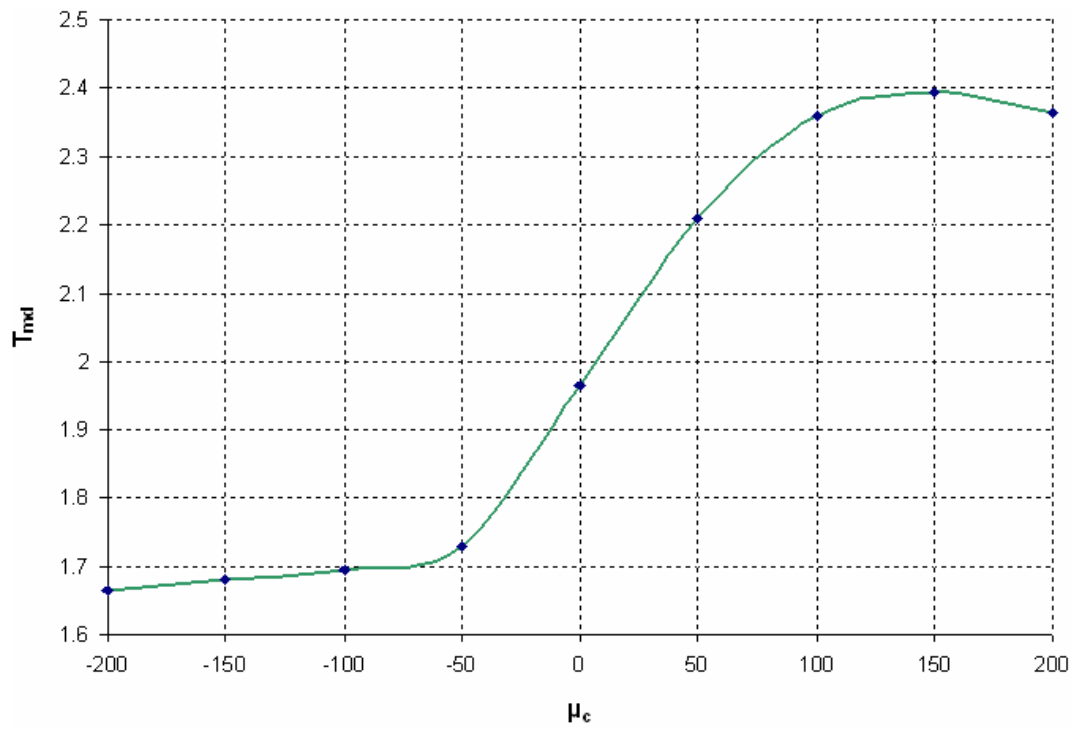
**Figure 5.8-5** *Temperature of maximum density versus $\mu_c$ for a mixture of 'o' and 's' waters ( $\mu_d$ = 0 throughout).*
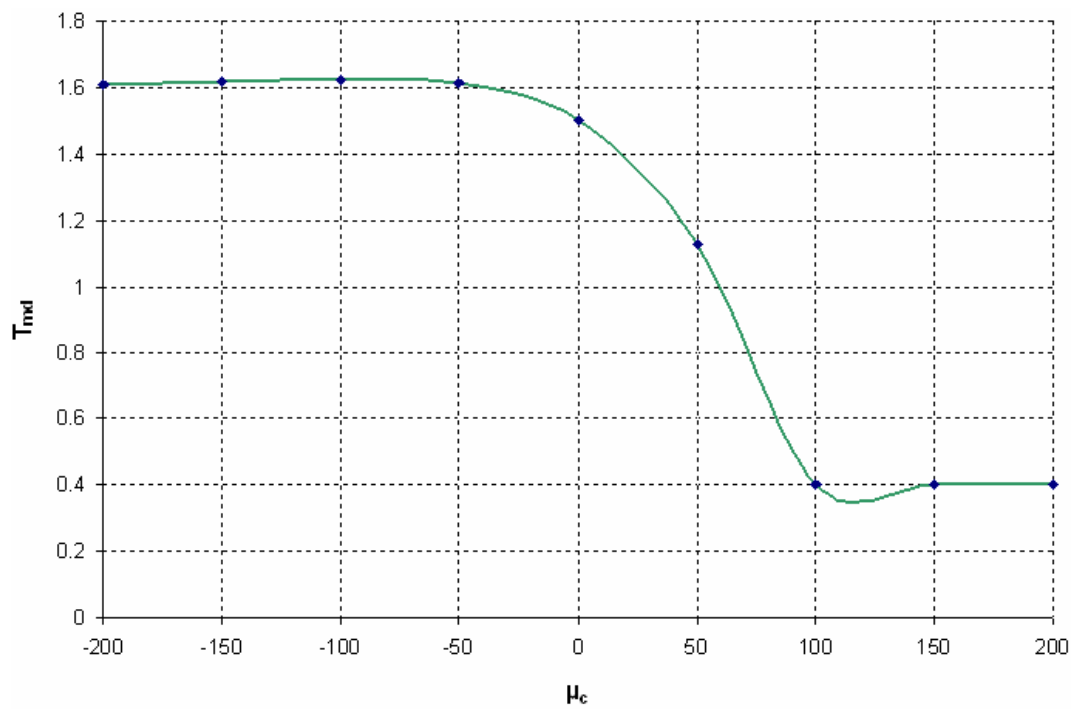


**Figure 5.8-6** *Temperature of maximum density versus $\mu_c$ for a mixture of 'o' and 'w' waters ( $\mu_d$ = 0 throughout).*

Using this model attempts were made to reproduce experimental results. In order to carry out this analysis mixtures were investigated at various values of the concentration parameter ($\mu_c$) and pressures ($\mu_d$). For a set concentration the temperatures of maximum density at various pressure values were extracted from the density profiles. By plotting the temperature of maximum density against pressure a graph such as figure 5.8-2(b) was obtained. A restricted pressure range (-20 to +20) was chosen for this analysis. Over this pressure range the temperature of maximum versus pressure graph was linear. The slope of this linear trend is the rate of change of the temperature of maximum density with respect to pressure. Values of this rate of change were calculated for various concentrations of ordinary and strong waters and ordinary and weak waters (figure 5.8-7). For both trends the slopes become less negative as concentration increases. This trend is similar to that of the monohydric alcohols found experimentally.
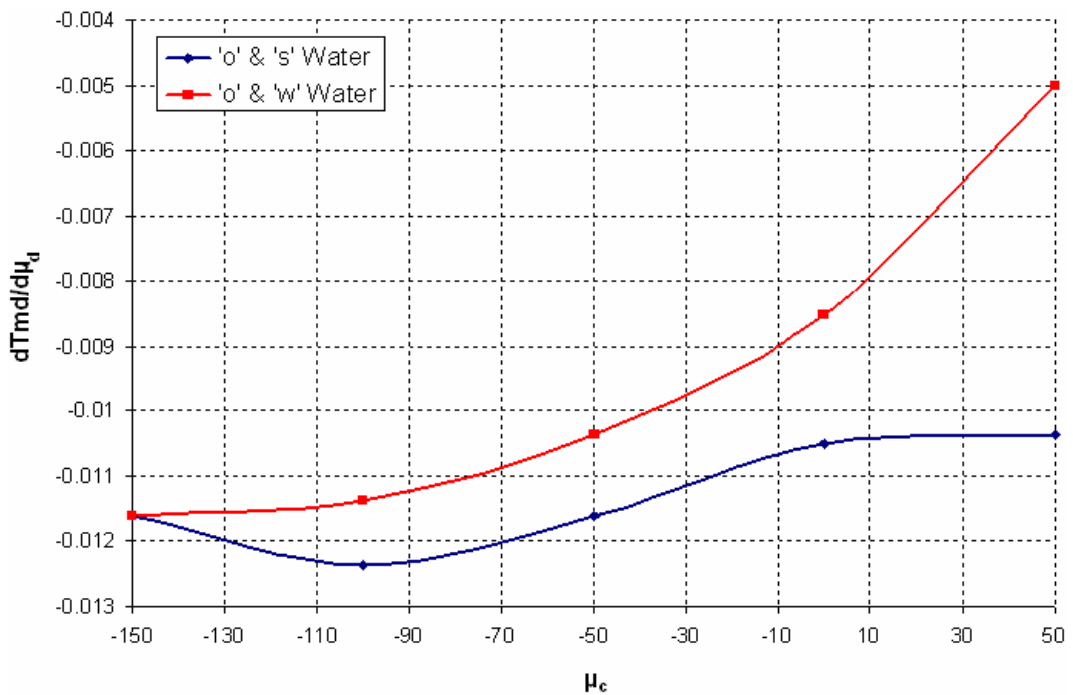


**Figure 5.8-7** *Rate of change of the temperature of maximum density with respect to pressure for various concentrations of 'o' and 's' waters and 'o' and 'w' waters.*

At concentration parameter values below -150 both the 'o' and 's' and the 'o' and 'w' trends do not vary as both mixtures behave like pure ordinary water at low concentrations. Above a concentration parameter value of +50 density maximums are no longer visible for the 'o' and 'w' mixture even in the restricted pressure range

of -20 to +20.  For these reasons the concentration parameter range has been restricted (-150 to +50) in figure 5.8-7.  These results will be discussed and compared with experimental results and results from macroscopic modelling in chapter 6.

# Chapter 6

# Conclusions

## 6.1 Conclusions

The investigations described in this thesis are mainly concerned with the behaviour of the temperature of maximum density of aqueous solutions under applied pressure. In order to carry out these investigations a pressure chamber and computer-controlled hydraulic system was designed and constructed. The experimental apparatus used was a modified version of the system described in Cawley et al [37]. Many modifications were made to this system including updating of the software and hardware. The pressure vessel and hydraulic system were additions to this apparatus. From experimental results the rate of change of the temperature of maximum density with respect to applied pressure was calculated for differing concentrations of various solutes. Results for sodium chloride solutions compare favourably to values extracted from the seawater equation [30] and the results of Caldwell [28]. Macroscopic and microscopic models have been explored to attempt to simulate experimental results.

The technique used to measure the temperature of maximum density was based on convective flows within the fluid under test. As a test sample was cooled to within the vicinity of the density maximum two convective cells were present in the liquid. By tracking the movement of the newly formed secondary cell the temperature of the density maximum was extracted. The movement of the secondary cell was tracked by an array of five equally spaced thermistors along the central axis of the fluid. The temperature profiles of these five thermistors showed an anomalous feature centred on the temperature of maximum density. In order to extract the exact value of the temperature of maximum density an area integration technique was used. Results using the convective flow technique compare favourably with results of other experimentalists using different techniques such as dilatometry.

For experimental runs above atmospheric pressure a computer controlled hydraulic system applied pressure to the fluid under test. The hydraulic system consisted of a bottle jack, hydraulic cylinder and a set of gears turned by a stepper motor which in turn was controlled in software. Between ramp runs the pressure system activated and increased the applied pressure to the desired value. For the subsequent ramp the

pressure was held at the required value. A rubber diaphragm was used as the interface between the test sample and hydraulic oil from the pressure system.

At atmospheric pressure the solutes studied behave very differently with increasing concentration. The temperature of maximum density of the ionic salts, the sugars and acetone decreased under increasing concentration (Despretz rule). Some of the monohydric alcohols showed an initial increase in the temperature of maximum density at low concentrations followed by a decrease at higher concentrations. This is in agreement with work carried out by Wada and Umeda [19] and Kaulgud [70]. Recent work at National University of Ireland Maynooth indicates that there is detailed structure in the temperature of maximum density profiles of the monohydric alcohol solutes [21].

At pressures above atmospheric pressure the behaviour of the temperature of maximum density of saline aqueous solutions have been investigated by various groups. Many researchers contributed to the formulation of the seawater equation which returns the density of water as a function of salinity, temperature and pressure [30]. Caldwell also carried out experiments on saline solutions under pressure [28]. To the author's knowledge only saline solutions have been investigated under pressure. In this work the rate of change of the temperature of maximum density with respect to applied pressure has been investigated as a function of concentration for a range of solutes. For pure water this rate of change has been measured to be $-0.0198 \pm 0.0005$ °C/bar. For increasing sodium chloride concentration this rate of change becomes more negative compared to pure water in agreement with the seawater equation and Caldwell (figure 3.5-2). Another ionic salt studied was potassium bromide which also follows this trend. Interestingly, the monohydric alcohols and acetone behave very differently. The rate of change of the temperature of maximum density with respect to applied pressure becomes less negative with increasing concentration compared to pure water for these solutes. The implication is that at least two groups of solutes exist. The sugars do not seem to be a part of either of these groups but further testing is required to conclusively exclude the sugars from either of these groups. The alcohols do not obey the Despretz rule over a concentration range at fixed pressure whereas the ionic salts do which also suggests at least two different classes of solutes. The behaviour of acetone is thus unusual as

161

at fixed pressure it follows the Despretz rule when tested over a range of concentrations but under pressure acetone joins the group with the monohydric alcohols. There is slight evidence that ethanol may have a nonlinear profiles whereas both ionic salts tested are compatible with linear fits. The probability that the ethanol points are compatible with a linear fit is 64% whereas both ionic salts are compatible with a linear model giving probabilities of over 95% (figure 3.6-1).

Attempts have been made to reproduce experimental results on a macroscopic level by investigating "ideal" solutions. There are no interactions between water and solute molecules with "ideal" mixing. In order to carry out this analysis density state functions for pure water [30] were combined with state functions for pure ethanol [46] and pure acetone [47] under pressure. Mixtures of water and ethanol gave rise to less negative rates of change of the temperature of maximum density with respect to applied pressure compared to the pure water point. This behaviour was also found to be true for mixtures of water and acetone. Although the slopes for both mixtures became less negative as solute concentration increases similar to the experimental results, the experimental results become less negative at a much faster rate (figure 4.3-3). The rate of change of the phase change with respect to applied pressure was investigated in the same way by combining the equation of state for the behaviour of the freezing point of pure water [30] with the similar state functions for pure ethanol [48] and pure acetone [49]. Mixtures of water and ethanol gave rise to less negative rates of change of the temperature of maximum density with respect to applied pressure compared to the pure water point. This behaviour was also found to be true for mixtures of water and acetone.

The behaviour of the temperature of maximum density as a function of pressure provides valuable test data for molecular models of water. Many models have attempted to reproduce the properties of water in fine detail. These models must be able to reproduce the key anomalous properties of water such as the density anomalies and high melting and boiling points. Vega and Abascal [71] examined a range of models which are capable of reproducing the density maximum of water. The models explored all reproduce the density maximum but over a wide range of absolute temperatures (180 K to 300 K). Vega and Abascal also studied the location of the temperature of maximum density relative to the temperature of the phase

change finding differences to be 11K for the TIP5P model and 37 K for the SPC model [71]. Noya et al. reported a temperature of maximum density of 280 K for the TIP4PQ/2005 model after he incorporated quantum effects [72]. Deeney and O'Leary believe that residual effects of quantum zero point energy account for the existence of the density maximum in water and aqueous solutions [73, 74].

The model used in this work to study water on a microscopic level was a two-dimensional gas-lattice model modified from the approach used by Buzano et al. [67]. Water molecules were in the shape of a Mercedes-Benz logo [64]. Monte Carlo simulations were used to evolve the system. Monte Carlo simulations were realised using Metropolis importance sampling [60] and the Wang-Landau method [61]. Using this model clear signatures of the density maximum were obtained. To study the effect of pressure on the temperature of maximum density the chemical potential parameter was varied. The chemical potential in a lattice model is analogous to pressure in an off lattice model as shown by Buzano et al. [67]. It was found that as pressure was increased the temperature of maximum density shifted to lower values in agreement with experimental results.

Hydrophilic molecules were added to the lattice to simulate the addition of a solute to water. Simulations were carried out for different concentrations of added molecules. At fixed pressure the temperature of maximum density was shifted to higher values under increasing concentration. The rate of change of the temperature of maximum density with respect to pressure became less negative as the number of added molecules increased. This was similar to the behaviour of the experimental results for the monohydric alcohols. Non-bonding molecules were added to the lattice to simulate the addition of hydrophobic molecules to water. In contrast to the addition of hydrophilic molecules the temperature of maximum density was shifted to lower values under increasing concentration at fixed pressure. However, the rate of change of the temperature of maximum density with respect to pressure became less negative as the number of hydrophobic molecules added increased. The addition of hydrophobic molecules to the lattice reproduced the behaviour of the monohydric alcohols similar to the addition of hydrophilic molecules to the lattice (figure 5.7-18).

A third approach investigated was to study the behaviour of the temperature of maximum density with respect to pressure as the hydrogen bond strength of all molecules in the lattice was increased. At fixed pressure the temperature of maximum density was shifted to higher values under increasing concentration. Under increasing global hydrogen bond strength the rate of change of the temperature of maximum density with respect to pressure became less negative again reproducing the experimental behaviour of the monohydric alcohol solutes.

Another approach used involved mixing three different types of fluid: 'ordinary', 'strong' and 'weak' water which effectively either strengthened or weakened hydrogen bond strength. 'Weak' water mixed with 'ordinary' water caused the temperature of maximum density to be shifted to lower values. 'Strong' water mixed with 'ordinary' water caused the temperature of maximum density to be shifted to higher values. Under pressure it was found that the rate of change of the temperature of maximum density with respect to pressure became less negative under increasing concentration for both mixtures. This was similar to the behaviour of the experimental results for the monohydric alcohols. Using macroscopic and microscopic approaches the behaviour of the monohydric alcohols has been reproduced. The behaviour of ionic salts was not achieved using either approach.

## 6.2 Future Work

The experimental system used for this work has undergone major changes but yet more alterations would further improve the capabilities of the system. The system can apply pressure to a sample fluid under test and hold the sample at a required applied pressure. Pressure is applied to the fluid by ramping up to the desired value in a controlled way. There is no way of controlling the release of pressure. Currently, pressure is released manually at the end of an experimental run via a pressure release valve. Control of this pressure release valve could be automated and controlled pressure release could be achieved through software. This would give the system a lot more flexibility in pressure testing. For example ramp runs could be performed at high applied pressures followed by lower pressures without having to restart the run. Pressure scanning could be carried out more efficiently as controlled

scans from 0 to 100 bar followed by scans from 100 to 0 bar could be carried out in sequence. Currently, during a pressure scan side wall temperatures are held constant and pressure is scanned from 0 to 100 bar at which point pressure must be manually released.

Between experimental runs the pressure chamber is removed from the system, emptied, cleaned and refilled with a solution of known concentration. The chamber is then placed back in the system. This process must be carried out every time a new solute concentration is tested. The author suggests that automating the filling and emptying process would greatly improve the efficiency of the system. If possible automating the addition of solute to the solution within the chamber would improve efficiency even further. If this were possible both concentration and pressure would be fully controlled in software and a single run could theoretically produce an entire trend for one solute (the rate of change of the temperature of maximum density with respect to applied pressure as a function of concentration).

The system could be altered further to allow investigations into the phase change of water and aqueous solutions under pressure. Currently, the system would not be able to cope with the significant volume change associated with ice formation. The diaphragm would rupture allowing oil to comtaminate the solution under test. The phase change of pure water and saline solutions have been investigated by Doherty and Kester [44] but no studies have been conducted on any other aqueous solutions. The rate of change of the phase change with respect to applied pressure changes minimally with respect to increasing concentration [44] in contrast to the behaviour of the temperature of maximum density. It would be very interesting to obtain information on the temperature of the phase change of other aqueous solutions to compare the behaviour of the temperature of maximum density to the behaviour of the temperature of the phase change under pressure.

The software can be altered to improve efficiency. Currently ramp runs begin so that the average temperature of the fluid is above the anomaly feature. Side wall temperatures are ramped down until the average temperature of the fluid is below the anomaly feature. The side wall temperatures are then ramped up again in a similar fashion. Both the down and up ramps are carried out over a fixed number of steps.

Hence, for a large period of time the system is not in an anomaly region. This time could be cut down by rewriting the software so that when the system reaches the end of the anomaly region it searches for the next anomaly and ramps through that anomaly immediately thereby cutting down time on either side of the anomaly region when the system is effectively idling. This adjustment to the software would vastly improve efficiency.

Further testing of solutes should be carried out under pressure. The only ketone tested in this work was acetone. Further studies into ketones are suggested by the author as acetone provided surprising results. At fixed pressure acetone follows the Despretz rule when tested over a range of concentrations in common with non-alcohol solutes such as sodium chloride. However, under pressure acetone follows the behaviour of the monohydric alcohols. Further testing of ketones would give information as to why acetone does not seem to follow the same behaviour as other solutes tested. The sugars should be investigated further also to resolve whether a third class of solutes exist with pressure analysis or whether in fact the sugars belong to one of the two classes investigated in this thesis.

An interesting extension of the work explored in this thesis would be to study aqueous solutions at negative pressures. Work has been carried out by Henderson and Speedy on pure water under negative pressure [29] but no work has been carried out on solutes at negative pressures. From the work of Henderson and Speedy the rate of change of the temperature of maximum density under tension was calculated to be -0.017 °C/bar [29] whereas a value of -0.02 °C/bar [28] has been measured under applied pressure. This is a significant difference for pure water so it would be interesting to extend the analysis to aqueous solutions.

Microscopically the two-dimensional gas-lattice modified Buzano model in conjunction with the Wang-Landau algorithm has produced results that reproduce the behaviour of the monohydric alcohols. No microscopic model explored in this work has reproduced the behaviour of the ionic salts as a function of pressure. This could be done by exploring the addition of various solutes to the lattice. The lattice size could be increased to allow for the addition of more solute molecules. This approach would be more versatile if the off-lattice model was explored further and made more

efficient. There would be more scope for adding more unusual molecules as solute particles in an off-lattice model. For example molecules that are of unusual shapes could be more easily introduced to an off-lattice model than a lattice model.

# Appendix A

# Experimental data acquisition and control software code
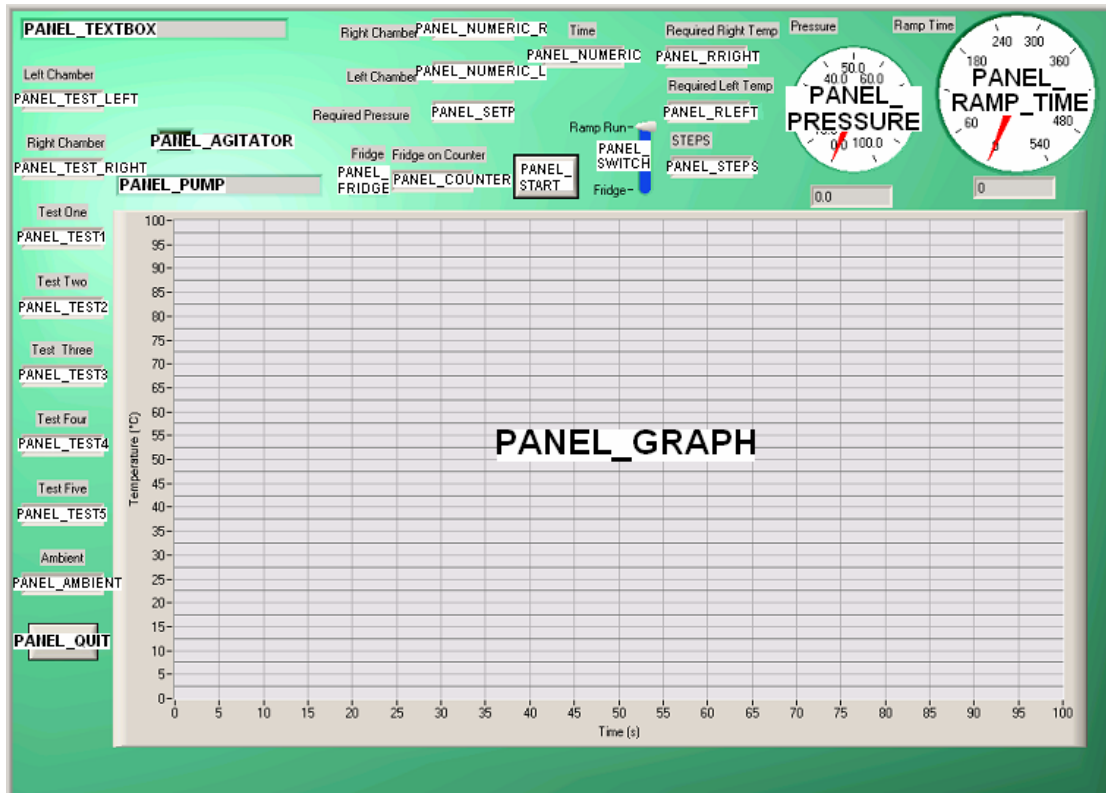
**Figure A** S*creen shot of the graphical user interface (GUI) with the controls labelled as per the source code.*

```
// Data acquisition software for Windows-operated systems
// modified version of P.O'Connor Heat-transfer.c
// incorporating thermistor and side chamber structures.
// Modified to include operation of stepper motor. GC
// Modified to read pressure from transducer and for
// multiple temperature ramps at static applied
// pressures. GC

#include <cvirte.h>
#include <userint.h>
#include "Heat_transfer.h"
#include <time.h>
#include <cbw.h>
#include <utility.h>
#include <ansi_c.h>
#include <stdio.h>
#define DO_8  for(n=0;n<8;n++)
#define DO_16 for(n=0;n<16;n++)
#define Max(x1,x2) (((x1) > (x2)) ? (x1):(x2))
#define PropZero(v) v.sum=v.sum2=0.0
#define PropAccum(v) v.sum += v.val, v.sum2 +=v.val*v.val
#define PropAve(v,n) \v.sum /= n, v.sum2=sqrt(Max
(v.sum2/n - v.sum*v.sum, 0.0))
```

```c
void terms(void);
void get_date(void);
int get_time(void);
void StartLog(void);
void record_results(void);
void delay(float);
void GUI_message(void);
void GUI_clear_message(void);
void error_file(void);
void InitialStates(void);
void ServoTemperatures(void);
void PumpActivate(int);
void AccumProps(int);
void InitializeRun(void);
void DoHoldRun(void);
void DoRampRun(void);
void DoFridgeRun(void);
void Fridge(void);
void Agitate(void);
void endRun(void);
void record_relay_results(void);
void StartRelayLog(void);
void stepper(void);
void Read_Pressure(void);

typedef struct{
    float adc,slope,intercept,t,loc;
} Thermistor;

typedef struct{
    int pc,ph,agit;
    float t_want;
    Thermistor therm;
    char loc[10];
}SideChamber;

typedef struct{
    float val,sum,sum2;
}Prop;

Thermistor therm[16];
SideChamber sc[2];
Prop thstats[16];
int n,pump,nmeasure,caldate,attempt,attempt1, num, usbOn;
int stepOn, time2_real, samples;
int relayFlagRC = 0, relayFlagRH = 0, relayFlagLH = 0;
int relayFlagLC = 0, pumpNum;
int day,month,year,hours,minutes,seconds;
int log_flag,run_flag;
unsigned int time_int,time_orig;
```

```c
static int panelHandle;
double ubound,lbound,tleft,tright,t_val,f,Req_Pressure;
double time_limit,time_real,Period;
char date_val[40],syscode;
char bufstring[20];
char file_date[250],file_date2[250];
long Rate = 80;
USHORT ADData[8], numline, numAct, PData[1];
FILE *data, *calib, *test, *relayLog;
long double Pressure;

int main (int argc, char *argv[])
{
     test=fopen("c:\\Data\\atest.dat","w");
     if (InitCVIRTE (0, argv, 0) == 0) return -1; //out
     of memory
     if ((panelHandle = LoadPanel (0,
     "Heat_transfer.uir",  PANEL)) < 0) return -1;
     InitialStates();
     DisplayPanel (panelHandle);   //front user panels
     are initialised
     RunUserInterface();
     DiscardPanel (panelHandle);
     return 0;
}


int CVICALLBACK quit (int panel, int control, int event,
void *callbackData, int eventData1, int eventData2)
{
     switch (event)
         {
         case EVENT_COMMIT:
             cbDOut (0, FIRSTPORTA, 0);
             cbDOut (0, FIRSTPORTB, 0);
             cbDOut (1, FIRSTPORTA, 0);
             cbDOut (1, FIRSTPORTB, 0);
             QuitUserInterface (0);   // exits program
             break;
         }
     return 0;
}


void InitialStates(void)
{
     int ii=0;
     cbFlashLED(0); // flashes LED on USB device
     cbDConfigPort(0, FIRSTPORTA, DIGITALOUT); //ports
     are initialised on the USB device
     cbDConfigPort(0, FIRSTPORTB, DIGITALOUT);
     cbDConfigPort(1, FIRSTPORTA, DIGITALOUT);
     cbDConfigPort(1, FIRSTPORTB, DIGITALOUT);
```

```
        cbDOut (0, FIRSTPORTA, 0);
        cbDOut (0, FIRSTPORTB, 0);

        AccumProps(0); //initialize all counters in
        thstats[16]
        nmeasure=0;
        attempt=0;
        log_flag=1; //always log for now - later get this
        flag set via GUI button
        run_flag=1; //default to hold run - later get this
        flag set via GUI option
        time_limit=999999; //max duration of holding run
        (seconds)

        calib=fopen("c:\\Data\\atest.cal","r");
        fscanf(calib,"%d %c", &caldate, &syscode);
        fprintf(test,"%10d %3c\n",caldate,syscode);
        DO_8{
                fscanf(calib,"%d %f %f",&ii, &therm[n].slope,
                &therm[n].intercept);
                fprintf(test,"%5d %10.3f %10.3f\n"
                ,ii,therm[n].slope,therm[n].intercept);
        }
        fclose(calib);
        fclose(test);

        DO_8 therm[n].loc=n*0.1; //fix later

        for(n=0;n<2;n++){
                if(n==0){
                //    sc[n].loc='r'; //fix later
                        sc[n].pc=128; //right, cold pump
                        sc[n].ph=64; //right, hot pump
                        sc[n].agit=0; //insert agitator port
                        address later
                }
                if(n==1){
                //    sc[n].loc='l'; //fix later
                        sc[n].pc=2; //port address, left chamber
                        cold pump
                        sc[n].ph=1; //left, hot pump
                        sc[n].agit=0; //insert agitator port
                        address later
                }
        }
}

void ServoTemperatures(void)
{
        for(n=0;n<2;n++){
                ubound=sc[n].t_want+0.1;
```

```c
        lbound=sc[n].t_want-0.1;
        t_val=sc[n].therm.t;
        if(t_val>ubound)PumpActivate(sc[n].pc);
        if(t_val<lbound)PumpActivate(sc[n].ph);
    }
}


void PumpActivate(int pump)
{
    if(therm[7].t<(((sc[0].t_want + sc[1].t_want)/2))){
        int ii=0, fridgeFlag = 0;
        usbOn = pump;
        cbDOut(0,FIRSTPORTA,ii);
        //Agitate();//checks to see if agitators need
        to be turned on
        cbDOut(0,FIRSTPORTA,pump);
        //if(fridgeFlag % 12 ==0){Fridge();}//checks
        the fridge temp and turns on if its too hot
        if(pump == 64){SetCtrlVal(panelHandle,
        PANEL_PUMP,"Right Hot Pump");}
        if(pump == 128){SetCtrlVal(panelHandle,
        PANEL_PUMP,"Right Cold Pump");}
        if(pump == 2){SetCtrlVal(panelHandle,
        PANEL_PUMP,"Left Cold Pump");}
        if(pump == 1){SetCtrlVal(panelHandle,
        PANEL_PUMP,"Left Hot Pump");}
        delay(5);
        record_relay_results();      //NEW
        usbOn = 0;              //NEW
        ResetTextBox (panelHandle, PANEL_PUMP, "");
        cbDOut(0,FIRSTPORTA,ii);
        //fridgeFlag = fridgeFlag + 1; // every 12
        cycles the fridge temp is checked to see if it
        needs to be turned on or off.
        Fridge();
    }

    if(therm[7].t>(((sc[0].t_want + sc[1].t_want)/2))){
        int ii=0, fridgeFlag = 0;
        usbOn = pump;
        pump = pump + 4;
        cbDOut(0,FIRSTPORTA,ii);
        //Agitate();//checks to see if agitators need
        to be turned on
        cbDOut(0,FIRSTPORTA,pump);
        //if(fridgeFlag % 12 ==0){Fridge();}//checks
        the fridge temp and turns on if its too hot
        if(pump == 68){SetCtrlVal(panelHandle,
        PANEL_PUMP,"Right Hot Pump");}
        if(pump == 132){SetCtrlVal(panelHandle,
        PANEL_PUMP,"Right Cold Pump");}
```

```
        if(pump == 6){SetCtrlVal(panelHandle,
        PANEL_PUMP,"Left Cold Pump");}
        if(pump == 5){SetCtrlVal(panelHandle,
        PANEL_PUMP,"Left Hot Pump");}
        delay(5);
        record_relay_results();      //NEW
        usbOn = 0;               //NEW
        ResetTextBox (panelHandle, PANEL_PUMP, "");
        cbDOut(0,FIRSTPORTA,ii);
        //fridgeFlag = fridgeFlag + 1; // every 12
        cycles the fridge temp is checked to see if it
        needs to be turned on or off.
        Fridge();
    }
}

void terms(void)
{
    GetCtrlVal (panelHandle, PANEL_NUMERIC_L, &tleft);
    GetCtrlVal (panelHandle, PANEL_NUMERIC_R, &tright);
    sc[1].t_want=tleft;
    sc[0].t_want=tright;
    SetCtrlVal (panelHandle, PANEL_SYSTEM, 1); // System
    LED on screen go green
}

int get_time(void)  // the amount of time since the
program was started is obtained
{
    SetCtrlVal (panelHandle, PANEL_NUMERIC, ((clock() /
    1000) - time_orig));
    GetCtrlVal (panelHandle, PANEL_NUMERIC, &time_int);
    if(run_flag == 0)SetCtrlVal (panelHandle,
    PANEL_RAMP_TIME, (time_int % 540));
    return time_int;
}

void get_date(void) //date and time in character format
for display
{
    GetSystemDate (&month, &day, &year); // the date and
    time from the system clock
    GetSystemTime(&hours, &minutes, &seconds);
    sprintf(date_val, "            %d/%d/%d
    %d:%d:%d",day,month,year,hours,minutes,seconds);
}

void delay(float seconds)
{
    clock_t ticks = seconds * CLOCKS_PER_SEC;
    clock_t start = clock();
```

```c
    while (\
        clock() - start < ticks)
    {    }
}


void error_file(void)
{
    char text4[30];
    sprintf(text4, " Data file not found     "); //
    error message printed to text box
    SetCtrlVal (panelHandle, PANEL_TEXTBOX, text4);
}


void GUI_message(void)
{
    char text8[30];
    if(run_flag == 1)sprintf(text8, "      HOLDING
    TEMPERATURE "); //message printed to text box
    if(run_flag == 0)sprintf(text8, "      RAMPING
    TEMPERATURE ");
    if(run_flag == 2)sprintf(text8, "      RUNNING FRIDGE
    ");
    ResetTextBox (panelHandle, PANEL_TEXTBOX, "");
    SetCtrlVal (panelHandle, PANEL_TEXTBOX, text8);
}


void GUI_clear_message(void)
{
    char text[55];        //text bar is cleared
    sprintf(text, "
    ");
    ResetTextBox (panelHandle, PANEL_TEXTBOX, "");
}


void StartLog(void)
{
    year=year-2000;
    attempt++;
    sprintf(file_date,"C:\\Data\\testing\\a%02d%02d%02d_%
    d.dat",day,month,year,attempt);
}


void StartRelayLog(void)
{
    attempt1++;
    sprintf(file_date2,"C:\\Data\\testing\\RelayLog\\a%02
    d%02d_%d.dat",day,month,attempt);
}


void record_results(void)
{
```

```c
      time_int=get_time();
      if((data = fopen(file_date, "at"))==NULL)
      {
        error_file();
      }
      else
      {
        time_real=time_int-time_orig;
        fprintf(data," %lf\t",time_real);
        for(n=0;n<8;n++) fprintf(data,"
        %lf\t",therm[n].t);
        fprintf(data," %lf\t",Pressure);
        fprintf(data, "\n");
        fclose(data);
      }
}

void record_relay_results(void)
{
      time_int=get_time();
      if((relayLog = fopen(file_date2, "at"))==NULL)
      {
        error_file();
      }
      else
      {
        time2_real=time_int-time_orig;
        fprintf(relayLog," %01d\t",time2_real);
        fprintf(relayLog," %03d\t",usbOn);
        fprintf(relayLog," %03d\t",stepOn);
        fprintf(relayLog, "\n");
        fclose(relayLog);
      }
}

void AccumProps(int icode)
{
      if(icode==0){
          DO_8 PropZero(thstats[n]);
      }else if(icode==1){
          DO_8 PropAccum(thstats[n]);
      }else if(icode==2){
          DO_8 PropAve(thstats[n],nmeasure);
      }
}

int CVICALLBACK hold_temperatures (int panel, int
control, int event, void *callbackData, int eventData1,
int eventData2)
{
      switch (event)
```

```
                    {
                    case EVENT_COMMIT:
                            InitializeRun();
                            GetCtrlVal(panelHandle, PANEL_SWITCH,
                            &run_flag);
                            if(run_flag==1)DoHoldRun();
                            if(run_flag==0)DoRampRun();
                            else DoFridgeRun();
                            break;
                    }
            return 0;
      }


void InitializeRun(void)
{
      GUI_message();
      terms(); //get tleft and tright information from GUI
      get_date();
      time_orig=get_time();
      if(log_flag==1)StartLog();
      StartRelayLog();
}


void DoHoldRun(void)
{
      int start_time=get_time();
      time_int=get_time();
      if(run_flag==1)time_limit=999999;
      while( (time_int-start_time) < time_limit){
            AccumProps(0);
            nmeasure=0;
            samples = 0;
            cbAInScan (0,0,7,10,&Rate, BIP10VOLTS,
            ADData, CONVERTDATA);
      //    cbAConvertData (0, 10, ADData, NULL);
      //    AccumProps(2);
      //    DO_8 therm[n].adc=thstats[n].sum;
            DO_8 therm[n].adc=ADData[n]-2048; //shift
            required as adc range is -10V to +10V
            DO_8 if(therm[n].adc < 1.0)therm[n].adc=1.0;
            DO_8 therm[n].t=therm[n].slope/(log(therm[n]
            .adc)+therm[n].intercept)-273.15;

            SetCtrlVal (panelHandle, PANEL_TEST_RIGHT,
            therm[0].t);
            SetCtrlVal (panelHandle, PANEL_TEST_LEFT,
            therm[1].t);
            SetCtrlVal (panelHandle, PANEL_TEST1,
            therm[2].t);  //try to condense this later
            SetCtrlVal (panelHandle, PANEL_TEST2,
            therm[3].t);
```

```c
            SetCtrlVal (panelHandle, PANEL_TEST3,
            therm[4].t);
            SetCtrlVal (panelHandle, PANEL_TEST4,
            therm[5].t);
            SetCtrlVal (panelHandle, PANEL_TEST5,
            therm[6].t);
            SetCtrlVal (panelHandle, PANEL_AMBIENT,
            therm[7].t);
            Read_Pressure();

            PlotPoint (panelHandle, PANEL_GRAPH, time_int,
            therm[0].t, VAL_SOLID_CIRCLE, VAL_RED);
            //Plots the Left chamber, Right Chamber and the
            Fridge Ambient temperature.
            PlotPoint (panelHandle, PANEL_GRAPH, time_int,
            therm[1].t, VAL_SOLID_CIRCLE, VAL_BLUE);
            PlotPoint (panelHandle, PANEL_GRAPH, time_int,
            therm[7].t, VAL_SOLID_CIRCLE, VAL_GREEN);

            //copy appropriate thermistor data to side
            chamber structures
            for(n=0;n<2;n++)sc[n].therm=therm[n];
            ServoTemperatures(); //uses pumps to servo on
            desired temperatures
            if(log_flag==1)record_results();
            stepper();
            //    plot_results();          //bring back in
            later (tidy up plotting function)
            time_int=get_time();
        }
}

void DoRampRun(void) //Selected using the toggle switch
{
        int ii,kk;

        for(kk=0;kk<4;kk++){
            ii=0;
            while(ii<40){
                time_limit=540.0;
                tleft=tleft-0.1;
                tright=tright-0.1;
                sc[1].t_want=tleft;
                sc[0].t_want=tright;
                SetCtrlVal(panelHandle, PANEL_RLEFT,
                tleft);
                SetCtrlVal(panelHandle, PANEL_RRIGHT,
                tright);
                SetCtrlVal(panelHandle, PANEL_STEPS, ii);
                DoHoldRun();
                ii++;
```

```
            }

            time_limit=1.0;
            DoHoldRun();

            ii=0;
            while(ii<40){
                time_limit=540.0;
                tleft=tleft+0.1;
                tright=tright+0.1;
                sc[1].t_want=tleft;
                sc[0].t_want=tright;
                SetCtrlVal(panelHandle, PANEL_RLEFT,
                tleft);
                SetCtrlVal(panelHandle, PANEL_RRIGHT,
                tright);
                SetCtrlVal(panelHandle, PANEL_STEPS, ii);
                DoHoldRun();
                ii++;
            }

            time_limit=1.0;
            DoHoldRun();

            ii=0;
            if(kk<3){
                Req_Pressure=20.0*(kk+1);
                while(ii<10){
                    time_limit=540.0;
                    sc[1].t_want=tleft;
                    sc[0].t_want=tright;
                    SetCtrlVal(panelHandle, PANEL_RLEFT,
                    tleft);
                    SetCtrlVal(panelHandle, PANEL_RRIGHT,
                    tright);
                    SetCtrlVal(panelHandle, PANEL_STEPS,
                    ii);
                    DoHoldRun();
                    ii++;
                }
            }

            time_limit=1.0;
            DoHoldRun();
        }

        time_limit=9999999;
        cbDOut(1, FIRSTPORTA, 0);
        DoFridgeRun();
    }
```

```
void DoFridgeRun(void)
{
     time_int=get_time();
     while( (time_int-time_orig) < 99999999){
          cbAInScan (0,0,7,10,&Rate, BIP10VOLTS, ADData,
          CONVERTDATA);//reads 8 ADC's
          cbAConvertData (0, 10, ADData, NULL);
          samples = 0;
          DO_8 therm[n].adc=ADData[n]-2048; //shift
          required as adc range is -10V to +10V
          DO_8 if(therm[n].adc < 1.0)therm[n].adc=1.0;
          DO_8 therm[n].t=therm[n].slope/(log(therm[n]
          .adc)+therm[n].intercept)-273.15;
          SetCtrlVal (panelHandle, PANEL_AMBIENT,
          therm[7].t);
          PlotPoint (panelHandle, PANEL_GRAPH, time_int,
          therm[7].t, VAL_SOLID_CIRCLE, VAL_GREEN);
          if(therm[7].t > (4.5))
          {
               cbDOut(0, FIRSTPORTB, 1);
               SetCtrlVal(panelHandle, PANEL_FRIDGE, 1);
               Delay(4);

          }
          else
          {
               cbDOut(0, FIRSTPORTB, 0);
               SetCtrlVal(panelHandle, PANEL_FRIDGE, 0);
               Delay(4);
          }
          //record_results();
          time_int=get_time();
     }
}

double counter;

void Fridge(void)
{
     if(therm[7].t > (((sc[0].t_want + sc[1].t_want)/2)))
     {
          counter = counter + 1;
          cbDOut(0, FIRSTPORTB, 1);
          SetCtrlVal(panelHandle, PANEL_FRIDGE, 1);
          SetCtrlVal(panelHandle, PANEL_COUNTER, (counter
          * 2.5));
     }
     else
     {
          cbDOut(0, FIRSTPORTB, 0);
          SetCtrlVal(panelHandle, PANEL_FRIDGE, 0);
```

```c
        }
}

void Agitate(void){
    if(time_int % 10 == 0){
        cbDOut(0, FIRSTPORTB, 9); //turns on the
        agitator for 1.5 sec if the time mod 4 is zero
        delay(2); cbDOut(0, FIRSTPORTB, 0);//turns the
        agitator back off
    }
    else{delay(0.5);}
}

void Read_Pressure(void){
    cbAInScan (1,0,7,10,&Rate, BIP10VOLTS, PData,
    CONVERTDATA);//reads 8 ADC's
    // cbAConvertData (1, 10, PData, NULL);//convert to
    12bit numbers
    samples=0;
    while (samples<3){  //collects 3 samples
        Pressure = Pressure + PData[0];    // all 3
        samples are then added together
        samples++;
    }

    Pressure = (((100/3063.51045)*Pressure)-
    200.7579099);
    SetCtrlVal (panelHandle, PANEL_PRESSURE, Pressure);
}

void stepper(void){
    //SetCtrlVal(panelHandle,PANEL_SETP,Req_Pressure);
    if(Pressure < Req_Pressure){
        cbDOut(1, FIRSTPORTA, 1);
    }
    else{
        cbDOut(1, FIRSTPORTA, 0);
    }
}
```

# Appendix B

# Area integration code for the extraction of the temperature of maximum density from ramp runs

```
c--routine which integrates area under curves given in
c--arrays
c--this version finds half-area point by integrating from
c--bottom to top;
c--this gives a value for Tmd directly
c--GC 8/2/10
c
      implicit none
      integer i,j,n,ndim,ihalf
      integer index_d1,index_d2
      real c1(50000),c2(50000),time(50000),s
      real d1(50000),d2(50000)
      real t1(50000),t2(50000),t3(50000)
      real t4(50000),t5(50000)
      real t6(50000)

      real yscale,ythresh,ymin,ymax
      real area1,area2,diff,totdiff,Tmd
      real c1_lower,c1_upper,c2_lower,c2_upper
      real area_half

      open(1,file='do_int.in',status='unknown')
      open(7,file='do_int.out', status ='unknown',ACCESS =
     'APPEND')

      i=0
10    continue
      i=i+1
c--following assumes that curve c1 is above c2; if not,
c--reverse order
c--total area difference will be negative if order is
c--incorrect
c     read(1,*,end=99)time(i),c1(i),c2(i)
      read(1,*,end=99)time(i),t1(i),t2(i),c1(i),t3(i),t4(i
     ),t5(i),c2(i),t6(i)

      goto 10
99    ndim=i-1
      write(6,*)'number of points: ',ndim
      write(7,*)'number of points: ',ndim


      do n=1,10
      call trapzd1(n,time,c1,ndim,s)
      area1=s
      enddo

      do n=1,10
      call trapzd1(n,time,c2,ndim,s)
      area2=s
      enddo
```

```fortran
      totdiff=area1-area2
      write(6,*)'Total area difference: ',totdiff
      write(7,*)'Total area difference: ',totdiff


c--now find point where area diffence is half the above
c--value
      ymin=10000000.0
      ymax=0.0
c--following assumes that min and max values are similar
c--for c1 and c2
      do i=1,ndim
      if(c1(i).lt.ymin)ymin=c1(i)
      if(c1(i).gt.ymax)ymax=c1(i)
      enddo
      yscale=(ymax-ymin)/float(ndim)

      do i=1,ndim

      do j=1,ndim
c--for both down and up ramps, the threshold is initially
c--set high
c--and then moved down; this gives a gradually increasing
c--area
        ythresh=ymin+float(ndim-i)*yscale
        d1(j)=c1(j)-ythresh
        if(d1(j).lt.0.0)d1(j)=0.0
        d2(j)=c2(j)-ythresh
        if(d2(j).lt.0.0)d2(j)=0.0
      enddo

      do n=1,10
        call trapzd1(n,time,d1,ndim,s)
        area1=s
      enddo
      do n=1,10
        call trapzd1(n,time,d2,ndim,s)
        area2=s
      enddo
      diff=area1-area2
c     write(6,*)'x, area difference: ',i,diff
c     write(7,*)'x, area difference: ',i,diff

      area_half=totdiff/2.0
c     area_half=totdiff/2.0+sqrt(totdiff)/2.0
      if(diff.ge.area_half)then
       ihalf=i
       Tmd=ythresh
       write(6,*)'index for half-area, Tmd: ',ihalf,Tmd
       write(7,*)'index for half-area, Tmd: ',ihalf,Tmd
```

```fortran
         do j=1,ndim
         if(d1(ndim-j).gt.0.0)then
         index_d1=ndim-j
         goto 981
         endif
         enddo
981   continue
         do j=1,ndim
         if(d2(ndim-j).gt.0.0)then
         index_d2=ndim-j
         goto 982
         endif
         enddo
982   continue

c     write(6,*)index_d1,c1(index_d1),index_d2,
c     2(index_d2)
c     write(7,*)index_d1,c1(index_d1),index_d2,c2(index_d2
c     )
c     c1_lower=c1(index_d1-10)
c     c1_upper=c1(index_d1+10)
c     c2_lower=c2(index_d2-10)
c     c2_upper=c2(index_d2+10)
c     write(6,*)'c1_lower,upper, c2_lower,upper: ',
c     1 c1_lower,c1_upper,c2_lower,c2_upper
c     write(7,*)'c1_lower,upper, c2_lower,upper: ',
c     1 c1_lower,c1_upper,c2_lower,c2_upper

      stop
      endif

      enddo !end i loop


      stop
      end

      SUBROUTINE TRAPZD1(n,time,CURVE,NDIM,S)
c--modified version of Press et al. trapezoidal rule
      implicit none
      integer ndim,ia,ib,n,it,ix,j
      real a,b,s,scale,curve(ndim),time(ndim)
      real tnm,del,sum,x

      ia=1
      ib=ndim
      scale=float(ndim)/time(ndim)

      IF (N.EQ.1) THEN
      a=float(ia)/scale
      b=float(ib)/scale
```

```fortran
          s=0.5*(b-a)*(curve(ia)+curve(ib))
          IT=1
      ELSE
          TNM=IT
          DEL=(B-A)/TNM
          X=A+0.5*DEL
      ix=int(x*scale)
          SUM=0.
          DO 11 J=1,IT
             SUM=SUM+curve(ix)
             X=X+DEL
        ix=int(x*scale)
11        CONTINUE
          S=0.5*(S+(B-A)*SUM/TNM)
          IT=2*IT
        ENDIF
        RETURN
        END
```

# Appendix C

# Modified Buzano model using the Wang-Landau method code

```c
//hexagonal lattice model using Mercedes-Benz molecules
//uses Wang-Landau algorithm to calculate density of
//states
//GC 17/11/08
//add weighting to arm-arm interactions: x2 if mb is
//twice bonded,
//and x5 if mb is triple bonded
//17/11/08

#include <stdio.h>
#include <stdlib.h>
#include <string.h>
#include <math.h>
#include "in_mddefs.h"
#include "ran1.c"

int nspin;
//nx should be multiple of 3; ny should be multiple of 2
//nx=12,ny=8;
double pi=3.1415926;
int nx=9.0,ny=6.0;
double xregion,yregion,yscale,plotradius;

typedef struct {
  double x,y;
} rvec;

typedef struct {
  rvec r;
  int phi,rad;
  double eta;
} tspin;

tspin spin[9][6];

int ii,jj,iii,jjj,iiii,jjjj,ir,jr,ic,jc,nn;
int phi0,phi_nn,narray,imin,jmin;
int phiold,radold,count;
int nnx1,nny1,nnx2,nny2;
int min_steps,e_states,m_states,mc_steps;
int b_old,b_new,m_old,m_new;
int nskip,count,count1,flag,aflag;
double ehist[1000][1000];
double ghist[1000][1000],gdiff;
double energy,etot,buf;
double f,min_f,lnf;
double flat_thresh;
double nactive,min_ghist;
double emin,emax,mmin,mmax,nbin,nsteps;
double eps_lj,eps_hb,c_hb,penalty;
long int dum;
```

```c
void total_e(void);
void RandomFlip(void);
void calc_coords(void);
void wrap(void);
void wrap2(void);
void wrap3(void);
void energy_hb2(void);
void arm_arm(void);
void energy_hb(void);
void energy_cc(void);
void energy_hb2(void);
void buzano(void);

FILE *fout, *fend, *temp_energy;

/*******************************************************
***********/
int main(void){

    int i,j;
    fout=fopen("wl_buzano.out","w");
    nx=9;
    ny=6;
    dum=-56465658;
    buf=ran1(&dum);
    yscale=0.8660254;
    narray=1000;
    e_states=narray; //max number of energy states-some
    remain empty
    m_states=narray; //max number of magnetization states
    emin=-12.0*nx*ny;
    //emin=-8.0*nx*ny; //-5 for arm-arm; -3 for centre-
    centre
    emax=0.0; //penalty if no bonds aligned
    mmin=0.0;
    mmax=nx*ny;

    for(i=0;i<e_states;i++){
      for(j=0;j<m_states;j++){
          ehist[i][j]=0;
          ghist[i][j]=1.0;
      }
    }

    f=2.71828;
    min_f=1.0001;
    min_steps=1000; //min number of MC sweeps for each f
    value
    nskip=1000;
    flat_thresh=0.8; //NB large value is more stringent
    (e.g. 0.9)
```

```c
        calc_coords();
        total_e();
        b_old=(energy-emin)/(emax-emin)*(narray-1)+1;
        m_old=(nactive-mmin)/(mmax-mmin)*(narray-1)+1;
        fprintf(stdout,"Initial Energy:%.3lf\t,
        density:%.3f\t,
        levels:%i\t,%i\n",energy,nactive,b_old,m_old);

//start outermost loop - repeat until f reaches min value
        while(f>min_f){
          lnf=log(f);

           for(i=0;i<e_states;i++){
             for(j=0;j<m_states;j++){
               ehist[i][j]=0;
             }
            }

          nsteps=0;
          mc_steps=0;
          count1=nskip+1;
          flag=1;

//repeat groups of MC sweeps until energy histogram is
//flat
          thousand:
          for(iii=0;iii<nx*ny;iii++){
             nsteps=nsteps+1;
             RandomFlip();
             b_new=(energy-emin)/(emax-emin)*(narray-1)+1;
             m_new=(nactive-mmin)/(mmax-mmin)*(narray-1)+1;
             if(b_new<1 || b_new>narray)
               fprintf(stdout,"%.3lf\t, %.3f\n",b_new,m_new);
             if(m_new<1 || m_new>narray)
               fprintf(stdout,"%.3lf\t, %.3f\n",b_new,m_new);
//avoid taking exponent if ghist difference is large
//(avoid overflow)
             gdiff=ghist[b_old-1][m_old-1]-ghist[b_new-
              1][m_new-1];
             if(gdiff>=0.0){
               b_old=b_new;
               m_old=m_new;
             }
             else if(exp(gdiff)>ran1(&dum)){
               b_old=b_new;
               m_old=m_new;
             }
             else{
                spin[ir][jr].phi=phiold; //undo random flip
                spin[ir][jr].rad=radold; //undo random flip
             }
```

```
            ghist[b_old-1][m_old-1]=ghist[b_old-1][m_old-
            1]+lnf;
            ehist[b_old-1][m_old-1]=ehist[b_old-1][m_old-
            1]+1;
        }
        count1=count1+1;
        mc_steps=mc_steps+1;

//check for flatness - non-zero histogram entries only
        if(mc_steps>=min_steps && count1>=nskip){
            count1=0;
            nbin=0;
            for(i=0;i<e_states;i++){
                for(j=0;j<m_states;j++){
                    if(ehist[i][j]>0)
                        nbin=nbin+1;
                }
            }
            for(i=0;i<e_states;i++){
                for(j=0;j<m_states;j++){
                    if(ehist[i][j]>0){
                        if(((ehist[i][j]*nbin)/nsteps)<flat_thre
                        sh)goto thousand;
                    }
                }
            }
            flag=0;
        }
        if(flag==0)goto nine;
        goto thousand;
        nine:

//normalize (logarithmic) ghist values
        min_ghist=100000000.0;
        jmin=0;
        imin=0;

        for(i=1;i<e_states;i++){
            for(j=1;j<m_states;j++){
                if(ehist[i][j]>0.0){
                    if(ghist[i][j]<min_ghist){
                        min_ghist=ghist[i][j];
                        jmin=0;
                        imin=0;
                    }
                }
            }
        }

        for(i=1;i<e_states;i++){
            for(j=1;j<m_states;j++){
```

```c
            if(ehist[i][j]>0.0)
                ghist[i][j]=ghist[i][j]- min_ghist;
        }
    }

    f=sqrt(f); //decrement f value
    fprintf(stdout,"New f Value:%.8lf\n",f);
  } //close while loop

  for(i=0;i<e_states;i++){
    for(j=0;j<m_states;j++){
        energy=(i)*(emax-emin)/(narray-1)+emin;
        nactive=(j)*(mmax-mmin)/(narray-1)+mmin;
//adjust ghist values to allow for q ground states
//ghist[i][j]=ghist[i][j]+log((q)*0.1);
        if(ehist[i][j]>0)
            fprintf(fout,"%i\t %i\t %.3lf\t %.3lf\t
            %.3lf\t%.3lf\n",i+1,j+1,energy,nactive,ghist
            [i][j],ehist[i][j]);
//fprintf(stdout,"%i\t %i\t %.3lf\t %.3lf\t %.3lf\t
%.3lf\n",i,j,energy,nactive,ghist[i][j],ehist[i][j]);
    }
  }
}

//***********************************************
*********//
void RandomFlip(void){

    ir=nx*ran1(&dum);
    jr=ny*ran1(&dum);
    if(ir>=nx)ir=nx-1;
    if(jr>=ny)jr=ny-1;
    phiold=spin[ir][jr].phi;
    radold=spin[ir][jr].rad;
//next: control balance between flip of angle and radius

    if(ran1(&dum)<0.5){
        ten:
        spin[ir][jr].phi=ran1(&dum)*3.0;
        if(spin[ir][jr].phi==phiold)goto ten;
    }

    else{
        spin[ir][jr].rad=abs(spin[ir][jr].rad-1);
        goto four;
    }
    four:
    total_e();
}
```

```c
//*********************************************************
********//
void calc_coords(void){

    int i,j;
    for(i=0;i<nx;i++){
      for(j=0;j<ny;j++){
          if(j%2==0)
              spin[i][j].r.x=(i)+0.5-nx/2.0;
          else{
              spin[i][j].r.x=(i)-nx/2.0;
          }
          spin[i][j].r.y=(-(ny-1)/2.0+j)*yscale;
          spin[i][j].phi=(3.0*ran1(&dum));
          spin[i][j].rad=(2.0*ran1(&dum));
          spin[i][j].eta=3.0;
      }
    }
}

//*********************************************************
********//
void wrap(void){

    if(iiii>=nx)iiii=0;
    if(iiii<0)iiii=nx-1;
    if(jjjj>=ny)jjjj=0;
    if(jjjj<0)jjjj=ny-1;
}

//*********************************************************
********//
void wrap2(void){

    if(nnx1>=nx)nnx1=0;
    if(nnx1<0)nnx1=nx-1;
    if(nny1>=ny)nny1=0;
    if(nny1<0)nny1=ny-1;
  }

//*********************************************************
********//
void wrap3(void){

    if(nnx2>=nx)nnx2=0;
    if(nnx2<0)nnx2=nx-1;
    if(nny2>=ny)nny2=0;
    if(nny2<0)nny2=ny-1;
}
//*********************************************************
********//
```

```
void arm_arm(void){

    aflag=0;
    if(spin[iiii][jjjj].rad==0)return; //return if
     neighbour not active
    phi0=spin[ic][jc].phi;
    phi_nn=spin[iiii][jjjj].phi;

    if(phi0==0){
      if(nn==1 || nn==3 || nn==5){
       if(phi_nn==2)aflag=1;
      }
    }
    if(phi0==2){
      if(nn==2 || nn==4 || nn==6){
       if(phi_nn==0)aflag=1;
      }
    }
}

//*****************************************************
********//
void total_e(void){

    energy=0.0;
    nactive=0.0;
    for(ii=0;ii<nx;ii++){
      for(jj=0;jj<ny;jj++){
          energy_hb2(); //arm-arm interactions
          energy=energy+etot;
          nactive=nactive+(spin[ii][jj].rad);
      }
    }
    energy=energy/2;
}

//*****************************************************
********//
void energy_hb2(void){

//this version gives additional weight to multiple bonds
//for each mb
    double rad;
    count=0;
    etot=0;
    ic=ii;
    jc=jj;
    rad=spin[ic][jc].rad;
    if(spin[ic][jc].rad==0)return;
    if(jc%2==0){
      iiii=ic-1;        jjjj=jc;      wrap();  nn=4;
```

```
      nnx1=ic; nny1=jc+1; nnx2=ic; nny2=jc-1;
      wrap2(); wrap3(); buzano();

      iiii=ic+1;        jjjj=jc;        wrap();  nn=1;
      nnx1=ic+1; nny1=jc-1; nnx2=ic+1; nny2=jc+1;
      wrap2(); wrap3(); buzano();

      iiii=ic;          jjjj=jc-1;      wrap();  nn=5;
      nnx1=ic-1; nny1=jc; nnx2=ic+1; nny2=jc-1;
      wrap2(); wrap3(); buzano();

      iiii=ic+1;        jjjj=jc-1;      wrap();  nn=6;
      nnx1=ic; nny1=jc-1; nnx2=ic+1; nny2=jc;
      wrap2(); wrap3(); buzano();

      iiii=ic;          jjjj=jc+1;      wrap();  nn=3;
      nnx1=ic+1; nny1=jc+1; nnx2=ic-1; nny2=jc;
      wrap2(); wrap3(); buzano();

      iiii=ic+1;        jjjj=jc+1;      wrap();  nn=2;
      nnx1=ic+1; nny1=jc; nnx2=ic; nny2=jc+1;
      wrap2(); wrap3(); buzano();
    }

    else{
      iiii=ic-1;        jjjj=jc;        wrap();  nn=4;
      nnx1=ic-1; nny1=jc+1; nnx2=ic-1; nny2=jc-1;
      wrap2(); wrap3(); buzano();

      iiii=ic+1;        jjjj=jc;        wrap();  nn=1;
      nnx1=ic; nny1=jc-1; nnx2=ic; nny2=jc+1;
      wrap2(); wrap3(); buzano();

      iiii=ic-1;        jjjj=jc-1;      wrap();  nn=5;
      nnx1=ic-1; nny1=jc; nnx2=ic; nny2=jc-1;
      wrap2(); wrap3(); buzano();

      iiii=ic;          jjjj=jc-1;      wrap();  nn=6;
      nnx1=ic-1; nny1=jc-1; nnx2=ic+1; nny2=jc;
      wrap2(); wrap3(); buzano();

      iiii=ic-1;        jjjj=jc+1;      wrap();  nn=3;
      nnx1=ic; nny1=jc+1; nnx2=ic-1; nny2=jc;
      wrap2(); wrap3(); buzano();

      iiii=ic;          jjjj=jc+1;      wrap();  nn=2;
      nnx1=ic+1; nny1=jc; nnx2=ic-1; nny2=jc+1;
      wrap2(); wrap3(); buzano();
    }
    //if(count>0){
//at least one bond aligned - divide by two for sharing;
```

```
    //if(count==1)etot=etot+0.1*(count)*rad;
    //if(count==2)etot=etot+0.1*(count)*rad*2.0;
    //if(count==3)etot=etot+0.1*(count)*rad*5.0;
    //}
    //else{
//no bond aligned - set to +1 as penalty
    //  etot=etot+5.0*rad;
    //}
}

//****************************************************
**//

void buzano(void){

    eps_lj=1.0;
    eps_hb=spin[iiii][jjjj].eta;
    c_hb=0.8;
    penalty=c_hb*eps_hb/2.0;

    if(spin[iiii][jjjj].rad==1){ //neighbour is active
      etot=etot-eps_lj;
      arm_arm();
      if(aflag==1){ //bonds aligned - test neighbours
        etot=etot-eps_hb;
        count=count+1;
        if(spin[nnx1][nny1].rad==1)etot=etot+penalty;
        if(spin[nnx2][nny2].rad==1)etot=etot+penalty;
      }
    }
}

//****************************************************
**//
```

# Appendix D

# Post-processing code for the Wang-Landau method

```c
//process the density of states function obtained from
//Wang-Landau
//version to process lattice Mercedes-Benz model
//2-d version; g(E,N)
//GC 29/01/09

#include <stdio.h>
#include <stdlib.h>
#include <string.h>
#include <math.h>
#include "in_mddefs.h"
#include "ran1.c"

int i,ii,j,nx=9,ny=6,m,mm,narray=1025,nspin;
//nx=12; ny=8;
double ghist[1025][1025],ehist[1025][1025];
double energy[1025],density[1025];
double lnP[1025][1025],prob[1025][1025];
double kT,mu,e_states,m_states;
double lambda,partition,pnorm,area;
double
u_energy,u_prev,kT_prev,capacity,helmholtz,entropy;
double den_ave;
float fenergy,fghist,fehist,fden;

FILE *wl_mb_data,*fout,*t, *ftest;

int main(void){

    wl_mb_data=fopen("C:\\data\\artmdsim2\\src\\wl_buzano
    .out","r");
    fout=fopen("buzano_proc_2d.out","w");
    t=fopen("buzano_proc_t_2d.out","w");
    ftest=fopen("TESTWLBUZ.out","w");

    e_states=narray;
    m_states=narray;
    nspin=nx*ny;
    kT=0.01;
    mu=-1.5;

//next: max exponent value - inspect values of lnP to get
//this by
//setting lambda to zero for first run through processing

    lambda=0.0;

    for(i=0;i<e_states;i++){
      for(j=0;j<m_states;j++){
          energy[i]=0.0;
          density[j]=0.0;
```

```c
      ghist[i][j]=0.0;
      ehist[i][j]=0.0;
    }
  }

  for(ii=0;ii<7009;ii++){ //change condition accoording
  to number of columns in wl_mb_2d.out

      fscanf(wl_mb_data,"%i %i %f %f %f
      %f",&i,&j,&fenergy,&fden,&fghist,&fehist);
      energy[i]=fenergy;
      density[j]=fden;
      ghist[i][j]=fghist;
      ehist[i][j]=fehist;
      fprintf(ftest,"%i\t %i\t %.3lf\t %.3lf\t %.3lf\t
      %.3lf\n",i,j,energy[i],density[j],ghist[i][j],ehi
      st[i][j]);
  }

//starting point from U(T) plot - used to calculate C(T)
  kT_prev=0.0;
  u_prev=-1.0;
//outer loop: use for calculation of U(T) etc.
  for(mm=1;mm<6;mm++){
  mu=mm*0.5-2.0;
    for(m=1;m<401;m++){
      kT=m*0.005;
      lambda=0.0;
      for(i=0;i<e_states;i++){
        for(j=0;j<m_states;j++){
          if(ehist[i][j]>0.0){
            lnP[i][j]=ghist[i][j]-
            (energy[i]/kT)+(density[j]*mu/kT);
            if(lnP[i][j]>lambda)lambda=lnP[i][j];
          }
        }
      }

      partition=0.0;
      u_energy=0.0;
      den_ave=0.0;
      for(i=0;i<e_states;i++){
        for(j=0;j<m_states;j++){
          if(ehist[i][j]>0.0){
            lnP[i][j]=ghist[i][j]-
            energy[i]/kT+density[j]*mu/kT-lambda;
            //goto nineonine:
            prob[i][j]=exp(lnP[i][j]);
            partition=partition+prob[i][j];
            u_energy=u_energy+energy[i]*prob[i][j];
            den_ave=den_ave+density[j]*prob[i][j];
```

```c
                //nineonine:
            }
          }
        }

        fprintf(stdout,"m,kT,partition:%i\t, %.8lf\t,
        %.8f\n",m,kT,partition);

        //u_energy=u_energy/(nspin*partition);
        u_energy=u_energy/partition;
        //den_ave=den_ave/(real*partition);
        den_ave=den_ave/partition;
        capacity=(u_energy - u_prev)/(kT - kT_prev);
        //helmholtz=-
        1.0*kT*(log(partition)+lambda)/(nspin);
        helmholtz=-1.0*kT*(log(partition)+lambda);

//entropy calculation: note that u_energy and helmholtz
//are both
//per particle, so no need to divide by number of
//particles again
//also, Boltzmann constant assumed to be 1.0 in this
//work, so
//kT is equivalent to T (entropy=energy/T)

        entropy=(u_energy-helmholtz)/kT;
        u_prev=u_energy;
        kT_prev=kT;

         fprintf(t,"%.8lf\t %.8lf\t %.8lf\t %.8lf\t
        %.8lf\n",kT,u_energy/nspin,den_ave/nspin,helmhol
        tz,entropy);

    } //close temperature loop
  } //close pressure loop
}
```

# Bibliography

[1]   www.lsbu.ac.uk/**water**/anmlies.html.

[2]   P. Wiggins, Life depends upon Two Kinds of Water, PLoS ONE , 3(1), e1406, (2008).

[3]   S.N. Sundberg, Optical and Raman spectroscopy studies on $H_2O$ at high pressure, Acta Universitatis Upsaliensis, Digital Comprehensive Summaries of Uppsala Dissertations from the Faculty of Science and Technology 92. 77 pp. Uppsala, ISBN 91-554-6340-1, (2005).

[4]   L.A. Bloomfield, How Things Work The Physics of Everyday Life, John Wiley & Sons, Inc., 326-327, (1997).

[5]   Handbook of Chemistry and Physics, 64th ed., CRC Press (Bocas Raton, Florida), (1984).

[6]   Handbook of Chemistry and Physics, 83rd  ed., CRC Press (Bocas Raton, Florida), (2002).

[7]   V. Tchijov, Heat capacity of high-pressure ice polymorphs, J. Phys. Chem. Solids, 65, 851-854, (2004).

[8]   Court Scientists, The Art of Experimentation in the Galilean Accademia del Cimento (1657-1667), Institute and Museum of the History of Science, Florence, (2001).

[9]   T.C. Hope, Experiments and observations upon the contraction of water by heat at low temperatures, Trans. Royal Soc. Edinburgh 5, 349-405, (1805).

[10]  M. Thiesen, K. Scheel, H. Diesselhorst, Untersuchungen über die thermische Ausdehnung von festen und tropfbar flüssigen Körpern - Bestimmung der

Ausdehnung des Wassers für die zwischen 0° und 40° liegenden Temperaturen, Wiss. Abhandlungen der Physik.-Techn. Reischsanst., 3, 1-70, (1900).

[11] M. Thiesen, Untersuchungen über die thermische Ausdehnung von festen und tropfbar flüssigen Körpern - Bestimmung der Ausdehnung des Wassers für die zwischen 0° und 40° liegenden Temperaturen, Wiss. Abhandlungen der Physik.-Techn. Reischsanst., 4, 1-32, (1918).

[12] International Critical Tables of Numerical Data, Physics, Chemistry and Technology, National Research Council, Vol. III, 107-111, (1928), (Electronic Edition: Knovel, 2003).

[13] M. Despretz, Recherches sur le maximum de densite des dissolutions aqueuses, Annales de Chimie et de Physique, 70, 49-81, (1839).

[14] M. Despretz, Le maximum de densite et la dilatation de l'eau distille, Annales de Chimie et de Physique, 73, 296-310, (1840).

[15] R. Wright, The Effect of some simple electrolytes on the temperature of maximum density of water, J. Chemical Soc., 115, 119-126, (1919).

[16] M.F Rosetti, Sur le maximum de densite et la dilatation de l'eau distillee, Annales de Chimie et de Physique, 10, 461-473, (1867).

[17] M.F Rosetti, Sur le maximum de densite et la dilatation de l'eau distillee, de l'eau de le adriatique et de quelques solutions salines, Annales de Chimie et de Physique, 17, 370-384, (1869).

[18] A.G. Mitchell, W.F.K. Wynne-Jones, Thermodynamic and other properties of solutions involving hydrogen bonding, Discuss. Faraday Soc. 15, 161-168, (1953).

[19]  G. Wada, S. Umeda, Effects of nonelectrolytes on the temperature of the maximum density of water. I. alcohols, Bull. Soc. Jpn., 35 4, 646-652, (1962).

[20]  F. Franks, B. Watson, Maximum density effects in dilute aqueous solutions of alcohols and amines, Trans. Faraday Soc., 63, 329-334, (1967).

[21]  M.F. Cawley, G.J. Cotter, A. Stewart, Detailed structure observed in the temperature of maximum density of aqueous solutions as functions of pressure and solute concentration, J. Chem. Phys., (submitted).

[22]  F.J. Millero, A. Gonzalez, G.K. Ward, The density of seawater solutions at one atmosphere as a function of temperature and salinity, J. Marine Res., 34, 61-93, (1976).

[23]  A. Bradshaw, K.E. Schleicher, Direct measurement of thermal expansion of seawater under pressure, Deep-Sea Res., 17, 691-706, (1970).

[24]  C. T. Chen, F.J Millero, The Specific volume of seawater at high pressures, Deep-Sea Res., 23, 595-612, (1976).

[25]  C.T. Chen, F.J. Millero, The equation of state of seawater determined from sound speeds, J. Marine Res., 36, 657-691, (1978).

[26]  C.T Chen, R.A. Fine, F.J. Millero, The equation of state of pure water determined from speed sounds, J. Chem. Phys., 66, 2142-2144, (1977).

[27]  F.J. Millero, C.T Chen, A. Bradshaw, K. Schleicher, A new high pressure equation of state for seawater, Deep-Sea Res., 27A, 255-264, (1980).

[28]  D.R. Caldwell, The maximum density points of pure and saline water, Deep-Sea Res., 25, 175-181, (1978).

[29]  S.J. Henderson, R.J. Speedy, Temperature of maximum density in water at negative pressure, J. Phys. Chem., 91, 3062-3068, (1978).

[30]  P. Fofonoff, R.C. Millard, Unesco 1983. Algorithms for computation of the fundamental properties of seawater, Unesco Tech. Pap. In Mar. Sci., 44, 53, (1983).

[31]  F.J. Millero, J.H. Knox, R.T. Emmet, A high pressure variable pressure magnetic float densimeter, J. Solution Chem., 1, 173-186, (1972).

[32]  Standard Test Method for Determination of Isothermal Secant and Tangent Bulk Modulus, Annual Book of ASTM Standards, 05.04, (2004).

[33]  D.R. Jackett, T.J. McDougall, R. Feistel, D.G. Wright, S.M. Griffies, Algorithms for density, potential temperature, conservative temperature and the freezing temperature of seawater, J. Atmos. Ocean. Technol., 23, 1709-1728, (2006).

[34]  R. Feistel, D.G. Wright, K. Miyagawa, A.H. Harvey, J. Hruby, D.R. Jackett, T.J. McDougall, W. Wagner, Mutually consistent thermodynamic potentials for fluid water, ice and seawater: a new standard in oceanography, Ocean Sci., 4, 275-291, (2008).

[35]  R. Feistel, G.M. Marion, A Gibbs-Pitzer function for high-salinity seawater thermodynamics, Progress in Oceanography, 74 (4), 515-539, ISSN 0079-6611, DOI: 10.1016/j.pocean.2007.04.020, (2007).

[36]  J. Safarov, F.J. Millero, R. Feistel, A. Heintz, E. Hassel, Pressure, density and temperature properties and vapour pressure of seawater in various salinities, Chemie Ingenieur Technik, 82, 1587, DOI: 10.1002/cite.201050649, (2010).

[37] M.F. Cawley, D. McGlynn, P.A. Mooney, Measurement of the temperature of density maximum of water solutions using a convective flow technique, Int. J. Heat and Mass Transfer, 49, 1763–1772, (2006).

[38] COMSOL Multiphysics User's Guide, Version 3.3a, (2007).

[39] D.S. Lin, M.W. Nansteel, Natural convection heat transfer in a square enclosure containing water near its density maximum, Int. J. Heat and Mass Transfer, 30, 2319-2328, (1987).

[40] M.F. Cawley, P.A. Mooney, P. O'Connor, Asymmetrical heat transfer through composites of water and aqueous solutions in the presence of the density maximum, Int. J. Heat and Mass Transfer, 51, 224-236, (2008).

[41] Solubility Data Series, International Union of Pure and Applied Chemistry, Vol. 15, Pergamon Press, Oxford, (1982).

[42] Solubility Data Series, International Union of Pure and Applied Chemistry, Vol. 37, Pergamon Press, Oxford, (1988).

[43] R.M. Stephenson, J. Stuart, M. Tabak, Mutual solubility of water and aliphatic alcohols, J. Chem. Eng. Data, 29(3), 287-290, (1984).

[44] B.T. Doherty, D.R. Kester, Freezing point of seawater, J. Marine Res., 32, 285-300, (1974).

[45] Numerical Recipes in C, 2nd ed., Cambridge University Press, 664-666, (1995).

[46] H.E. Dillon, S.G. Penoncello, A fundamental equation for calculation of the thermodynamic properties of ethanol, Int. J. Thermophysics, 25, 2, 321-335, (2004).

[47] S. Lago, P.A.G. Albo, Thermodynamic properties of acetone calculated from accurate experimental speed of sound measurements at low temperatures and high pressures, J. Chem. Thermodynamics, 41, 506-512, (2009).

[48] T.F. Sun, J.A. Schouten, N.J. Trappeniers, S.N. Biswas, Accurate measurement of the melting line of methanol and ethanol at pressures up to 270 MPa, Berichte der Bunsen-Gesellschaft für Physikalische Chemie, 92, 652-655, (1988).

[49] P.W. Richter, W.F.T Pistorius, The effect of pressure on the melting point of acetone, Zeitschrift für Physikalische Chemie Neue Folge, Bd. 85, 82-85, (1973).

[50] http://server.ccl.net/cca/documents/molecular-modeling/node9.html#SECTION00680000000000000000.

[51] W.C. Röntgen, Über die constitution des flüssigen Wassers, Ann. Phys. u. Chem. 45, (1892).

[52] G.W. Robinson, S. Zhu, S. Singh, Water in biology, chemistry and physics: experimental overview and computational methodologies, World Scientific Publishing Co. Pte Ltd., Singapore, (1996).

[53] C.H. Cho, S. Singh, G.W. Robinson, An explanation of the density maximum in water, Phys. Rev. Lett., 76 (10), 1651-1654, (1996).

[54] C.H. Cho, S. Singh, G.W. Robinson, Understanding all of water's anomalies with nonlocal potential, J. Chem. Phys., 107 (19), 7979-7988, (1997).

[55] H. Tanaka, Simple physical explanation of the unusual thermodynamic behaviour of liquid water, Phys. Rev. Lett., 80 (26), 5750-5753, (1998).

[56] P. Jedlovszky, M. Mezei, R. Vallauri, A molecular explanation of the density maximum of liquid water from computer simulations with a polarizable potential model, Chem. Phys. Lett., 318, 155-160, (2000).

[57] S. Chatterjee, H.S Ashbaugh, P.G. Debenedetti, Effects of nonpolar solutes on the thermodynamic response functions of aqueous mixtures, J. Chem. Phys., 123, 164503, (2005).

[58] H.S. Ashbaugh, T.M. Truskett, P.G. Debenedetti, A simple thermodynamic theory of hydrophobic hydration, J. Chem. Phys., 116 (7), 2907-2921, (2002).

[59] T.M. Truskett, P.G. Debenedetti, S. Sastry, A single-bonded approach to orientation-dependent interactions and its implication for liquid water, J. Chem. Phys., 111 (6), 2647-2656, (1999).

[60] N. Metropolis, A.W. Rosenbluth, M.N. Rosenbluth, A.H. Teller, E. Teller, Equations of state calculations by fast computing machines, J. Chem. Phys., 21 (6), 1087-1092, DOI: 10.1063/1.1699114, (1953).

[61] D.P. Landau, Shan-Ho Tsai, M. Exler, A new approach to Monte Carlo simulations in statistical physics: Wang-Landau sampling, Am. J. Phys., 72 (10), 1294-1302, (2004).

[62] C. Gervais, T. Wüst, D.P. Landau, Y. Xu, Application of the Wang-Landau algorithm to the dimerization of glycophorin A, J. Chem. Phys., 130, 215106, (2009).

[63] F. Wang, D.P. Landau, Efficient, Multiple-range random walk algorithm to calculate the density of states, Phys. Rev. Lett., 86 (10), 2050-2053, (2001).

[64] K.A.T. Silverstein, A.D.J. Haymet, K.A. Dill, A simple model of the hydrophobic effect, J. Am. Chem. Soc., 120, 3166-3175, (1998).

[65] Ben-Naim, Statistical mechanics of "waterlike" particles in two dimensions. I. physical model and application of the Percus-Yevick equation, Am. J. of Chem. Phys., 54, 3682-3695, (1971).

[66] D.C. Rappaport, The Art of Molecular Dynamics Simulation, 2$^{nd}$ ed., Cambridge University Press, (2004).

[67] C. Buzano, E. De Stefanis, Low-temperature swelling of a hydrophobic polymer: a lattice approach, J. of Chem. Phys., 126, 074904 (2007).

[68] C. Buzano, E. De Stefani, M. Pretti, Hydration of an apolar solute in a two-dimensional waterlike lattice fluid, Phys. Rev. E, 71, 051502, (2005).

[69] C. Buzano, E. De Stefani, M. Pretti, Two-dimensional lattice-fluid model with waterlike anomalies, Phys. Rev. E, 69, 061502, (2004).

[70] M.V. Kaulgud, Temperature of maximum density behaviour of non-electrolytes in water, , J. Chem. Soc. Faraday Trans., 86 (6), 911-915, (1990).

[71] C. Vega, J.L.F. Abascal, Relation between the melting temperature and the temperature of maximum density for the most common models of water, J. Chem. Phys., 123, 144504, (2005).

[72] E.G. Noya, C. Vega, L.M. Sesé, R. Ramírez, Quantum effects on the maximum density of water as described by the TIP4PQ/2005 model, J. Chem. Phys., 131, 124518, (2009).

[73] F.A. Deeney, J.P. O'Leary, Zero point energy and the origin of the density maximum in water, Phys. Lett. A, 372, 1551-1554, (2008).

[74] F.A. Deeney, J.P. O'Leary, A rapid method for measuring maximum density measurements in water and aqueous solutions for the study of quantum zero point energy effects in these liquids, Euro. J. Phys., 29, 871-877, (2008).